A SMALL MOLECULE BASED APPROACH TO STUDY MAMMARY GLAND BIOLOGY REVEALS NEW MECHANISTIC INSIGHTS ON HOW ENVIRONMENTAL TOXINS DISRUPT MAMMARY FUNCTION

by

Kaitlin J. Basham

A dissertation submitted to the faculty of
The University of Utah
in partial fulfillment of the requirements for the degree of

Doctor of Philosophy

Department of Oncological Sciences

The University of Utah

August 2014

The University of Utah Graduate School

STATEMENT OF DISSERTATION APPROVAL

The following faculty members served as the supervisory committee chair and members for the dissertation of Kaitlin J. Basham.

Dates at right indicate the members' approval of the dissertation.

Bryan Welm, Chair	06/03/2014 Date Approved
Rodney Stewart, Member	06/03/2014 Date Approved
Katharine Ullman, Member	06/03/2014 Date Approved
Mark Metzstein, Member	06/03/2014 Date Approved
Ryan Looper, Member	06/03/2014 Date Approved

The dissertation has also been approved by Bradley Cairns Chair of the Department/School/College of Oncological Sciences.

and by David B. Kieda, Dean of The Graduate School.

ABSTRACT

Through the production of milk, the mammary gland provides nutritional and immunological protection for newborns. However, lactation is required for only short periods of time in the adult animal, which allows the mammary gland to develop through a series of distinct stages. During embryogenesis and puberty, the gland establishes an extensive network of epithelial ducts, which then undergo widespread branching and differentiation during pregnancy to maximize milk production. Throughout this process, the mammary gland relies on coordination of major cellular processes, including proliferation, invasion, and differentiation. As many of these pathways become aberrantly regulated during breast cancer, understanding mechanisms that regulate mammary gland development has important disease implications.

Although previous studies have characterized several systemic hormones and local factors central to mammary development, little is known about the downstream mediators of these pathways. To identify new factors, we established a three-dimensional model of mammary branching morphogenesis using primary mammary epithelial cells (MECs) stimulated with fibroblast growth factor-2 (FGF2). We performed a forward chemical genetic screen to identify compounds that modulate FGF2-induced branching and discovered a novel *bis*-aryloxadiazole, called 1023, which completely blocks branching through activation of the aryl hydrocarbon receptor (AHR).

Using 1023 as a molecular probe, we found AHR activation blocks mammary branching through upregulation of desmosomal adhesion. These results identified desmosomes as a novel target of AHR signaling and suggested desmosomes are downregulated to facilitate mammary branching. Supporting this hypothesis, we found desmosomes absent in the mammary glands of pregnant mice in a cell-type specific manner. These results suggest desmosomes control initiation of mammary branching, and may also be targeted during breast cancer to promote cellular invasion.

We also investigated mechanisms of AHR activation and the impact of AHR on mammary differentiation. We performed a structure activity relationship study of 1023 and defined moieties of the molecule critical for AHR stimulation. Moreover, we investigated the effect of AHR on mammary differentiation and elucidated a transcriptional mechanism through which the AHR pathway directly blocks lactation in MECs. Since several environmental pollutants stimulate AHR, these studies provide mechanistic insight for how toxins impair mammary function.

In memory of my mother: a great story teller, mentor, and friend.

“The more we see, the more we are capable of seeing.”
Maria Mitchell

TABLE OF CONTENTS

LIST OF FIGURES

LIST OF TABLES

ACKNOWLEDGEMENTS

First, I would like to thank my mentor Dr. Bryan Welm for the freedom he has given me to pursue my own hypotheses and develop as an independent scientist. I appreciate all that he has contributed to my Ph.D. training and particularly admire his sense of innovation and willingness to take chances, which has helped shape the way I think about big questions.

I would also like to thank my thesis committee, Dr. Rodney Stewart, Dr. Katharine Ullman, Dr. Mark Metzstein, and Dr. Ryan Looper, for always being approachable and generous with their time and feedback. Additionally, the Developmental Biology Training Grant, led by Dr. Joseph Yost and Dr. Richard Dorsky, has been an integral part of my PhD training. I appreciate their support of my graduate studies through funding, career development, and community events.

Leading up to graduate school, two professors profoundly shaped my career decisions. Dr. Larry Neznanski (a.k.a. Doc Nez) was my high school physics teacher and the first person to force me to think critically and learn without memorizing. This experience completely changed my view of science and inspired me to pursue biology in college. At Saint Mary's College of California, Dr. Allan Hansell was an incredibly influential mentor during my studies. He was the first professor to give me the opportunity to do bench science and the first to challenge me to understand a question or

problem simply for the sake of knowing. Together, Doc Nez and Dr. Hansell helped me find my passion for research and I am grateful for their influence and inspiration.

During graduate school, I feel fortunate to have been surrounded and supported by incredible colleagues and friends. The former and current members of the Welm lab have greatly impacted my graduate school experience. From baked goods and coffee breaks to feedback on experiments and presentations, the lab was a unique and fun environment. I will always be grateful for the help celebrating successes and the support through challenging times from Brittni, Daria, Rachel, and Celine. Beyond the lab, many close friends were a vital part of finding balance, especially Shelly, Elena, and Jo. I will always cherish the time skiing, canyoneering, and rafting in the Utah backcountry together.

Lastly, I am grateful to my entire family, who have endlessly supported my passions. My parents always prioritized education and created every opportunity possible. My brother never ceases to amaze me with his sense of creativity and innovation and my in-laws have a wonderful and contagious curiosity of the world. Finally, I am lucky to be married to my best friend, Andy, who inspires me to be a better person. Thank you for accompanying me in this adventure.

CHAPTER 1

INTRODUCTION

Mammary Gland Biology

The origin and function of the mammary gland

As a defining feature of mammals, the mammary gland has long been recognized as a unique organ. In 1758, Carolus Linnaeus used the mammary gland as the basis for classifying and naming the *Mammalia* class of the animal kingdom (1). Meaning "of the breast," *Mammalia* describes a diverse group of species that, among other definitive features, utilize the mammary gland for milk production to support the perinatal growth of offspring.

Through the production of milk, the mammary gland provides nutritional and immunological protection for newborns. Although lactation fulfills this duel role, increasing evidence suggests the gland first evolved to carry out a protective function (2-5). Initially, the ancestral mammary structure is thought to have secreted antimicrobial molecules, including lysozyme (5) and xanthine oxidoreductase (XOR) (2). These enzymes later evolved additional roles to augment the nutritional content of secretions. For example, lysozyme evolved to synthesize and secrete milk sugars (i.e., lactose) (5) while XOR obtained the ability to promote milk fat droplet secretion (2).

Mammary gland composition

To successfully produce and deliver milk for newborn animals, the mammary gland establishes an elaborate network of epithelial ducts. Initially, a rudimentary ductal tree is formed during embryogenesis, which then undergoes significant growth and branching during puberty to create a mature ductal network. During pregnancy, this framework of epithelial ducts supports further branching and formation of alveoli, which

functionally differentiate to produce milk. As a highly complex process, development of the mammary gland relies on coordination between its two cellular compartments: the epithelium and the surrounding stroma.

The epithelium is derived embryonically from ectoderm and gives rise to mammary ducts, which are composed of luminal epithelial and myoepithelial cells (Figure 1.1) (6). Luminal epithelial cells form the inner layer of ducts and give rise to milk-producing alveoli during pregnancy. In contrast, myoepithelial cells form the outer layer of mammary ducts and lie adjacent to the basement membrane. These more specialized cells contract in response to hormonal cues during lactation to move milk along the ductal network. While still controversial, recent studies suggest each of these cell types is maintained by a small stem cell population, which allows for expansion of the gland during puberty and pregnancy (7).

The mammary epithelium is supported by the surrounding stroma, or mammary fat pad (Figure 1.1). The stromal compartment is derived embryonically from mesoderm and includes a condensed layer of cells and extracellular matrix (ECM) near the ducts in addition to more distal adipocytes, vascular endothelial cells, fibroblasts, and immune cells (8). The importance of the stromal compartment during mammary gland development has been elegantly demonstrated by transplantation studies. Recombination of mammary epithelium and salivary mesenchyme gives rise to a structure with salivary morphology (9). In contrast, transplantation of skin epithelium and mammary mesenchyme results in mammary structures capable of lactogenic differentiation (10). These studies demonstrate mesenchyme-derived signals significantly impact mammary morphogenesis and cell fate.

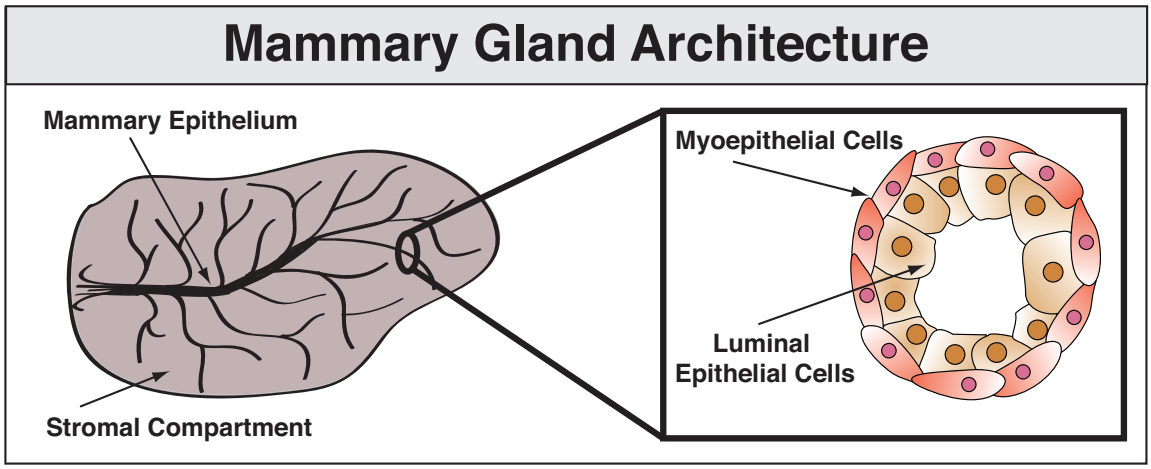

Figure 1.1. Schematic representation of mammary gland architecture. (Left) The mammary gland contains two cellular compartments, the epithelium and the stroma, which function together to produce and deliver milk for newborn animals. (Right) Within the mammary epithelium, luminal epithelial cells line the inside of mammary ducts and myoepithelial cells form an outer, contractile layer.

Stages of mammary gland development

Together, the mammary epithelium and stromal compartment function to promote growth and expansion of the mammary gland at each stage of development. During embryogenesis, puberty, and pregnancy, the gland undergoes extensive branching morphogenesis to increase its surface area and thereby maximize the capacity for milk production. However, each stage of development is governed by unique branching mechanisms and regulatory signals.

Embryogenesis. The earliest stage of morphogenesis in the mammary gland begins at embryonic day 10.5 (E10.5) in mice (11). Initially, bilateral ridges of epidermal cells, called milk lines, are specified ventrally from forelimb to hindlimb. Ectodermal cells within each milk line migrate into clusters by E11.5 (12,13), forming 5 pairs of placodes at the site of each future nipple. Although these initial events in the mouse mammary gland closely mirror human development, the mammary line forms earlier in

humans during the first trimester and only gives rise to one pair of placodes (14). However, in both humans and mice, crosstalk between the epithelial and mesenchymal layers coordinates these early events.

Somite-derived fibroblast growth factors (FGFs) and Wnt signaling in the ectoderm are among the critical factors for early mammary development. FGF signaling, which acts through receptors in the ectoderm, stimulates TBX3 expression in the underlying mesenchyme (15). This is one of the first observable regulatory events and occurs at E10.25 (16). TBX3 then activates Wnt signaling in the ectoderm, particularly *Wnt10b*, to ultimately specify the mammary line. The importance of these major signaling pathways has been demonstrated by loss-of-function approaches. Mice deficient in FGFR2b only develop one pair of placodes (17) and *Tbx3-/-* mice fail to activate Wnt signaling or form placodes (18). Furthermore, overexpression of the diffusible Wnt inhibitor, DKK1, in the ectoderm completely blocks placode formation (19). Together, these studies suggest local FGFs, TBX3 and Wnt ligands collectively regulate mammary line specification and placode development.

Following formation, each placode grows into the underlying mesenchyme to form a primary anlage, or bulb-shaped mammary rudiment. As growth continues, the mammary bud invades the preadipocyte layer beneath the mesenchyme, which represents the future mammary fat pad. Here, between E15.5 and E16.5, the mammary bud sprouts into a rudimentary ductal tree. This structure is the culmination of embryonic mammary development and is composed of a primary duct with 15-20 secondary branches (11). However, in humans, multiple independent ductal trees develop and join together at each nipple.

This first phase of mammary development occurs independent of hormonal stimulation, since mice deficient in the estrogen receptor (20,21), progesterone receptor (22), or prolactin receptor (23) display normal embryonic mammary gland development. Rather, parathyroid hormone-related protein (PTHLH), which is produced in the mammary epithelium and signals through its receptor in the mammary mesenchyme (24), is one of the key regulators of embryonic mammary branching. *Pthlh-/-* mice display normal mammary bud development, but fail to form a ductal tree, suggesting PTHLH is required for fetal mammary branching (25). These studies demonstrate the critical role of localized factors in early morphogenesis, as compared to the dual role of local and systemic signals that function during later stages (Figure 1.2).

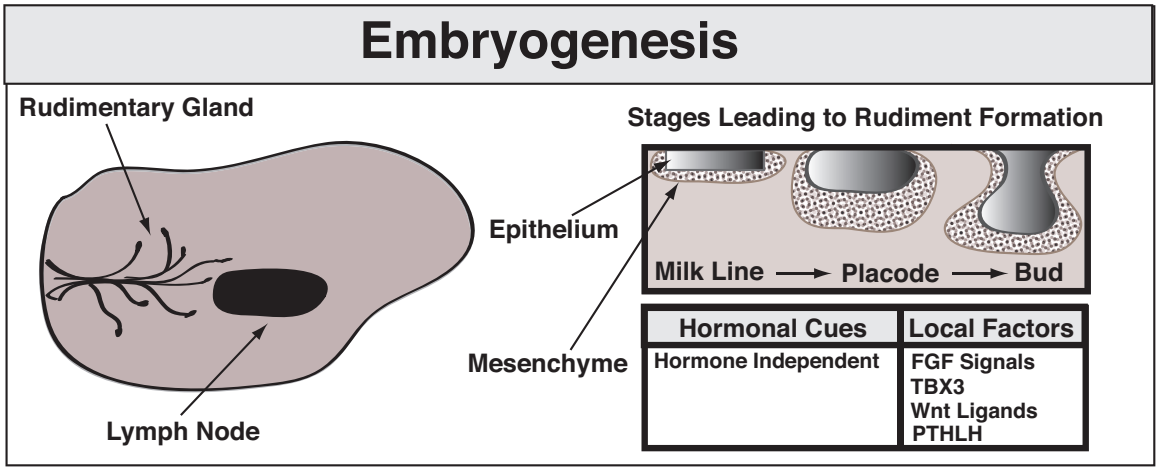

Figure 1.2. Summary of mammary gland development during embryogenesis. (Left) A rudimentary ductal network is established in the mammary gland during embryogenesis. (Right) Initially, bilateral ridges of epidermal cells (milk lines) are specified, which then migrate to form placodes. Each placode grows into the underlying mesenchyme to form a mammary bud that sprouts into a small ductal tree. Rather than hormonal cues, this stage of mammary development is regulated by local factors.

Puberty. Following embryogenesis, the mammary gland enters an isometric growth phase in which the rudimentary ductal tree grows proportional to the body. Growth continues in this manner until puberty, when hormone-dependent branching transforms the mammary gland into an elaborate ductal network (26) (Figure 1.3). During puberty, branching occurs through two main mechanisms: bifurcation of terminal end buds (TEBs) and sprouting of side branches.

TEBs are club-shaped structures that form at the tips of elongating ducts and contain a multilayered inner core of body cells surrounded by an outer layer of undifferentiated cap cells (26). Through proliferation and invasion of the fat tissue, TEBs drive elongation of immature ducts and undergo bifurcation to create new primary branches. TEBs are heavily regulated by rates of mitosis, as ectopic overexpression of transforming growth factor beta1 (TGFB1), which inhibits epithelial proliferation,

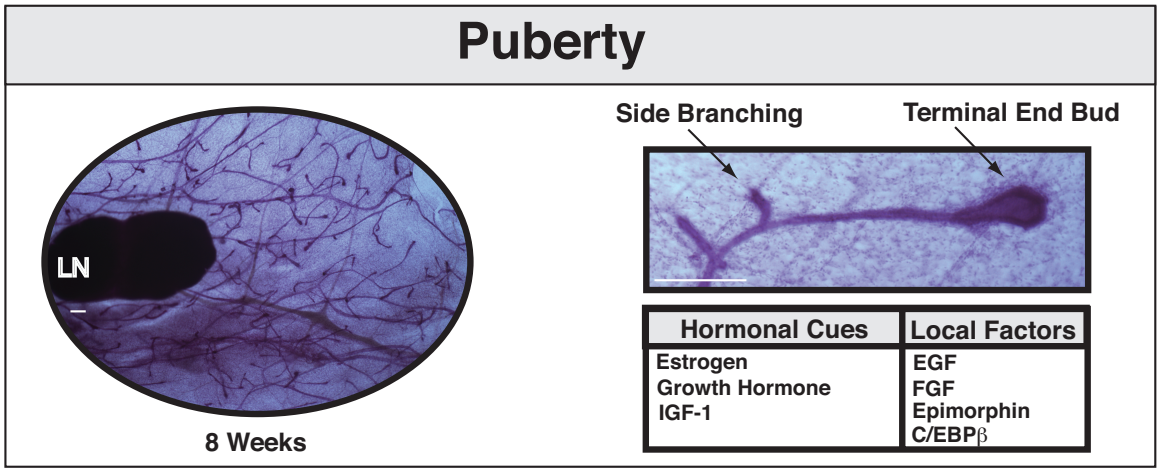

Figure 1.3. Summary of mammary gland development during puberty. (Left) An elaborate ductal network is established in the mammary gland during puberty. Representative whole mount analysis from a mature, female FVB/n mouse. The mammary gland was collected at 8 weeks of age and stained with carmine alum. LN: lymph node. (Right) During puberty, branching occurs through two mechanisms: side branching and terminal end bud formation. These processes are controlled by several hormonal and local factors. Scale bars: 0.25mm.

significantly restricts ductal elongation and bifurcation (27,28). Additionally, the surrounding stroma has a significant influence on growth and branching of TEBs, particularly components of the ECM and infiltrating macrophages (reviewed in (26)).

Concurrent with TEBs, side branches emerge laterally from the trailing portion of primary ducts. C/EBPβ is one factor required in the mammary epithelium for this process, as evidenced by the dramatic decrease in secondary branches observed after targeted deletion in the mouse (29). C/EBPβ is a transcription factor induced through paracrine signaling by epimorphin, which is expressed by neighboring fibroblasts and subsequently released by matrix metalloproteinases (MMPs) (30). In addition to C/EBPβ, epimorphin also promotes side branching through upregulation of MMPs. Inhibition of MMP activity in mammary organoid cultures blocks branching, suggesting these factors are also required for normal mammary branching morphogenesis (31). These mechanisms of lateral branching, together with elongation and bifurcation of TEBs, create a ductal network that fills approximately 60% of the mammary fat pad area by the end of puberty (32), leaving space for alveoli formation during pregnancy.

In addition to localized signaling pathways that control specific branching mechanisms, systemic hormones globally regulate mammary development during puberty. Removal of either the ovaries (ovariectomy) or pituitary gland (hypophysectomy) results in failed mammary morphogenesis during puberty (33), implicating a critical role for both ovarian and pituitary hormones. In particular, estrogens produced in the ovaries and growth hormone (GH) and insulin-like growth factor (IGF-1) from the pituitary are critical factors required for morphogenesis.

A central role for estrogen signaling during adolescent development has been demonstrated by gain-of-function and loss-of-function studies. In initial experiments, estrogen was delivered in Elvax pellets to the mammary glands of ovariectomized mice and was found to stimulate ductal growth. In contrast, loss of estrogen receptor-alpha (ERα) (21,34) or loss of enzymes critical for estrogen biosynthesis (35), resulted in formation of a rudimentary ductal tree that failed to elongate and grow during puberty. These studies defined a central role for estrogen in puberty-associated growth of the mammary gland. Similar approaches were also used to define critical roles for GH and IGF-1 during puberty. Specifically, mice lacking GH receptor (36) or IGF-1 (37) display a significant reduction in ductal development. Moreover, estrogens are capable of rescuing ductal development in hypophysectomized animals only if GH or IGF-1 is also provided (37), suggesting estrogen cooperates with pituitary hormones to promote mammary development.

Although these early experiments demonstrated the importance of estrogen signaling during mammary ductal morphogenesis, it wasn't until later that transplantation studies showed estrogen acts through stromal-derived growth factors, rather than directly on mammary ducts. In these seminal experiments, recombination of estrogen receptor knockout mammary epithelium and wild type mammary stroma in the subrenal capsule of nude mice displayed normal epithelial proliferation (38). These results demonstrated that hormonal regulation of epithelial growth was mediated by estrogen-induced stromal factors, which were later shown to include epidermal growth factor (EGF) (39,40).

This link between ER and EGF is based on observations that EGF receptor (EGFR) activation rescues ductal development in ovariectomized (39) and ER-α-

deficient mice (40). EGFR is a receptor tyrosine kinase that can be activated by a variety of ligands to promote cell proliferation and survival. Amphiregulin (AREG) is the only EGFR ligand known to be required for normal ductal development (41). Mechanistically, AREG is induced in mammary epithelial cells in response to estrogen and IGF-1 signaling, and is proteolytically released from epithelial cells by ADAM metallopeptidase domain 17 (ADAM17). AREG then activates EGFR on stromal cells to induce release of stromal factors that promote epithelial growth. These EGFR-stimulated factors are essential for mammary development, as EGFR-null stroma is unable to support growth of wild type epithelium in cotransplantation studies (42).

Although still ongoing, a number of studies suggest FGF signaling is the critical downstream pathway stimulated by EGFR activation. FGFs are upregulated in the stroma during puberty (43) and growth of EGFR-null mammary organoids in culture can be rescued by FGF2 and FGF7 (41). However, FGF signaling during adolescent mammary development was initially difficult to study, as deletion of FGF receptor-2b (FGFR2b) resulted in the failure of most embryonic placodes to form (17). Later conditional deletion of FGFR2 during puberty in the mammary epithelium caused impaired ductal development (44). Moreover, mosaic inactivation of FGFR2, due to inefficiency of the MMTV-Cre transgene, found FGFR2-null epithelial cells were outcompeted by their wild type counterparts, particularly within TEBs. Taken together, these results strongly support FGF as the key downstream mediator of EGFR activation during ductal morphogenesis.

Overall, hormonal and local signals function during puberty to create an extensive ductal network. Estrogen produced in the ovary and GH and IGF-1 from the pituitary

gland, act in concert to stimulate the production and release of EGFR ligands from the mammary epithelium. These factors activate stromal EGFR signaling and subsequent production of FGF ligands, which act on mammary epithelial cells to promote ductal morphogenesis. These major hormonal and local factors critical during mammary development have been largely studied through recombination experiments and genetically engineered mice. Although powerful, the cellular complexity of these systems limits our understanding of the direct cellular targets of these signals, particularly the downstream mediators of FGFR activation. Through the use of new techniques that allow more precise manipulation of specific factors within certain cell types, we will be able to study these pathways in greater detail and further elucidate mechanisms of cellular proliferation and invasion during ductal morphogenesis.

Pregnancy. In preparation for lactation, rapid expansion of the mammary gland occurs during pregnancy (Figure 1.4). The network of ducts established during puberty undergoes extensive secondary and tertiary branching. Moreover, epithelial proliferation results in formation of alveolar buds, which differentiate into mature alveoli primed for milk production. Overall, alveolar morphogenesis increases epithelial surface area to maximize the capacity of milk production in the mammary gland. Similar to pubertal development, both local and systemic signals are key mediators of this developmental phase.

Progesterone and prolactin are the primary hormonal regulators of mammary development during pregnancy. Produced in the ovary, progesterone acts on mammary epithelial cells to elicit branching and alveolar differentiation. The requirement of progesterone signaling during mammary development has been demonstrated in

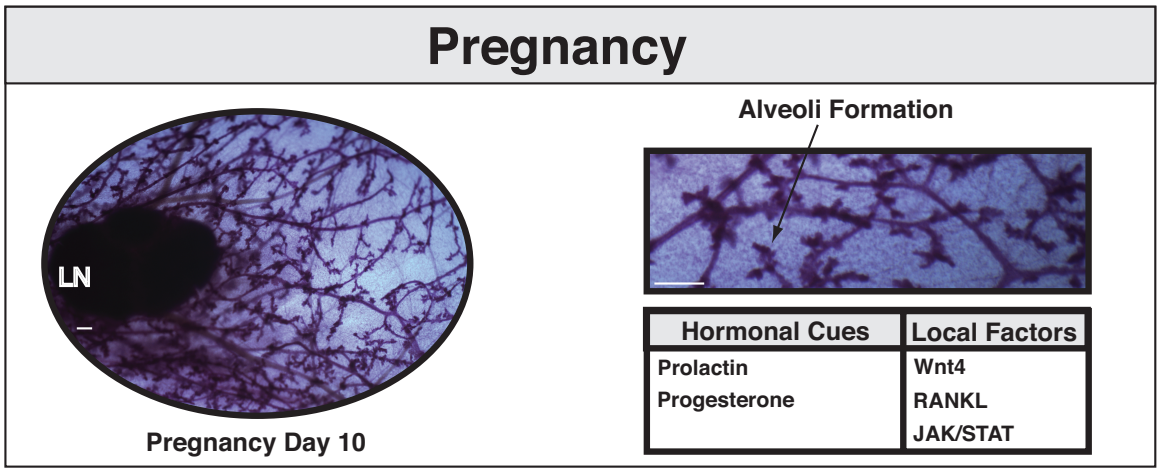

Figure 1.4. Summary of mammary gland development during pregnancy. (Left) High levels of secondary and tertiary branching occur in the mammary gland during pregnancy. Representative whole mount analysis from a pregnant, female FVB/n mouse. The mammary gland was collected at day 10 of pregnancy and stained with carmine alum. LN: lymph node. (Right) Lobuloalveolar branching occurs during pregnancy to form alveoli, which are primed for milk production. This developmental stage is controlled by several hormonal and local factors. Scale bars: 0.25mm.

progesterone receptor (*Pgr*) knockout mice. Specifically, loss of *Pgr* in the mammary epithelium limits mammary development to a small ductal network that fails to expand and differentiate during pregnancy (45).

Synergistic with progesterone, prolactin (PRL) is also critical for mammary development during pregnancy. PRL is produced in both the pituitary and the mammary epithelium, which parallels its dual role as a systemic and local regulator of mammary development. Systemically, PRL is required to stimulate progesterone production in the ovaries. This role was elucidated from *Prl* knockout mice, which show impaired alveolar development (46) that is rescued when *Prl-/-* mammary tissue is transplanted into wild type recipient mice (47) or when progesterone levels are exogenously restored in *Prl-/-* mice (48). In addition to the impact of PRL on the ovaries, it also directly targets mammary epithelium, as loss of the prolactin receptor (*Prlr*) in the mammary epithelium

impairs alveolar development (23). These studies demonstrate a key role for prolactin in both systemic and local control of mammary development.

Progesterone and prolactin cooperate to promote mammary development and differentiation during pregnancy. As a result, many of their proposed downstream pathways overlap. For example, PGR (49) and PRLR (50) both regulate Wnt4, which is required for paracrine activation of tertiary branching (49). However, Wnt4 only appears to be required during early pregnancy, suggesting involvement of other parallel or compensatory pathways. For instance, receptor activator of NFKB1 ligand (RANKL) and its receptor, RANK, are thought to play a critical role downstream of PGR and PRLR. RANKL is induced by prolactin (50) and also by progesterone (51) in epithelial cells expressing PGR (52). Moreover, loss of RANK or RANKL phenocopies *Pgr-/-* glands (53) and ectopic expression of RANKL rescues alveolar development in *Pgr* null glands (54). As a common mediator of PGR and PRLR signaling, RANK activation is thought to drive high levels of epithelial proliferation required during formation of alveolar structures.

In addition to shared pathways, progesterone and PRL also maintain unique targets. In particular, PRLR activates JAK/STAT (Janus kinase/ Signal transducer and activator of transcription) signaling through phosphorylation of JAK2 and subsequent activation of STAT5. As a key transcription factor, STAT5 mediates expression of genes important for alveolar development and differentiation, including milk proteins (reviewed in (55)). Overall, progesterone and prolactin act through a number of downstream pathways to precisely control mammary differentiation and lactation.

Involution. The final phase of mammary morphogenesis, called involution, occurs after weaning to restore the gland to a virgin-like state. In this process, milk-producing epithelial cells are destroyed in two distinct phases. The first period of involution lasts for 48 hours after weaning and is characterized by detachment of epithelial cells from the extracellular matrix, which induces cell death and shedding (56). As no major architectural changes occur, this process is reversible if suckling is reinitiated. Teat-sealing experiments, in which individual glands are physically closed off, have demonstrated this phase is regulated by local factors (57,58). Although several signaling pathways influence early involution, a switch in STAT signaling is thought to have a critical role (59). Specifically, the accumulation of milk within ducts, called milk stasis, leads to decreased Stat5 phosphorylation and increased Stat3 phosphorylation, which has a significant impact on both cell survival and apoptosis (60).

After the initial wave, a more aggressive and irreversible period of involution begins. Collapse of alveoli, breakdown of the extracellular matrix (ECM), and widespread apoptosis removes nearly all of the secretory cells from the mammary gland within 6 days (61). Unlike the first phase, this later portion of involution is regulated by systemic hormones and can be suppressed with glucocorticoid (62,63). Moreover, serine proteases and matrix metalloproteinases (MMPs) expressed by stromal cells have a critical role (64). As the surrounding matrix is remodeled, epithelial cells lose cellular contacts and undergo apoptosis. To compensate for the loss in epithelial tissue, MMPs also promote adipocyte differentiation, thus restoring the original structure of the gland.

In vitro models of mammary development

The mouse mammary gland has been the primary model system used to study mammary gland biology. Compared to the human breast, the mouse mammary gland is composed of the same epithelial cell types, similarly responds to hormonal cues including estrogen and progesterone, and progresses through a remarkably similar series of developmental stages. Moreover, the mouse mammary gland is amenable to a wide range of elegant *in vivo* manipulations, including tissue recombination, transplantation, and genetic engineering (65). These techniques have been widely used to study both normal mammary gland development and breast cancer biology. However, these approaches are not well suited for study of the human mammary gland and are both cost and time intensive.

To complement studies in the mouse, several *in vitro* models of the mammary gland have been developed. Specifically, three-dimensional (3D) models have been highly successful in recapitulating the *in vivo* physiology and differentiation of the mammary gland (66,67). These models can be performed with both mouse and human cells and are highly amenable to genetic and pharmacological manipulations, which has allowed for in depth analysis of signaling pathways and has facilitated the development of novel breast cancer therapeutics.

The first 3D model of the mammary gland was created over 30 years ago, when mouse mammary epithelial cells were cultured on floating collagen gels (68). In contrast to the more rigid matrices of plastic, glass, and fixed collagen, flexible collagen gels allowed mammary epithelial cells to functionally differentiate and produce milk proteins in the presence of lactogenic hormones (69,70). Since these early experiments, a large

number of studies have been performed to understand the role of the extracellular matrix (ECM) in mammary gland development and function (reviewed in (71)). Much more than a scaffold, the ECM and its specific composition are now known to significantly impact cellular response, growth, and differentiation.

In the mammary gland, the epithelial compartment is surrounded by basement membrane, which contains large amounts of collagen IV and laminin (72). Given these observations, it is not surprising that 3D models of mammary morphology have significantly evolved over time to more closely mimic the endogenous setting. In particular, Matrigel is now widely used, which is a laminin-rich extracellular matrix derived from Engelbreth-Holm-Swarm tumors (73).

When embedded in Matrigel, mammary cells from both mice (74) and humans (75) reorganize to form polarized, spherical structures. Moreover, human MCF-10A mammary epithelial cells grown in Matrigel form polarized acini-like spheres (76). These phenotypes more closely resemble *in vivo* mammary morphology compared to cultures with collagen I gels, which induce purified luminal epithelial cells to form structures with inverse polarity (77). In addition to the appropriate cellular morphology, Matrigel promotes differentiation of mouse mammary epithelial cells in response to lactogenic hormones (74). Furthermore, malignant human breast cells form disorganized cellular structures in Matrigel (75), highlighting the ability of this system to also mimic the disease state.

The establishment of 3D models has significantly advanced our ability to study the mammary gland *in vitro*. These techniques allow for the rapid *ex vivo* culture of mammary cells and are highly accessible to experimental manipulations. Moreover, 3D

models are particularly well suited for the study of signaling pathways, as both mono- and co-culture, consisting of combinations of epithelium and stroma, can be performed. For example, individual mammary cell types can be grown alone or in combination to study cell autonomous signaling as well as crosstalk between neighboring cells. These studies demonstrate the wide range of experimental questions that can be addressed using 3D culture systems.

Perspectives on mammary gland biology

Through a series of distinct developmental stages, the mammary gland undergoes a unique pattern of growth and differentiation. Early developmental phases give rise to a framework of ducts, which temporarily undergo functional differentiation and milk production to support the growth of offspring. This segmented growth pattern precisely links the differentiation state of the gland with the birth of offspring, thus limiting the high-energy expenditure of lactation to the short timeframe necessary to nurse newborns.

In order to precisely coordinate this process, the gland relies on tight regulation of key signaling pathways that underlie mammary development. Through *in vivo* and *in vitro* approaches, many of the major hormonal and local cues have been identified. Estrogen, progesterone, prolactin, growth hormone, and insulin-like growth factor are among the dominant hormonal signals, while EGF and FGF remain a few of the major local factors. These signaling pathways facilitate communication between the epithelial and stromal compartments of the mammary gland and control critical morphological and functional changes.

To build upon this initial framework, one of the critical next steps in mammary gland biology is to identify and understand the downstream mediators of the major signaling pathways. The molecular connection between primary signaling molecules and actual cellular changes, such as proliferation, invasion, and differentiation, remain elusive. Specifically, the targets of FGF signaling that drive ductal elongation and lateral branching are unknown. To address this question, we developed a novel *in vitro* model of mammary branching morphogenesis using primary mammary epithelial cells stimulated with FGF2. We then used a small molecule-based approach to rapidly identify novel targets important for mammary branching (Chapter 2) and have begun to validate our initial studies *in vivo* (Chapter 5). Since the normal cellular processes governing mammary morphogenesis also underlie the mechanisms of breast cancer, our study of mammary gland development has significant implications for both normal and cancer biology.

Aryl Hydrocarbon Receptor Signaling

Discovery of the aryl hydrocarbon receptor

The aryl hydrocarbon receptor (AHR) was first described by Alan Poland's laboratory in 1976 (78). However, a number of key experiments dating back to the 1950s set the stage for this important discovery. Early on, it was known that aminoazo dyes, such as 3'-methyl-4-dimethylaminoazobenzene, caused liver cancer in rats (79). Yet the carcinogenic effect of these compounds could be abrogated by simultaneous injection of 3-methylcholanthrene (3-MC) (80). As a polyaromatic hydrocarbon (PAH), 3-MC was hypothesized to protect animals from carcinogenesis by altering metabolism of the

aminoazo dye. Through a series of studies on 3-MC and related chemicals, PAHs were shown to selectively induce metabolism of certain drugs (81,82), suggestive of a specific signaling pathway protective against chemical exposures. Furthermore, the induction of metabolic enzymes by PAHs varied across mouse strains (83,84) and segregated in what appeared to be an autosomal dominant fashion (85-87). These studies defined a new genetic locus, named the *Ah* locus, based on aromatic hydrocarbon sensitivity. C57BL/6 mice, who displayed a strong metabolic response to PAHs, were characterized by the "responsive" Ah^b allele, while DBA2 mice were associated with the "nonresponsive" Ah^d allele (88).

Just as the *Ah* locus emerged as an important mediator of toxin metabolism, Alan Poland began studying factory-produced toxins that caused skin ailments in workers. Poland focused on 2,4,5-trichlorophenol (2,4,5-T) and its active contaminant, 2,3,7,8-tetrachlorodibenzo-p-dioxin (TCDD), which was thought to be responsible for chemically induced acne (chloracne) and skin blistering (porphyria cutanea tarda). Over the course of many studies, TCDD was found to induce the same metabolic enzymes as 3-MC, but was 30,000 times more toxic (89). Taking advantage of TCDD's potency and genetic differences between mouse strains, Poland was ultimately able to show the *Ah* locus produced a soluble protein, now referred to as the aryl hydrocarbon receptor (AHR), that specifically bound radiolabeled TCDD (78). Furthermore, mutation in the *Ah* locus of "nonresponsive" mice was shown to produce a receptor with decreased affinity for PAHs (90,91), accounting for the variable chemical response observed in different strains of mice.

Classical AHR-mediated signaling

After his landmark discovery, Poland hypothesized AHR activation by PAHs mimicked that of steroid hormone receptors (78). More specifically, Poland predicted activated AHR localized to the nucleus to alter specific metabolic target genes. However, later cloning and sequencing of AHR (92,93) found little in common with steroid hormone receptors. Rather, AHR contained a basic helix-loop-helix (bHLH) domain and a PER/ARNT/SIM (PAS) domain, classifying it as a member of the bHLH/PAS family of transcriptional regulators.

Although not structurally related to steroid hormone receptors, AHR does function as a ligand-activated transcription factor, as Poland predicted (Figure 1.5). In the absence of ligands, AHR interacts with a multiprotein chaperone complex to remain inactive in the cytoplasm (94). Among the members of this complex, p23 and two molecules of heat shock protein 90 (Hsp90) interact with AHR to prevent degradation and premature dimerization, and to promote a conformation of AHR capable of ligand binding (95,96). Additionally, hepatitis B virus X-associated protein 2 (XAP2) increases the stability of AHR and promotes cytoplasmic retention of the receptor (97,98). Together, the protein complex associated with the inactive form of AHR regulates its stability, ligand binding ability, and subcellular trafficking.

Ligand binding induces a conformational change in the AHR complex, which exposes a nuclear localization sequence (NLS) on AHR to promote its nuclear translocation (98). Once nuclear, AHR dissociates from its chaperone proteins, which allows interaction with other binding partners. In particular, AHR forms a heterodimer with the AHR nuclear translocator (ARNT). (99). AHR/ARNT complexes directly bind

Figure 1.5. Model of classical AHR signaling. In the absence of ligands, AHR remains inactive in the cytoplasm, bound to a chaperone complex. Upon ligand activation, AHR translocates to the nucleus and dissociates from its chaperone proteins. This allows AHR to interact with ARNT and form transcriptional activating complexes. As a heterodimer, AHR/ARNT binds specific response elements located upstream of AHR-regulated genes to promote their transcription. Abbreviations: AHR, aryl hydrocarbon receptor; ARNT, AHR nuclear translocator.

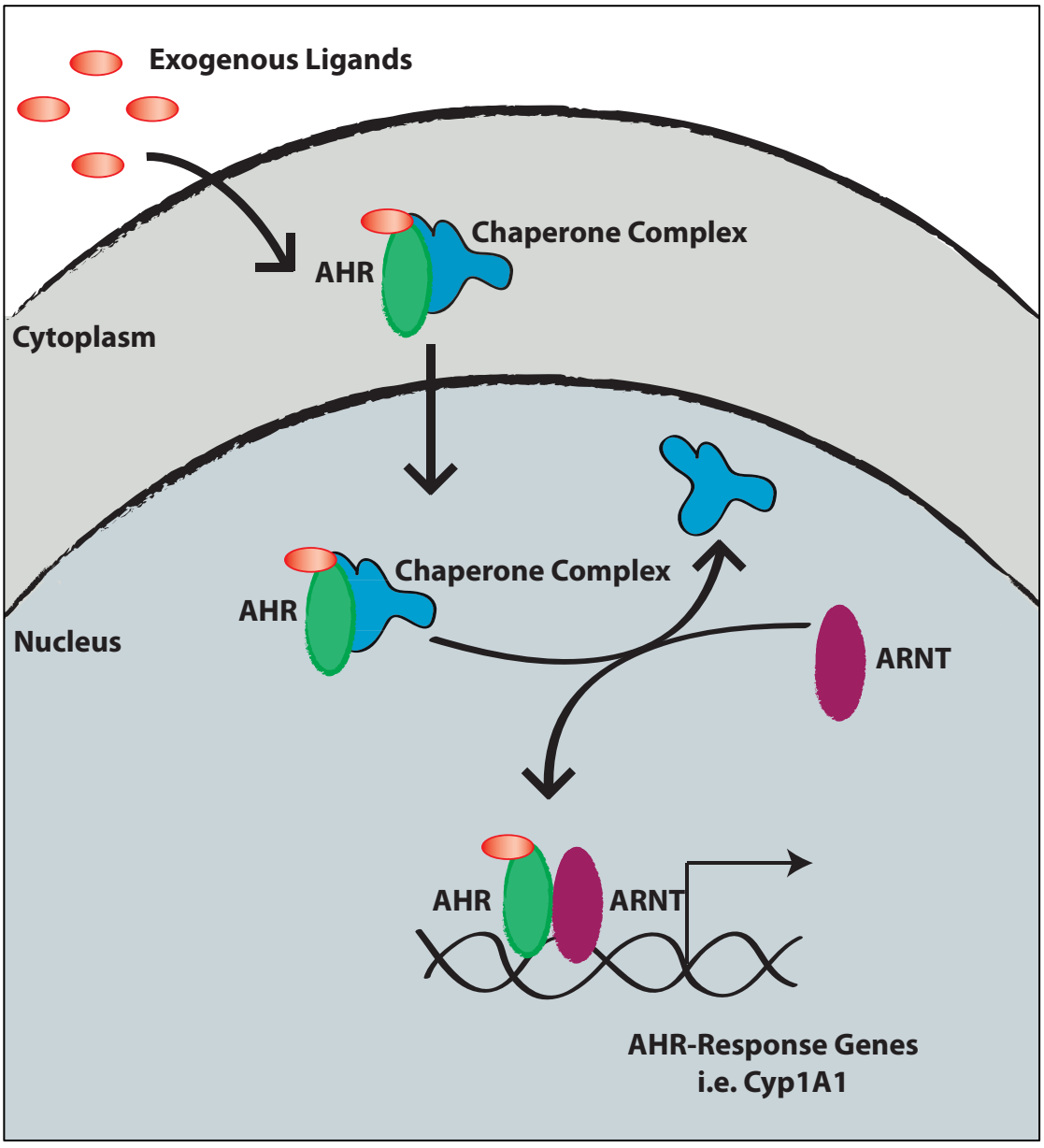
Exogenous Ligands
Chaperone Complex
AHR
Cytoplasm
Chaperone Complex
AHR
Nucleus
ARNT
AHR
ARNT
AHR-Response Genes
i.e. Cyp1A1

DNA and specifically interact with the core nucleotide sequence 5'-TNGCGTG-3' in the 5' flanking region of gene targets (100,101). Referred to as the AHR-responsive element (AHRE), this consensus sequence is found near AHR-regulated genes. Some of the most well characterized AHR response genes include metabolic enzymes such as CYP1A1, CYP1A2, CYP1B1, NAD(P)H:quinone oxidoreductase (NQO1), aldehyde dehydrogenase (ALDH) 3A1, UDP-glucuronosyltransferase (UGT) 1A1, and glutathione-S-transferase (GST) A1 (102). These enzymes catalyze critical reactions, such as oxidation, reduction, and hydrolysis, to increase clearance of toxic substrates. In the case of aminoazo dyes, the protective effect of 3-MC against liver cancer is attributed to 3-MC activation of AHR and subsequent metabolism of the dye through these enzymatic reactions.

Negative regulation of AHR

Once activated, AHR signaling is downregulated by multiple mechanisms, suggesting the importance of precise pathway control and prevention of overstimulation. Proteasome-mediated degradation was the first mechanism found to attenuate AHR activity (103-105). This pathway has primarily been studied in cultured cells treated with TCDD. In this system, AHR is ubiquitinated (104) and steadily declines in a time-dependent manner (106). Proteasome inhibitors block receptor turnover (103-105), increase nuclear AHR/ARNT complexes (105), and amplify target gene expression (104). Moreover, proteasome-mediated degradation of AHR depends on transcriptional activation (104) and subsequent nuclear export (103,105), as inhibition of either process blocks turnover.

In addition to degradation by the proteasome, AHR activity is also dampened by a negative feedback loop driven by the aryl hydrocarbon receptor repressor (AHRR). AHRR is a bHLH/PAS family member that is constitutively expressed at very low levels in many tissues (107,108). However, AHRR contains 3 copies of the AHRE in its promoter region, which results in high AHR-mediated induction (109). A portion of AHRR is highly similar to the N-terminal region of AHR (107), and facilitates ARNT interaction and DNA binding. As a result, AHRR is able to form competitive ARNT heterodimers that bind and transcriptionally repress AHR response genes (110). Mechanistically, AHRR is SUMOylated at three specific residues following dimerization (111). Modification of these sites is required for interaction between AHRR and a corepressor complex, containing ankyrin repeat family A protein 2 (ANKRA2), histone deacetylase (HDAC) 4, and HDAC 5 (112). This complex blocks transcription of AHR target genes. The ability of AHRR to negatively regulate AHR signaling helps prevent sustained activation of the pathway.

AHR ligands

Historically, AHR was defined based on its ability to respond to toxic chemicals, including 3-MC and TCDD. Although these compounds are among the most well characterized and high-affinity ligands, AHR is able to bind structurally diverse molecules. This is largely attributed to the promiscuous nature of the AHR ligand binding domain (LBD), which is both necessary and sufficient for ligand-mediated activation.

The LBD of AHR is located within a structural repeat of the PAS domain, called PAS B. Since this region also interacts with Hsp90, deletion of PAS B disrupts cytoplasmic retention of the receptor by its chaperone complex and results in ligand-independent, constitutive AHR activation (113). Conversely, expression of PAS B alone binds TCDD with a comparable affinity to wild type AHR (114). Structural information about the AHR binding pocket is limited, as no X-ray or NMR structures of AHR have been solved. However, homology models of the AHR LBD have been built based on crystal structures of homologous proteins in the PAS family (115,116). These models have further defined residues of the AHR LBD important for binding and revealed a wide range of compound characteristics able to confer activity.

The diverse range of known AHR ligands is broadly classified into two groups: synthetic and naturally occurring (117,118). Synthetic AHR ligands are typified by halogenated aromatic hydrocarbons (HAHs) derived from industrial sources, which include polychlorinated dibenzo-*p*-dioxins, dibenzofurans, and biphenyls, and polycyclic aromatic hydrocarbons (PAHs), including 3-MC and benzo[*a*]pyrene, released by the process of combustion (118). In addition to synthetic ligands, numerous naturally occurring compounds activate AHR (117). These include indigo (119), indirubin (119), dietary flavonoids (120), and metabolites of both arachidonic acid (121) and heme (122). Although these compounds show AHR-specific activity, many are present at very low levels in vertebrate tissues and display varying degrees of receptor activation.

Despite the large number of exogenous activators, no known endogenous ligands of AHR have been identified. While AHR may function only to protect against harmful toxins, it is also possible that AHR has a role in normal physiology and thus, an

endogenous ligand. In fact, the role for AHR in normal developmental processes is argued to predate its role in toxicity. This idea is supported by the presence of AHR homologs in most major groups of animals, including many of the earliest bilateral metazoans that evolved more than 500 million years ago (123). Although the ancestral AHR was a transcriptional activator, it was unable to bind PAHs (124), suggesting AHR originally functioned as a regulatory gene during development. The ability of AHR to bind PAHs did not emerge until jawed vertebrates. In particular, AHR regulation of Cyp1A1 was first evidenced in bony fishes (123), which is thought to be in response to the emergence of natural halogenated products in marine species (125). In addition to phylogenetic evidence, AHR knockout mice also support an important physiological function for AHR. Specifically, AHR-null mice (126,127) display vascular, immune, and skin defects, among others. Together, these studies are consistent with a role for AHR beyond toxicity and support the continued effort to identify an endogenous ligand.

AHR in the mammary gland

Mammary gland development is among the physiological pathways proposed to be regulated by AHR signaling. This idea is supported by expression analysis, which has found key AHR pathway components expressed at different stages of mammary growth and differentiation. AHR, which is present in both the epithelial and stromal compartment, is highly expressed during puberty and into pregnancy and declines dramatically at lactation and involution (128). Similarly, ARNT is expressed throughout the gland and is highest in the virgin and pregnant state (129). ARNT remains highly expressed during lactation and decreases significantly at involution. In addition to AHR

and ARNT proteins, readouts of pathway activation are also seen in the developing gland. Specifically, mammary glands from C57Bl/6 mice show nuclear AHR localization in ~15% of ductal and lobular epithelial cells (128). Moreover, AHR targets, including Cyp1A1 and Cyp1B1, are increased in these animals, as well as in organ explants stimulated with hormone treatment. Together, these studies show the AHR pathway is expressed and activated in the mammary gland.

In addition to expression studies, knockout animals also support a potential role for AHR signaling during mammary development. AHR null animals show a 50% reduction in TEBs (128), which are structures highly active during puberty-associated branching, when AHR is also highly expressed. Moreover, loss of AHR results in severe reproductive phenotypes, as evidenced by difficulty maintaining pregnancies and high mortality of null mothers during pregnancy (130). Of those that survive, less than half of dams are able to support their pups until weaning. In addition to AHR, loss of ARNT impacts mammary development and function. Complete loss of ARNT is lethal, but conditional ARNT inactivation has been performed in the mammary gland. Loss of ARNT at puberty using MMTV-Cre, which is expressed in luminal epithelial cells, impairs subsequent alveolar development and results in more than half of mothers that are unable to nutritionally support their offspring (129). However, transplantation of these glands into normal recipient mice rescues alveolar development and milk production, suggesting the stromal compartment mediates the observed defect in ARNT loss. Furthermore, inactivation of ARNT during pregnancy using WAP-Cre, with is active in luminal epithelial cells during pregnancy, does not appear to decrease mammary function. This approach does not inactivate ARNT until the onset of pregnancy and only

reduces ARNT levels by 80%, leaving residual protein expression. As a result, further *in vivo* analysis is needed to interpret these conflicting results.

While loss of function studies remain unclear about the role of the AHR pathway in the mammary gland, activation of AHR undoubtedly disrupts mammary development and function. Rats exposed to TCDD during gestation (131) or at 4-5 weeks of age (132) display decreased branching and TEB formation during puberty, resulting in immature, small mammary glands. Furthermore, numerous studies show adverse effects of AHR activation during pregnancy. For example, C57Bl/6 mice exposed to TCDD during pregnancy display branching defects, particularly within alveolar structures (133). Consequently, expression of milk proteins is reduced and dams are unable to support their litter. Reciprocal transplant studies with AHR knockout mice suggest TCDD exposure blocks mammary differentiation through multiple mechanisms (134). In these experiments, both wild type mammary epithelial cells (MECs) transplanted into AHR knockout recipients and AHR knockout MECs transplanted into wild type recipients showed mammary defects after TCDD treatment during pregnancy. However, mutant mice that express an AHR protein lacking the DNA binding domain show normal alveolar development in the presence of TCDD. These results suggest AHR:DNA interactions mediate the toxic effects of TCDD and strongly implicate a direct consequence of AHR stimulation on mammary epithelial cells. Despite these studies, the downstream functional targets of activated AHR that affect mammary gland development remain unclear.

Crosstalk between AHR and ER

Beyond its classical signaling axis, AHR converges with several other important physiological pathways. In particular, AHR activation antagonizes the estrogen receptor (ER) (reviewed in (135)), which likely contributes to the reproductive phenotypes observed in TCDD-treated animals. This relationship between AHR and ER has been observed in humans and rodent models through both *in vitro* and *in vivo* approaches. Specifically, TCDD inhibits estrogen-dependent growth of human breast cancer cells (136) and significantly reduces the incidence of mammary and uterine tumors in chronically exposed rats (137). Similar results have also been observed in women from Seveso, Italy who were exposed to TCDD during a 1976 industrial explosion. Compared to control individuals, women who experienced TCDD exposure have a lower incidence of breast cancer (138). These data suggest antagonism of ER signaling by AHR activation reduces ER-dependent breast cancer, although the precise connection between breast cancer subtype specificity and the AHR pathway requires further investigation.

The mechanism of interaction between AHR and ER appears to be multifaceted and may be tissue- or cell-type dependent. AHR complexes have been shown to bind regulatory regions within ER target genes and sterically hinder transcription (139). In addition, AHR and ER compete for similar coactivators (140), which limits the activation capacity of each pathway. Finally, activated AHR increases proteasome-mediated degradation of ER (141) as well as metabolism of circulating estrogens (142). Given the importance of estrogen signaling during mammary gland development, this complex relationship between AHR and ER likely plays a role in TCDD-mediated toxicity.

Perspectives on the AHR pathway

Since Alan Poland's initial discovery, the field of AHR research has rapidly expanded. AHR was originally defined based on its central role mediating toxicity. However, more than 6,000 studies on AHR have been published to date and researchers now appreciate a dual role for AHR in both toxicology and normal physiology.

In terms of toxicity, it is clear that many hazardous chemicals elicit their harmful effects through AHR. Furthermore, the AHR binding pocket is promiscuous in nature and different types of ligands seemingly display different binding requirements. As a result, structure activity relationship (SAR) studies for different classes of agonists are needed to more definitively define mechanisms of AHR activation. We identified 1,2,4-*bis*-aryloxadiazole as a potent AHR agonist and performed a SAR study to determine which moieties of the molecule are critical for AHR activation (Chapter 3). Insight from these studies will not only help detect other harmful chemicals that bind AHR, but will also aid in identifying and validating potential endogenous ligands.

In addition to toxicology, the involvement of AHR in normal biological processes is still a highly active area of investigation. In the mammary gland, exposure to AHR agonists notably disrupts mammary development and function. However, these effects likely stem from both systemic hormone changes and local AHR signaling within the epithelial compartment. To uncouple these effects, we used an epithelial-based model of mammary lactation to recapitulate lactogenesis in the presence of AHR agonists. We found AHR activation directly blocked milk production in mammary epithelial cells, and elucidated a novel role for AHRR in mediating this response (Chapter 4).

References

1. Linnaeus, C. (1758) *Systema Naturae* The 10th edition ed., Holmiae : Impensis Direct. Laurentii Salvii, 1758-1759, Stockholm

2. Vorbach, C., Capecchi, M. R., and Penninger, J. M. (2006) Evolution of the mammary gland from the innate immune system? *Bioessays* **28**, 606-616

3. Capuco, A. V., and Akers, R. M. (2009) The origin and evolution of lactation. *J. Biol.* **8**, 37

4. Blackburn, D. G., Hayssen, V., and Murphy, C. J. (1989) The origins of lactation and the evolution of milk: A review with new hypotheses. *Mammal Rev.* **19**, 1-26

5. Goldman, A. S. (2002) Evolution of the mammary gland defense system and the ontogeny of the immune system. *J. Mammary Gland Biol. Neoplasia* **7**, 277-289

6. Visvader, J. E. (2009) Keeping abreast of the mammary epithelial hierarchy and breast tumorigenesis. *Genes Dev.* **23**, 2563-2577

7. Rios, A. C., Fu, N. Y., Lindeman, G. J., and Visvader, J. E. (2014) In situ identification of bipotent stem cells in the mammary gland. *Nature* **506**, 322-327

8. Neville, M. C., Medina, D., Monks, J., and Hovey, R. C. (1998) The mammary fat pad. *J. Mammary Gland Biol. Neoplasia* **3**, 109-116

9. Sakakura, T., Nishizuka, Y., and Dawe, C. J. (1976) Mesenchyme-dependent morphogenesis and epithelium-specific cytodifferentiation in mouse mammary gland. *Science* **194**, 1439-1441

10. Cunha, G. R., Young, P., Christov, K., Guzman, R., Nandi, S., Talamantes, F., and Thordarson, G. (1995) Mammary phenotypic expression induced in epidermal cells by embryonic mammary mesenchyme. *Acta. Anat.* **152**, 195-204

11. Hens, J. R., and Wysolmerski, J. J. (2005) Key stages of mammary gland development: Molecular mechanisms involved in the formation of the embryonic mammary gland. *Breast Cancer Res.* **7**, 220-224

12. Balinsky, B. I. (1950) On the prenatal growth of the mammary gland rudiment in the mouse. *J. Anat.* **84**, 227-235

13. Propper, A. Y. (1978) Wandering epithelial cells in the rabbit embryo milk line. A preliminary scanning electron microscope study. *Dev. Biol.* **67**, 225-231

14. Howard, B. A., and Gusterson, B. A. (2000) Human breast development. *J. Mammary Gland Biol. Neoplasia* **5**, 119-137

15. Eblaghie, M. C., Song, S. J., Kim, J. Y., Akita, K., Tickle, C., and Jung, H. S. (2004) Interactions between FGF and Wnt signals and Tbx3 gene expression in mammary gland initiation in mouse embryos. *J. Anat.* **205**, 1-13

16. Jerome-Majewska, L. A., Jenkins, G. P., Ernstoff, E., Zindy, F., Sherr, C. J., and Papaioannou, V. E. (2005) Tbx3, the ulnar-mammary syndrome gene, and Tbx2 interact in mammary gland development through a p19Arf/p53-independent pathway. *Dev. Dyn.* **234**, 922-933

17. Mailleux, A. A., Spencer-Dene, B., Dillon, C., Ndiaye, D., Savona-Baron, C., Itoh, N., Kato, S., Dickson, C., Thiery, J. P., and Bellusci, S. (2002) Role of FGF10/FGFR2b signaling during mammary gland development in the mouse embryo. *Development* **129**, 53-60

18. Davenport, T. G., Jerome-Majewska, L. A., and Papaioannou, V. E. (2003) Mammary gland, limb and yolk sac defects in mice lacking Tbx3, the gene mutated in human ulnar mammary syndrome. *Development* **130**, 2263-2273

19. Chu, E. Y., Hens, J., Andl, T., Kairo, A., Yamaguchi, T. P., Brisken, C., Glick, A., Wysolmerski, J. J., and Millar, S. E. (2004) Canonical WNT signaling promotes mammary placode development and is essential for initiation of mammary gland morphogenesis. *Development* **131**, 4819-4829

20. Krege, J. H., Hodgin, J. B., Couse, J. F., Enmark, E., Warner, M., Mahler, J. F., Sar, M., Korach, K. S., Gustafsson, J. A., and Smithies, O. (1998) Generation and reproductive phenotypes of mice lacking estrogen receptor beta. *Proc. Natl. Acad. Sci. U. S. A.* **95**, 15677-15682

21. Lubahn, D. B., Moyer, J. S., Golding, T. S., Couse, J. F., Korach, K. S., and Smithies, O. (1993) Alteration of reproductive function but not prenatal sexual development after insertional disruption of the mouse estrogen receptor gene. *Proc. Natl. Acad. Sci. U. S. A.* **90**, 11162-11166

22. Lydon, J. P., DeMayo, F. J., Conneely, O. M., and O'Malley, B. W. (1996) Reproductive phenotpes of the progesterone receptor null mutant mouse. *J. Steroid Biochem. Mol. Biol.* **56**, 67-77

23. Ormandy, C. J., Camus, A., Barra, J., Damotte, D., Lucas, B., Buteau, H., Edery, M., Brousse, N., Babinet, C., Binart, N., and Kelly, P. A. (1997) Null mutation of the prolactin receptor gene produces multiple reproductive defects in the mouse. *Genes Dev.* **11**, 167-178

24. Juppner, H., Abou-Samra, A. B., Freeman, M., Kong, X. F., Schipani, E., Richards, J., Kolakowski, L. F., Jr., Hock, J., Potts, J. T., Jr., Kronenberg, H. M., and et al. (1991) A G protein-linked receptor for parathyroid hormone and parathyroid hormone-related peptide. *Science* **254**, 1024-1026

25. Wysolmerski, J. J., Philbrick, W. M., Dunbar, M. E., Lanske, B., Kronenberg, H., and Broadus, A. E. (1998) Rescue of the parathyroid hormone-related protein knockout mouse demonstrates that parathyroid hormone-related protein is essential for mammary gland development. *Development* **125**, 1285-1294

26. Sternlicht, M. D. (2006) Key stages in mammary gland development: The cues that regulate ductal branching morphogenesis. *Breast Cancer Res.* **8**, 201

27. Silberstein, G. B., and Daniel, C. W. (1987) Reversible inhibition of mammary gland growth by transforming growth factor-beta. *Science* **237**, 291-293

28. Ingman, W. V., and Robertson, S. A. (2008) Mammary gland development in transforming growth factor beta1 null mutant mice: Systemic and epithelial effects. *Biol. Reprod.* **79**, 711-717

29. Seagroves, T. N., Krnacik, S., Raught, B., Gay, J., Burgess-Beusse, B., Darlington, G. J., and Rosen, J. M. (1998) C/EBPbeta, but not C/EBPalpha, is essential for ductal morphogenesis, lobuloalveolar proliferation, and functional differentiation in the mouse mammary gland. *Genes Dev.* **12**, 1917-1928

30. Radisky, D. C., Hirai, Y., and Bissell, M. J. (2003) Delivering the message: Epimorphin and mammary epithelial morphogenesis. *Trends Cell Biol.* **13**, 426-434

31. Simian, M., Hirai, Y., Navre, M., Werb, Z., Lochter, A., and Bissell, M. J. (2001) The interplay of matrix metalloproteinases, morphogens and growth factors is necessary for branching of mammary epithelial cells. *Development* **128**, 3117-3131

32. Macias, H., and Hinck, L. (2012) Mammary gland development. *Wiley Interdiscip. Rev. Dev. Biol.* **1**, 533-557

33. Daniel, C. W., Silberstein, G. B., and Strickland, P. (1987) Direct action of 17 beta-estradiol on mouse mammary ducts analyzed by sustained release implants and steroid autoradiography. *Cancer Res.* **47**, 6052-6057

34. Korach, K. S., Couse, J. F., Curtis, S. W., Washburn, T. F., Lindzey, J., Kimbro, K. S., Eddy, E. M., Migliaccio, S., Snedeker, S. M., Lubahn, D. B., Schomberg, D. W., and Smith, E. P. (1996) Estrogen receptor gene disruption: Molecular characterization and experimental and clinical phenotypes. *Recent Prog. Horm. Res.* **51**, 159-186; discussion 186-158

35. Fisher, C. R., Graves, K. H., Parlow, A. F., and Simpson, E. R. (1998) Characterization of mice deficient in aromatase (ArKO) because of targeted disruption of the cyp19 gene. *Proc. Natl. Acad. Sci. U. S. A.* **95**, 6965-6970

36. Gallego, M. I., Binart, N., Robinson, G. W., Okagaki, R., Coschigano, K. T., Perry, J., Kopchick, J. J., Oka, T., Kelly, P. A., and Hennighausen, L. (2001) Prolactin, growth hormone, and epidermal growth factor activate Stat5 in different compartments of mammary tissue and exert different and overlapping developmental effects. *Dev. Biol.* **229**, 163-175

37. Kleinberg, D. L., Feldman, M., and Ruan, W. (2000) IGF-I: An essential factor in terminal end bud formation and ductal morphogenesis. *J. Mammary Gland Biol. Neoplasia* **5**, 7-17

38. Cunha, G. R., Young, P., Hom, Y. K., Cooke, P. S., Taylor, J. A., and Lubahn, D. B. (1997) Elucidation of a role for stromal steroid hormone receptors in mammary gland growth and development using tissue recombinants. *J. Mammary Gland Biol. Neoplasia* **2**, 393-402

39. Coleman, S., Silberstein, G. B., and Daniel, C. W. (1988) Ductal morphogenesis in the mouse mammary gland: Evidence supporting a role for epidermal growth factor. *Dev. Biol.* **127**, 304-315

40. Kenney, N. J., Bowman, A., Korach, K. S., Barrett, J. C., and Salomon, D. S. (2003) Effect of exogenous epidermal-like growth factors on mammary gland development and differentiation in the estrogen receptor-alpha knockout (ERKO) mouse. *Breast Cancer Res. Treat.* **79**, 161-173

41. Sternlicht, M. D., Sunnarborg, S. W., Kouros-Mehr, H., Yu, Y., Lee, D. C., and Werb, Z. (2005) Mammary ductal morphogenesis requires paracrine activation of stromal EGFR via ADAM17-dependent shedding of epithelial amphiregulin. *Development* **132**, 3923-3933

42. Wiesen, J. F., Young, P., Werb, Z., and Cunha, G. R. (1999) Signaling through the stromal epidermal growth factor receptor is necessary for mammary ductal development. *Development* **126**, 335-344

43. Chakravorti, S., and Sheffield, L. (1996) Acidic and basic fibroblast growth factor mRNA and protein in mouse mammary glands. *Endocrine* **4**, 175-182

44. Lu, P., Ewald, A. J., Martin, G. R., and Werb, Z. (2008) Genetic mosaic analysis reveals FGF receptor 2 function in terminal end buds during mammary gland branching morphogenesis. *Dev. Biol.* **321**, 77-87

45. Brisken, C., Park, S., Vass, T., Lydon, J. P., O'Malley, B. W., and Weinberg, R. A. (1998) A paracrine role for the epithelial progesterone receptor in mammary gland development. *Proc. Natl. Acad. Sci. U. S. A.* **95**, 5076-5081

46. Horseman, N. D., Zhao, W., Montecino-Rodriguez, E., Tanaka, M., Nakashima, K., Engle, S. J., Smith, F., Markoff, E., and Dorshkind, K. (1997) Defective mammopoiesis, but normal hematopoiesis, in mice with a targeted disruption of the prolactin gene. *EMBO J.* **16**, 6926-6935

47. Brisken, C., Kaur, S., Chavarria, T. E., Binart, N., Sutherland, R. L., Weinberg, R. A., Kelly, P. A., and Ormandy, C. J. (1999) Prolactin controls mammary gland development via direct and indirect mechanisms. *Dev. Biol.* **210**, 96-106

48. Vomachka, A. J., Pratt, S. L., Lockefeer, J. A., and Horseman, N. D. (2000) Prolactin gene-disruption arrests mammary gland development and retards T-antigen-induced tumor growth. *Oncogene* **19**, 1077-1084

49. Brisken, C., Heineman, A., Chavarria, T., Elenbaas, B., Tan, J., Dey, S. K., McMahon, J. A., McMahon, A. P., and Weinberg, R. A. (2000) Essential function of Wnt-4 in mammary gland development downstream of progesterone signaling. *Genes Dev.* **14**, 650-654

50. Ormandy, C. J., Naylor, M., Harris, J., Robertson, F., Horseman, N. D., Lindeman, G. J., Visvader, J., and Kelly, P. A. (2003) Investigation of the transcriptional changes underlying functional defects in the mammary glands of prolactin receptor knockout mice. *Recent Prog. Horm. Res.* **58**, 297-323

51. Fernandez-Valdivia, R., Mukherjee, A., Creighton, C. J., Buser, A. C., DeMayo, F. J., Edwards, D. P., and Lydon, J. P. (2008) Transcriptional response of the murine mammary gland to acute progesterone exposure. *Endocrinology* **149**, 6236-6250

52. Mulac-Jericevic, B., Lydon, J. P., DeMayo, F. J., and Conneely, O. M. (2003) Defective mammary gland morphogenesis in mice lacking the progesterone receptor B isoform. *Proc. Natl. Acad. Sci. U. S. A.* **100**, 9744-9749

53. Fata, J. E., Kong, Y. Y., Li, J., Sasaki, T., Irie-Sasaki, J., Moorehead, R. A., Elliott, R., Scully, S., Voura, E. B., Lacey, D. L., Boyle, W. J., Khokha, R., and Penninger, J. M. (2000) The osteoclast differentiation factor osteoprotegerin-ligand is essential for mammary gland development. *Cell* **103**, 41-50

54. Mukherjee, A., Soyal, S. M., Li, J., Ying, Y., He, B., DeMayo, F. J., and Lydon, J. P. (2010) Targeting RANKL to a specific subset of murine mammary epithelial cells induces ordered branching morphogenesis and alveologenesis in the absence of progesterone receptor expression. *FASEB J.* **24**, 4408-4419

55. Furth, P. A., Nakles, R. E., Millman, S., Diaz-Cruz, E. S., and Cabrera, M. C. (2011) Signal transducer and activator of transcription 5 as a key signaling pathway in normal mammary gland developmental biology and breast cancer. *Breast Cancer Res.* **13**, 220

56. Lund, L. R., Romer, J., Thomasset, N., Solberg, H., Pyke, C., Bissell, M. J., Dano, K., and Werb, Z. (1996) Two distinct phases of apoptosis in mammary gland involution: Proteinase-independent and -dependent pathways. *Development* **122**, 181-193

57. Marti, A., Feng, Z., Altermatt, H. J., and Jaggi, R. (1997) Milk accumulation triggers apoptosis of mammary epithelial cells. *Eur. J. Cell Biol.* **73**, 158-165

58. Li, M., Liu, X., Robinson, G., Bar-Peled, U., Wagner, K. U., Young, W. S., Hennighausen, L., and Furth, P. A. (1997) Mammary-derived signals activate programmed cell death during the first stage of mammary gland involution. *Proc. Natl. Acad. Sci. U. S. A.* **94**, 3425-3430

59. Clarkson, R. W., Boland, M. P., Kritikou, E. A., Lee, J. M., Freeman, T. C., Tiffen, P. G., and Watson, C. J. (2006) The genes induced by signal transducer and activators of transcription (STAT)3 and STAT5 in mammary epithelial cells define the roles of these STATs in mammary development. *Mol. Endocrinol.* **20**, 675-685

60. Chapman, R. S., Lourenco, P. C., Tonner, E., Flint, D. J., Selbert, S., Takeda, K., Akira, S., Clarke, A. R., and Watson, C. J. (1999) Suppression of epithelial apoptosis and delayed mammary gland involution in mice with a conditional knockout of Stat3. *Genes Dev.* **13**, 2604-2616

61. Watson, C. J. (2006) Involution: Apoptosis and tissue remodelling that convert the mammary gland from milk factory to a quiescent organ. *Breast Cancer Res.* **8**, 203

62. Zettl, K. S., Sjaastad, M. D., Riskin, P. M., Parry, G., Machen, T. E., and Firestone, G. L. (1992) Glucocorticoid-induced formation of tight junctions in mouse mammary epithelial cells in vitro. *Proc. Natl. Acad. Sci. U. S. A.* **89**, 9069-9073

63. Feng, Z., Marti, A., Jehn, B., Altermatt, H. J., Chicaiza, G., and Jaggi, R. (1995) Glucocorticoid and progesterone inhibit involution and programmed cell death in the mouse mammary gland. *J. Cell Biol.* **131**, 1095-1103

64. Green, K. A., and Lund, L. R. (2005) ECM degrading proteases and tissue remodelling in the mammary gland. *Bioessays* **27**, 894-903

65. Smith, B. A., Welm, A. L., and Welm, B. E. (2012) On the shoulders of giants: A historical perspective of unique experimental methods in mammary gland research. *Semin. Cell Dev. Biol.* **23**, 583-590

66. Nelson, C. M., and Bissell, M. J. (2005) Modeling dynamic reciprocity: Engineering three-dimensional culture models of breast architecture, function, and neoplastic transformation. *Semin. Cancer Biol.* **15**, 342-352

67. Schmeichel, K. L., and Bissell, M. J. (2003) Modeling tissue-specific signaling and organ function in three dimensions. *J. Cell Sci.* **116**, 2377-2388

68. Emerman, J. T., and Pitelka, D. R. (1977) Maintenance and induction of morphological differentiation in dissociated mammary epithelium on floating collagen membranes. *In Vitro* **13**, 316-328

69. Emerman, J. T., Enami, J., Pitelka, D. R., and Nandi, S. (1977) Hormonal effects on intracellular and secreted casein in cultures of mouse mammary epithelial cells on floating collagen membranes. *Proc. Natl. Acad. Sci. U. S. A.* **74**, 4466-4470

70. Lee, E. Y., Parry, G., and Bissell, M. J. (1984) Modulation of secreted proteins of mouse mammary epithelial cells by the collagenous substrata. *J. Cell Biol.* **98**, 146-155

71. Weigelt, B., and Bissell, M. J. (2008) Unraveling the microenvironmental influences on the normal mammary gland and breast cancer. *Semin. Cancer Biol.* **18**, 311-321

72. Timpl, R. (1989) Structure and biological activity of basement membrane proteins. *Eur. J. Biochem.* **180**, 487-502

73. Kleinman, H. K., McGarvey, M. L., Hassell, J. R., Star, V. L., Cannon, F. B., Laurie, G. W., and Martin, G. R. (1986) Basement membrane complexes with biological activity. *Biochemistry* **25**, 312-318

74. Barcellos-Hoff, M. H., Aggeler, J., Ram, T. G., and Bissell, M. J. (1989) Functional differentiation and alveolar morphogenesis of primary mammary cultures on reconstituted basement membrane. *Development* **105**, 223-235

75. Petersen, O. W., Ronnov-Jessen, L., Howlett, A. R., and Bissell, M. J. (1992) Interaction with basement membrane serves to rapidly distinguish growth and differentiation pattern of normal and malignant human breast epithelial cells. *Proc. Natl. Acad. Sci. U. S. A.* **89**, 9064-9068

76. Debnath, J., Muthuswamy, S. K., and Brugge, J. S. (2003) Morphogenesis and oncogenesis of MCF-10A mammary epithelial acini grown in three-dimensional basement membrane cultures. *Methods* **30**, 256-268

77. Gudjonsson, T., Ronnov-Jessen, L., Villadsen, R., Rank, F., Bissell, M. J., and Petersen, O. W. (2002) Normal and tumor-derived myoepithelial cells differ in their ability to interact with luminal breast epithelial cells for polarity and basement membrane deposition. *J. Cell Sci.* **115**, 39-50

78. Poland, A., Glover, E., and Kende, A. S. (1976) Stereospecific, high affinity binding of 2,3,7,8-tetrachlorodibenzo-p-dioxin by hepatic cytosol. Evidence that the binding species is receptor for induction of aryl hydrocarbon hydroxylase. *J. Biol. Chem.* **251**, 4936-4946

79. Kirby, A. H. (1945) Studies in carcinogenesis with azo compounds; the action of azo compounds in mice, and the bearing thereof on theories of azo dye carcinogenesis. *Cancer Res.* **5**, 683-696

80. Richardson, H. L., Stier, A. R., and Borsos-Nachtnebel, E. (1952) Liver tumor inhibition and adrenal histologic responses in rats to which 3'-methyl-4-dimethylaminoazobenzene and 20-methylcholanthrene were simultaneously administered. *Cancer Res.* **12**, 356-361

81. Conney, A. H., Miller, E. C., and Miller, J. A. (1957) Substrate-induced synthesis and other properties of benzpyrene hydroxylase in rat liver. *J. Biol. Chem.* **228**, 753-766

82. Conney, A. H., Gillette, J. R., Inscoe, J. K., Trams, E. R., and Posner, H. S. (1959) Induced synthesis of liver microsomal enzymes which metabolize foreign compounds. *Science* **130**, 1478-1479

83. Nebert, D. W., and Bausserman, L. L. (1970) Genetic differences in the extent of aryl hydrocarbon hydroxylase induction in mouse fetal cell cultures. *J. Biol. Chem.* **245**, 6373-6382

84. Nebert, D. W., and Gelboin, H. V. (1969) The in vivo and in vitro induction of aryl hydrocarbon hydroxylase in mammalian cells of different species, tissues, strains, and developmental and hormonal states. *Arch. Biochem. Biophys.* **134**, 76-89

85. Nebert, D. W., and Gielen, J. E. (1972) Genetic regulation of aryl hydrocarbon hydroxylase induction in the mouse. *Fed. Proc.* **31**, 1315-1325

86. Gielen, J. E., Goujon, F. M., and Nebert, D. W. (1972) Genetic regulation of aryl hydrocarbon hydroxylase induction. II. Simple Mendelian expression in mouse tissues in vivo. *J. Biol. Chem.* **247**, 1125-1137

87. Nebert, D. W., Goujon, F. M., and Gielen, J. E. (1972) Aryl hydrocarbon hydroxylase induction by polycyclic hydrocarbons: Simple autosomal dominant trait in the mouse. *Nat. New. Biol.* **236**, 107-110

88. Nebert, D. W., Negishi, M., Lang, M. A., Hjelmeland, L. M., and Eisen, H. J. (1982) The Ah locus, a multigene family necessary for survival in a chemically adverse environment: Comparison with the immune system. *Adv. Genet.* **21**, 1-52

89. Poland, A., and Glover, E. (1974) Comparison of 2,3,7,8-tetrachlorodibenzo-p-dioxin, a potent inducer of aryl hydrocarbon hydroxylase, with 3-methylcholanthrene. *Mol. Pharmacol.* **10**, 349-359

90. Poland, A., Palen, D., and Glover, E. (1994) Analysis of the four alleles of the murine aryl hydrocarbon receptor. *Mol. Pharmacol.* **46**, 915-921

91. Ema, M., Ohe, N., Suzuki, M., Mimura, J., Sogawa, K., Ikawa, S., and Fujii-Kuriyama, Y. (1994) Dioxin binding activities of polymorphic forms of mouse and human arylhydrocarbon receptors. *J. Biol. Chem.* **269**, 27337-27343

92. Burbach, K. M., Poland, A., and Bradfield, C. A. (1992) Cloning of the Ah-receptor cDNA reveals a distinctive ligand-activated transcription factor. *Proc. Nat. Acad. Sci. U. S. A.* **89**, 8185-8189

93. Ema, M., Sogawa, K., Watanabe, N., Chujoh, Y., Matsushita, N., Gotoh, O., Funae, Y., and Fujii-Kuriyama, Y. (1992) cDNA cloning and structure of mouse putative Ah receptor. *Biochem. Biophys. Res. Commun.* **184**, 246-253

94. Petrulis, J. R., and Perdew, G. H. (2002) The role of chaperone proteins in the aryl hydrocarbon receptor core complex. *Chem. Biol. Interact.* **141**, 25-40

95. Antonsson, C., Whitelaw, M. L., McGuire, J., Gustafsson, J. A., and Poellinger, L. (1995) Distinct roles of the molecular chaperone hsp90 in modulating dioxin receptor function via the basic helix-loop-helix and PAS domains. *Mol. Cell. Biol.* **15**, 756-765

96. Kazlauskas, A., Poellinger, L., and Pongratz, I. (1999) Evidence that the co-chaperone p23 regulates ligand responsiveness of the dioxin (Aryl hydrocarbon) receptor. *J. Biol. Chem.* **274**, 13519-13524

97. Meyer, B. K., and Perdew, G. H. (1999) Characterization of the AhR-hsp90-XAP2 core complex and the role of the immunophilin-related protein XAP2 in AhR stabilization. *Biochemistry* **38**, 8907-8917

98. Petrulis, J. R., Hord, N. G., and Perdew, G. H. (2000) Subcellular localization of the aryl hydrocarbon receptor is modulated by the immunophilin homolog hepatitis B virus X-associated protein 2. *J. Biol. Chem.* **275**, 37448-37453

99. Reyes, H., Reisz-Porszasz, S., and Hankinson, O. (1992) Identification of the Ah receptor nuclear translocator protein (Arnt) as a component of the DNA binding form of the Ah receptor. *Science* **256**, 1193-1195

100. Shen, E. S., and Whitlock, J. P., Jr. (1992) Protein-DNA interactions at a dioxin-responsive enhancer. Mutational analysis of the DNA-binding site for the liganded Ah receptor. *J. Biol. Chem.* **267**, 6815-6819

101. Yao, E. F., and Denison, M. S. (1992) DNA sequence determinants for binding of transformed Ah receptor to a dioxin-responsive enhancer. *Biochemistry* **31**, 5060-5067

102. Tijet, N., Boutros, P. C., Moffat, I. D., Okey, A. B., Tuomisto, J., and Pohjanvirta, R. (2006) Aryl hydrocarbon receptor regulates distinct dioxin-dependent and dioxin-independent gene batteries. *Mol. Pharmacol.* **69**, 140-153

103. Roberts, B. J., and Whitelaw, M. L. (1999) Degradation of the basic helix-loop-helix/Per-ARNT-Sim homology domain dioxin receptor via the ubiquitin/proteasome pathway. *J. Biol. Chem.* **274**, 36351-36356

104. Ma, Q., and Baldwin, K. T. (2000) 2,3,7,8-tetrachlorodibenzo-p-dioxin-induced degradation of aryl hydrocarbon receptor (AhR) by the ubiquitin-proteasome pathway. Role of the transcription activaton and DNA binding of AhR. *J. Biol. Chem.* **275**, 8432-8438

105. Davarinos, N. A., and Pollenz, R. S. (1999) Aryl hydrocarbon receptor imported into the nucleus following ligand binding is rapidly degraded via the cytosplasmic proteasome following nuclear export. *J. Biol. Chem.* **274**, 28708-28715

106. Pollenz, R. S. (1996) The aryl-hydrocarbon receptor, but not the aryl-hydrocarbon receptor nuclear translocator protein, is rapidly depleted in hepatic and nonhepatic culture cells exposed to 2,3,7,8-tetrachlorodibenzo-p-dioxin. *Mol. Pharmacol.* **49**, 391-398

107. Mimura, J., Ema, M., Sogawa, K., and Fujii-Kuriyama, Y. (1999) Identification of a novel mechanism of regulation of Ah (dioxin) receptor function. *Genes Dev.* **13**, 20-25

108. Bernshausen, T., Jux, B., Esser, C., Abel, J., and Fritsche, E. (2006) Tissue distribution and function of the Aryl hydrocarbon receptor repressor (AhRR) in C57BL/6 and Aryl hydrocarbon receptor deficient mice. *Arch. Toxicol.* **80**, 206-211

109. Baba, T., Mimura, J., Gradin, K., Kuroiwa, A., Watanabe, T., Matsuda, Y., Inazawa, J., Sogawa, K., and Fujii-Kuriyama, Y. (2001) Structure and expression of the Ah receptor repressor gene. *J. Biol. Chem.* **276**, 33101-33110

110. Evans, B. R., Karchner, S. I., Allan, L. L., Pollenz, R. S., Tanguay, R. L., Jenny, M. J., Sherr, D. H., and Hahn, M. E. (2008) Repression of aryl hydrocarbon receptor (AHR) signaling by AHR repressor: Role of DNA binding and competition for AHR nuclear translocator. *Mol. Pharmacol.* **73**, 387-398

111. Oshima, M., Mimura, J., Sekine, H., Okawa, H., and Fujii-Kuriyama, Y. (2009) SUMO modification regulates the transcriptional repressor function of aryl hydrocarbon receptor repressor. *J. Biol. Chem.* **284**, 11017-11026

112. Oshima, M., Mimura, J., Yamamoto, M., and Fujii-Kuriyama, Y. (2007) Molecular mechanism of transcriptional repression of AhR repressor involving ANKRA2, HDAC4, and HDAC5. *Biochem. Biophys. Res. Commun.* **364**, 276-282

113. McGuire, J., Okamoto, K., Whitelaw, M. L., Tanaka, H., and Poellinger, L. (2001) Definition of a dioxin receptor mutant that is a constitutive activator of transcription: Delineation of overlapping repression and ligand binding functions within the PAS domain. *J. Biol. Chem.* **276**, 41841-41849

114. Coumailleau, P., Poellinger, L., Gustafsson, J. A., and Whitelaw, M. L. (1995) Definition of a minimal domain of the dioxin receptor that is associated with Hsp90 and maintains wild type ligand binding affinity and specificity. *J. Biol. Chem.* **270**, 25291-25300

115. Procopio, M., Lahm, A., Tramontano, A., Bonati, L., and Pitea, D. (2002) A model for recognition of polychlorinated dibenzo-p-dioxins by the aryl hydrocarbon receptor. *Eur. J. Biochem.* **269**, 13-18

116. Pandini, A., Denison, M. S., Song, Y., Soshilov, A. A., and Bonati, L. (2007) Structural and functional characterization of the aryl hydrocarbon receptor ligand binding domain by homology modeling and mutational analysis. *Biochemistry* **46**, 696-708

117. Nguyen, L. P., and Bradfield, C. A. (2008) The search for endogenous activators of the aryl hydrocarbon receptor. *Chem. Res. Toxicol.* **21**, 102-116

118. Denison, M. S., and Nagy, S. R. (2003) Activation of the aryl hydrocarbon receptor by structurally diverse exogenous and endogenous chemicals. *Annu. Rev. Pharmacol. Toxicol.* **43**, 309-334

119. Adachi, J., Mori, Y., Matsui, S., Takigami, H., Fujino, J., Kitagawa, H., Miller, C. A., 3rd, Kato, T., Saeki, K., and Matsuda, T. (2001) Indirubin and indigo are potent aryl hydrocarbon receptor ligands present in human urine. *J. Biol. Chem.* **276**, 31475-31478

120. Zhang, S., Qin, C., and Safe, S. H. (2003) Flavonoids as aryl hydrocarbon receptor agonists/antagonists: Effects of structure and cell context. *Environ. Health Perspect.* **111**, 1877-1882

121. Kroetz, D. L., and Zeldin, D. C. (2002) Cytochrome P450 pathways of arachidonic acid metabolism. *Curr. Opin. Lipidol.* **13**, 273-283

122. Phelan, D., Winter, G. M., Rogers, W. J., Lam, J. C., and Denison, M. S. (1998) Activation of the Ah receptor signal transduction pathway by bilirubin and biliverdin. *Arch. Biochem. Biophys.* **357**, 155-163

123. Hahn, M. E. (2002) Aryl hydrocarbon receptors: Diversity and evolution. *Chem. Biol. Interact.* **141**, 131-160

124. Butler, R. A., Kelley, M. L., Powell, W. H., Hahn, M. E., and Van Beneden, R. J. (2001) An aryl hydrocarbon receptor (AHR) homologue from the soft-shell clam, Mya arenaria: Evidence that invertebrate AHR homologues lack 2,3,7,8-tetrachlorodibenzo-p-dioxin and beta-naphthoflavone binding. *Gene* **278**, 223-234

125. Hahn, M. E. (1998) The aryl hydrocarbon receptor: A comparative perspective. *Comp. Biochem. Physiol. C. Pharmacol. Toxicol. Endocrinol.* **121**, 23-53

126. Schmidt, J. V., Su, G. H., Reddy, J. K., Simon, M. C., and Bradfield, C. A. (1996) Characterization of a murine Ahr null allele: Involvement of the Ah receptor in hepatic growth and development. *Proc. Natl. Acad. Sci. U. S. A.* **93**, 6731-6736

127. Fernandez-Salguero, P., Pineau, T., Hilbert, D. M., McPhail, T., Lee, S. S., Kimura, S., Nebert, D. W., Rudikoff, S., Ward, J. M., and Gonzalez, F. J. (1995) Immune system impairment and hepatic fibrosis in mice lacking the dioxin-binding Ah receptor. *Science* **268**, 722-726

128. Hushka, L. J., Williams, J. S., and Greenlee, W. F. (1998) Characterization of 2,3,7,8-tetrachlorodibenzofuran-dependent suppression and AH receptor pathway gene expression in the developing mouse mammary gland. *Toxicol. Appl. Pharmacol.* **152**, 200-210

129. Le Provost, F., Riedlinger, G., Hee Yim, S., Benedict, J., Gonzalez, F. J., Flaws, J., and Hennighausen, L. (2002) The aryl hydrocarbon receptor (AhR) and its nuclear translocator (Arnt) are dispensable for normal mammary gland development but are required for fertility. *Genesis* **32**, 231-239

130. Abbott, B. D., Schmid, J. E., Pitt, J. A., Buckalew, A. R., Wood, C. R., Held, G. A., and Diliberto, J. J. (1999) Adverse reproductive outcomes in the transgenic Ah receptor-deficient mouse. *Toxicol. Appl. Pharmacol.* **155**, 62-70

131. Fenton, S. E., Hamm, J. T., Birnbaum, L. S., and Youngblood, G. L. (2002) Persistent abnormalities in the rat mammary gland following gestational and lactational exposure to 2,3,7,8-tetrachlorodibenzo-p-dioxin (TCDD). *Toxicol. Sci.* **67**, 63-74

132. Brown, N. M., and Lamartiniere, C. A. (1995) Xenoestrogens alter mammary gland differentiation and cell proliferation in the rat. *Environ. Health Perspect.* **103**, 708-713

133. Vorderstrasse, B. A., Fenton, S. E., Bohn, A. A., Cundiff, J. A., and Lawrence, B. P. (2004) A novel effect of dioxin: Exposure during pregnancy severely impairs mammary gland differentiation. *Toxicol. Sci.* **78**, 248-257

134. Lew, B. J., Manickam, R., and Lawrence, B. P. (2011) Activation of the aryl hydrocarbon receptor during pregnancy in the mouse alters mammary development through direct effects on stromal and epithelial tissues. *Biol. Reprod.* **84**, 1094-1102

135. Safe, S., and Wormke, M. (2003) Inhibitory aryl hydrocarbon receptor-estrogen receptor alpha cross-talk and mechanisms of action. *Chem. Res. Toxicol.* **16**, 807-816

136. Safe, S., Wormke, M., and Samudio, I. (2000) Mechanisms of inhibitory aryl hydrocarbon receptor-estrogen receptor crosstalk in human breast cancer cells. *J. Mammary Gland Biol. Neoplasia* **5**, 295-306

137. Kociba, R. J., Keyes, D. G., Beyer, J. E., Carreon, R. M., Wade, C. E., Dittenber, D. A., Kalnins, R. P., Frauson, L. E., Park, C. N., Barnard, S. D., Hummel, R. A., and Humiston, C. G. (1978) Results of a two-year chronic toxicity and oncogenicity study of 2,3,7,8-tetrachlorodibenzo-p-dioxin in rats. *Toxicol. Appl. Pharmacol.* **46**, 279-303

138. Bertazzi, P. A., Consonni, D., Bachetti, S., Rubagotti, M., Baccarelli, A., Zocchetti, C., and Pesatori, A. C. (2001) Health effects of dioxin exposure: A 20-year mortality study. *Am. J. Epidemiol.* **153**, 1031-1044

139. Klinge, C. M., Bowers, J. L., Kulakosky, P. C., Kamboj, K. K., and Swanson, H. I. (1999) The aryl hydrocarbon receptor (AHR)/AHR nuclear translocator (ARNT) heterodimer interacts with naturally occurring estrogen response elements. *Mol. Cell. Endocrinol.* **157**, 105-119

140. Brunnberg, S., Pettersson, K., Rydin, E., Matthews, J., Hanberg, A., and Pongratz, I. (2003) The basic helix-loop-helix-PAS protein ARNT functions as a potent coactivator of estrogen receptor-dependent transcription. *Proc. Natl. Acad. Sci. U. S. A.* **100**, 6517-6522

141. Wormke, M., Stoner, M., Saville, B., Walker, K., Abdelrahim, M., Burghardt, R., and Safe, S. (2003) The aryl hydrocarbon receptor mediates degradation of estrogen receptor alpha through activation of proteasomes. *Mol. Cell. Biol.* **23**, 1843-1855

142. Takemoto, K., Nakajima, M., Fujiki, Y., Katoh, M., Gonzalez, F. J., and Yokoi, T. (2004) Role of the aryl hydrocarbon receptor and Cyp1b1 in the antiestrogenic activity of 2,3,7,8-tetrachlorodibenzo-p-dioxin. *Arch. Toxicol.* **78**, 309-315

CHAPTER 2

CHEMICAL GENETIC SCREEN REVEALS A ROLE FOR DESMOSOMAL ADHESION IN MAMMARY BRANCHING MORPHOGENESIS

This research was originally published in The Journal of Biological Chemistry. Kaitlin J. Basham, Collin Kieffer, Dawne N. Shelton, Christopher J. Leonard, Vasudev R. Bhonde, Hariprasad Vankayalapati, Brett Milash, David J. Bearss, Ryan E. Looper, and Bryan E. Welm. Chemical genetic screen reveals a role for desmosomal adhesion in mammary branching morphogenesis. *The Journal of Biological Chemistry*. 2013*;* 288: 2261-2270.

Supplemental Material can be found at:
http://www.jbc.org/content/suppl/2012/12/03/M112.411033.DC1.html

⌘ *Author's Choice*

THE JOURNAL OF BIOLOGICAL CHEMISTRY VOL. 288, NO. 4, pp. 2261–2270, January 25, 2013

Chemical Genetic Screen Reveals a Role for Desmosomal Adhesion in Mammary Branching Morphogenesis*[S]

Received for publication, August 16, 2012, and in revised form, November 15, 2012 Published, JBC Papers in Press, December 3, 2012, DOI 10.1074/jbc.M112.411033

Kaitlin J. Basham[‡1], Collin Kieffer[‡1,2], Dawne N. Shelton[‡], Christopher J. Leonard[‡], Vasudev R. Bhonde[§], Hariprasad Vankayalapati[¶], Brett Milash[‖], David J. Bearss[¶], Ryan E. Looper[§], and Bryan E. Welm[‡3]**

*From the [‡]Department of Oncological Sciences, Huntsman Cancer Institute, the [§]Department of Chemistry, the [¶]Center for Investigational Therapeutics, Huntsman Cancer Institute, the [‖]Microarray and Genomic Analysis Core Facility, Huntsman Cancer Institute, and the **Department of Surgery, University of Utah, Salt Lake City, Utah 84112*

Background: Mammary gland branching morphogenesis is a highly regulated developmental process often disrupted in breast cancer.
Results: A chemical genetic screen in primary three-dimensional culture revealed that activation of the aryl hydrocarbon receptor promotes desmosomes to block branching.
Conclusion: Down-regulation of desmosomes is required for proper mammary branching morphogenesis.
Significance: Desmosomes are a novel mechanism through which exposure to environmental pollutants may affect mammary development.

During the process of branching morphogenesis, the mammary gland undergoes distinct phases of remodeling to form an elaborate ductal network that ultimately produces and delivers milk to newborn animals. These developmental events rely on tight regulation of critical cellular pathways, many of which are probably disrupted during initiation and progression of breast cancer. Transgenic mouse and *in vitro* organoid models previously identified growth factor signaling as a key regulator of mammary branching, but the functional downstream targets of these pathways remain unclear. Here, we used purified primary mammary epithelial cells stimulated with fibroblast growth factor-2 (FGF2) to model mammary branching morphogenesis *in vitro*. We employed a forward chemical genetic approach to identify modulators of this process and describe a potent compound, 1023, that blocks FGF2-induced branching. In primary mammary epithelial cells, we used lentivirus-mediated knockdown of the aryl hydrocarbon receptor (AHR) to demonstrate that 1023 acts through AHR to block branching. Using 1023 as a tool, we identified desmosomal adhesion as a novel target of AHR signaling and show that desmosomes are critical for AHR agonists to block branching. Our findings support a functional role for desmosomes during mammary morphogenesis and also in blocking FGF-induced invasion.

Branching morphogenesis is a developmental process that maximizes surface area in order to enhance gas, nutrient, and waste exchange by tissue (1). Consequently, branching morphogenesis occurs during development of a variety of organs, including *Drosophila* trachea, mammalian lungs, kidneys, and salivary and mammary glands (2). Because this developmental event relies on coordination of major cellular processes, including proliferation, invasion, differentiation, and apoptosis (1), understanding the pathways that drive branching morphogenesis may lead to discoveries of mechanisms involved in human diseases, such as cancer, where these fundamental cellular pathways are aberrantly regulated.

In contrast to other organs, the mammary gland undergoes key stages of development postnatally. Due to its delayed development and capacity to branch in organotypic systems *in vitro*, the mammary gland is a uniquely accessible model organ of branching morphogenesis (3). At birth, the mammary gland consists of a small ductal network embedded in adipose tissue. Hormonal cues stimulate its development during puberty, which results in elongation of ducts that eventually fill the fat pad (4). Importantly, mammary ducts are composed of an epithelial bilayer, with a basal layer consisting of myoepithelial cells and inner layer of luminal cells. Each layer contains progenitor and differentiated cell populations that are poised to respond to developmental and hormonal changes. During pregnancy, alveolar buds branch from ducts and develop into lobuloalveolar acini, where functionally differentiated luminal cells produce milk during lactation. In addition, differentiated myoepithelial cells contract in response to oxytocin to facilitate milk delivery (5). Cumulatively, mammary branching morphogenesis functions to establish an extensive tubular gland capable of producing and delivering milk to newborn animals.

Studies using genetically modified mice and three-dimensional organotypic culture of mammary tissue have identified several molecular pathways important for mammary gland development. Among these pathways, epidermal growth factor (EGF) receptor and fibroblast growth factor (FGF) receptor

* This work was supported, in whole or in part, by National Institutes of Health Grants R01-CA143815 and R01-CA140296. This work was also supported by Department of Defense Breast Cancer Research Program Grant W81XWH-09-1-04310. K. J. B. is supported by an NIH Developmental Biology Training Grant (5T32 HD07491).
⌘ *Author's Choice*—Final version full access.
[S] This article contains supplemental Experimental Procedures, Tables S1 and S2, Figs. S1–S4, and Movies S1 and S2.
[1] Both authors contributed equally to this work.
[2] Present address: Division of Biology, California Institute of Technology, Pasadena, CA 91125.
[3] To whom correspondence should be addressed: Dept. of Surgery, Dept. of Oncological Sciences, Huntsman Cancer Institute, University of Utah, 2000 Circle of Hope Dr., Salt Lake City, UT 84112. Tel.: 801-587-4633; Fax: 801-585-9872; E-mail: Bryan.Welm@hci.utah.edu.

have been shown to be critical drivers of proliferation and invasion, respectively (5). Although these studies support a pivotal role for EGF and FGF signaling in mammary development, the downstream cellular targets of these cascades remain unclear.

We sought to develop an *in vitro* model of mammary development well suited to define intracellular pathways targeted by growth factor signaling. In previously established organotypic models of mammary morphogenesis, fragments of murine mammary epithelium, called organoids, were embedded in extracellular matrix and stimulated with specific growth factors to induce branching (6–9). However, organoids are complex tissue structures consisting of both epithelial and stromal cells. As a result, one limitation of these studies is the inability to distinguish the effects of growth factor signaling directly on epithelial cells from the indirect effects exerted through stromal cells. We developed an *in vitro* three-dimensional branching model consisting of enriched, primary mammary epithelial cells (MECs)[4] and employed a forward chemical genetic screen to identify modulators of branching morphogenesis. We describe a compound, 1023, which effectively blocks FGF2-induced branching while maintaining cells as normal mammary cysts. We demonstrate that 1023 acts through the aryl hydrocarbon receptor (AHR) to functionally inhibit branching by regulating desmosome adhesion complexes in mammary epithelium.

EXPERIMENTAL PROCEDURES

Isolation of Primary MECs—Organoids from the fourth inguinal mammary glands were isolated from 8–12-week-old female FVB/n mice as described previously (10). Protocol modifications and dissociation of organoids into single cells are described in the supplemental material.

Aggregation and Culture of Primary MECs in Matrigel—Frozen primary MECs were thawed, washed, and pelleted three times with 5 ml of DMEM/F-12 (HyClone) (150 × *g*, 3 min) to remove DMSO. To form aggregates, 2×10^6 primary MECs were resuspended in 1 ml of primary MEC growth medium (DMEM/F-12 supplemented with 5 μg/ml ITS-X (Invitrogen), 1 μg/ml hydrocortisone, 10 ng/ml murine EGF (BD Biosciences), 10% FBS (HyClone), and 1× penicillin/streptomycin/glutamine (Invitrogen)) and incubated overnight at 37 °C with 5% CO_2 in a 24-well ultra-low attachment tissue culture plate (Costar). After 16 h, stromal contaminants were removed by differential centrifugation as described previously (6). To create a base layer, 20 μl of growth factor-reduced Matrigel (BD Biosciences) was plated in the center of each well of a 24-well glass SensoPlate (Greiner Bio-One) and allowed to solidify at 37 °C. Aggregates (250 per well) were plated on top of the hardened base layer in 40 μl of Matrigel per well and incubated at 37 °C with 5% CO_2 to solidify Matrigel. Embedded aggregates were cultured in DMEM/F-12 supplemented with 5 μg/ml ITS-X, 1× penicillin/streptomycin/glutamine, and either murine EGF or human FGF2 (Invitrogen) (2.5 nM unless otherwise indicated). 1023, 1023-CF_3, and 2,3,7,8-tetrachlorodibenzodioxin (TCDD) were added as indicated. Cells were incubated at 37 °C with 5% CO_2 with medium changes every 48 h. When single cells were cultured in Matrigel, 2,500 single trypsinized primary MECs were embedded in 40 μl of Matrigel per well of a 24-well plate. For peptide experiments, aggregates were plated on top of Matrigel as described previously (11). Briefly, 50 μl of Matrigel was plated in each well of a 96-well plate and incubated at 37 °C to harden. Aggregates (250 per well) were resuspended in 100 μl of medium containing 2% Matrigel and plated on top of the base layer. We used this overlay technique to ensure that the peptides could access aggregates. To calculate the percentage of branching in all assays, samples were fixed in 4% paraformaldehyde and imaged with bright field microscopy at low magnification (×4). At least 100 aggregates/well were scored, with branching counted as three ducts or more, as established previously in organoid culture models (6). At least 3 independent samples/condition were averaged for each experiment.

Small Molecule Library Screen—Compound stocks were obtained from the University of Utah Department of Chemistry Collection and diluted to 10 μM in serum-free medium (DMEM/F-12 supplemented with 5 μg/ml ITS-X, 1× penicillin/streptomycin/glutamine, and 2.5 nM human FGF2). Aggregates were embedded as described above in 48-well tissue culture plates (BD Biosciences) with a 5-μl Matrigel base layer and 200 aggregates suspended in 10 μl of Matrigel on top. Medium was replaced with fresh compound-containing medium after 72 h in culture. After 144 h total, cells were fixed in 4% paraformaldehyde, and an Olympus CKX41 inverted microscope was used to score each compound based on the phenotype observed in greater than 50% of aggregates in each well.

Homology Modeling—Sequence alignment, homology modeling, and molecular docking of 1023 with human AHR is described in detail in the supplemental material.

Construction of shRNA Lentiviral Plasmids—RNA sequences (supplemental Table S2) for shRNA *Ahr* or *Arnt* (aryl hydrocarbon receptor nuclear translocator) knockdown were designed using the Dharmacon siDESIGN Center (available on the Thermo Scientific Web site). Oligonucleotides were annealed and ligated into HpaI and XhoI sites in pLentiLox5.0-GFP (12) following the molecular cloning protocol detailed in the supplemental material.

Virus Production and Transduction of Primary MECs—Lentivirus was produced and titrated as previously described (10, 13). High efficiency lentiviral transduction of primary MECs was conducted as described previously (14) with modifications detailed in the supplemental material.

Statistical Analysis—All values are shown as means ± S.E. or S.D., as indicated. *p* values were determined using Student's *t* test with two-tailed distribution and unequal variance.

Additional Experimental Procedures—Additional methodology is provided in the supplementary material.

RESULTS

Development of in Vitro Three-dimensional Branching Assay Using Primary MECs—To study the direct effect of growth factor signaling on epithelial cells, we developed a three-dimensional branching assay using isolated primary MECs devoid of

[4] The abbreviations used are: MEC, mammary epithelial cell; AHR, aryl hydrocarbon receptor; K8, keratin-8; K14, keratin-14; TCDD, 2,3,7,8-tetrachlorodibenzodioxin; ARNT, aryl hydrocarbon receptor nuclear translocator; DIC, differential interference contrast.

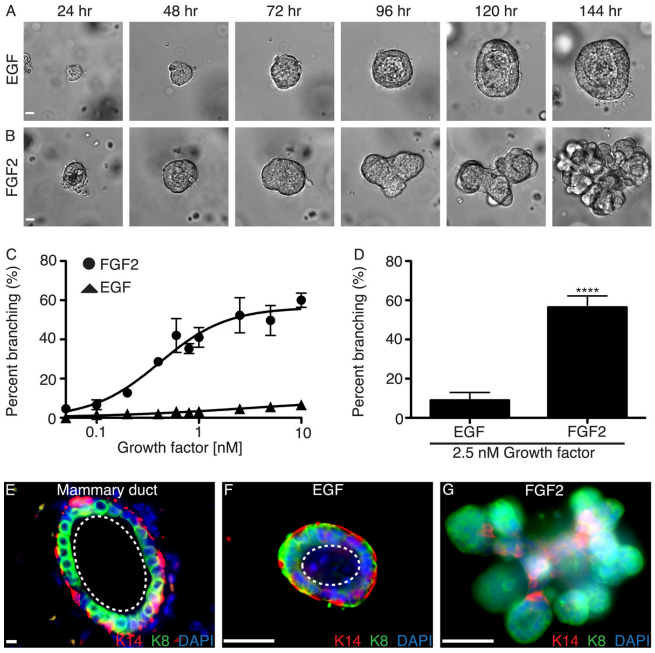

FIGURE 1. **Primary MECs branch in the presence of FGF2.** *A*, aggregated primary MECs grown in Matrigel with 2.5 nM EGF underwent extensive reorganization to form a fluid-filled cyst between 72 and 96 h in culture. Continued growth was observed through 144 h. *B*, 2.5 nM FGF2 stimulated robust branching. Aggregates initially reorganized to form a cyst, which collapsed near 72 h in culture. Extensive branching and increased growth was observed through 144 h in culture. Representative time course DIC images are shown. *C*, dose-response analysis for EGF- and FGF2-induced branching over 144 h. *D*, quantification of percentage of branching in primary MECs grown for 144 h with 2.5 nM EGF or 2.5 nM FGF2. Statistical analysis was performed using Student's *t* test. Results are shown as mean ± S.D. (*error bars*); $n = 3$; ****, $p < 0.0001$. *E*, mammary ducts are composed of an epithelial bilayer, as shown by immunofluorescence staining of a cross-section of a duct from a virgin FVB/n mouse with a luminal epithelial marker, K8 (*green*), and a myoepithelial marker, K14 (*red*). *F*, immunofluorescence staining for K8 and K14 in our three-dimensional primary MEC culture model with 2.5 nM EGF. *G*, immunofluorescence staining for K8 and K14 in our three-dimensional primary MEC culture model with 2.5 nM FGF2. *E–G*, interactions between luminal epithelial and myoepithelial cells were similar to those observed *in vivo*. Nuclei were stained with DAPI (in *blue*). The *dashed white line* defines the lumen. *A*, *B*, and *E–G*, *scale bar*, 40 μm.

stromal components. Primary MECs were prepared as single cells from the fourth inguinal mammary glands of 8–12-week-old FVB/n mice. Dissociated primary MECs were cultured in suspension to allow aggregation of epithelial cells, and after 16 h, the cell clusters were enriched from stromal cells by differential centrifugation as described previously (6). The MEC aggregates were embedded in Matrigel and grown in culture for 144 h in serum-free medium supplemented with either EGF or FGF2. In this assay, aggregates cultured with either growth factor underwent considerable reorganization, motility, and proliferation (Fig. 1, *A* and *B*). However, EGF and FGF2 induced distinct differences in morphology. Unlike *in vitro* organoid cultures (7), aggregated primary MECs in our assay did not branch efficiently in the presence of EGF and predominately formed hollow cysts with a fluid-filled lumen (Fig. 1*A*). The significantly reduced branching observed with EGF further supports its role as an indirect mediator of branching (8, 15) and is in agreement with the lack of stromal cells in our aggregate culture model (10) compared with the organoid model (16). In contrast to EGF, FGF2 stimulated extensive branching of MECs (Fig. 1*B*), which is consistent with the robust branching phenotype elicited by activation of the FGF receptor in mammary epithelial cells *in vivo* (17). To determine the optimal concentration of FGF2 required to stimulate branching in the aggregate model, we performed a dose-response analysis and found the half-maximal effective concentration (EC_{50}) for FGF2-induced branching to be 0.41 ± 0.053 nM (Fig. 1*C*). Based on these results, we used 2.5 nM growth factor for all subsequent assays, which was the minimum concentration required to achieve maximal branching. At this concentration, 56.4% of primary MECs branched in the presence of FGF2 compared with only 8.9% with EGF (Fig. 1*D*).

We next used immunofluorescence to assess the cellular architecture of cyst and branched structures. Both EGF and FGF2 induced a cellular organization similar to that observed *in vivo*. Immunofluorescence staining showed that like *in vivo* mammary ducts (Fig. 1*E*), EGF-induced cysts were composed of an epithelial bilayer (Fig. 1*F*), with keratin-8 (K8)-positive luminal epithelial cells surrounded by keratin-14 (K14)-positive myoepithelial cells. In branched structures induced by FGF2, we found K8-positive luminal epithelial cells invading into the Matrigel at branch points and K14-positive myoepithe-

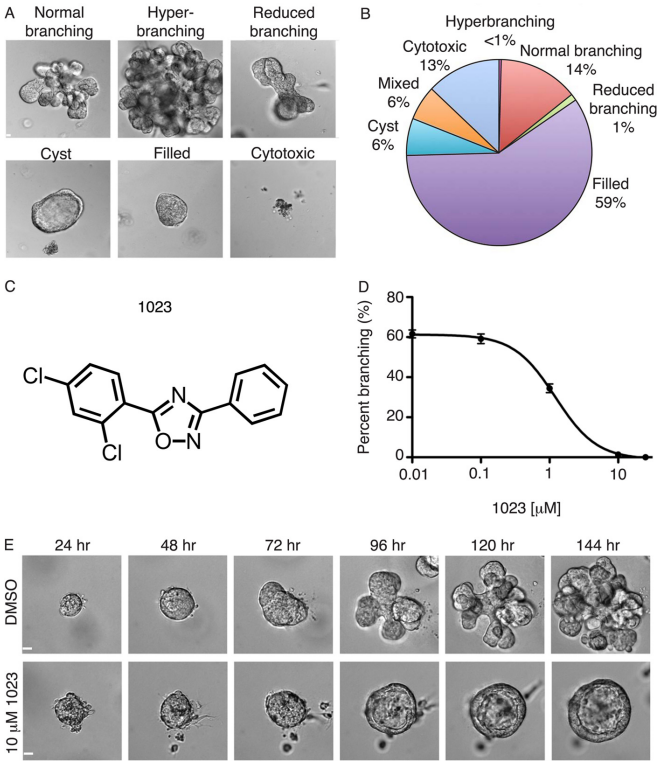

FIGURE 2. **Chemical library screen identifies 1023 as a potent inhibitor of *in vitro* branching morphogenesis.** *A*, six dominant phenotypes were observed in a chemical library screen for alterations on FGF2-induced branching. Representative DIC images of the phenotypes observed are shown. *B*, quantification of the percentage of total compounds that induced each phenotype. *C*, structure of 1023, which was one of the most potent compounds to cause cyst arrest. *D*, dose-response analysis for FGF2-induced branching in the presence of 1023 over 144 h. *E*, representative time course DIC images of MECs grown in the FGF2 branching assay with DMSO (vehicle control) (*top*) or 10 μM 1023 (*bottom*). *A* and *E*, *scale bar*, 40 μm. *Error bars*, S.D.

lial cells retained at points of constriction at the base of branches (Fig. 1*G*), which is consistent with previous studies showing that branch points arise at breaks in the myoepithelial layer (16). Thus, our aggregate-based model recapitulated key aspects of *in vivo* mammary branching morphogenesis and allowed us to uncouple epithelial induced morphogenesis from stromal mediated events.

Chemical Genetic Screen to Identify Modulators of Branching Morphogenesis—With our three-dimensional assay, we next conducted a chemical genetic screen to identify strong modulators of branching, with the goal to use these compounds to elucidate signaling pathways in epithelial cells critical for this developmental process. We were specifically interested in compounds that completely blocked FGF2-induced invasion yet maintained the normal, bilayered morphology of the growing aggregate. Thus, we were interested in compounds that induced cyst morphology similar to EGF-treated aggregates. We hypothesized that compounds causing cyst arrest in FGF2-treated aggregates would more specifically target invasion rather than growth-stimulating pathways.

587 compounds from the University of Utah Chemistry Department Collection were screened in the FGF2 branching assay. Six dominant phenotypes were observed (Fig. 2, *A* and *B*): normal branching, hyperbranching, reduced branching, cyst arrest, filled, and cytotoxic. Additionally, 6% of compounds caused a mixed phenotype consisting of two or more dominant characteristics (Fig. 2*B*). The most potent compound that caused cyst arrest, a diphenyl oxadiazole named 1023 (Fig. 2*C*), exhibited an EC_{50} of 1.2 ± 0.050 μM in our branching assay (Fig. 2*D*) and had no significant toxicity or effect on growth compared with DMSO treatment (vehicle control) (Fig. 2*E* and supplemental Movies S1 and S2). The effect of impairing branching while simultaneously maintaining normal cyst growth (supplemental Fig. S1) suggested 1023 was a specific modulator of FGF2-induced branching. Thus, we reasoned that elucidating the target of 1023 would lead to better understanding of the molecular mechanisms downstream of FGF2 during mammary branching morphogenesis.

Activation of the Aryl Hydrocarbon Receptor Blocks Branching Morphogenesis—For insight into the biological mechanism of action of 1023, we evaluated alterations in gene expression

TABLE 1
Genes of interest up-regulated by microarray in MECs treated for 72 h with 1023
Known AHR response genes are shown in boldface type.

Gene identifier	Gene name	Gene symbol	Ratio[a]
NM_009992	**Cytochrome P450, family 1, subfamily a, polypeptide 1, transcript variant 1**	***Cyp1a1***	**49.61**
NM_009644	**Aryl-hydrocarbon receptor repressor**	***Ahrr***	**22.37**
XM_484705	Desmoglein 1 α	*Dsg1*	10.51
BY704100	Desmocollin 1	*Dsc1*	9.39
NM_010356	**Glutathione *S*-transferase, α 3, transcript variant 2**	***Gsta3***	**7.13**
NM_007436	**Aldehyde dehydrogenase family 3, subfamily A1, transcript variant 1**	***Aldh3a1***	**5.37**
NM_008706	**NAD(P)H dehydrogenase, quinone 1**	***Nqo1***	**4.09**
NM_009994	**Cytochrome P450, family 1, subfamily b, polypeptide 1**	***Cyp1b1***	**3.49**
NM_030596	Desmoglein 3	*Dsg3*	3.38
NM_201410	**UDP glucuronosyltransferase 1 family, polypeptide A6B**	***Ugt-1a***	**2.91**

[a] Log_2 ratio for 1023-treated *versus* DMSO.

following compound treatment. We conducted microarray gene expression analysis on primary MECs grown in Matrigel for 72 h with FGF2 and either DMSO or 10 μM 1023. Compared with DMSO, 1023 highly up-regulated *Cyp1a1*, *Ahrr*, *Gsta3*, *Aldh3a1*, *Nqo1*, *Cyp1b1*, and *Ugt-1a* (Table 1, boldface type), an expression profile known to be induced by activation of AHR (18).

AHR is a ligand-activated transcription factor and member of the Per-Arnt-Sim family of basic helix-loop-helix proteins. Known for binding aromatic compounds (19, 20), AHR mediates response to chemicals by up-regulating expression of metabolic enzymes (21). However, a growing number of studies suggest that AHR has a wider physiologic role in regulating critical cellular processes, including proliferation, differentiation, and apoptosis (22, 23). To assess AHR as a potential target of 1023, we used a homology model structure of human AHR to predict binding modes of 1023 (24). Using the lowest energy conformer, 1023 was predicted to bind AHR with a free energy of −20.83 kcal/mol (Fig. 3*A*), which suggested a strong interaction between 1023 and AHR. In addition to van der Waals contacts, our modeling predicted Phe-287, His-291, Phe-324, Cys-300, His-337, and Gln-383 in the AHR binding cavity significantly contributed to the binding mode of 1023 through hydrogen bonding and other non-bonded contacts. Furthermore, the modeling data indicated that the addition of a trifluoromethyl group to the phenyl ring of 1023 would drastically reduce its ability to bind AHR due to steric clashes with His-291 and Phe-287. As a result, we synthesized the 1023-CF_3 analog (Fig. 3*B*, *top*), which had a predicted binding energy of −11.21 kcal/mol, to use as a negative control in our assays.

With AHR as the putative cellular target of 1023, we hypothesized that TCDD (Fig. 3*B*, *bottom*), a widespread environmental pollutant and known activator of AHR (25, 26), would phenocopy 1023. In our three-dimensional branching assay, TCDD blocked branching of primary MECs (EC_{50} = 3.93 ± 0.17 pM) (Fig. 3*C*) and induced a strong cyst arrest phenotype (Fig. 3*E*, *top right*), similar to 1023 (Fig. 3*E*, *bottom left*). In contrast, 1023-CF_3 did not efficiently block branching (EC_{50} = 71.1 ± 1.9 μM) compared with 1023 (EC_{50} = 1.2 ± 0.05 μM) (Fig. 3, *D* and *E*, *bottom panels*), as predicted by our modeling data. These results suggested that activation of AHR is sufficient to block mammary branching morphogenesis *in vitro*.

1023 Activates AHR to Disrupt Mammary Branching Morphogenesis—We next probed the AHR pathway to verify that 1023 was a strong activator of AHR. Following ligand binding, AHR undergoes nuclear translocation, dimerizes with ARNT, and activates transcription of downstream target genes (19, 27, 28). Considering this mechanism, we wanted to determine whether 1023 treatment led to an increased accumulation of AHR in the nucleus. To do so, we expressed an HA-tagged AHR construct, pACTAG2-HA-AHR, in HEK-293T cells. After 24 h of drug treatment, we performed immunofluorescence for HA and found that both 10 nM TCDD and 10 μM 1023 significantly increased the amount of nuclear AHR compared with DMSO or 10 μM 1023-CF_3 (Fig. 3*F* and supplemental Fig. S2).

The increase in AHR nuclear translocation also correlated with induction of AHR response genes. *Cyp1a1* (cytochrome P4501A1) is a direct AHR target and is used as a readout for AHR activation (29). In primary MECs treated for 48 h, 10 nM TCDD and 10 μM 1023 increased *Cyp1a1* gene expression by 23.3- and 4.5-fold, respectively, compared with DMSO or 10 μM 1023-CF_3 (Fig. 3*G*). Furthermore, we tested the specificity of *Cyp1a1* induction and asked whether AHR and its transcriptional binding partner, ARNT, were required for 1023 to activate *Cyp1a1* expression. We generated mouse mammary HC11 cell lines stably expressing either a nonspecific control shRNA, shRNA against *Ahr* (shAHR-1), or shRNA against *Arnt* (shARNT-1 or shARNT-2). In these cell lines, *Ahr* expression was reduced by 61% (shAHR-1) (supplemental Fig. S3*A*) and *Arnt* expression by 60% (shARNT-1) or 75% (shARNT-2) (supplemental Fig. S3*B*). Cells with *Ahr* or *Arnt* knockdown showed considerably reduced expression of *Cyp1a1* than control cells after treatment with 10 nM TCDD (supplemental Fig. S3*C*) or 10 μM 1023 (Fig. 4*A*). Together, these results confirmed that 1023 activated AHR, leading to its nuclear translocation and induction of downstream gene targets.

Although 1023 activated AHR, it was still unclear whether AHR was required for the observed branching defect. To address this, we used lentiviral shRNA constructs to knock down *Ahr* in primary MECs. Briefly, primary MECs were infected in monolayer with a lentiviral control hairpin or shRNA construct against *Ahr* (shAHR-1 or shAHR-2), and knockdown of *Ahr* was confirmed by RT-PCR (supplemental Fig. S3*D*). Following infection, primary MECs were embedded as single cells in Matrigel and grown for 21 days with FGF2. Within each well, single cells grew into clonal outgrowths that were either untransduced or transduced, as distinguished by GFP expression. As expected, control transduced outgrowths (Fig. 4, *B* and *C*) branched in the presence DMSO but generated cysts in the presence of 10 nM TCDD or 10 μM 1023. Similar results were observed with untransduced outgrowths that grew in the same well as transduced outgrowths (supplemental Fig. S3*E*). In contrast, transduction of MECs with lentiviruses containing either of two different shRNA hairpins against *Ahr* sig-

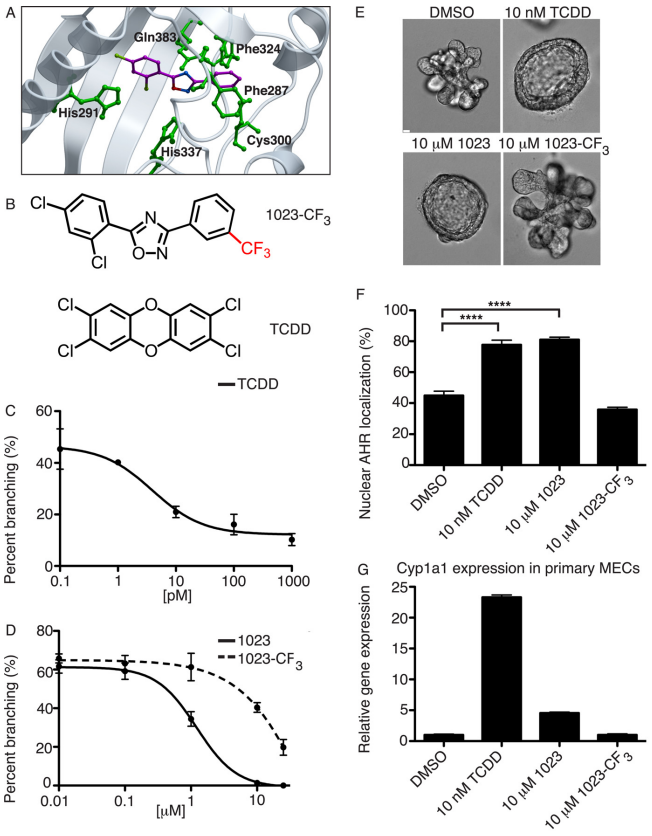

FIGURE 3. **1023 activates the aryl hydrocarbon receptor.** *A*, docking of 1023 (*purple*) with the homology model structure of human AHR (*gray*). Important interacting residues are noted in *green*. The binding free energy was estimated at −20.83 kcal/mol, suggesting a favorable interaction between 1023 and AHR. *B*, chemical structures of 1023-CF_3 (*top*), a predicted inactive analog of 1023, and TCDD (*bottom*), a known activator of AHR. *C*, dose-response analysis for FGF2-induced branching in primary MECs treated with TCDD for 144 h. *D*, 1023-CF_3 was less effective at blocking branching than 1023, as shown by dose-response analysis over 144 h for FGF2-induced branching. *Error bars* S.D. *E*, representative DIC images of the dominant phenotype observed in primary MECs grown in the FGF2 branching assay with DMSO (*top left*), 10 nM TCDD (*top right*), 10 μM 1023 (*bottom left*), or 10 μM 1023-CF_3 (*bottom right*). *Scale bar*, 40 μm. *F*, in HEK-293T cells transiently expressing pACTAG2-HA-AHR, 10 nM TCDD and 10 μM 1023 increased nuclear localization of AHR compared with DMSO or 10 μM 1023-CF_3 after 24 h of treatment. Quantification was based on immunofluorescence for HA. Results are shown as mean ± S.D.; $n = 7$; ****, $p < 0.0001$. *G*, relative gene expression of *Cyp1a1*, a known AHR response gene, was elevated in primary MECs treated for 48 h with 10 nM TCDD or 10 μM 1023 compared with DMSO or 10 μM 1023-CF_3. *Cyp1a1* gene expression was measured by RT-PCR and normalized to *β-actin* expression. Results are shown as mean ± S.E. (*error bars*); $n = 3$; ***, $p < 0.001$; **, $p < 0.01$. *F* and *G*, statistical analysis was performed using Student's *t* test.

nificantly rescued branching in the presence of 10 nM TCDD or 10 μM 1023 (Fig. 4, *B* and *D* and supplemental Fig. S3*F*). These results demonstrated that AHR was required for TCDD and 1023 to block FGF2-induced branching morphogenesis.

Desmosomal Adhesion Is Regulated by the AHR Pathway—After determining that 1023 targeted the AHR pathway, we sought to mechanistically understand how activation of AHR blocks mammary branching. Strikingly, our microarray analysis showed up-regulation of several genes involved in cellular adhesion, including desmosomal cadherins (Table 1 and supplemental Table S1). Because desmosomes are known to induce very tight intercellular contacts (30, 31) and are one of the dominant adhesion complexes found in the mammary gland (32), we hypothesized that desmosomal adhesion would be critical for maintenance of cysts caused by AHR activation.

First, we confirmed our microarray analysis by measuring gene expression of desmosomal cadherins in primary MECs treated for 96 h. RT-PCR results showed that both 10 nM TCDD and 10 μM 1023 significantly up-regulated gene expression of *Dsc1* (desmocollin 1) (supplemental Fig. S4*A*), *Dsg1* (desmoglein 1) (supplemental Fig. S4*B*), and *Dsg3* (desmoglein 3) (Fig. 5*A*) compared with DMSO. Moreover, desmosomal cadherins were up-regulated in primary MECs grown in the presence of EGF compared with FGF2 (Fig. 5*A* and supplemental Fig. S4, *A*

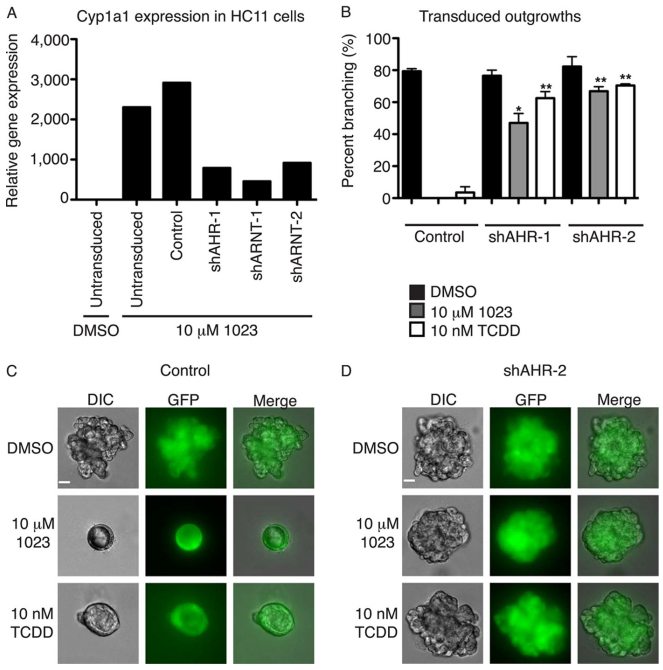

FIGURE 4. **AHR is the biological target of 1023.** *A*, induction of *Cyp1a1* by 1023 was lower in HC11 cells stably expressing an shRNA against *Ahr* (shAHR-1) or *Arnt* (shARNT-1 or shARNT-2) than untransduced or control transduced cells. *Cyp1a1* gene expression was measured after 6 days of treatment with DMSO or 10 μM 1023 and normalized to *β-actin* expression. Results are shown as mean ± S.E. (*error bars*). *B*, knockdown of *Ahr* in primary MECs rescued branching in the presence of AHR agonists. Shown is a quantification of the percentage of branching in transduced outgrowths from primary MECs infected with a lentiviral control shRNA (Control) or shRNA against *Ahr* (shAHR-1 or shAHR-2). Statistical analysis was performed using Student's *t* test. Results are shown as mean ± S.D. (*error bars*); $n = 2$; *, $p < 0.05$; **, $p < 0.01$. *C*, representative images of a clonal outgrowth from primary MECs transduced with a control shRNA. *D*, representative images of a clonal outgrowth from primary MECs transduced with shAHR-2. *B–D*, following transduction, cells were embedded in Matrigel as single cells and grown for 21 days in the presence of 2.5 nM FGF2 and DMSO, 10 nM TCDD, or 10 μM 1023. *C* and *D*, *scale bar*, 40 μm.

and *B*). To assess protein levels, we performed a Western blot for DSG3 in primary MECs extracted from Matrigel after 96 h of treatment. Consistent with our RT-PCR results, DSG3 protein levels were highly up-regulated in primary MECs grown with EGF, 10 nM TCDD, or 10 μM 1023 compared with FGF2 alone (Fig. 5*B*). Finally, knockdown of *Ahr* or *Arnt* significantly reduced induction of desmosomal cadherins (supplemental Fig. S4, *C* and *D*). Like *Cyp1a1*, *Dsg1* gene expression was lower in HC11 cell lines with stable knockdown of *Ahr* or *Arnt* after treatment with 10 nM TCDD or 10 μM 1023. These experiments identified *Dsc1*, *Dsg1*, and *Dsg3* as novel downstream targets of the AHR signaling pathway.

Inhibition of Desmosomal Adhesion Promotes Branching of the Mammary Epithelium—To assess the functional importance of desmosomal adhesion in AHR-mediated disruption of branching morphogenesis, we sought to inhibit desmosome formation. Desmocollin and desmoglein are members of the cadherin family of proteins and require calcium to form functional desmosomes *in vitro* (33–36). We predicted that if cadherin junctions were required to maintain the cyst phenotype, then chelation of calcium would rescue the branching defect elicited by 1023. Thus, we added 10 μM EGTA (pH 7.4) to chelate calcium in our branching assay. After 144 h in culture, we found a significant increase in branching with EGTA in the presence 10 nM TCDD or 10 μM 1023 compared with vehicle control (Fig. 5, *C* and *D*). Furthermore, calcium chelation significantly increased branching in the presence of EGF, suggesting that desmosomes play a central role in the transition to a branched epithelial state.

Based on these results, we went on to selectively inhibit the formation of desmosome complexes using blocking peptides. These 10-mer peptides bind the cell adhesion recognition site (37) of a specific desmosome cadherin and functionally inhibit its ability to form adhesion complexes (38, 39). Accordingly, we added 2 mM peptide against DSC3 or DSG3 to primary MECs after 48 h in culture with 10 μM 1023 and observed a significant increase in branching at 144 h. In contrast, a nonspecific control peptide and a previously published peptide against E-cadherin (38) did not significantly affect branching in the presence of 10 μM 1023 (Fig. 5, *E* and *F*), suggesting a specific role for desmosomes. Together, these results demonstrate that desmosomes are a novel downstream target of ligand-induced AHR signaling and critical to block branching morphogenesis of the mammary gland.

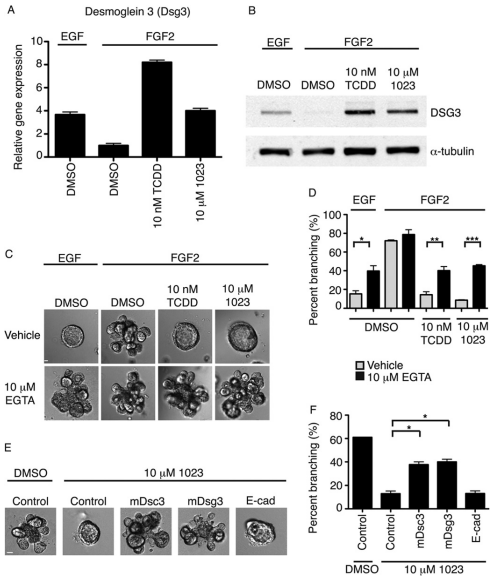

FIGURE 5. **AHR signaling promotes desmosomal adhesion to block mammary branching morphogenesis.** *A*, relative gene expression of *Dsg3* (desmoglein 3) in aggregated primary MECs grown for 96 h in Matrigel with 2.5 nM EGF or 2.5 nM FGF2 and DMSO or 10 nM TCDD or 10 μM 1023. Gene expression was measured by RT-PCR and normalized to *β-actin* expression. Results are shown as mean ± S.E. (*error bars*). *B*, Western blot analysis of DSG3 in aggregated primary MECs grown for 96 h in Matrigel with 2.5 nM EGF or 2.5 nM FGF2 and DMSO or 10 nM TCDD or 10 μM 1023. *C*, the addition of 10 μM EGTA significantly increased branching of primary MECs grown in the presence of 2.5 nM EGF or in the presence of 2.5 nM FGF2 and 10 nM TCDD or 10 μM 1023 compared with vehicle control. Representative DIC images are shown. *D*, quantification of branching shown as mean ± S.D. (*error bars*); $n = 3$; *, $p < 0.05$; **, $p < 0.01$; ***, $p < 0.001$. *C* and *D*, EGTA was added after 48 h in culture, and branching was scored at 144 h. *E*, the addition of 2 mM blocking peptide against DSC3 or DSG3, but not E-cadherin or a nonspecific control peptide, significantly increased branching of primary MECs grown in the presence of FGF2 and 10 μM 1023. Representative DIC images are shown. *F*, quantification of branching shown as mean ± S.D. (*error bars*); $n = 3$; *, $p < 0.05$. *E* and *F*, peptide was added after 48 h in culture, and branching was scored at 144 h. *C* and *E*, *scale bar*, 40 μm. *D* and *F*, statistical analysis was performed using Student's *t* test.

DISCUSSION

Using a three-dimensional epithelial cell-based model of branching, we demonstrate that FGF2, but not EGF, is sufficient to drive morphogenesis of mammary epithelial cells, which is in agreement with the role of growth factors in mammary development (5, 40). In addition, we employed a novel chemical genetic approach to identify molecular pathways controlling the dynamics of mammary branching morphogenesis. The use of chemical genetics rather than a standard genetic approach allowed us to specifically activate the AHR signaling pathway and identify a new role for AHR in regulating adhesion complexes in the mammary gland.

Environmental exposure to chemical pollutants, including TCDD, is thought to contribute significantly to lactation deficiencies in women (41). These findings are supported by studies in rodents, which showed that TCDD exposure during gestation (42, 43) and pregnancy (44) decreased alveolar development and milk production, respectively. It remains controversial whether local or systemic mechanisms mediate the effect of TCDD on mammary differentiation. Although TCDD is known to modulate estrogen receptor signaling (45), studies have shown that it does not decrease circulating levels of prolactin, estradiol, or progesterone in compound-treated mice (44). Additionally, TCDD was shown to reduce alveolar development in *ex vivo* cultures of whole mammary glands (46). In agreement with these observations, our data show that AHR activation has direct effects on mammary cells.

The key mediators of the effects of TCDD have been difficult to study with *in vitro* organoid and *in vivo* transgenic models, due to the complex interactions between epithelial and stromal cells in these systems. Studies have shown that the DNA-binding domain of AHR is required for the deleterious effects of TCDD on the mammary gland (46), implicating AHR transcriptional regulation as a critical mechanism. Additionally, reciprocal transplant experiments with AHR knock-out mice suggest that both epithelial and stromal transcriptional targets of AHR contribute to the block in branching (46). Here, we demonstrate an epithelial mediated mechanism, in which AHR blocks alveolar development through desmosomal adhesion, which is a novel target of the AHR pathway.

There is growing evidence to suggest that desmosomes contribute significantly to mammary morphogenesis. In the 1970s, electron microscopy was used to assess the ultrastructure of the mouse mammary gland (47). These studies showed that desmosomes were a major adhesion component in the mammary gland, with large desmosome complexes connecting ductal epithelial cells in the virgin gland. Interestingly, desmosomal complexes were highly dynamic. At the onset of lactation, desmosomal adhesion was increased in major, nonsecretory ducts, whereas milk-producing alveoli lost all desmosome contacts during lactation. This stage-dependent shift in adhesion suggested that desmosomes may have a critical role maintaining ductal structure, and their down-regulation may functionally contribute to productive lactation in lobuloalveoli.

Since these early studies, a functional role for desmosomal adhesion in mammary epithelial cells has been slowly emerging. During branching morphogenesis, luminal epithelial cells migrate collectively through the outer myoepithelial layer of a cyst to form new branch points (16). EM studies on organoids grown in Matrigel showed that despite an overall loss of adhesion during this process, desmosomal adhesion is maintained between luminal epithelial cells (32). In another study, desmosome-blocking peptides disrupted the ability of a clonal cell line derived from mouse luminal epithelial cells to form clusters in an *in vitro* assay (38). Taken together, these results suggest that desmosomes are a critical form of adhesion between luminal epithelial cells.

Although our results show that down-regulation of desmosomal adhesion facilitates branching morphogenesis, the specific role of these adhesion complexes in myoepithelial and luminal cells is not clear. Our data suggest that the myoepithelial-specific desmosome cadherins, Dsc3 and Dsg3 (38), must be down-regulated for branching morphogenesis. Because branch points are known to initiate from breaks in the myoep-

ithelial layer (16), the mechanical integrity of desmosomes may be selectively lost in myoepithelial cells to promote branching and differentiation. Loss of robust adhesion between myoepithelial cells would also facilitate contraction and milk delivery required during lactation.

Our data demonstrate that desmosomes form a critical and functional adhesion complex between mammary epithelial cells. Because desmosome cadherins are commonly mutated or silenced in human breast cancer (48, 49), desmosomes may be a critical adhesion complex that is lost in order to promote tumorigenesis. These findings are supported by previous work, which showed overexpression of desmosomal components inhibited invasion of nonadhesive cells in collagen (39). In our assay, desmosomal adhesion was sufficient to block the invasive mechanisms mediated by FGF2, consistent with an ability to promote tight epithelial cell interactions. Similarly, AHR agonists have been shown to inhibit invasion and increase differentiation of breast cancer cells (50). Thus, dissecting the role and regulation of desmosomes *in vivo* will be a critical next step toward understanding morphogenesis and transformation of the mammary gland.

Acknowledgments—We thank Dr. Oliver Hankinson (UCLA, Los Angeles, CA) for providing the AHR expression plasmid and Drs. James Bear (University of North Carolina, Chapel Hill, NC) and Thomas Marshall (University of Utah, Salt Lake City, UT) for providing the pLentiLox5.0-GFP vector.

REFERENCES

1. Lu, P., and Werb, Z. (2008) Patterning mechanisms of branched organs. *Science* **322,** 1506–1509
2. Lu, P., Sternlicht, M. D., and Werb, Z. (2006) Comparative mechanisms of branching morphogenesis in diverse systems. *J. Mammary Gland Biol. Neoplasia* **11,** 213–228
3. Smith, B. A., Welm, A. L., and Welm, B. E. (2012) On the shoulders of giants: A historical perspective of unique experimental methods in mammary gland research. *Semin. Cell Dev. Biol.* **23,** 583–590
4. Sternlicht, M. D. (2006) Key stages in mammary gland development. The cues that regulate ductal branching morphogenesis. *Breast Cancer Res.* **8,** 201
5. Sternlicht, M. D., Kouros-Mehr, H., Lu, P., and Werb, Z. (2006) Hormonal and local control of mammary branching morphogenesis. *Differentiation* **74,** 365–381
6. Fata, J. E., Mori, H., Ewald, A. J., Zhang, H., Yao, E., Werb, Z., and Bissell, M. J. (2007) The MAPK(ERK-1,2) pathway integrates distinct and antagonistic signals from TGFα and FGF7 in morphogenesis of mouse mammary epithelium. *Dev. Biol.* **306,** 193–207
7. Simian, M., Hirai, Y., Navre, M., Werb, Z., Lochter, A., and Bissell, M. J. (2001) The interplay of matrix metalloproteinases, morphogens, and growth factors is necessary for branching of mammary epithelial cells. *Development* **128,** 3117–3131
8. Sternlicht, M. D., Sunnarborg, S. W., Kouros-Mehr, H., Yu, Y., Lee, D. C., and Werb, Z. (2005) Mammary ductal morphogenesis requires paracrine activation of stromal EGFR via ADAM17-dependent shedding of epithelial amphiregulin. *Development* **132,** 3923–3933
9. Wiseman, B. S., Sternlicht, M. D., Lund, L. R., Alexander, C. M., Mott, J., Bissell, M. J., Soloway, P., Itohara, S., and Werb, Z. (2003) Site-specific inductive and inhibitory activities of MMP-2 and MMP-3 orchestrate mammary gland branching morphogenesis. *J. Cell Biol.* **162,** 1123–1133
10. Welm, B. E., Dijkgraaf, G. J., Bledau, A. S., Welm, A. L., and Werb, Z. (2008) Lentiviral transduction of mammary stem cells for analysis of gene function during development and cancer. *Cell Stem Cell* **2,** 90–102
11. Lee, G. Y., Kenny, P. A., Lee, E. H., and Bissell, M. J. (2007) Three-dimensional culture models of normal and malignant breast epithelial cells. *Nat. Methods* **4,** 359–365
12. Cai, L., Marshall, T. W., Uetrecht, A. C., Schafer, D. A., and Bear, J. E. (2007) Coronin 1B coordinates Arp2/3 complex and cofilin activities at the leading edge. *Cell* **128,** 915–929
13. Klages, N., Zufferey, R., and Trono, D. (2000) A stable system for the high-titer production of multiply attenuated lentiviral vectors. *Mol. Ther.* **2,** 170–176
14. Vafaizadeh, V., Klemmt, P., Brendel, C., Weber, K., Doebele, C., Britt, K., Grez, M., Fehse, B., Desriviéres, S., and Groner, B. (2010) Mammary epithelial reconstitution with gene-modified stem cells assigns roles to Stat5 in luminal alveolar cell fate decisions, differentiation, involution, and mammary tumor formation. *Stem Cells* **28,** 928–938
15. Wiesen, J. F., Young, P., Werb, Z., and Cunha, G. R. (1999) Signaling through the stromal epidermal growth factor receptor is necessary for mammary ductal development. *Development* **126,** 335–344
16. Ewald, A. J., Brenot, A., Duong, M., Chan, B. S., and Werb, Z. (2008) Collective epithelial migration and cell rearrangements drive mammary branching morphogenesis. *Dev. Cell* **14,** 570–581
17. Welm, B. E., Freeman, K. W., Chen, M., Contreras, A., Spencer, D. M., and Rosen, J. M. (2002) Inducible dimerization of FGFR1. Development of a mouse model to analyze progressive transformation of the mammary gland. *J. Cell Biol.* **157,** 703–714
18. Tijet, N., Boutros, P. C., Moffat, I. D., Okey, A. B., Tuomisto, J., and Pohjanvirta, R. (2006) Aryl hydrocarbon receptor regulates distinct dioxin-dependent and dioxin-independent gene batteries. *Mol. Pharmacol.* **69,** 140–153
19. Denison, M. S., and Nagy, S. R. (2003) Activation of the aryl hydrocarbon receptor by structurally diverse exogenous and endogenous chemicals. *Annu. Rev. Pharmacol. Toxicol.* **43,** 309–334
20. Denison, M. S., Pandini, A., Nagy, S. R., Baldwin, E. P., and Bonati, L. (2002) Ligand binding and activation of the Ah receptor. *Chem. Biol. Interact.* **141,** 3–24
21. Nebert, D. W., Dalton, T. P., Okey, A. B., and Gonzalez, F. J. (2004) Role of aryl hydrocarbon receptor-mediated induction of the CYP1 enzymes in environmental toxicity and cancer. *J. Biol. Chem.* **279,** 23847–23850
22. Furness, S. G., and Whelan, F. (2009) The pleiotropy of dioxin toxicity–xenobiotic misappropriation of the aryl hydrocarbon receptor's alternative physiological roles. *Pharmacol. Ther.* **124,** 336–353
23. Lawrence, B. P., and Sherr, D. H. (2012) You AhR what you eat? *Nat. Immunol.* **13,** 117–119
24. Motto, I., Bordogna, A., Soshilov, A. A., Denison, M. S., and Bonati, L. (2011) New aryl hydrocarbon receptor homology model targeted to improve docking reliability. *J. Chem. Inf. Model.* **51,** 2868–2881
25. Fernandez-Salguero, P. M., Hilbert, D. M., Rudikoff, S., Ward, J. M., and Gonzalez, F. J. (1996) Aryl-hydrocarbon receptor-deficient mice are resistant to 2,3,7,8-tetrachlorodibenzo-*p*-dioxin-induced toxicity. *Toxicol. Appl. Pharmacol.* **140,** 173–179
26. Mimura, J., and Fujii-Kuriyama, Y. (2003) Functional role of AhR in the expression of toxic effects by TCDD. *Biochim. Biophys. Acta* **1619,** 263–268
27. Heid, S. E., Pollenz, R. S., and Swanson, H. I. (2000) Role of heat shock protein 90 dissociation in mediating agonist-induced activation of the aryl hydrocarbon receptor. *Mol. Pharmacol.* **57,** 82–92
28. Pollenz, R. S., Sattler, C. A., and Poland, A. (1994) The aryl hydrocarbon receptor and aryl hydrocarbon receptor nuclear translocator protein show distinct subcellular localizations in Hepa 1c1c7 cells by immunofluorescence microscopy. *Mol. Pharmacol.* **45,** 428–438
29. Whitlock, J. P., Jr. (1999) Induction of cytochrome P4501A1. *Annu. Rev. Pharmacol. Toxicol.* **39,** 103–125
30. Garrod, D., and Chidgey, M. (2008) Desmosome structure, composition and function. *Biochim. Biophys. Acta* **1778,** 572–587
31. Garrod, D., and Kimura, T. E. (2008) Hyper-adhesion. A new concept in cell-cell adhesion. *Biochem. Soc. Trans.* **36,** 195–201
32. Ewald, A. J., Huebner, R. J., Palsdottir, H., Lee, J. K., Perez, M. J., Jorgens, D. M., Tauscher, A. N., Cheung, K. J., Werb, Z., and Auer, M. (2012) Mammary collective cell migration involves transient loss of epithelial

features and individual cell migration within the epithelium. *J. Cell Sci.* **125,** 2638–2654
33. Demlehner, M. P., Schäfer, S., Grund, C., and Franke, W. W. (1995) Continual assembly of half-desmosomal structures in the absence of cell contacts and their frustrated endocytosis. A coordinated Sisyphus cycle. *J. Cell Biol.* **131,** 745–760
34. Garrod, D. (2010) Desmosomes *in vivo*. *Dermatol. Res. Pract.* **2010,** 212439
35. Penn, E. J., Burdett, I. D., Hobson, C., Magee, A. I., and Rees, D. A. (1987) Structure and assembly of desmosome junctions. Biosynthesis and turnover of the major desmosome components of Madin-Darby canine kidney cells in low calcium medium. *J. Cell Biol.* **105,** 2327–2334
36. Nagar, B., Overduin, M., Ikura, M., and Rini, J. M. (1996) Structural basis of calcium-induced E-cadherin rigidification and dimerization. *Nature* **380,** 360–364
37. Blaschuk, O. W., Sullivan, R., David, S., and Pouliot, Y. (1990) Identification of a cadherin cell adhesion recognition sequence. *Dev. Biol.* **139,** 227–229
38. Runswick, S. K., O'Hare, M. J., Jones, L., Streuli, C. H., and Garrod, D. R. (2001) Desmosomal adhesion regulates epithelial morphogenesis and cell positioning. *Nat. Cell Biol.* **3,** 823–830
39. Tselepis, C., Chidgey, M., North, A., and Garrod, D. (1998) Desmosomal adhesion inhibits invasive behavior. *Proc. Natl. Acad. Sci. U.S.A.* **95,** 8064–8069
40. Lu, P., Ewald, A. J., Martin, G. R., and Werb, Z. (2008) Genetic mosaic analysis reveals FGF receptor 2 function in terminal end buds during mammary gland branching morphogenesis. *Dev. Biol.* **321,** 77–87
41. Neville, M. C., and Walsh, C. T. (1995) Effects of xenobiotics on milk secretion and composition. *Am. J. Clin. Nutr.* **61,** 687S–694S
42. Fenton, S. E., Hamm, J. T., Birnbaum, L. S., and Youngblood, G. L. (2002) Persistent abnormalities in the rat mammary gland following gestational and lactational exposure to 2,3,7,8-tetrachlorodibenzo-*p*-dioxin (TCDD). *Toxicol. Sci.* **67,** 63–74
43. Lewis, B. C., Hudgins, S., Lewis, A., Schorr, K., Sommer, R., Peterson, R. E., Flaws, J. A., and Furth, P. A. (2001) *In utero* and lactational treatment with 2,3,7,8-tetrachlorodibenzo-*p*-dioxin impairs mammary gland differentiation but does not block the response to exogenous estrogen in the postpubertal female rat. *Toxicol. Sci.* **62,** 46–53
44. Vorderstrasse, B. A., Fenton, S. E., Bohn, A. A., Cundiff, J. A., and Lawrence, B. P. (2004) A novel effect of dioxin. Exposure during pregnancy severely impairs mammary gland differentiation. *Toxicol. Sci.* **78,** 248–257
45. Swedenborg, E., and Pongratz, I. (2010) AhR and ARNT modulate ER signaling. *Toxicology* **268,** 132–138
46. Lew, B. J., Manickam, R., and Lawrence, B. P. (2011) Activation of the aryl hydrocarbon receptor during pregnancy in the mouse alters mammary development through direct effects on stromal and epithelial tissues. *Biol. Reprod.* **84,** 1094–1102
47. Pitelka, D. R., Hamamoto, S. T., Duafala, J. G., and Nemanic, M. K. (1973) Cell contacts in the mouse mammary gland. I. Normal gland in postnatal development and the secretory cycle. *J. Cell Biol.* **56,** 797–818
48. Klus, G. T., Rokaeus, N., Bittner, M. L., Chen, Y., Korz, D. M., Sukumar, S., Schick, A., and Szallasi, Z. (2001) Down-regulation of the desmosomal cadherin desmocollin 3 in human breast cancer. *Int. J. Oncol.* **19,** 169–174
49. Oshiro, M. M., Kim, C. J., Wozniak, R. J., Junk, D. J., Muñoz-Rodriguez, J. L., Burr, J. A., Fitzgerald, M., Pawar, S. C., Cress, A. E., Domann, F. E., and Futscher, B. W. (2005) Epigenetic silencing of DSC3 is a common event in human breast cancer. *Breast Cancer Res.* **7,** R669–R680
50. Barhoover, M. A., Hall, J. M., Greenlee, W. F., and Thomas, R. S. (2010) Aryl hydrocarbon receptor regulates cell cycle progression in human breast cancer cells via a functional interaction with cyclin-dependent kinase 4. *Mol. Pharmacol.* **77,** 195–201

SUPPLEMENTARY DATA

Chemical Genetic Screen Reveals a Role for Desmosomal Adhesion in Mammary Branching Morphogenesis*

Kaitlin J. Basham[1,7], Collin Kieffer[1,6,7], Dawne N. Shelton[1], Christopher J. Leonard[1], Vasudev R. Bhonde[2], Hariprasad Vankayalapati[3], Brett Milash[4], David J. Bearss[3], Ryan E. Looper[2], and Bryan E. Welm[1,5]

From the [1]Department of Oncological Sciences, Huntsman Cancer Institute, [2]the Department of Chemistry, [3]the Center for Investigational Therapeutics, Huntsman Cancer Institute, [4]the Microarray and Genomic Analysis Core Facility, Huntsman Cancer Institute, [5]the Department of Surgery, University of Utah, Salt Lake City, UT 84112 USA. [6]Present address: Division of Biology, California Institute of Technology, Pasadena, CA 91125. [7]These authors contributed equally to this work.

*Running title: *Chemical screen shows desmosomes regulate mammary branching*

To whom correspondence should be addressed: Bryan E. Welm, PhD, Department of Surgery, Department of Oncological Sciences, Huntsman Cancer Institute, University of Utah, 2000 Circle of Hope Dr., Salt Lake City, UT, 84112, USA, Tel.: (801) 587-4633; Fax: (801) 585-9872; E-mail: Bryan.Welm@hci.utah.edu

Keywords: aryl hydrocarbon receptor; chemical genetics; desmosomes; drug screen; mammary gland

SUPPLEMENTAL RESULTS

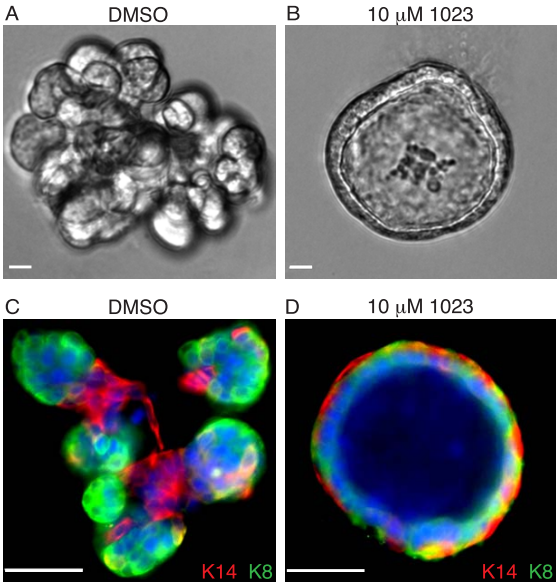

SUPPLEMENTAL FIGURE S1. MECs treated with 1023 maintain an epithelial bilayer. A. Representative DIC image of a primary MEC aggregate grown with 2.5 nM FGF2 and DMSO. B. Representative DIC image of a primary MEC aggregate grown with 2.5 nM FGF2 and 10 μM 1023. C-D. Immunofluorescence staining of a luminal epithelial marker, keratin-8 (K8, in green), and a myoepithelial marker, keratin-14 (K14, in red) in MEC aggregates grown in the FGF2 branching assay. Nuclei were stained with DAPI (in blue). C. Representative staining of a primary MEC aggregate grown with 2.5 nM FGF2 and DMSO. D. Representative staining of a primary MEC aggregate grown with 2.5 nM FGF2 and 10 μM 1023. 1023 maintained an epithelial bilayer, with luminal epithelial cells (in green) surrounded by myoepithelial cells (in red). A-D. Aggregates were grown for 144 hours in Matrigel. Scale bar = 40 μm.

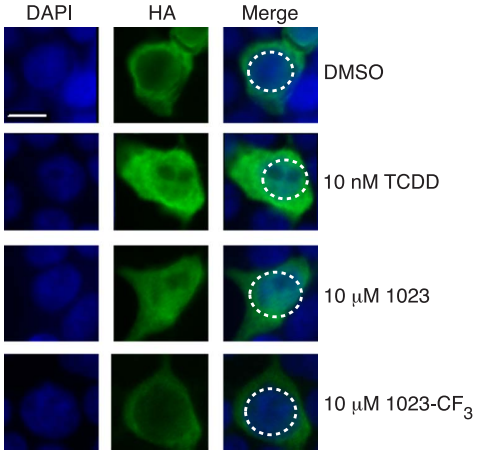

SUPPLEMENTAL FIGURE S2. 1023 and TCDD activate AHR to translocate to the nucleus. Representative images of HEK-293T cells transiently expressing pACTAG2-HA-AHR after 24 hours of treatment. 10 nM TCDD and 10 μM 1023 increased nuclear localization of AHR compared to DMSO or 10 μM 1023-CF_3. Dashed white line defines nuclei. Scale bar = 10 μm.

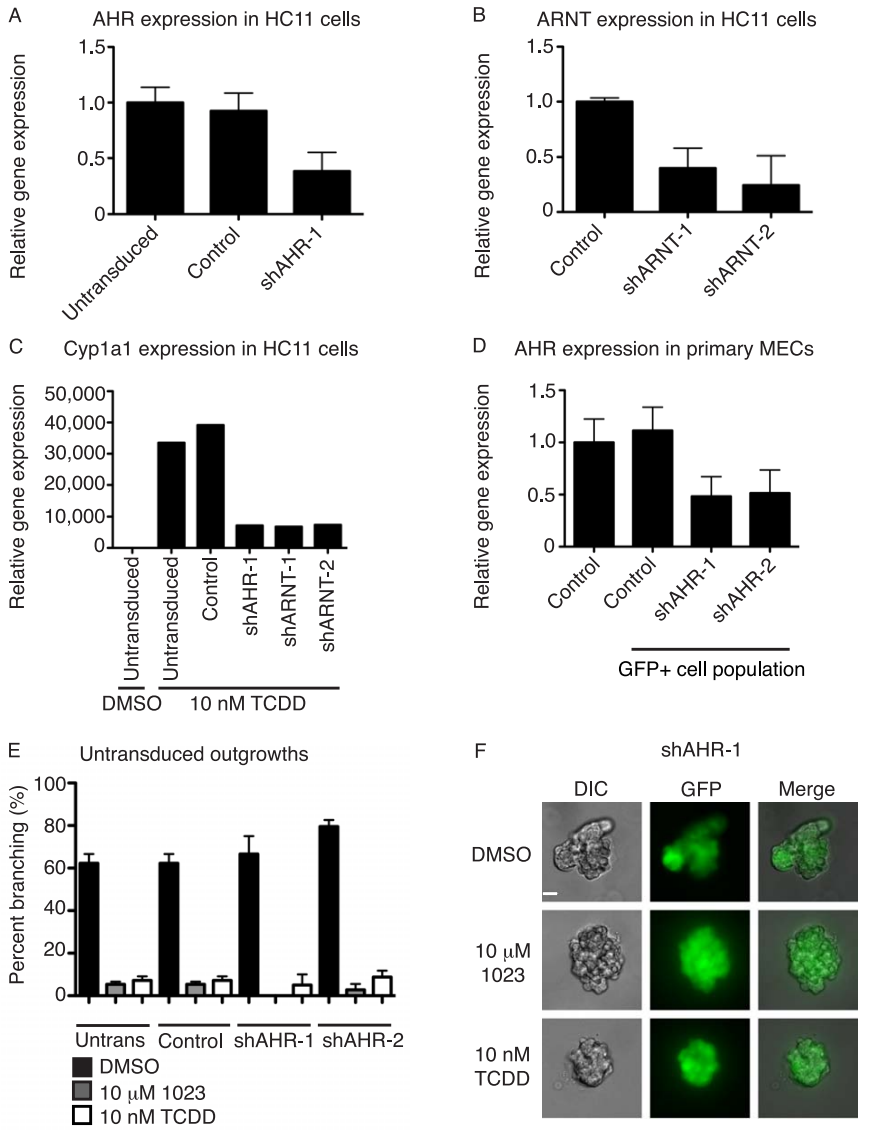
A
AHR expression in HC11 cells
Relative gene expression
1.5
1.0
0.5
0
Untransduced
Control
shAHR-1
B
ARNT expression in HC11 cells
Relative gene expression
1.5
1.0
0.5
0
Control
shARNT-1
shARNT-2
C
Cyp1a1 expression in HC11 cells
Relative gene expression
50,000
40,000
30,000
20,000
10,000
0
Untransduced
Untransduced
Control
shAHR-1
shARNT-1
shARNT-2
DMSO
10 nM TCDD
D
AHR expression in primary MECs
Relative gene expression
1.5
1.0
0.5
0
Control
Control
shAHR-1
shAHR-2
GFP+ cell population
E
Untransduced outgrowths
Percent branching (%)
100
80
60
40
20
0
Untrans
Control
shAHR-1
shAHR-2
DMSO
10 μM 1023
10 nM TCDD
F
shAHR-1
DIC
GFP
Merge
DMSO
10 μM 1023
10 nM TCDD

SUPPLEMENTAL FIGURE S3. AHR is the biological target of 1023. A. AHR gene expression in HC11 cells stably expressing shAHR-1. B. ARNT gene expression in HC11 cells stably expressing either shARNT-1 or shARNT-2. A-B. Gene expression was measured by RT-PCR in stable cell lines 7 days after lentiviral transduction and normalized to beta-actin. Results are shown as mean ± s.e.m. C. Cyp1a1 gene expression in untransduced HC11 cells or cells stably expressing a control shRNA, an shRNA against AHR (shAHR-1), or an shRNA against ARNT (shARNT-1 or shARNT-2). Cyp1a1 gene expression was measured by RT-PCR after 6 days of treatment with DMSO or 10 nM TCDD and normalized to beta-actin expression. Results are shown as mean ± s.e.m. D. AHR gene expression in primary MECs after transduction with lentiviral shRNA constructs against AHR. Gene expression was measured by RT-PCR in primary MECs sorted by FACS for GFP expression and normalized to beta-actin. Results are shown as mean ± s.e.m. E. Quantification of percent branching in untransduced outgrowths from primary MECs infected with a lentiviral control shRNA (Control) or shRNA against AHR (shAHR-1 or shAHR-2). Results are shown as mean ± s.d; n = 2. F. Representative images of a clonal outgrowth from primary MECs transduced with shAHR-1. Scale bar = 40 μm. E-F. Following transduction, cells were embedded in Matrigel as single cells and grown for 21 days in the presence of 2.5 nM FGF2 and DMSO, 10 nM TCDD, or 10 μM 1023.

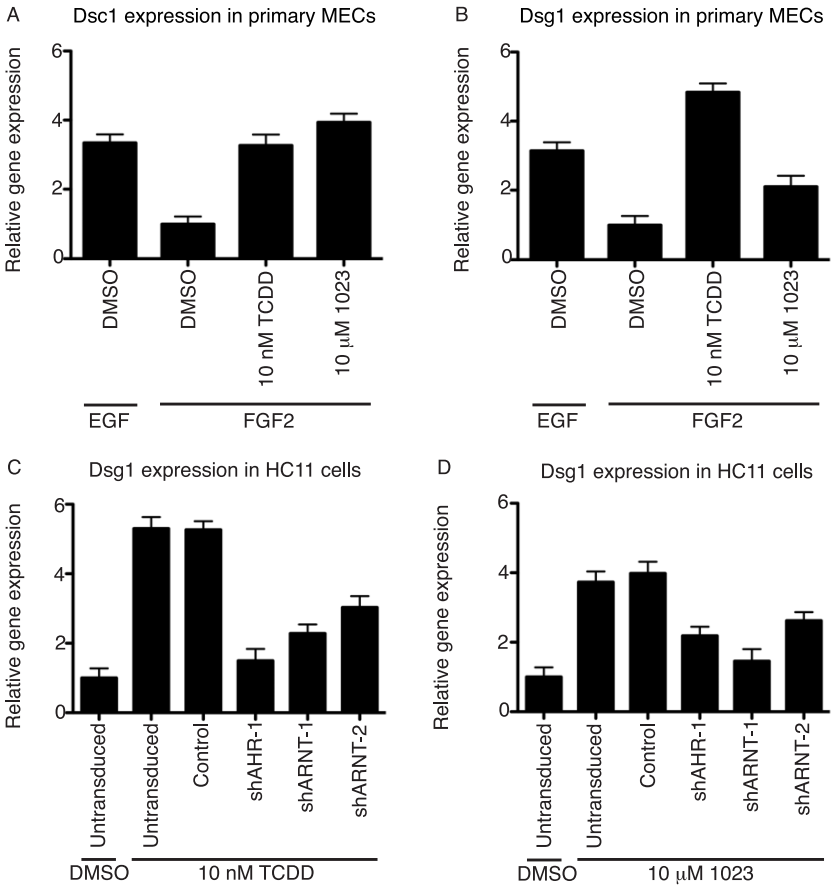

SUPPLEMENTAL FIGURE S4. AHR activation increases expression of desmosomal cadherins. A. Relative gene expression of desmocollin 1 (Dsc1). B. Relative gene expression of desmoglein 1 (Dsg1). A-B. Aggregated primary MECs were grown for 96 hours in Matrigel with 2.5 nM EGF or 2.5 nM FGF2 and DMSO, 10 nM TCDD, or 10 μM 1023. C. Relative gene expression of Dsg1 in HC11 cells after treatment with 10 nM TCDD. D. Relative gene expression of Dsg1 in HC11 cells after treatment with 10 μM 1023. C-D. Gene expression was measured in untransduced HC11 cells or cells stably expressing a control shRNA, an shRNA against AHR (shAHR-1), or an shRNA against ARNT (shARNT-1 or shARNT-2) after 6 days of compound treatment. A-D. Gene expression was measured by RT-PCR and normalized to beta-actin expression. Results are shown as mean ± s.e.m.

SUPPLEMENTAL MOVIE S1. FGF2 induces branching in primary MECs. Time-lapse imaging of a primary MEC aggregate embedded in Matrigel and grown in the presence of 2.5 nM FGF2 and 0.1% DMSO for 120 hours. MECs initially reorganized to form a fluid-filled cyst, which collapsed near 72 hours in culture and led to extensive branching through 120 hours in culture. Images were captured every 30 minutes.

SUPPLEMENTAL MOVIE S2. 1023 blocks branching of primary MECs. Time-lapse imaging of a primary MEC aggregate embedded in Matrigel and grown in the presence of 2.5 nM FGF2 and 10 μM 1023 for 120 hours. MECs initially reorganized to form a fluid-filled cyst, which continued to grow through 120 hours in culture. Images were captured every 30 minutes.

SUPPLEMENTAL TABLE S2. Primer and shRNA sequences

Primer sequences used for RT-PCR

Target	Forward	Reverse
β-actin	5'-GGCTGTGCTGTCCCTGTATG-3'	5'-CAAGAAGGAAGGCTGGAAAA-3'
Cyp1A1	5'-GGTTAACCATGACCGGGAACT-3'	5'-TGCCCAAACCAAAGAGAGTGA-3'
AHR	5'-CTTTGCTGAACTCGGCTTGC-3'	5'-TTGCTGGGGGCACACCATCT-3'
ARNT	5'-CTAAGAGACAGCTTTCAGCAGGT-3'	5'-AGGGTTTTGGAAGGTAAAGGAG-3'
Dsc1	5'-CAGTAGTGGCGACAGATACA-3'	5'-CCTTCTCCTGCTGACAAATG-3'
Dsg1	5'-GGGATAACCACCATCTGTGT-3'	5'-CCTCCCAGATCTTGCATTTC-3'
Dsg3	5'-AGGTTCTGGCCATAGACGAA-3'	5'-TCACTGAGAGGGTCACAGAA-3'

Oligo and shRNA sequences for shRNA lentiviral plasmids

	Oligo (5'→3')	Mature shRNA
Control Fwd	TGCGCTTGGGCGAGAGTAAGTTCAAGAGACTTACTCTCGCCCAAGC GCTTTTTTC	GCGCTTGGGCGAGAGTAAG
Control Rev	TCGAGAAAAAAGCGCTTGGGCGAGAGTAAGTCTCTTGAAATTACT CTCGCCCAAGCGCA	
shAHR-1 Fwd	TGGACAGAACAAGAAAGGGGTTCAAGAGATCCCTTTCTTGTTCTGT CCTTTTTTC	GGACAGAACAAGAAAGGGG
shAHR-1 Rev	TCGAGAAAAAAGGACAGAACAAGAAAGGGATCTCTTGAACCCCTT TCTTGTTCTGTCCA	
shAHR-2 Fwd	TGGACCAAACACAAGCTAGGTTCAAGAGATCTAGCTTGTGTTTGGT CCTTTTTTC	GGACCAAACACAAGCTAGG
shAHR-2 Rev	TCGAGAAAAAAGGACCAAACACAAGCTAGATCTCTTGAACCTAGC TTGTGTTTGGTCCA	
shARNT-1 Fwd	TGGGAAGAGCTGCAGATATGTTCAAGAGAAATATCTGCAGCTCTTC CCTTTTTTC	GGGAAGAGCTGCAGATATG
shARNT-1 Rev	TCGAGAAAAAAGGGAAGAGCTGCAGATATTTCTCTTGAACATATCT GCAGCTCTTCCCA	
shARNT-2 Fwd	TGGACAGAGATCCAAGGTTGTTCAAGAGAAAACCTTGGATCTCTGT CCTTTTTTC	GGACAGAGATCCAAGGTTG
shARNT-2 Rev	TCGAGAAAAAAGGACAGAGATCCAAGGTTTTCTCTTGAACAACCTT GGATCTCTGTCCA	

SUPPLEMENTAL EXPERIMENTAL PROCEDURES

Mice–FVB/n mice were maintained following protocols reviewed and approved by the University of Utah Institutional Animal Care and Use Committee.

Isolation of primary MECs–Organoids from the fourth inguinal mammary gland were isolated from 8-12 week-old female FVB/n mice as previously described (1). All plasticware was pre-coated with sterile 3% bovine serum albumin (BSA) in phosphate buffered saline (PBS) in order to minimize cell loss during preparation. Organoids were washed once in PBS without calcium or magnesium (Gibco), pelleted at 500 x g for 30 seconds, resuspended in 3 mL of PBS containing 750 µL 0.05% Trypsin/EDTA (Gibco), placed in a 6-well plate (Falcon) and incubated at 37 ºC. Every 3 minutes, cells were pipetted to break up organoids and visualized under a light microscope. This process was repeated until approximately 90% of the organoids dissociated into single cells or for a maximum of 20 minutes to minimize cell death. Hanks' balanced salt solution (HBSS) (Gibco) with 2% fetal bovine serum (FBS) (HyClone) was added to neutralize the trypsin and cells were pelleted (450 x g, 3 minutes). The cell pellet was resuspended in 10 mL serum-free DMEM/F-12 (HyClone) containing 100 µg/mL DNase I (Sigma) and incubated at room temperature for 3 minutes with gentle mixing. Cells were filtered through a 40 µm cell strainer (BD Falcon), counted, pelleted at 450 x g for 3 minutes, and used for branching assays. Extra cells were pelleted and resuspended in DMEM/F-12 containing 20% FBS and 10% DMSO (Sigma) at a concentration of $4x10^6$ cells/mL, and frozen in liquid nitrogen.

Antibody staining–Staining for K8 (Developmental Studies Hybridoma Bank, Troma-1, 1:100) and K14 (Covance, PRB-155P-100, 1:400) was done on sections of mammary gland from virgin FVB/n mice and on primary MECs grown for 144 hours in 8-chamber culture slides (BD Falcon). Staining on sections was done using standard microtome sectioning, deparaffinization and hydration, and antigen retrieval with boiling 10 mM sodium citrate buffer, pH 6.0. For primary MECs, aggregates were embedded as described using 5 µL of Matrigel as the base layer and 200 aggregates suspended in 10 µL Matrigel on top. Aggregates were fixed with 4% PFA for 30 minutes at room temperature (RT), washed three times with PBS, and permeablized with 0.5% triton X-100 (Omnipure) for 90 minutes at RT. All samples were blocked in 5% BSA (Cell Signaling Technologies) + 1% normal goat serum for 1 hour at RT and incubated with primary antibody diluted in 1% BSA overnight at 4 ºC. For HA (Covance, MMS-101R, 1:500) staining, HEK-293T cells were fixed with 4% PFA for 15 minutes at RT, washed once with 50 nM ammonium chloride (Sigma), and permeablized with 0.2% triton X-100 in PBS for 8 minutes at RT. Cells were washed once in 1% BSA in PBS and blocked with fresh 1% BSA in PBS for 10 minutes. Following block, samples were incubated with primary antibody diluted in 1% BSA in PBS for 1 hour at RT. After primary antibody incubations, samples were washed three times with PBS and incubated with secondary antibodies (Invitrogen, Alexa series, all 1:1000 in 1% BSA in PBS) for 1 hour at RT. Nuclei were stained with 50 ng/mL DAPI (Molecular Probes) for 5 minutes at RT. Coverslips were mounted with ProLong Gold anti-fade reagent (Invitrogen).

Chemical compounds–TCDD (Cambridge Isotopes Laboratories, Inc., Andover, MA) was obtained as a DMSO stock solution. 1023 and 1023-CF_3 were synthesized as described below and dissolved in DMSO at a stock concentration of 10 mM.

Chemical synthesis–***(5-(2,4-dichlorophenyl)-3-phenyl-1,2,4-oxadiazole [1023]:*** To a stirring solution of benzamidoxime (500 mg, 3.67 mmol) in dioxane (35 mL), was added 2,4 dichlorobenzoyl chloride (770 mg, 3.67 mmol) followed by BF_3•OEt_2 (114 µL, 0.80 mmol) at 0 °C. The reaction mixture was stirred at room temperature for 30 minutes and heated to reflux for 12 hrs. After completion of the reaction, the dioxane was removed by rotary evaporation and the residue was cooled in an ice bath and quenched with ice water. The aqueous layer was then extracted with EtOAc (2 x 50 ml). The combined organic layers were dried over Na_2SO_4, and concentrated under reduced pressure. The resulting crude product was purified by flash column chromatography (10% EtOAc in hexanes) to yield **1023** (850 mg, 80%) as a colorless solid.

^{1}H NMR (500 MHz, $CDCl_3$) δ 8.18 (dd, J = 7.5, 1.4 Hz, 2H), 8.13 (d, J = 8.3 Hz, 1H), 7.61 (d, J = 1.9 Hz, 1H), 7.56 – 7.70 (m, 3H), 7.43 (dd, J = 8.3, 1.9 Hz, 1H) ppm; ^{13}C NMR (100 MHz, $CDCl_3$): δ (ppm) 137.7, 168.9, 139.2, 134.9, 132.9, 131.6, 131.6, 129.1, 127.8, 126.8, 122.3 ppm; IR (neat) 2152, 1595,

1569, 1452, 1392, 1363, 1135, 1104, 748, 707, 691 cm^{-1}; HRMS (ESI) calcd for $C_{14}H_9Cl_2N_2O$ (M+H): 291.0092, found: 291.0090. Mp; 55-56 ^oC.

(5-(2,4-dichlorophenyl)-3-(3-(trifluoromethyl)phenyl)-1,2,4-oxadiazole [1023-CF_3]: To a stirring solution of 3-trifluorobenzamidoxime (346 mg, 1.69 mmol) in dioxane (17 mL), was added 2,4 dichlorobenzoyl chloride (425 mg, 2.03 mmol) followed by BF_3•OEt_2 (52 µL, 0.42 mmol) at 0 °C. The reaction mixture was stirred at room temperature for 30 minutes and heated to reflux for 12 hrs. After completion of the reaction, the dioxane was removed by rotary evaporation and the residue was cooled in an ice bath and quenched with ice water. The aqueous layer was then extracted with EtOAc (2 x 50 ml). The combined organic layers were dried over Na_2SO_4, and concentrated under reduced pressure. The resulting crude product was purified by flash column chromatography (10 % EtOAc in hexanes) to yield **1023-CF_3** (415 mg, 68%) as a colorless solid.

^1H NMR ($CDCl_3$, 500 MHz) δ 8.45 (s, 1H), 8.36 (d, J= 7.8 Hz, 1H), 8.15 (d, J= 8.2 Hz, 1H), 7.80 (d, J= 7.8 Hz, 1H), 7.68- 7.63 (m, 2H), 7.48- 7.44 (m, 1H) ppm; ^{13}C NMR (400MHz, CDCl3) δ 174.5, 167.9, 139.5, 135.0, 132.9, 131.9, 131.7, 131.6, 130.9, 129.7, 128.1, 128.1, 128.1, 127.9, 127.7, 125.3, 124.8, 124.7, 124.7, 124.7, 122.5, 122.0 ppm; IR (neat) 1590, 1569, 1493, 1390, 1323, 1313, 1169, 1116, 1073, 811, 707 cm^{-1}; HRMS (ESI) calcd for $C_{15}H_8Cl_2N_2OF_3Cl_2$ (M+H): 358.9966, found: 358.9956. Mp; 83-84 ^oC.

Microscopy–Live time-lapse imaging was performed using a Zeiss Axiovert S-100 microscope equipped with a digital CTI-Controller 3700 and Tempcontrol-37-2 to maintain cells at 37 ^oC with 5% CO_2. Images were captured using a 10x A-Plan objective lens every 30 minutes using OpenLab 4.0.2 software (Improvision, Inc.). All other imaging was performed using an Olympus IX81-ZDC microscope with an ORCAER CCD camera and Slidebook 5.0.0.24 software (Intelligent Imaging Innovations, Inc). DIC images were captured using a 10X Plan or 20X long working distance objective lens. Immunofluorescence imaging was performed using a 60X Plan oil objective lens (mammary sections) or 40x U-Plan objective lens (Matrigel samples and AHR nuclear localization). Imaging of single cell primary MEC outgrowths was done using a 20X U-Plan objective lens. For immunofluorescence imaging of Matrigel samples, deconvolution was performed using Slidebook software and the nearest neighbor method.

Microarray processing and analysis–Total RNA was isolated using the Qiagen RNeasy kit and assayed for quality on the Bioanalyzer RNA 6000 nano chip. Samples were labeled with the Agilent Two-Color Low RNA Input Linear Amplification Kit and hybridized to the Agilent Whole Mouse Gene Expression array (Agilent microarray design ID 014868, GEO platform ID GPL7202) using standard Agilent two-color gene expression hybridization and wash protocols. Microarray slides were scanned on an Agilent Technologies G2505B scanner at 5 micron resolution. The slide images were processed using Agilent Feature Extraction software version 9.5.1.1, which performs linear Lowess normalization to correct for dye bias. In this experiment DMSO controls were labeled with Cy3, and compound-treated samples were labeled with Cy5. The Lowess normalized data from the arrays was filtered to remove control features and features flagged as nonuniform or feature population outliers. Remaining features for any probe were averaged to yield a single value for each unique probe sequence. The normalized data set was loaded into GeneSifter software (Geospiza Inc) for analysis. The microarray data from this publication have been submitted to the Gene Expression Omnibus database (http://www.ncbi.nlm.nih.gov/geo/) and assigned the accession number GSE39249.

Sequence alignment and homology modeling of the aryl hydrocarbon receptor (AHR)– Sequences of human AHR (hAHR) (NP_001612) and murine AHR (mAHR) (NP_038492) were extracted from the NCBI protein sequence database. All sequences were imported into the ClustalW program (2) and the sequence alignment editor, BioEdit (3), for multiple pairwise alignments. The resulting alignments were examined manually. hAHR and mAHR had 27% and 50% sequence identity and similarity, respectively, to the solved crystal structure of the high affinity heterodimer of HIF2 alpha and ARNT C-terminal PAS domain (4) (PDB: 3F1O). This crystal structure was used as a template for hAHR homology modeling in ICM. Sequence similarity, 3D-PSSM threading, and ICM searches with hAHR provided the HIF2 alpha and ARNT C-terminal PAS domain as a template structure for homology modeling of hAHR. In the

HIF2 PAS-B Domain, an internal cavity was located using the Site Map with ICM, and electrostatic surfaces were generated using the identified binding sites with ICM force field. A grid spacing of 0.5 Å and dielectric constant of 80 for the solvent were employed.

Molecular docking–**1023** and **1023-CF_3** were used for regular docking with the hAHR homology model. Docking calculations were performed using the ICM (5) docking module with default setup. The structure of each complex was energy minimized in the same environment and saved in PDB format. These energy-minimized complexes were then reposed into ICM and converted into an ICM object, and MMFF charges were assigned for the select ligand. The compounds were docked using the "interactive docking" menu of ICM. A stack of different docked conformations were generated and visually checked. 100 conformers of each ligand docking were performed on a four AMD 64-bit processors Red Hat Linux server. The best docking conformations were selected on the basis of docking energies and RMSD of the ligand from the initial ligand conformation. The docking conformation validated as most realistic for each compound was used for calculation the ligand−hAHR binding energy (Cal. ΔG) using the ICM script for binding energy calculations.

Plasmids–The HA-tagged mouse AHR expression plasmid (pACTAG-HA-mAHR) was kindly provided by Dr. Oliver Hankinson (University of California, Los Angeles, CA). The pLentiLox5.0-GFP vector used for creating lentiviral shRNA constructs was a gift from Dr. James Bear (University of North Carolina, Chapel Hill, NC). The following plasmids for generating lentivirus have been previously described: pMDLg/pRRE (6), pRSV-Rev (6), and pVSV-G (Clontech). The identity of each plasmid was confirmed by sequencing.

AHR nuclear localization assay–In 6-well tissue culture plates, 25,000 HEK-293T cells in DMEM (Gibco) with 10% charcoal-stripped FBS (CSFBS) (Dextran-coated charcoal: Sigma) were seeded onto lysine-coated glass coverslips. The media was replaced 12 hours later with DMEM containing 2% CSFBS, and 2 µg pACTAG-HA-AHR was used for polyethyleneimine (PEI) (Polysciences) mediated transfection as follows. For each well, 6 µg PEI was combined with 200 uL Opti-MEM (Invitrogen), inverted several times to mix, and incubated for 5 minutes at room temperature. Plasmid DNA was added dropwise to the PEI / Opti-MEM solution, mixed by inverting several times, and incubated at RT for 15-45 minutes. Transfection mixtures were added dropwise to each well and mixed with gentle agitation. Media was replaced 16 hours post-transfection and cells were dosed 48 hours post-transfection with 0.1% DMSO (Sigma), 10 µM 1023, or 10 nM TCDD. Samples were stained 24 hours after dosing. For each condition, a minimum of 100 cells per sample were scored.

RNA extraction and real-time PCR–HC11 cells were washed twice with PBS and scraped into 1 mL cold PBS. Cells were pelleted at 1250 x g for 5 minutes at 4 ºC and resuspended in 600 uL RLT buffer (Qiagen). For primary MECs, 1,000 aggregates were embedded per well and three wells were combined for each condition. Cells were washed twice with PBS and suspended in 600 µL RLT buffer (Qiagen) containing beta-mercaptoethanol (BME) (1:100) in order to lyse cells and solubilize Matrigel. RNA was isolated and DNase I treated using the Qiagen RNeasy Mini Kit according to manufacturers instructions. Total RNA was quantified using a Nanodrop (Thermo Scientific) and 1 µg of RNA was used to generate cDNA with the Superscript III Reverse Transcriptase Kit (Invitrogen) according to manufacturers instructions. RNase H (Qiagen) was used to remove excess RNA and cDNA was diluted 1:20 in TE buffer, pH 8.0. For real-time detection, 5 uL reactions were performed with the LightCycler 480 (Roche) in quadruplicate using 2x KAPA SYBR FAST qPCR Master Mix (Kapa Biosystems) and 200 nM each of the forward and reverse PCR primers. Beta-actin was used as an internal reference gene and relative gene expression was calculated by direct CT comparison (7). Primer sequences are listed in supplemental Table S2.

Molecular cloning–For shRNA constructs, oligonucleotides were diluted in TE Buffer pH 8.0 (Ambion) to a final concentration of 60 µM. Forward and reverse primers were combined at a final concentration of 1.2 µM each in annealing buffer (100 mM potassium acetate, 30 mM HEPES-KOH pH 7.4, 2 mM magnesium acetate) and incubated at 95 ºC for 5 minutes followed by stepwise 1 minute incubations at 0.5 ºC temperature decrements until 4 ºC was obtained. The pLentiLox5.0-GFP vector (8) was digested for 1 hour with HpaI-XhoI and dephosphorylated. Annealed oligos were diluted at 1:20 and

ligated overnight at 16 ºC with 50 ng digested pLentiLox5.0-GFP vector. Positive clones were identified using an XbaI restriction digest.

Production and titration of lentivirus–HEK-293T cells were plated on 10-cm tissue culture dishes at $7x10^6$ cells per plate in DMEM (Gibco) with 10% FBS (HyClone) 24 hours prior to transfection. The culture medium was changed 2 hours prior to transfection and a total of 10.1 µg of DNA was used for PEI mediated transfection of each 10-cm dish. For 1 mL transfection mixture per 10-cm plate, 30 µg of PEI was combined with Opti-MEM, inverted several times to mix, and incubated for 5-15 minutes at RT. Plasmids for transfection were combined at the following ratios per 10-cm plate: 5 µg transfer plasmid, 1.7 µg pMDLg/pRRE packaging plasmid, 1.7 µg pRSV-Rev export plasmid, and 1.7 µg pVSVG envelope plasmid. Plasmid DNA was added dropwise to the PEI / Opti-MEM solution, mixed by inverting several times, and incubated at RT for 15-45 minutes. Transfection mixtures were added dropwise to each plate and mixed with gentle agitation. The culture medium was replaced 12 hours after transfection and the viral supernatant was collected 24 and 48 hours later and kept at 4 ºC for all subsequent manipulations. The viral supernatants were cleared of large cell debris by centrifugation at 2450 x g for 10 minutes and filtered through a 0.45 µm cellulose acetate filter (Corning). Viral supernatants were concentrated by ultracentrifugation at 100,000 x g for 1 h 45 min. Viral pellets were resuspended in DMEM/F-12 by gentle pipetting and stored overnight at 4 ºC. The following day, concentrated virus was aliquoted and stored at -80 ºC. Viral titers were determined on HEK-293T cells as previously described with the following modifications (1). In six-well plates, $2x10^5$ cells per well were plated and allowed to adhere for 12 hours. The medium was replaced with 1 mL of either 1:200, 1:1,000, or 1:10,000 diluted viral concentrate. The number of cells per well was counted at the time of virus addition and the average of three wells was used to calculate the viral titer. Culture medium was replaced 12 hours after infection and 60 hours later, cells were harvested and analyzed for fluorescent protein expression by FACS. Viral titers were calculated (TU/ml) according to the equation [cell number x (% fluorescent cells / 100)] x 1000/µl of viral concentrate (9). Only transductions that resulted in fewer than 15% fluorescent cells were used for titer calculations.

HC11 cell culture and production of stable lines–HC11 cells were grown at 37 ºC with 5% CO_2 in RPMI (HyClone) supplemented with 10% FBS, ITS-X, Pen Strep Glutamine, and 10 ng/mL murine EGF. For all compound treatments, FBS was reduced to 2% 12 hours after seeding cells. For stable shRNA expression, $1.25x10^6$ cells were seeded in a 10-cm tissue dish, cultured for 12 hours, and transduced at an MOI of 20. The transduction efficiency was determined by FACS 72 hours after infection and lines with greater than 80% transduction were used for experiments as indicated.

Lentiviral transduction of primary MECs–High efficiency lentiviral transduction of primary MECs was conducted as previously described (10) with the following modifications. Primary MECs were seeded in a 6-well tissue culture plate at a concentration of $2x10^5$ cells per well or a 10-cm tissue culture plate at a concentration of $1x10^6$ cells per plate and incubated in PMEC growth media. After 48 hours, media was aspirated and replaced with 1 mL (6-well plate) or 8 mL (10-cm dish) of fresh PMEC growth media. Lentiviral particles were layered onto primary MECs at a MOI of 40 and gently mixed. After 16 hours, virus-containing media was replaced with 2 mL (6-well plate) or 10 mL (10-cm dish) DMEM/F-12 containing ITS-X, Pen Strep, and 2.5 nM murine EGF or human FGF2. 48 hours later, primary MECs were trypsinized down to single cells, collected, and embedded in Matrigel as described.

RNA isolation from transduced primary MECs–To measure knockdown of AHR in primary cells, MECs were seeded in 10-cm tissue culture plates and transduced as described above. After 96 hours, cells were sorted by FACS based on GFP expression using a FACSAria-II SORP high-speed cell sorter. Untransduced (GFP negative) and transduced (GFP positive) cell populations were collected on ice in RLT buffer. The ratio of sample:RLT was adjusted to 100 uL:350 uL for each sample and RNA was isolated and DNase I treated using the Qiagen RNeasy Mini Kit according to manufacturers instructions.

Western blot–400 µL BD cell recovery solution (BD Biosciences#354253) per well was used to isolate primary MECs from Matrigel according to manufacturers instructions. For each sample, 3 wells of a 24 well plate (1,000 aggregates per well) were combined. Isolated primary MECs were lysed in RIPA buffer (50 mM Tris-HCl pH 8.0, 150 mM NaCl, 0.1% SDS, 0.5% sodium deoxycholate, 1% Triton

X-100, 1 mM DTT, 1X protease/phosphatase inhibitor cocktail) and sonicated at 4 ºC for 20 seconds. 30 µg whole cell lysate was separated by 10% SDS-polyacrylamide gel electrophoresis and transferred to PVDF membrane (Millipore) for detection of mDsg3 (1:200, MBL #D218-3) and α-tubulin (1:1000, Sigma-Aldrich #T6199).

Peptides–The peptides used have been previously described (11): mouse Dsc3 (LIAYASTADG), mouse Dsg3 (ITCRALNALG), E-cadherin (LYSHAVSSNG), and control (YTGDAFPALT). Peptides were synthesized by the University of Utah DNA/Peptide Synthesis Facility (Salt Lake City, UT), purified (>96% purity) by high-performance liquid chromatography, and identified by laser desorption mass spectrometry. Concentrations were determined using Ellman's reagent (12) for mouse Dsg3, which does not contain tryptophan or tyrosine residues, and Edelhoch's method (13) for all other peptides. Freeze-dried peptides were reconstituted in distilled water at a stock concentration of 40 mM.

SUPPLEMENTAL REFERENCES

1. Welm, B. E., Dijkgraaf, G. J., Bledau, A. S., Welm, A. L., and Werb, Z. (2008) *Cell Stem Cell* **2**, 90-102
2. Thompson, J. D., Higgins, D. G., and Gibson, T. J. (1994) *Nucleic Acids Res* **22**, 4673-4680
3. Hall, T. A. (1999) *Nuclei Acids Symposium Series* **41**, 95-98
4. Scheuermann, T. H., Tomchick, D. R., Machius, M., Guo, Y., Bruick, R. K., and Gardner, K. H. (2009) *Proc Natl Acad Sci U S A* **106**, 450-455
5. Totrov, M., and Abagyan, R. (1997) *Proteins* **Suppl 1**, 215-220
6. Dull, T., Zufferey, R., Kelly, M., Mandel, R. J., Nguyen, M., Trono, D., and Naldini, L. (1998) *J Virol* **72**, 8463-8471
7. Schefe, J. H., Lehmann, K. E., Buschmann, I. R., Unger, T., and Funke-Kaiser, H. (2006) *J Mol Med (Berl)* **84**, 901-910
8. Cai, L., Marshall, T. W., Uetrecht, A. C., Schafer, D. A., and Bear, J. E. (2007) *Cell* **128**, 915-929
9. Klages, N., Zufferey, R., and Trono, D. (2000) *Mol Ther* **2**, 170-176
10. Vafaizadeh, V., Klemmt, P., Brendel, C., Weber, K., Doebele, C., Britt, K., Grez, M., Fehse, B., Desrivieres, S., and Groner, B. (2010) *Stem Cells* **28**, 928-938
11. Runswick, S. K., O'Hare, M. J., Jones, L., Streuli, C. H., and Garrod, D. R. (2001) *Nat Cell Biol* **3**, 823-830
12. Riddles, P. W., Blakeley, R. L., and Zerner, B. (1979) *Anal Biochem* **94**, 75-81
13. Edelhoch, H. (1967) *Biochemistry* **6**, 1948-1954

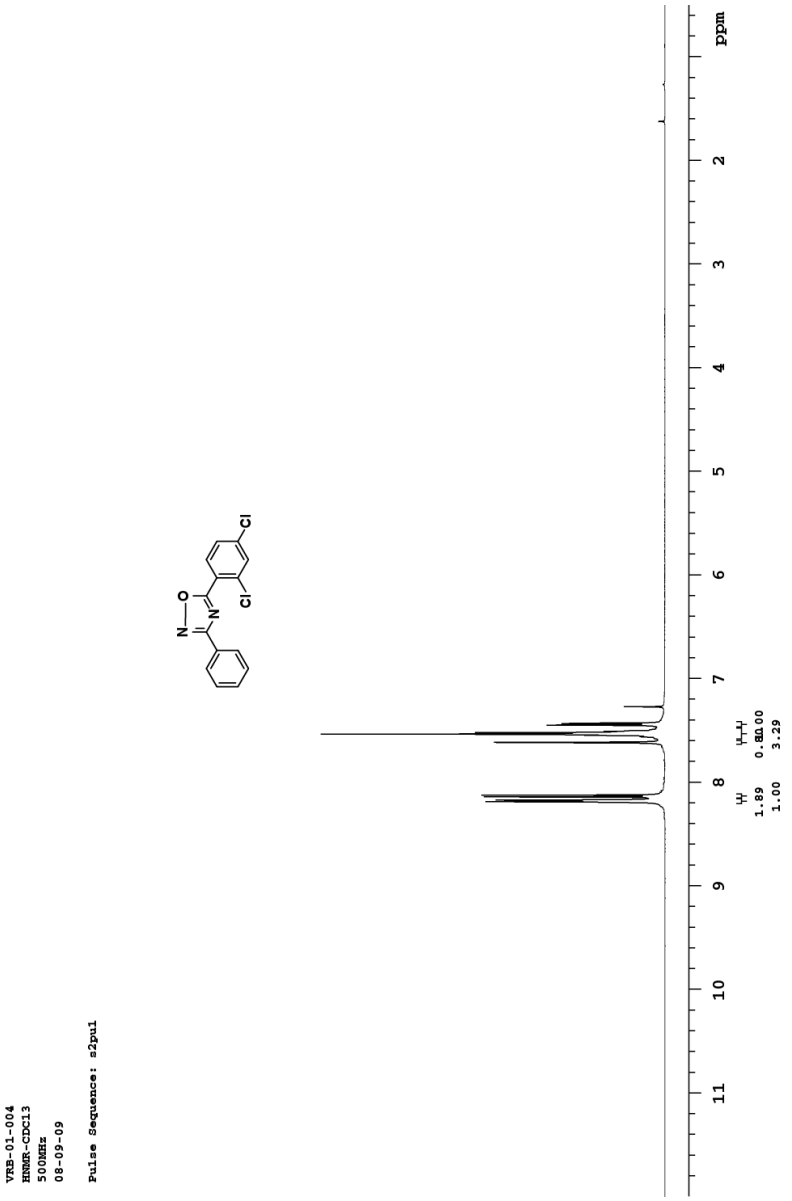
VRB-01-004
HNMR-CDCl3
500MHz
08-09-09
Pulse Sequence: s2pul
Cl
Cl
O
N
N
ppm
1
2
3
4
5
6
7
8
9
10
11
1.89
1.00
0.80
3.29

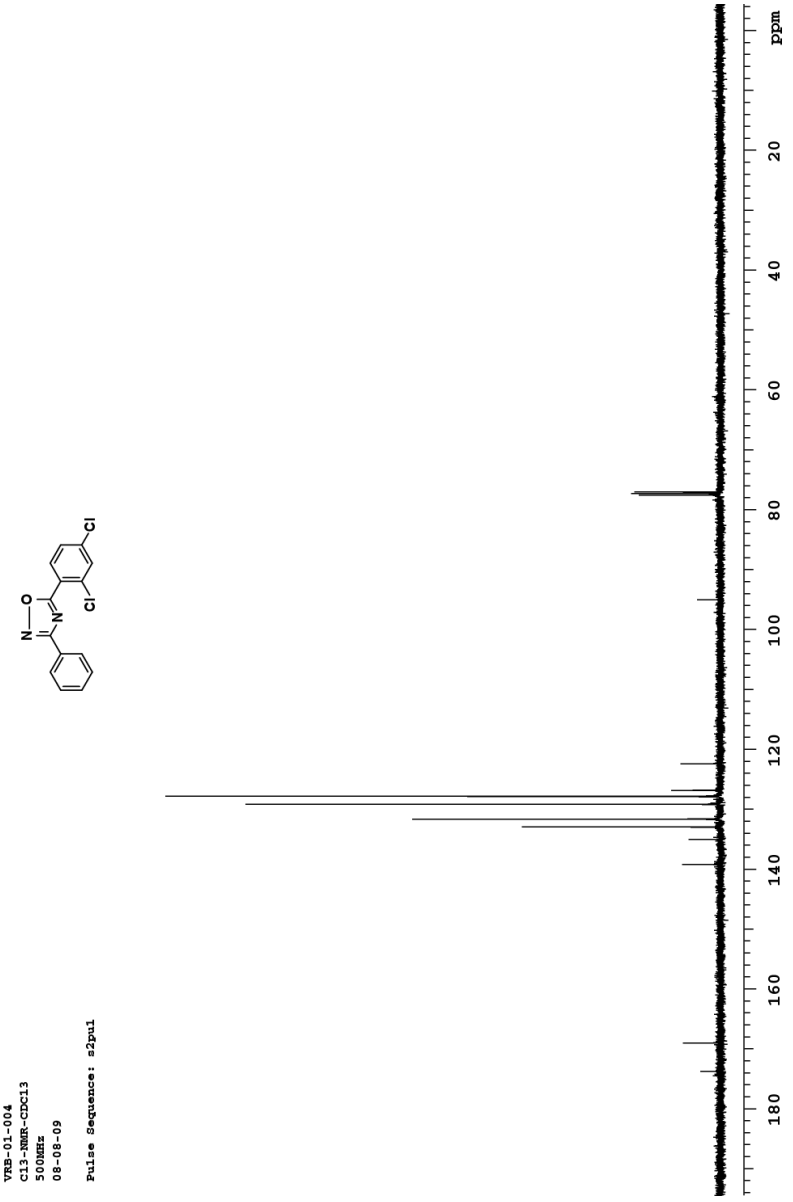
VRB-01-004
C13-NMR-CDC13
500MHz
08-08-09
Pulse Sequence: s2pul
O
N
N
Cl
Cl
ppm
20
40
60
80
100
120
140
160
180

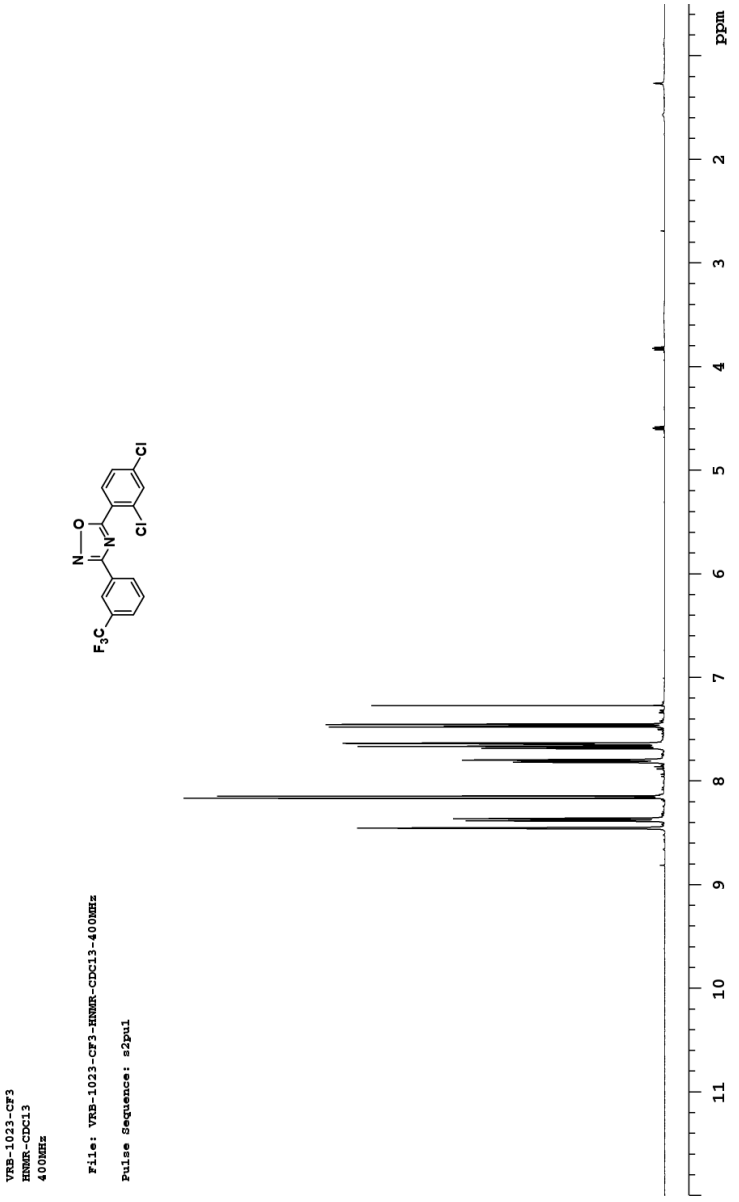
VRB-1023-CF3
HNMR-CDCl3
400MHz
File: VRB-1023-CF3-HNMR-CDCl3-400MHz
Pulse Sequence: s2pul
Cl
Cl
N
O
N
F3C
ppm
11
10
9
8
7
6
5
4
3
2

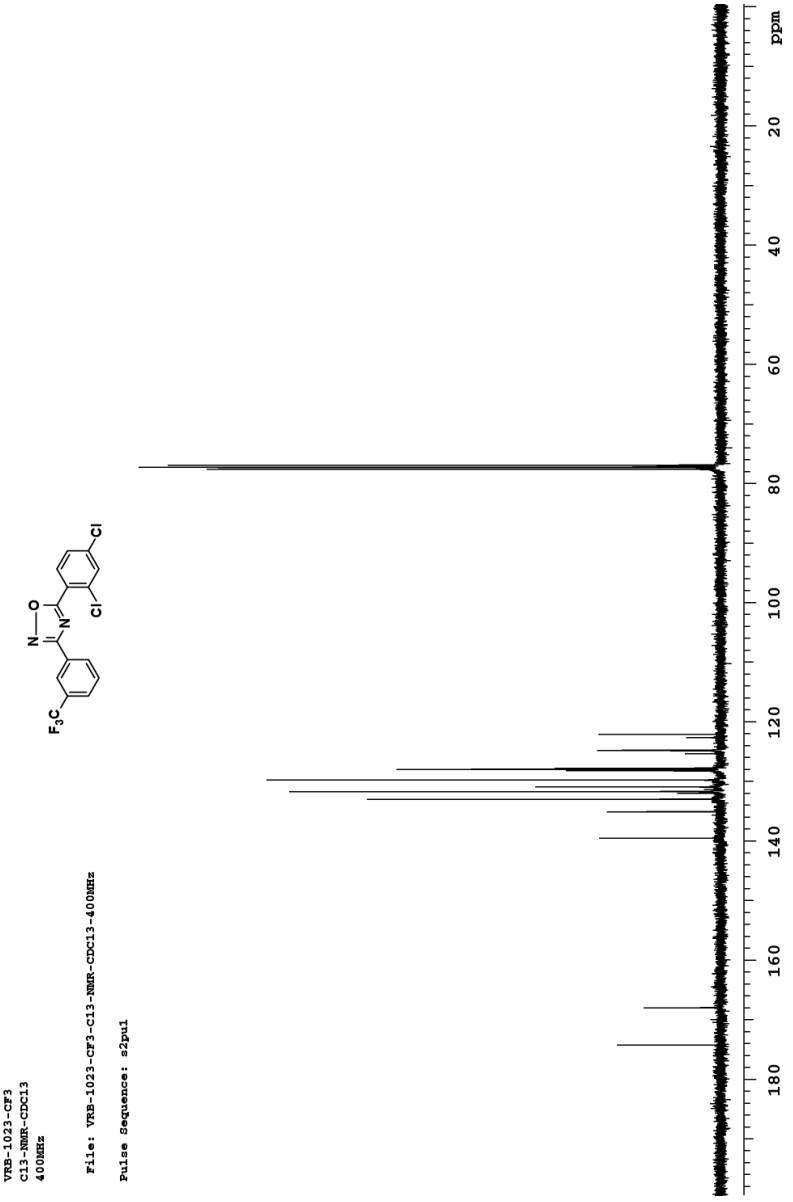
VRB-1023-CF3
C13-NMR-CDC13
400MHz
File: VRB-1023-CF3-C13-NMR-CDC13-400MHz
Pulse Sequence: s2pul
Cl
Cl
O
N
N
F3C
ppm
20
40
60
80
100
120
140
160
180

CHAPTER 3

BIS-ARYLOXADIAZOLES AS EFFECTIVE ACTIVATORS OF THE ARYL HYDROCARBON RECEPTOR

This research was originally published in Bioorganic and Medicinal Chemistry Letters. Kaitlin J. Basham, Vasudev R. Bhonde, Collin Kieffer, James B.C. Mack, Matthew Hess, Bryan E. Welm, and Ryan E. Looper. *Bis*-aryloxadiazoles as effective activators of the aryl hydrocarbon receptor. *Bioorganic and Medicinal Chemistry Letters*. 2014; 24(11): 2473-2476. http://dx.doi.org/10.1016/j.bmcl.2014.04.013.

Reprinted with permission

Graphical Abstract

***Bis*-aryloxadiazoles as effective activators of the aryl hydrocarbon receptor**

Kaitlin J. Basham[a,#], Vasudev R. Bhonde[b,#], Collin Kieffer[a,d], James B.C. Mack[b], Matthew Hess[b], Bryan E. Welm[a,c], and Ryan E. Looper[b,*]

[a]*Department of Oncological Sciences, Huntsman Cancer Institute, University of Utah, Salt Lake City, UT 84112, USA*

[b]*Department of Chemistry, University of Utah, Salt Lake City, UT 84112, USA*

[c]*Department of Surgery, University of Utah, Salt Lake City, UT 84112, USA*

[d]*Present address: Division of Biology, California Institute of Technology, Pasadena, CA 91125, USA*

[#]*These authors contributed equally*

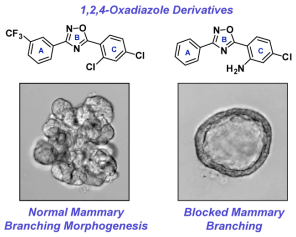

Bioorganic & Medicinal Chemistry Letters 24 (2014) 2473–2476

Contents lists available at ScienceDirect

Bioorganic & Medicinal Chemistry Letters

journal homepage: www.elsevier.com/locate/bmcl

Bis-aryloxadiazoles as effective activators of the aryl hydrocarbon receptor

Kaitlin J. Basham [a,†], Vasudev R. Bhonde [b,†], Collin Kieffer [a,‡], James B. C. Mack [b], Matthew Hess [b], Bryan E. Welm [a,c], Ryan E. Looper [b,*]

[a] Department of Oncological Sciences, Huntsman Cancer Institute, University of Utah, Salt Lake City, UT 84112, USA
[b] Department of Chemistry, University of Utah, Salt Lake City, UT 84112, USA
[c] Department of Surgery, University of Utah, Salt Lake City, UT 84112, USA

ARTICLE INFO

Article history:
Received 31 January 2014
Revised 2 April 2014
Accepted 4 April 2014
Available online 13 April 2014

Keywords:
Oxadiazole
Aryl hydrocarbon receptor
Mammary gland
Branching morphogenesis
Dioxin

ABSTRACT

Bis-aryloxadiazoles are common scaffolds in medicinal chemistry due to their wide range of biological activities. Previously, we identified a 1,2,4-bis-aryloxadiazole that blocks mammary branching morphogenesis through activation of the aryl hydrocarbon receptor (AHR). In addition to defects in mammary differentiation, AHR stimulation induces toxicity in many other tissues. We performed a structure activity relationship (SAR) study of 1,2,4-bis-aryloxadiazole to determine which moieties of the molecule are critical for AHR activation. We validated our results with a functional biological assay, using desmosome formation during mammary morphogenesis to indicate AHR activity. These findings will aid the design of oxadiazole derivative therapeutics with reduced off-target toxicity profiles.

Small molecule libraries are widely used as a tool in chemical biology,[1] both to probe biological pathways and to develop new therapeutics. However, the success of chemical library screening efforts is limited by library composition and size. One strategy to produce a large number of drug-like compounds is to use scaffolds that have previously generated biologically active chemicals.[2] In particular, the oxadiazole nucleus has been used extensively as a scaffold in drug development[3] due to the range of activities reported for its derivatives, including antimicrobial, anticancer, anti-inflammatory, and antiviral effects.[4–7]

As a heteroaromatic ring, oxadiazoles can be prepared as several constitutional isomers. The 1,2,4-oxadiazole isomer has been used in numerous pharmacologic drugs, including metabotropic glutamate subtype 5 receptor antagonists,[8] sphingosine-1-phosphate-1 receptor agonists,[9] and anticancer apoptosis inducers.[10] Additionally, we previously identified a derivative of this isoform as a potent compound that blocks mammary branching morphogenesis.[11] In our assay, 1,2,4-bis-aryloxadiazole **1** (referred as 1023 in our previous communication) was the lead compound identified in a chemical genetic screen for molecules that block mammary branching morphogenesis. Further analysis showed **1** had an EC_{50} of 1.2 ± 0.050 μM and blocked branching through activation of the aryl hydrocarbon receptor (AHR).

In addition to influencing mammary branching, AHR agonists also block differentiation and lactation in the mammary gland[12–14] and exhibit a wide range of toxic effects in other tissues.[15,16] Our previous observations that compound **1** potently activated AHR suggested that other 1,2,4-oxadiazole derivatives may display unwanted drug effects due to AHR stimulation. Given the structural relationship of these derivatives to 2,3,7,8-tetrachlorodibenzo-*p*-dioxin (TCDD), a known carcinogen and environmental toxin that also activates AHR, we performed structure–activity relationship (SAR) studies of **1** to identify key elements of the molecule that contribute to AHR activation. A library of bis-aryloxadiazoles was prepared by Lewis-acid mediated coupling of benzoyl chlorides with benzamidoximes (Scheme 1). The activity of each analog was determined by measuring expression of the AHR target gene, *Cyp1a1*,[17,18] in HC11 mammary epithelial cells (MECs) treated for 48 h with 10 μM compound.

We initially made systematic modifications on the C-ring of **1** (Table 1). Based on a previous homology model,[11] this ring was predicted to form charge/polar interactions with amino acid residues His-291 and Gln-383 in the AHR binding pocket. Our results indicated that replacing the *o*-Cl substituent with an amino group (compound **2**) increased AHR activity ~5-fold, as shown by

* Corresponding author. Tel.: +1 (801) 585 0408.
E-mail address: r.looper@utah.edu (R.E. Looper).
† These authors contributed equally.
‡ Present address: Division of Biology, California Institute of Technology, Pasadena, CA 91125, USA.

http://dx.doi.org/10.1016/j.bmcl.2014.04.013
0960-894X/

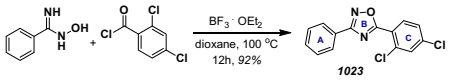

Scheme 1. General strategy for synthesis of bis-aryloxadiazoles.

Table 1
SAR study of the C-ring of 1,2,4-bis-aryloxadiazole

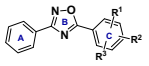

Compound	R^1	R^2	R^3	Relative *Cyp1a1*
1	*o*-Cl	*p*-Cl	H	128.53 ± 0.17
2	*o*-NH_2	*p*-Cl	H	638.80 ± 0.14
3	*o*-NO_2	*p*-CF_3	H	0.36 ± 0.15
4	*o*-NO_2	*p*-OMe	H	0.42 ± 0.25
5	*o*-NO_2	*p*-OH	H	0.25 ± 0.14
6	*o*-NO_2	*p*-OCO_2Me	H	0.39 ± 0.16
7	*o*-NO_2	*p*-*O*-Propargyl	H	2.43 ± 0.19
8	*o*-NO_2	p-F	H	122.64 ± 0.12
9	*o*-NH_2	*p*-CF_3	H	58.63 ± 0.15
10	*o*-Cl	*p*-Cl	*m*-Cl	25.79 ± 0.17

Expression of an AHR response gene, *Cyp1a1*, was measured in HC11 MECs treated with 10 μM compound for 48 h.

increased *Cyp1a1* gene expression with compound **2**. In contrast, placement of an electron-withdrawing group (NO_2) at the *ortho* position of the C-ring dramatically decreased AHR activity (compounds **3**–**7**). These results suggested that the C-ring of bis-aryloxadiazole is compatible with an electroneutral or protic-polar substitution that can be stabilized by hydrogen bonding with His-291 (Fig. 1). This was confirmed by replacing the nitro group at the *ortho* position of compound **3** with an amino group (compound **9**), which partially restored *Cyp1a1* gene expression.

In addition to the *ortho* position, the *para* group of the C-ring also influenced AHR activity. Specifically, *p*-CF_3 (compound **9**) showed significantly lower *Cyp1a1* gene expression compared to *p*-Cl (compound **2**). This result is likely due to the electron withdrawing and sterically bulky nature of CF_3. Surprisingly, *p*-F (compound **8**) offset the decreased activity of *o*-NO_2 observed in other analogs. This may be explained by the small size of *p*-F, which would decrease van der Waals repulsion and contribute to aromatic stabilization through charge interaction. Together, modifications on the C-ring suggested bis-aryloxadiazole requires subtle

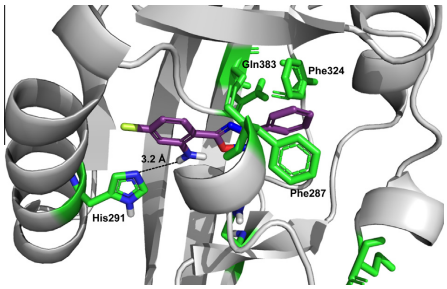

Figure 1. Homology model structure of human AHR (gray) and compound **2** (purple), with residues predicted to contribute to compound binding shown in green. Hydrogen bonding between the amino group at the *ortho* position of the C-ring and His-291 is predicted to stabilize binding.

Table 2
SAR study of the A-ring of 1,2,4-bis-aryloxadiazole

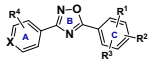

Compound	X	R^1	R^2	R^3	R^4	Relative *Cyp1a1*
11	CH	*o*-Cl	*p*-Cl	H	*m*-CF_3	1.84 ± 0.28
12	CH	*o*-Cl	*p*-Cl	H	*m*-CO_2Me	0.18 ± 0.49
13	CH	*o*-F	H	H	*m*-CO_2Me	0.29 ± 0.74
14	CH	*o*-F	H	H	*m*-CO_2H	3.71 ± 0.22
15	CH	*o*-Cl	*p*-Cl	H	*o*-Cl	5.91 ± 0.18
16	CH	*o*-Cl	*p*-Cl	H	*m*-Cl	1.59 ± 0.30
17	CH	*o*-Cl	*p*-Cl	H	*p*-Cl	8.15 ± 0.14
18	CH	*o*-Cl	*p*-Cl	H	*p*-*O*-Propargyl	0.66 ± 0.26
19	CH	*o*-NO_2	*p*-Cl	H	*p*-*O*-Propargyl	0.29 ± 0.35
20	CH	*o*-NH_2	*p*-Cl	H	*p*-*O*-Allyl	0.62 ± 0.16
21	CH	*o*-NH_2	*p*-Cl	H	*p*-*O*-Propargyl	0.38 ± 0.42
22	N	*o*-Cl	*m*-Cl	*p*-Cl	H	0.53 ± 0.28
23	N	*o*-Cl	*p*-Cl	H	H	0.37 ± 0.13
24	N	*o*-NO_2	*p*-Cl	H	H	8.25 ± 0.13
25	N	*o*-NO_2	*p*-OAc	H	H	0.35 ± 0.41

Expression of an AHR response gene, *Cyp1a1*, was measured in HC11 MECs treated with 10 μM compound for 48 h.

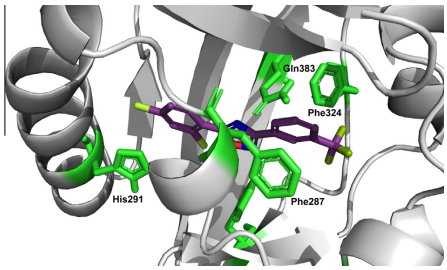

Figure 2. Homology model structure of human AHR (gray) and compound **11** (purple). Residues predicted to contribute to compound binding are shown in green. Steric interactions of the A-ring with Phe324 and Phe287 lead to decreased AHR activation.

electronic demand at the *ortho* and *para* positions and tight van der Waals radii at the *para* position to elicit significant AHR activation.

Next, we extended our SAR study to the A-ring of bis-aryloxadiazole (Table 2). Previous modeling studies[11,19] suggested this portion of the molecule binds within a tight hydrophobic cavity of AHR and is stabilized by aromatic π-stacking of Phe-324 and Phe-287. As a result, we hypothesized that functional groups on the A-ring of bis-aryloxadiazole able to distort this π-stacking would also diminish AHR activation (Fig. 2). Supporting this hypothesis, we previously showed that addition of *m*-CF_3 to the A-ring (compound **11**) dramatically decreased AHR activity.[11] Similarly, polar carbomethoxy or carboxylate substituents at R_4 (compounds **12**–**14**) showed low *Cyp1a1* gene expression, irrespective of identities at R_1 and R_2. Importantly, these substitution patterns are seen in lead compounds for the treatment of nonsense mutation disorders (e.g., Ataluren).[20]

In addition to *meta* substitutions, we altered other positions of the A-ring and modified the A-ring itself. Substitution of CF_3 with Cl at different positions resulted in only subtle AHR activation, with *p*-Cl showing the highest *Cyp1a1* gene induction (compound **15**–**17**). Similarly, larger *para*-substituents on the A-ring (compounds **18**–**21**) or substitution of the A-ring with a heterocycle

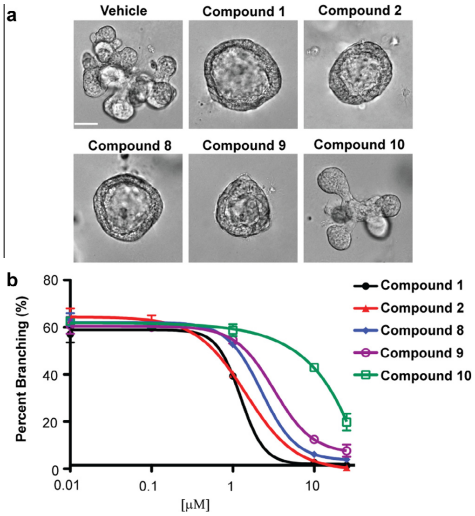

Figure 3. Characterization of mammary branching morphogenesis in the presence of 1,2,4-bis-aryloxadiazole analogs. (a) Representative images and (b) dose–response analysis for branching in primary MECs. Scale bar = 40 μm. Calculated EC_{50} values: compound **1** (1.2 ± 0.4 μM), compound **2** (1.4 ± 0.1 μM), compound **8** (2.2 ± 0.1 μM), compound **9** (3.2 ± 0.1 μM), compound **10** (>10 μM).

(pyridine) nearly abolished AHR activity (compounds **22**–**25**). Taken together, these results show that any modification of the A-ring of bis-aryloxadiazole has a profound effect on AHR binding and activation.

From our SAR study, we identified 4 analogs of 1,2,4-bis-aryloxadiazole that retained significant *Cyp1a1* gene expression (compounds **2**, **8**, **9**, and **10**). We next validated these compounds as AHR agonists in a functional biological assay. Previously, we showed **1** potently blocked mammary branching morphogenesis of primary MECs.[11] Using this same assay, we observed that compounds **2**, **8**, and **9** recapitulated the unbranched, cyst phenotype (Fig. 3a) and displayed an EC_{50} similar to compound **1** (Fig. 3b). In contrast, compound **10**, which induced the lowest level of *Cyp1a1* gene expression compared to the other active analogs, did not inhibit branching and displayed a relatively high EC_{50} (Fig. 3).

Finally, we assessed the level of desmosomal adhesion in primary MECs treated with compounds **2**, **8**, **9**, and **10**. We previously identified desmosomes as a novel target of activated AHR, which functionally disrupts mammary branching morphogenesis.[11] Using desmoglein 3 (DSG3) protein levels as an indicator of desmosome complexes,[21] we observed high levels of desmosomal proteins in primary MECs treated with 10 nM TCDD, which is a known AHR agonist, and 10 μM of compounds **1**, **2**, **8**, and **9** (Fig. 4a and b). Interestingly, compounds **10** and **11** showed the lowest levels of DSG3, which correlated with their low *Cyp1a1* gene expression levels and poor EC_{50} values in our branching assay (Fig. 4b and c). The shared patterns of *Cyp1a1* gene expression and DSG3 protein levels in these biological assays suggest DSG3 is a functional indicator of AHR activity.

In summary, we performed SAR studies of 1,2,4-bis-aryloxadiazole to identify components of the molecule critical for AHR activation. Our results indicated the C-ring is agonistic when substituted with electronically neutral or protic-polar moieties, particularly when tight van der Waals radii at the *para* position are maintained. In contrast, modification of the A-ring dramatically reduced AHR activity in all cases, suggesting this portion of the molecule significantly contributes to AHR binding and activation. These findings indicate that chemical substitutions of the A-ring that minimize AHR activation, but do not significantly alter therapeutic activity, should be considered for bis-aryloxadiazole compounds. We validated our findings by assessing the biological effects of these compounds on mammary branching morphogenesis. In agreement with our previous observations, there was a

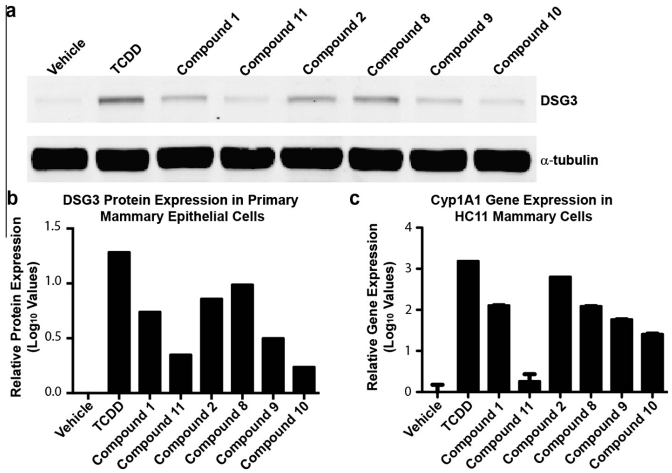

Figure 4. Effect of analog compounds on desmosomal adhesion and AHR readout genes in MECs. (a) Western blot analysis and (b) quantification of desmoglein 3 (DSG3) in primary MECs. (c) Relative *Cyp1a1* gene expression in HC11 MECs.

strong correlation between *Cyp1a1* induction, activation of desmosomal adhesion, and a block in mammary branching morphogenesis. Since loss of desmosomes is sufficient for mammary branching,[11] these results identified DSG3 as a functional readout of AHR activation. These results will aid the design and use of 1,2,4-bis-aryloxadiazoles in order to maintain biological activity of therapeutics while minimizing the activation of AHR.

Acknowledgments

We thank Prof. David J. Bearss and Dr. Hariprasad Vankayalapati at the Center for Investigational Therapeutics, Huntsman Cancer Institute, for the modeling studies of compound **1** with human AHR. National Institutes of Health (R01-GM090082, R01-CA143815, R01-CA140296) and the Department of Defense Breast Cancer Research Program (W81XWH-09-1-04310) supported this work. K.J.B. is supported by National Institutes of Health Developmental Biology Training Grant 5T32 HD07491.

Supplementary data

Supplementary data associated with this article can be found, in the online version, at http://dx.doi.org/10.1016/j.bmcl.2014.04.013.

References and notes

1. Mayr, L. M.; Bojanic, D. *Curr. Opin. Pharmacol.* **2009**, *9*, 580.
2. Welsch, M. E.; Snyder, S. A.; Stockwell, B. R. *Curr. Opin. Chem. Biol.* **2010**, *14*, 347.
3. Bostrom, J.; Hogner, A.; Llinas, A.; Wellner, E.; Plowright, A. T. *J. Med. Chem.* **1817**, *2012*, 55.
4. Summa, V.; Petrocchi, A.; Bonelli, F.; Crescenzi, B.; Donghi, M.; Ferrara, M.; Fiore, F.; Gardelli, C.; Gonzalez Paz, O.; Hazuda, D. J.; Jones, P.; Kinzel, O.; Laufer, R.; Monteagudo, E.; Muraglia, E.; Nizi, E.; Orvieto, F.; Pace, P.; Pescatore, G.; Scarpelli, R.; Stillmock, K.; Witmer, M. V.; Rowley, M. *J. Med. Chem.* **2008**, *51*, 5843.
5. Pace, A.; Pierro, P. *Org. Biomol. Chem.* **2009**, *7*, 4337.
6. Kumar, D.; Patel, G.; Johnson, E. O.; Shah, K. *Bioorg. Med. Chem. Lett.* **2009**, *19*, 2739.
7. Somani, R. R.; Bhanushali, U. V. *Indian J. Pharm. Sci.* **2011**, *73*, 634.
8. Roppe, J.; Smith, N. D.; Huang, D.; Tehrani, L.; Wang, B.; Anderson, J.; Brodkin, J.; Chung, J.; Jiang, X.; King, C.; Munoz, B.; Varney, M. A.; Prasit, P.; Cosford, N. D. *J. Med. Chem.* **2004**, *47*, 4645.
9. Li, Z.; Chen, W.; Hale, J. J.; Lynch, C. L.; Mills, S. G.; Hajdu, R.; Keohane, C. A.; Rosenbach, M. J.; Milligan, J. A.; Shei, G. J.; Chrebet, G.; Parent, S. A.; Bergstrom, J.; Card, D.; Forrest, M.; Quackenbush, E. J.; Wickham, L. A.; Vargas, H.; Evans, R. M.; Rosen, H.; Mandala, S. *J. Med. Chem.* **2005**, *48*, 6169.
10. Zhang, H. Z.; Kasibhatla, S.; Kuemmerle, J.; Kemnitzer, W.; Ollis-Mason, K.; Qiu, L.; Crogan-Grundy, C.; Tseng, B.; Drewe, J.; Cai, S. X. *J. Med. Chem.* **2005**, *48*, 5215.
11. Basham, K. J.; Kieffer, C.; Shelton, D. N.; Leonard, C. J.; Bhonde, V. R.; Vankayalapati, H.; Milash, B.; Bearss, D. J.; Looper, R. E.; Welm, B. E. *J. Biol. Chem.* **2013**, *288*, 2261.
12. Collins, L. L.; Lew, B. J.; Lawrence, B. P. *Reprod. Toxicol.* **2009**, *28*, 11.
13. Lew, B. J.; Manickam, R.; Lawrence, B. P. *Biol. Reprod.* **2011**, *84*, 1094.
14. Vorderstrasse, B. A.; Fenton, S. E.; Bohn, A. A.; Cundiff, J. A.; Lawrence, B. P. *Toxicol. Sci.* **2004**, *78*, 248.
15. Furness, S. G.; Whelan, F. *Pharmacol. Ther.* **2009**, *124*, 336.
16. Mandal, P. K. *J. Comp. Physiol. B.* **2005**, *175*, 221.
17. Tijet, N.; Boutros, P. C.; Moffat, I. D.; Okey, A. B.; Tuomisto, J.; Pohjanvirta, R. *Mol. Pharmacol.* **2006**, *69*, 140.
18. Whitlock, J. P., Jr. *Annu. Rev. Pharmacol. Toxicol.* **1999**, *39*, 103.
19. Motto, I.; Bordogna, A.; Soshilov, A. A.; Denison, M. S.; Bonati, L. *J. Chem. Inf. Model.* **2011**, *51*, 2868.
20. Welch, E. M.; Barton, E. R.; Zhuo, J.; Tomizawa, Y.; Friesen, W. J.; Trifillis, P.; Paushkin, S.; Patel, M.; Trotta, C. R.; Hwang, S.; Wilde, R. G.; Karp, G.; Takasugi, J.; Chen, G.; Jones, S.; Ren, H.; Moon, Y. C.; Corson, D.; Turpoff, A. A.; Campbell, J. A.; Conn, M. M.; Khan, A.; Almstead, N. G.; Hedrick, J.; Mollin, A.; Risher, N.; Weetall, M.; Yeh, S.; Branstrom, A. A.; Colacino, J. M.; Babiak, J.; Ju, W. D.; Hirawat, S.; Northcutt, V. J.; Miller, L. L.; Spatrick, P.; He, F.; Kawana, M.; Feng, H.; Jacobson, A.; Peltz, S. W.; Sweeney, H. L. *Nature* **2007**, *447*, 87.
21. Garrod, D.; Chidgey, M. *Biochim. Biophys. Acta* **2008**, *1778*, 572.

Supporting Information

Bis-aryloxadiazoles as effective activators of the aryl hydrocarbon receptor

Kaitlin J. Basham[a,#], Vasudev R. Bhonde[b,#], Collin Kieffer[a], James B.C. Mack[b], Matthew Hess[b], Bryan E. Welm[a,c], and Ryan E. Looper[b,*]
[a]*Department of Oncological Sciences, Huntsman Cancer Institute, University of Utah, Salt Lake City, UT 84112, USA*
[b]*Department of Chemistry, University of Utah, Salt Lake City, UT 84112, USA*
[c]*Department of Surgery, University of Utah, Salt Lake City, UT 84112, USA*
[#]*These authors contributed equally*

1. Chemistry:

2. Biological Experiments:

1. Chemistry

A. General experimental considerations:

All reactions requiring anhydrous conditions were conducted in flame-dried glassware under a positive pressure of either nitrogen or argon. Commercially available reagents were used as received; otherwise, materials were purified according to *Purification of Laboratory Chemicals*.[1] Dichloromethane (CH_2Cl_2), acetonitrile (CH_3CN) tetrahydrofuran (THF) diethyl ether (Et_2O) were degassed with nitrogen and passed through a solvent purification system (Innovative Technologies Pure Solv). Triethylamine (Et_3N) was distilled from CaH_2 immediately prior to use. Reactions were monitored by TLC and visualized by a dual short wave/long wave UV lamp and stained with aqueous solution of ceric ammonium molybdate. Flash chromatography was performed on Merck silica gel Kieselgel 60 (230-400 mesh) from EM Science with the indicated HPLC grade solvent.

Infrared spectra were obtained using a Nicolet 380-FT IR spectrometer fitted with a Smart Orbit sample system. Mass spectra were determined on a Micromass Quattro II (ESI/APCI-TOF) for HRMS at the University of Utah Mass Spectrometry Facility. ^{1}H NMR and ^{13}C NMR spectra were recorded at 500 MHz and 125 MHz, respectively. Proton resonances were reported relative to the deuterated solvent peak: 7.27 ppm for $CDCl_3$ 7.15 ppm for C_6D_6, 3.31 ppm (center line signal) for CD_3OD and 4.80 ppm for D_2O using the following format: chemical shift (δ) (multiplicity (s= singlet, brs= broad singlet, d= doublet, dd= double of doublet, ddd= double of doublet of doublet, dddd= double of doublet of doublet of doublet, t= triplet, dtt= doublet of triplet of triplet, q= quartet, m= multiplet), coupling constant(s) *J* in Hz, integration).[2] Carbon resonances were reported as chemical shifts (δ) in parts per million, relative to the center line signal of the respective solvent peak: 77.23 ppm for $CDCl_3$, 128.0 ppm for C_6D_6 and 49.15 ppm for CD_3OD and 164.2 ppm for TFA.

[1] *Purification of Laboratory Chemicals*. 2003, 5th Ed. Armarego, W. L. F.; Chai, C. L. L.
[2] Hoye, T.R.; Hansen, P.R.; Vyvyan, J.R. *J. Org. Chem.* **1994**; *59*(15); 4096-4103.

B. Experimental procedures

General procedure for the preparation of the *bis*-aryloxadiazoles

5-(2,4-dichlorophenyl)-3-phenyl-1,2,4-oxadiazole (1)

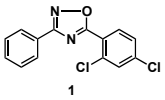

1

To a solution of benzamidoxime (500 mg, 3.67 μmol) in dioxane (35 mL) at 0 °C was added 2, 4-dichlorobenzoyl chloride (770 mg, 3.67 mmol) and BF_3•OEt_2 (114 μL, 0.80 mmol). The reaction mixture was stirred at rt for 30 min and heated to reflux for 12 h. The volatiles were evaporated under reduced pressure and the residue was cooled in an ice bath and diluted with ice-water (25 mL). This solution was then transferred to a separatory funnel and the aqueous layer was extracted with EtOAc (2 × 50 ml). The combined organic layers were dried over Na_2SO_4 and concentrated under reduced pressure. The resulting crude product was purified by flash column chromatography (10% EtOAc in hexanes) to yield *bis*-aryl oxadiazole **1** (850 mg, 80%) as a colorless solid.

Mp = 80 - 81 °C; ^{1}H NMR ($CDCl_3$, 500 MHz) δ 8.18 (dd, *J* = 7.5, 1.4 Hz, 2H), 8.13 (d, *J* = 8.3 Hz, 1H), 7.61 (d, *J* = 1.9 Hz, 1H), 7.56 - 7.70 (m, 3H), 7.43 (dd, *J* = 8.3, 1.9 Hz, 1H) ppm; ^{13}C NMR ($CDCl_3$, 100 MHz) δ 137.7, 168.9, 139.2, 134.9, 132.9, 131.6, 131.6, 129.1, 127.8, 126.8, 122.3 ppm; IR (neat) 2152, 1595, 1569, 1452, 1392, 1363, 1135, 1104, 748, 707, 691 cm^{-1}; HRMS (ESI) calcd for $C_{14}H_9Cl_2N_2O$ (M+H): 291.0092, found: 291.0090.

5-chloro-2-(3-phenyl-1,2,4-oxadiazol-5-yl)aniline (2)

5-(4-chloro-2-nitrophenyl)-3-phenyl-1,2,4-oxadiazole (2SM)

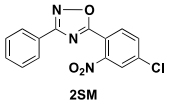

2SM

Mp = 104 - 105 °C; ^{1}H NMR (DMSO-d_6, 300 MHz) δ 8.16 - 8.12 (m, 2H), 8.03- 7.99 (m, 2H), 7.78 (dd, *J* = 8.3, 2.0 Hz, 1H), 7.58 - 7.48 (m, 3H) ppm; ^{13}C NMR ($CDCl_3$, 125 MHz) δ 171.6, 169.3, 149.4, 139.6, 133.1, 132.4, 131.8, 129.1, 127.8, 126.3, 125.1, 117.4 ppm; IR (neat) 3099, 2359, 2341, 1574, 1538, 1445, 1321, 1288, 1134, 1114 cm^{-}

^{1}; ESI-MS m/z 302.0 $[M+H]^{+}$.

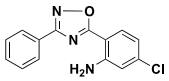

2

To a solution of nitro-oxadiazole **2SM** (455 mg, 1.51 mmol) obtained above in EtOH (25 mL) was added $SnCl_2 \bullet 2H_2O$ (858 mg, 4.48 mmol) and the resultant solution was heated to reflux for 3h. The volatiles were evaporated under reduced pressure and the residue obtained was diluted with water (20 mL) and basified (pH ≈ 12) with saturated aq. $NaHCO_3$ (10 mL). This solution was transferred to a separatory funnel and extracted with CH_2Cl_2 (4 × 25 mL). The combined organic layers were dried over Na_2SO_4 and concentrated under reduced pressure to afford the amino-oxadiazole **2** (275 mg, 88%) as an off-white solid.

Mp = 165 - 166 °C; ^{1}H NMR ($CDCl_3$, 300 MHz) δ 8.17 - 8.12 **(**m, 2H**),** 8.94 (d, *J* = 8.5, 1H), 7.58 - 7.48 (m, 3H), 6.84 (d, *J* = 1.9 Hz, 1H), 6.78 (dd, *J* = 8.5, 1.9 Hz, 1H), 6.09 (bs, 2H) ppm; ^{13}C NMR ($CDCl_3$, 125 MHz) δ 174.4, 168.1, 148.5, 140.1, 131.4, 130.6, 129.0, 127.7, 126.9, 117.8, 116.1, 104.7 ppm; IR (neat) 3422, 3329, 1628, 1613, 1604, 1566, 1546, 1375, 1251 cm^{-1}; ESI-MS m/z 272.0 $[M+H]^{+}$.

5-(2-nitro-4-(trifluoromethyl)phenyl)-3-phenyl-1,2,4-oxadiazole (3)

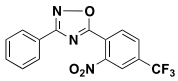

3

Mp = 102 -104 °C; ^{1}H NMR ($CDCl_3$, 500 MHz) δ□8.72 (d, *J* = 1.5Hz, 1H), 8.56 - 8.53 (m, 1H), 8.18- 8.16 (m, 1H), 8.17 (dd, *J* = 8.0, 1.5Hz, 1H), 8.06 (d, *J* = 8.0Hz, 1H), 7.59 - 7.52 (m, 3H) ppm; ^{13}C NMR ($CDCl_3$, 125 MHz) δ 172.3, 169.7, 129.4 (q, *J* = 7.2 Hz), 129.3 (q, *J* = 19.8 Hz), 129.2, 127.7, 127.0, 126.8, 126.1, 124.6, 121.6 (q, *J* = 273.9 Hz) ppm; IR (neat) 2359, 2342, 1733, 1646, 1575, 1541, 1506, 1472, 668 cm^{-1}.

5-(4-methoxy-2-nitrophenyl)-3-phenyl-1,2,4-oxadiazole (4)

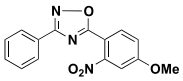

4

Mp = 102 - 104 °C; ^{1}H NMR ($CDCl_3$, 300 MHz) δ□8.16 - 8.11 (m, 2H), 7.99 (d, *J* = 8.7 Hz, 1H), 7.55- 7.47 (m, 2H), 7.45 (d, *J* = 4.5 Hz, 2H), 7.27 (s, 1H), 7.26 (dd, *J* = 8.7, 2.7 Hz, 1H), 3.98 (s, 3H) ppm; ^{13}C NMR ($CDCl_3$, 125 MHz) δ 172.4, 169.1, 163.1, 150.4, 132.7, 131.6, 129.1, 127.8, 126.7, 118.2, 110.8, 110.3, 56.5 ppm; IR (neat) 3079, 3019, 2844, 2359, 2341, 1617, 1538, 1497, 1443, 1360, 1290, 1245, 1135, 1030, 751 cm^{-1}.

3-nitro-4-(3-phenyl-1,2,4-oxadiazol-5-yl)phenol (5)

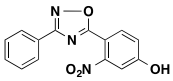

5

To a solution of methyl carbonate **6** (250 mg, 0.76 mmol) in EtOH: H_2O (3:2, 10 mL) was added crushed NaOH (91 mg, 2.28 mmol) at rt and the resultant solution was stirred for 2h. The volatiles were evaporated under reduced pressure and the residue obtained was diluted with water (10 mL) and extracted with CH_2Cl_2 (2 × 25 mL). The combined organic layers were dried over Na_2SO_4 and concentrated under reduced pressure to afford the nitro-phenol **5** (175 mg, 82%) as a yellow solid.

Mp = 260 - 262 °C; ^{1}H NMR (DMSO-d_6, 300 MHz) δ 8.62 (d, *J* = 1.5 Hz, 1H), 8.45 (dd, *J* = 8.0, 1.5, 1H), 8.32 (d, *J* = 7.9 Hz, 1H), 8.10 - 8.05 (m, 2H), 7.69- 7.59 (m, 3H) ppm; ^{13}C NMR ($CDCl_3$, 125 MHz) δ 171.9, 168.3, 164.7, 135.9, 135.9, 133.8, 132.2, 129.4, 127.1, 125.4, 125.2, 120.7 ppm; IR (neat) 3057, 1703, 1548, 1445, 1426, 1357, 1288 cm^{-1}.

methyl (3-nitro-4-(3-phenyl-1,2,4-oxadiazol-5-yl)phenyl) carbonate (6)

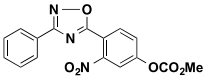

6

Mp = 116 - 118 °C; ^{1}H NMR ($CDCl_3$, 500 MHz) δ 8.64 (d, *J* = 1.5 Hz, 1H), 8.63 (dd, *J* = 8.1, 1.8 Hz, 1H), 8.16 - 8.13 (m, 3H), 7.58 - 7.49 (m, 3H), 4.03 (s, 3H) ppm; ^{13}C NMR ($CDCl_3$, 125 MHz) δ 171.7, 169.4, 164.1, 149.0, 134.9, 133.5, 131.8, 131.8, 129.2, 127.8, 126.2, 125.7, 122.5, 53.4 ppm; IR (neat) 3087, 2955, 1731, 1543, 1445, 1358, 1288, 1256, 1117 cm^{-1}.

5-(2-nitro-4-(prop-2-ynyloxy)phenyl)-3-phenyl-1,2,4-oxadiazole (7)

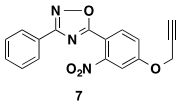
7

Mp = 111 - 113 °C; ^{1}H NMR ($CDCl_3$, 300 MHz) δ 8.66 (d, *J* = 1.6 Hz, 1H), 8.47 (dd, *J* = 8.1, 1.6 Hz, 1H), 8.19 - 8.12 (m, 3H), 7.59 - 7.49 (m, 3H) 5.03 (d, *J* = 2.4 Hz, 2H), 2.62 (t, *J* = 2.4 Hz, 1H) ppm; ^{13}C NMR ($CDCl_3$, 125 MHz) δ 171.5, 169.4, 162.9, 149.1, 134.2, 133.7, 131.9, 129.2, 127.8, 126.1, 125.8, 122.8,76.8, 76.3, 53.9 ppm; IR (neat) 3293, 3091, 1732, 1542, 1357, 1279, 1246, 1113 cm^{-1}.

5-(4-fluoro-2-nitrophenyl)-3-phenyl-1,2,4-oxadiazole (8)

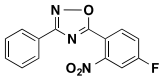
8

Mp = 94 - 95 °C; ^{1}H NMR ($CDCl_3$, 500 MHz) δ 8.14 (dd, *J* = 6.5, 1.5 Hz, 2H), 8.08 (dd, *J* = 9.0, 5.5 Hz, 1H), 7.76 (dd, *J* = 7.2, 4.5 Hz, 1H), 7.56- 7.50 (m, 4H) ppm; ^{13}C NMR ($CDCl_3$, 125 MHz) δ 171.6, 169.2, 165.4, 163.3, 133.6, 133.5, 131.8, 128.4 (d, *J* = 170.4 Hz), 126.3, 120.4 (d, *J* = 21.3 Hz), 115.4, 113.1 (d, *J* = 26.7 Hz) ppm; IR (neat) 3079, 2359, 2341, 1625, 1569, 1541, 1506, 1362, 1267, 1216, 668 cm^{-1}; ESI-MS m/z 286.4 $[M+H]^+$.

2-(3-phenyl-1,2,4-oxadiazol-5-yl)-5-(trifluoromethyl)aniline (9)

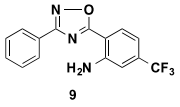
9

To a solution of nitro-oxadiazole **3** in EtOH (210 mg, 0.62 mmol) was added $SnCl_2 \bullet 2H_2O$ (356 mg, 1.88 mmol) and the resultant solution was heated to reflux for 3h. The volatiles were evaporated under reduced pressure and the residue obtained was diluted with water (20 mL) and basified (pH ≈ 12) with saturated aqueous $NaHCO_3$ (10 mL). This solution was transferred to a separatory funnel and extracted with CH_2Cl_2 (4 × 25 mL). The combined organic layers were dried over Na_2SO_4 and concentrated under reduced pressure to afford the amino-oxadiazole **9** (116 mg, 61%) as a yellow solid.

Mp = 146 - 147 °C; ^{1}H NMR ($CDCl_3$, 500 MHz) δ 8.19 - 8.15 (m, 2H), 7.61 (bs, 3H), 7.56 - 7.50 (m, 3H), 4.41 (bs, 2H) ppm; ^{13}C NMR ($CDCl_3$, 125 MHz) δ 174.7, 169.1, 145.0, 131.3, 128.9, 128.1, 127.6 (q, *J* = 8.0 Hz), 127.5, 126.6, 124.3 (q, *J* = 272.3 Hz), 117.0, 116.3, 116.2 ppm; IR (neat) 3369, 3257, 1655, 1581, 1567, 1528, 1509, 1370, 1327, 1092 cm^{-1}; ESI-MS m/z 306 $[M+H]^+$.

3-phenyl-5-(2,4,6-trichlorophenyl)-1,2,4-oxadiazole (10)

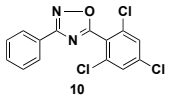
10

Mp = 95 - 96 °C; ^{1}H NMR ($CDCl_3$, 500 MHz) δ 8.24 (d, *J* = 6.8Hz, 2H), 8.19 (m, 2H), 7.63- 7.49 (m, 3H) ppm; ^{13}C NMR ($CDCl_3$, 125 MHz) δ 132.9, 131.7, 131.4, 129.3, 129.2, 129.0, 128.4, 128.3, 127.8, 127.7 ppm; IR (neat) 3366, 3221, 3078, 2360, 2340, 1743, 1634, 1578, 1548, 1410, 1369, 1258, 1114, 1055, cm^{-1}.

5-(2,4-dichlorophenyl)-3-(3-(trifluoromethyl)phenyl)-1,2,4-oxadiazole (11).

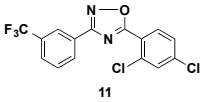
11

Mp =107 - 109 °C; ^{1}H NMR ($CDCl_3$, 500 MHz) δ 8.45 (s, 1H), 8.36 (d, *J* = 7.8 Hz, 1H), 8.15 (d, *J* = 8.2 Hz, 1H), 7.80 (d, *J* = 7.8 Hz, 1H), 7.68 - 7.63 (m, 2H), 7.48 - 7.44 (m, 1H) ppm; ^{13}C NMR ($CDCl_3$, 100 MHz) δ, 174.2, 167.9, 139.5, 135.0, 132.9, 131.9, 131.8 (q, *J* = 16.5 Hz), 130.9, 129.7, 128.1 (q, *J* = 5.7 Hz), 127.9, 127.7, 124.7 (q, *J* = 5.7 Hz), 123.9 (q, *J* = 273.1 Hz), 122.0 ppm; IR (neat) 1590, 1569, 1493, 1390, 1323, 1313, 1169, 1116, 1073, 811, 707 cm^{-1}; HRMS (ESI) calcd for $C_{15}H_8Cl_2N_2OF_3Cl_2$ (M+H): 358.9966, found: 358.9956.

methyl 3-(5-(2,4-dichlorophenyl)-1,2,4-oxadiazol-3-yl)benzoate (12)

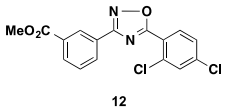
12

Mp = 132 - 133 °C; ^{1}H NMR ($CDCl_3$, 500 MHz) δ 8.84 (d, *J* = 2.0 Hz, 1H), 8.38 (d, *J* = 8.0 Hz, 1H), 8.23 (d, *J* = 8.0 Hz, 1H), 8.17 (d, *J* = 9.0 Hz, 1H), 7.64 - 7.60 (m, 2H), 7.47 (dd, *J* = 8.0, 2.0 Hz, 1H), 4.0 (s, 3H) ppm; ^{13}C NMR ($CDCl_3$, 125 MHz) δ 173.2, 166.4, 162.9, 156.8, 138.8, 133.4, 132.5, 131.7, 131.4, 131.2, 129.3, 127.9, 127.6, 52.62 ppm; IR (neat) 3477, 3352, 2360, 2399, 1723, 1632, 1585, 1272, 1097 cm^{-1}.

methyl 3-(5-(2-fluorophenyl)-1,2,4-oxadiazol-3-yl)benzoate (13)

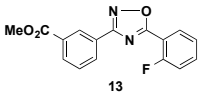

13

Mp = 124 - 126 °C; ^{1}H NMR ($CDCl_3$, 500 MHz) δ 8.81 (s, 1H), 8.33 (d, *J* = 5.2 Hz, 1H), 8.23 - 8.17 (m, 2H), 7.62 - 7.56 (m, 2H), 7.34 - 7.25 (m, 2H), 3.98 (s, 3H) ppm; ^{13}C NMR ($CDCl_3$, 125 MHz) δ 173.3, 168.2,166.5, 162.0, 159.9, 134.9 (d, *J*= 8.3 Hz), 132.4, 131.9, 130.2 (d, *J* = 240.3 Hz), 128.9, 127.4, 124.9, 124.9, 117.4 (d, *J* = 20.6), 112.8 (d, *J* = 11.4 Hz), 52.5 ppm; IR (neat) 1725, 1621, 1472, 1436, 1372, 1293, 1264, 1229 cm^{-1}.

3-(5-(2-fluorophenyl)-1,2,4-oxadiazol-3-yl)benzoic acid (14)

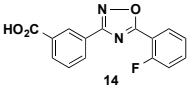

14

To a solution of methyl ester **13** (228 mg, 0.76 mmol) in EtOH: H_2O (3:2, 10 mL) was added crushed NaOH (91 mg, 2.27 mmol) and the solution was stirred at rt for 3h. The volatiles were evaporated under reduced pressure and the residue obtained was acidified with 1N aqueous HCl (pH ≈ 4). This solution was then transferred to a separatory funnel and extracted with EtOAc (3 × 20 mL). The combined organic layers were dried Na_2SO_4 and concentrated under reduced pressure to afford the title acid **14** (123 mg, 54%) as a white solid.

Mp = 239 - 240 °C; ^{1}H NMR (DMSO-d_6, 500 MHz) δ 8.64 (*J* = 1.4 Hz, 1H), 8.33 (ddd, *J* = 7.8, 2.9, 1.4 Hz, 1H), 8.27 (dt, *J* = 7.8, 1.9 Hz, 1H), 8.18 (ddd, *J* = 7.8, 2.9, 1.4 Hz, 1H), 7.83- 7.79 (m, 1H), 7.75 (t, *J* = 7.8 Hz, 1H), 7.57 (dd, *J* = 10.7, 8.7 Hz, 1H), 7.51 (dd, *J* = 7.3, 0.9 Hz, 1H) ppm; ^{13}C NMR (DMSO-d_6, 125 MHz) δ 172.7, 167.4, 166.5, 161.0, 158.9, 135.8 (d, *J* = 9.1 Hz), 132.3, 131.8, 131.0 (d, *J* = 22.8 Hz), 127.8, (d, *J* = 263.9 Hz) 126.3, 125.5, 125.5, 117.5 (d, *J* = 20.6 Hz), 111.7 (d, *J* = 10.6 Hz) ppm; IR (neat) 3145, 2359, 2342, 1733, 1699, 1646, 1575, 1472, 1305, 744, 668 cm^{-1}; ESI-MS m/z 285.1 $[M+H]^+$

5-(2-chlorophenyl)-3-(2,4-dichlorophenyl)-1,2,4-oxadiazole (15)

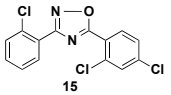

15

Mp = 99 - 101 °C; ^{1}H NMR ($CDCl_3$, 500 MHz) δ 8.16 (d, *J* = 8.3 Hz, 1H), 8.04 (d, *J* = 7.3 Hz, 1H), 7.64 (s, 1H), 7.59 (brd, *J* = 8.3 Hz, 1H), 7.50- 7.42 (m, 3H) ppm; ^{13}C NMR ($CDCl_3$, 125 MHz) δ 173.25, 167.80, 139.38, 135.07, 133.83, 132.98, 132.10, 132.05, 131.70, 131.25, 127.92, 127.18, 126.08, 122.13 ppm; IR (neat) 3076, 2360, 2341, 1698, 1588, 1555, 1476, 1418, 1375, 1311, 1265, 1109, 1052, 908, 868, 838, 771, 755 cm^{-1}; ESI-MS m/z 325.3 $[M+H]^+$.

5-(3-chlorophenyl)-3-(2,4-dichlorophenyl)-1,2,4-oxadiazole (16)

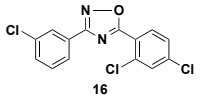

16

Mp = 133 - 134 °C; ^{1}H NMR (500 MHz, $CDCl_3$) δ 8.14 (t, *J* = 1.8 Hz, 1H), 8.10 (d, *J* = 8.4 Hz, 1H), 8.03 (*J* = 7.6, 1.34Hz, 1H), 7.59 (d, *J* = 2.1 Hz, 1H), 7.49 (ddd *J* = 7.9, 2.1, 1.1, 1H), 7.44 - 7.41 (m, 2H); ^{13}C NMR (125 MHz, $CDCl_3$) δ 173.9, 167.9, 139.4, 135.2, 135.0, 132.9, 131.7, 131.6, 130.4, 128.5, 127.9, 127.8, 125.8, 122.0 ppm; IR (neat) 3086, 1592, 1566, 1536, 1522, 1477, 1457, 1437, 1388, 1363, 1298, 1145, 1105, 1086, 1051, 892, 872, 839, 816, 792, 771, 757, 719, 674 cm^{-1}; ESI-MS m/z 325.2 $[M+H]^+$.

5-(4-chlorophenyl)-3-(2,4-dichlorophenyl)-1,2,4-oxadiazole (17)

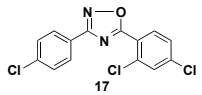

17

Mp 143 - 144 °C; ^{1}H NMR ($CDCl_3$, 500 MHz) δ 8.13- 8.10 (m, 3H), 7.62 (d, *J* = 1.95 Hz, 1H), 7.54- 7.49 (m, 3H) ppm; ^{13}C NMR ($CDCl_3$, 125 MHz) δ 139.5, 132.9, 131.6, 129.4, 129.0, 127.9, 125.3, 122.1, 95.2 ppm; IR (neat) 3079, 2359, 1703, 1592, 1410, 759 cm^{-1}; ESI-MS m/z 325.3 $[M+H]^+$.

5-(2,4-dichlorophenyl)-3-(4-(prop-2-ynyloxy)phenyl)-1,2,4-oxadiazole (18)

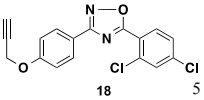

18

Mp = 139 - 141 °C; ^{1}H NMR ($CDCl_3$, 300 MHz) δ 8.13 (d, *J* = 8.9 Hz, 2H), 8.12 (d, *J* = 8.5 Hz, 1H), 7.62 (d, *J* = 2.0 Hz, 1H), 7.44 (dd, *J* = 8.5, 2.0 Hz, 1H),

7.11 (d, *J* = 8.9 Hz, 2H), 4.78 (d, *J* = 2.3 Hz, 2H), 2.57 (t, *J* = 2.3 Hz, 1H) ppm; ^{13}C NMR (DMSO-d_6, 125 MHz) δ 173.5, 168.5, 160.1, 139.1, 134.9, 132.8, 131.6, 129.4, 127.8, 122.4, 120.1, 115.4, 78.1, 76.2, 56.0 ppm; IR (neat): 3302, 3090, 1614, 1587, 1570, 1388, 1251 cm^{-1}; ESI-MS m/z 345 $[M+H]^+$.

5-(4-chloro-2-nitrophenyl)-3-(4-(prop-2-ynyloxy)phenyl)-1,2,4-oxadiazole (19)

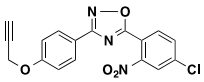

19

Mp = 133 - 134 °C; ^{1}H NMR ($CDCl_3$, 500 MHz) δ 8.08 (d, *J* = 9.5 Hz, 2H), 8.00 (d, *J* = 8.5 Hz, 1H), 7.98 (d, *J* = 2.5 Hz, 1H), 7.78 (dd, *J* = 8.5, 2.0 Hz, 1H), 7.10 (d, *J* = 9.5 Hz, 2H), 4.78 (d, *J* = 2.5 Hz, 2H), 2.57 (t, *J* = 2.5 Hz, 1H) ppm; ^{13}C NMR (125 MHz, $CDCl_3$) δ 171.3, 168.9, 160.3, 139.5, 134.1, 133.0, 132.4, 129.4, 125.1, 119.6, 117.4, 115.5, 78.1, 76.2, 56.0 ppm; IR (neat) 3293, 3265, 2360, 2340, 1620, 1544, 1487, 1422, 1357, 1233, 1023 cm^{-1}; ESI-MS m/z 356.1 $[M+H]^+$

2-(3-(4-(allyloxy)phenyl)-1,2,4-oxadiazol-5-yl)-5-chloroaniline (20)
3-(4-(allyloxy)phenyl)-5-(4-chloro-2-nitrophenyl)-1,2,4-oxadiazole (20SM)

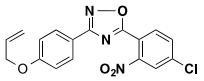

20SM

Mp = 160 - 163 °C; ^{1}H NMR ($CDCl_3$, 300 MHz) δ 8.05 (d, *J* = 9.0 Hz, 2H), 7.99 (d, *J* = 8.3 Hz, 2H), 7.76 (dd, *J* = 8.3, 2.0 Hz, 1H), 7.02 (d, *J* = 9.0 Hz, 2H), 6.07 (ddt, *J* = 17.1, 10.4, 5.2 Hz, 1H), 5.44 (ddt, *J* = 17.3, 3.1, 1.6 Hz, 1H), 5.33 (ddt, *J* = 10.4, 2.7, 1.3 Hz, 1H), 4.61 (ddd, *J* = 5.3, 1.5, 1.5 Hz, 2H) ppm; ^{13}C NMR ($CDCl_3$, 125 MHz) δ 171.2, 169.0, 161.4, 139.5, 133.0, 132.8, 132.4, 129.4, 125.1, 122.3, 118.8, 118.3, 117.4, 115.3, 69.0 ppm; IR (neat) 3093, 2874, 2359, 2340, 1699, 1610, 1589, 1534, 1352, 1249, 835, 770 cm^{-1}; ESI-MS m/z 357.5 $[M+H]^+$.

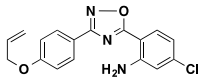

20

To a solution of nitro-oxadiazole **20SM** (225 mg, 0.63 mmol) obtained above in EtOH (25 mL) was added $SnCl_2 \bullet 2H_2O$ (358 mg, 1.89 mmol) and the resultant solution was heated to reflux for 3h. The volatiles were evaporated under reduced pressure and the residue obtained was diluted with water (20 mL) and basified (pH ≈ 12) with saturated aqueous $NaHCO_3$ (10 mL). This solution was transferred to a separatory funnel and extracted with CH_2Cl_2 (4 × 25 mL). The combined organic layers were dried over Na_2SO_4 and concentrated under reduced pressure to afford the amino-oxadiazole **20** (118 mg, 57%) as a light yellow solid.

Mp = 160 - 162 °C; ^{1}H NMR (DMSO-d_6, 300 MHz) δ 9.58 (brs, 1H), 9.35 (d, *J* = 1.2 Hz, 1H), 8.09 (d, *J* = 8.7 Hz, 2H), 7.96 (d, *J* = 8.3 Hz, 1H), 7.34(d, *J* = 2.0 Hz, 1H), 7.15 (d, *J* = 8.9 Hz, 2H), 6.95 (dd, *J* = 8.5, 2.0 Hz, 1H), 6.06 (ddt, *J* = 17.1, 10.4, 5.2 Hz, 1H), 5.44 (ddt, *J* = 17.3, 3.4, 1.6 Hz, 1H), 5.30 (ddt, *J* = 10.5, 3.0, 1.3 Hz, 1H), 4.67 (ddd, *J* = 5.2, 1.5, 1.5 Hz, 2H) ppm; ^{13}C NMR (DMSO-d_6, 125 MHz) δ 172.8, 167.2, 160.7, 151.1, 139.2, 133.2, 130.6, 129.0, 118.2, 118.0, 117.8, 115.3, 112.3, 103.2, 68.3 ppm; IR (neat) 3276, 2360, 2341, 1652, 1610, 1540, 1473, 1256, 836 cm^{-1}; ESI-MS m/z 328.1 $[M+H]^+$

5-chloro-2-(3-(4-(prop-2-ynyloxy)phenyl)-1,2,4-oxadiazol-5-yl)aniline (21)

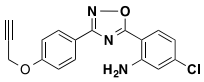

21

To a solution of propargyloxadiazole **19** in EtOH (410 mg, 1.15 mmol) was added $SnCl_2 \bullet 2H_2O$ (656 mg, 3.46 mmol) and the resultant solution was heated to reflux for 3h. The volatiles were evaporated under reduced pressure and the residue obtained was diluted with water (20 mL) and basified (pH ≈ 12) with saturated aqueous $NaHCO_3$ (10 mL). This solution was then transferred to a separatory funnel and extracted with CH_2Cl_2 (4 × 25 mL). The combined organic layers were dried over Na_2SO_4 and concentrated under reduced pressure to afford the amino-oxadiazole **21** (256 mg, 68%) as a yellow solid.

Mp = 178 - 179 °C; ^{1}H NMR (DMSO-d_6, 500 MHz) δ 8.12 (d, *J* = 8.9 Hz, 2H), 7.84 (d, *J* = 8.6 Hz, 1H), 7.21 (bs, 2H), 7.18 (d, *J* = 8.9 Hz, 2H), 7.03 (d, *J* = 1.9 Hz, 1H), 6.71 (dd, *J* = 8.5, 2.0 Hz, 1H), 4.92 (d, *J* = 2.3 Hz, 2H), 3.65 (t, *J* = 2.4 Hz, 1H) ppm; ^{13}C NMR (DMSO-d_6, 125 MHz) δ 173.7, 166.9, 59.6, 149.6, 138.5, 130.4, 128.9, 119.0, 115.6, 115.4, 115.3, 102.6, 78.8, 78.6, 55.6 ppm; IR (neat) 3472, 3350, 2359, 2341, 1734, 1717, 1669, 1506, 1373, 1251, 1014, 842, 759, 668 cm^{-1}; ESI-MS m/z 326.7 $[M+H]^+$.

3-(pyridin-4-yl)-5-(2,4,6-trichlorophenyl)-1,2,4-oxadiazole (22)

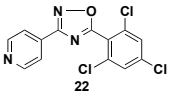
22

Mp = 173 - 174 °C; ^{1}H NMR (DMSO-d_6, 300 MHz) δ 8.73 (d, *J* = 4.8 Hz, 2H), 7.88 (s, 1H), 7.79 (s, 1H), 7.73 (d, *J* = 5.5 Hz, 2H) ppm; ^{13}C NMR (DMSO-d_6, 125 MHz) δ 164.8, 155.1, 149.2, 139.5, 135.6, 134.8, 130.8, 128.1, 121.4 ppm; IR (neat) 3332, 3176, 3077, 1744, 1641, 1603, 1577, 1546, 1409, 1370, 1255, 1111, 1054 cm^{-1}. ESI-MS m/z 348.3 $[M+K]^+$.

5-(2,4-dichlorophenyl)-3-(pyridin-4-yl)-1,2,4-oxadiazole (23)

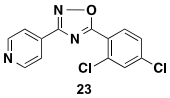
23

Mp = 136 - 137 °C; ^{1}H NMR ($CDCl_3$, 500 MHz) δ 8.83 (d, *J* = 4.4 Hz, 2H), 8.14 (d, *J* = 8.7 Hz, 1H), 8.04 (d, *J* = 5.8 Hz, 2H), 7.64 (d, *J* = 1.9 Hz, 1H), 7.47 (dd, *J* = 8.7, 1.9 Hz, 1H) ppm; ^{13}C NMR ($CDCl_3$, 125 MHz) δ 174.5, 167.4, 150.9, 139.6, 135.0, 134.2, 132.9, 131.7, 127.9, 121.8, 121.5 ppm; IR (neat) 3750, 3743, 3670, 2359, 2341, 1699, 1576 cm^{-1}; ESI-MS m/z 292.0 $[M+H]^+$

5-(4-chloro-2-nitrophenyl)-3-(pyridin-4-yl)-1,2,4-oxadiazole (24)

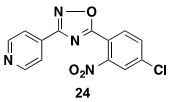
24

Mp = 172 - 174 °C; ^{1}H NMR ($CDCl_3$, 500 MHz) δ 8.83 (dd, *J* = 7.5, 2.5 Hz, 2H), 8.04 (d, *J* = 3.5 Hz, 1H), 8.02 (d, *J* = 14.0 Hz, 1H), 8.01 (dd, *J* = 7.5, 2.5 Hz, 2H), 7.81 (dd, *J* = 14.0, 3.5 Hz, 1H) ppm; ^{13}C NMR ($CDCl_3$, 125 MHz) δ 172.5, 167.8, 150.8, 140.1, 133.8, 133.2, 132.4, 131.8, 125.3, 121.6, 116.9 ppm; IR (neat) 3076, 2923, 1681, 1534, 1415, 1365, 1250, cm^{-1}; ESI-MS m/z 303.0 $[M+H]^+$

methyl 3-nitro-4-(3-(pyridin-4-yl)-1,2,4-oxadiazol-5-yl)benzoate (25)

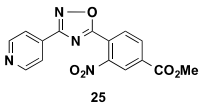
25

Mp = 138 - 140 °C; ^{1}H NMR (DMSO-d_6, 300 MHz) δ 8.95 (d, *J* = 6.5 Hz, 2H), 8.57 (d, *J* = 1.5 Hz, 1H), 8.40 (dd, *J* = 7.9, 1.6 Hz, 1H), 8.13- 7.56 (m, 3H), 3.95 (s, 3H) ppm; ^{13}C NMR (DMSO-d_6, 125 MHz) δ 163.9, 153.9, 147.0, 144.8, 134.2, 133.6, 132.9, 130.8, 130.3, 124.4, 124.2, 123.4, 53.1 ppm; IR (neat) 3099, 2359, 2341, 1723, 1636, 1537, 1494, 1287, 1236, 1100, 1052 cm^{-1}; ESI-MS m/z 327 $[M+H]^+$

C. [1]HNMR and [13]CNMR data of 1,2,4-bis-aryl oxadiazoles

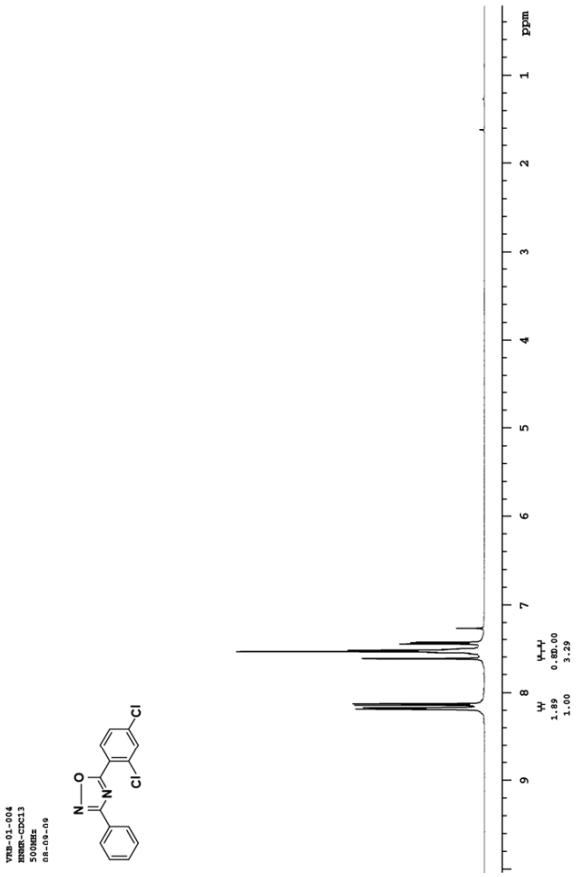

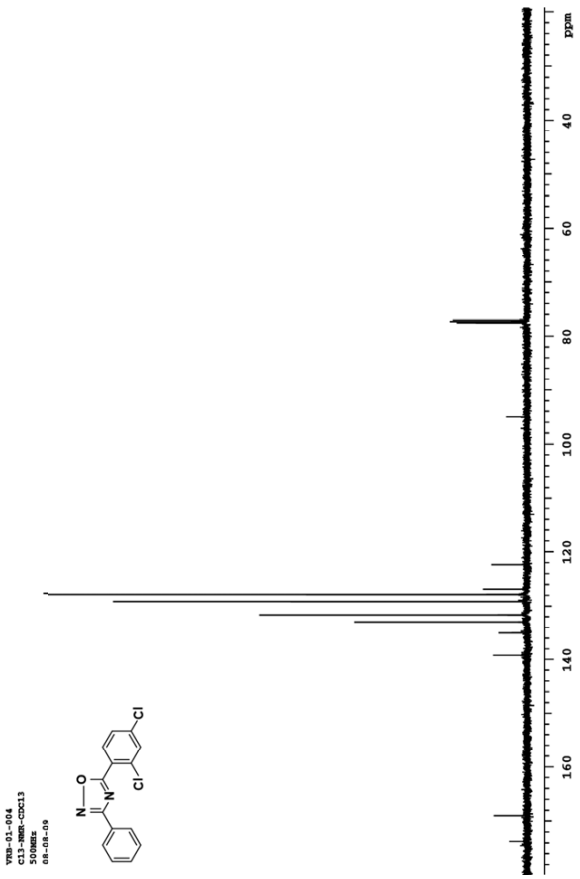
VRB-01-004
C13-NMR-CDCl3
500MHz
08-08-09
Cl
Cl
N
O
N
ppm
160
140
120
100
80
60
40

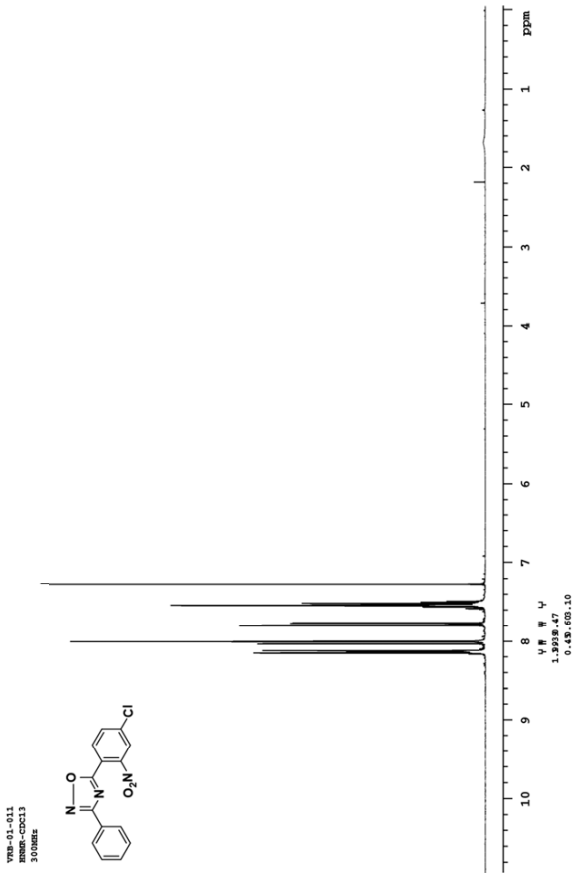
VRB-01-011
mmm-CDCl3
300MHz
Cl
O
N
N
O2N
ppm
1
2
3
4
5
6
7
8
9
10
1.9958.47
0.449.603.10

10

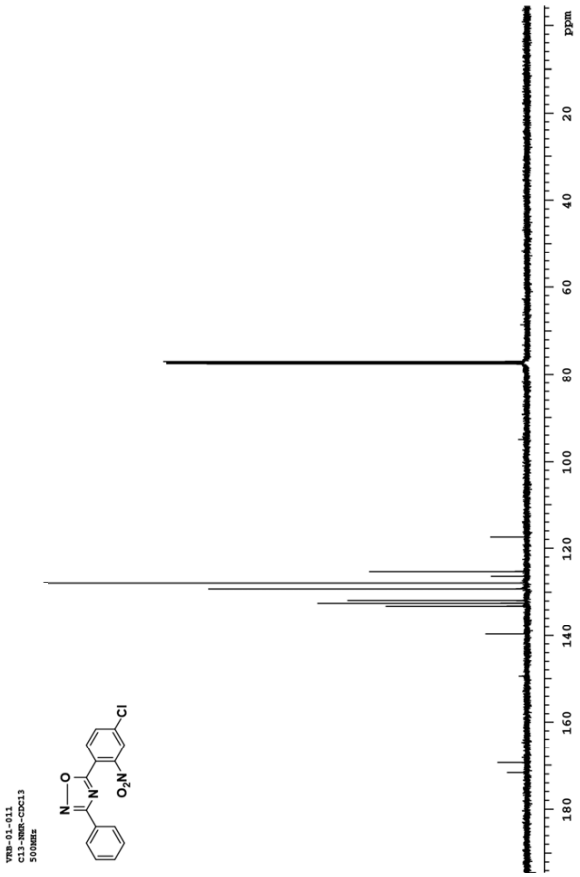
VRB-01-011
C13-NMR-CDCl3
500MHz
Cl
O2N
ppm
20
40
60
80
100
120
140
160
180

11

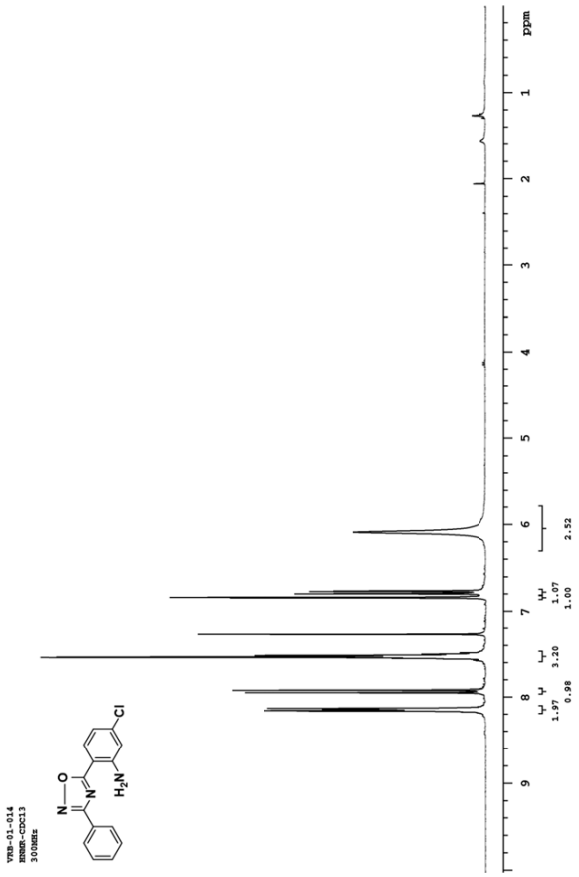
VRB-01-014
HNMR-CDCl3
300MHz
N
O
N
H2N
Cl
ppm
1
2
3
4
5
6
7
8
9
1.97
0.98
3.20
1.07
1.00
2.52

12

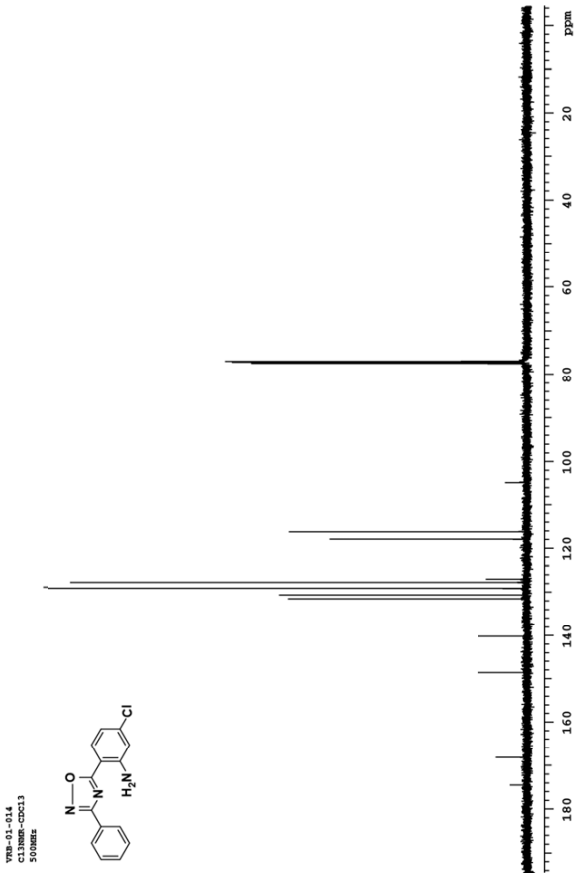
VRB-01-014
C13NMR-CDCl3
500MHz
Cl
O
N
N
H2N
ppm
20
40
60
80
100
120
140
160
180

13

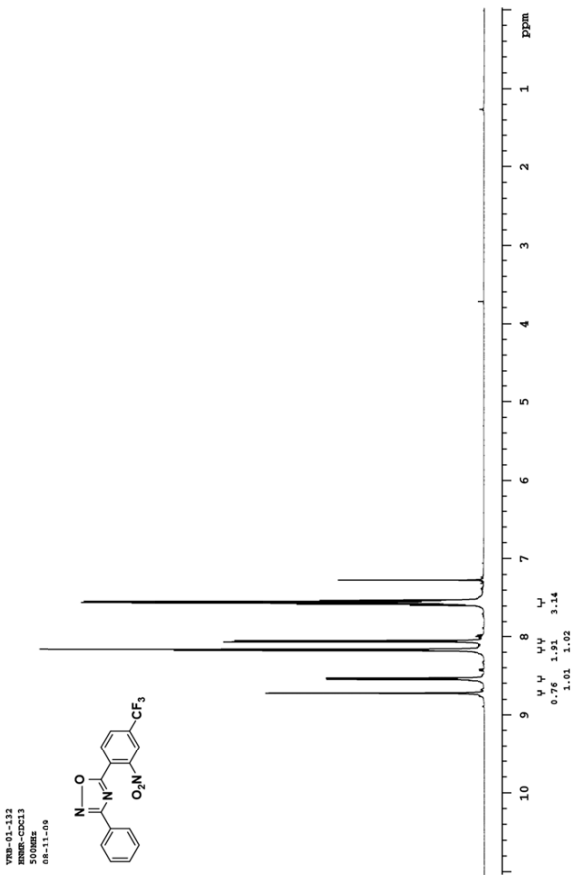
VRB-01-132
mmm-CDCl3
500MHz
08-11-06
ppm
0.76
1.01
1.91
1.02
3.14

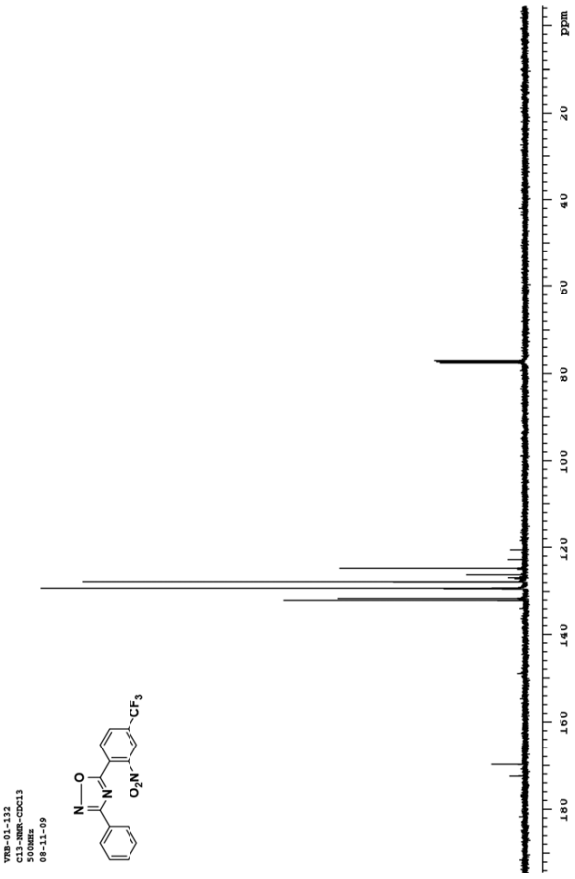
YRB-01-132
C13-NMR-CDCl3
500MHz
08-11-09
O
N
O2N
CF3
ppm

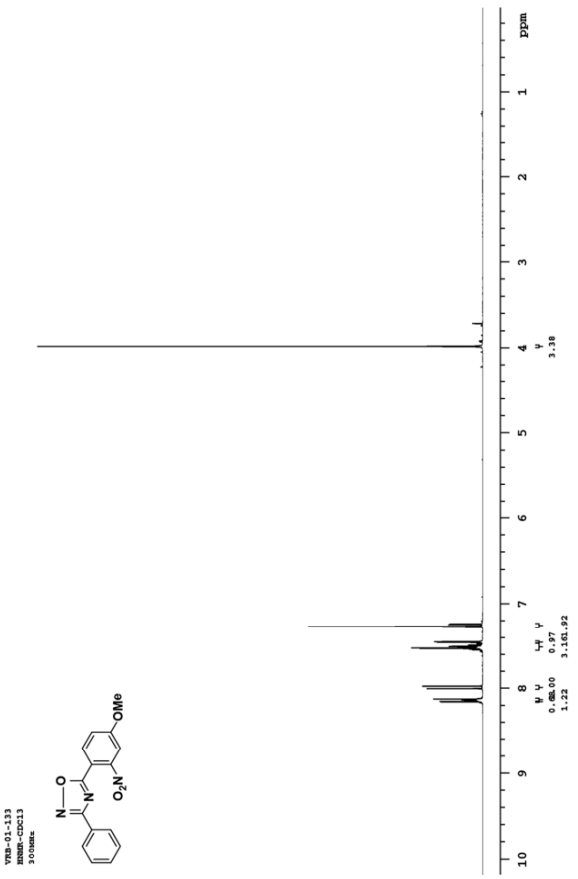

16

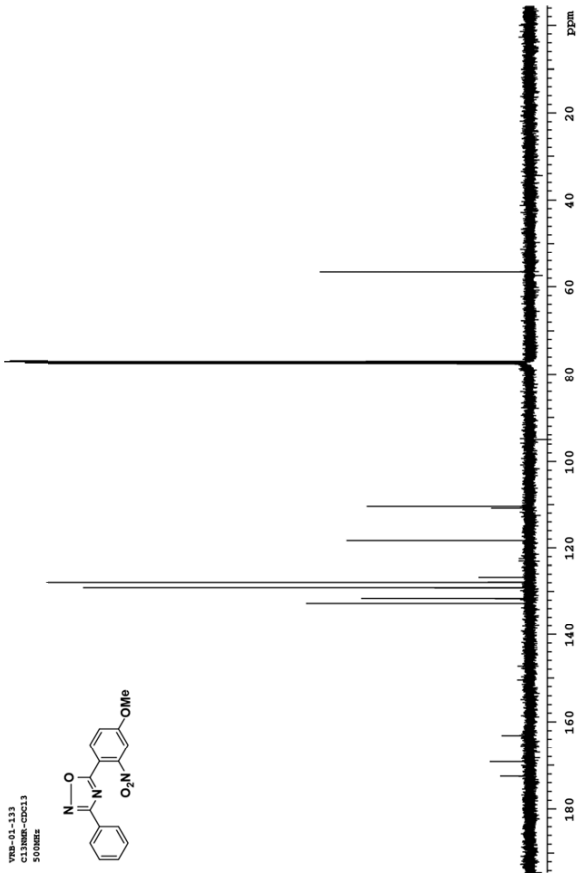
VRB-01-133
C13NMR-CDC13
500MHz
OMe
O2N
ppm
20
40
60
80
100
120
140
160
180

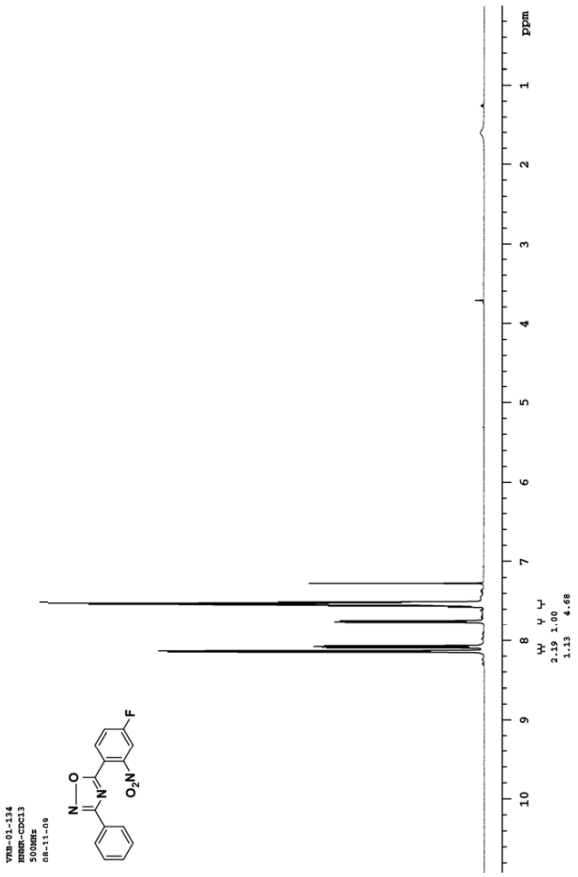
VRB-01-134
HNMR-CDCl3
500MHz
08-11-06
F
O2N
ppm
2.19 1.00
1.13 4.68

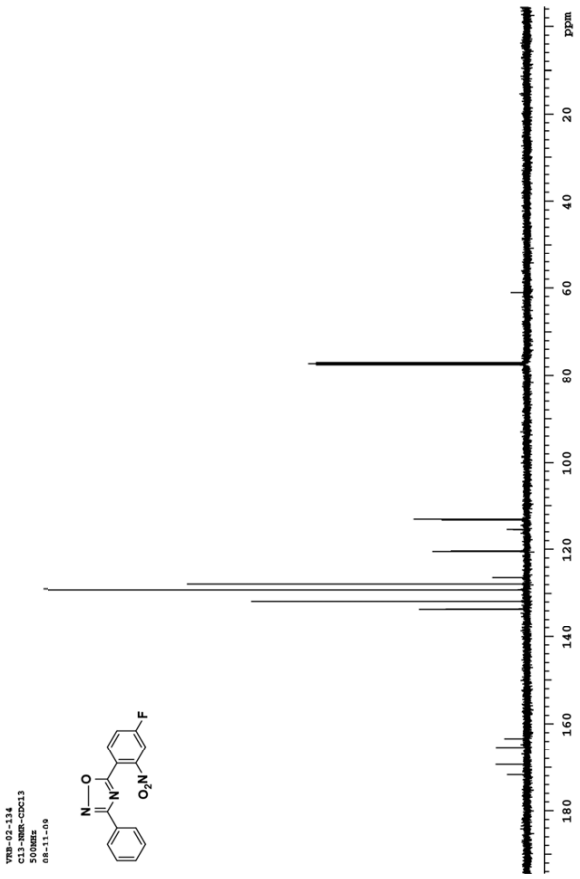
VRB-02-134
C13-NMR-CDCl3
500MHz
08-11-09
F
O2N
ppm
180
160
140
120
100
80
60
40
20

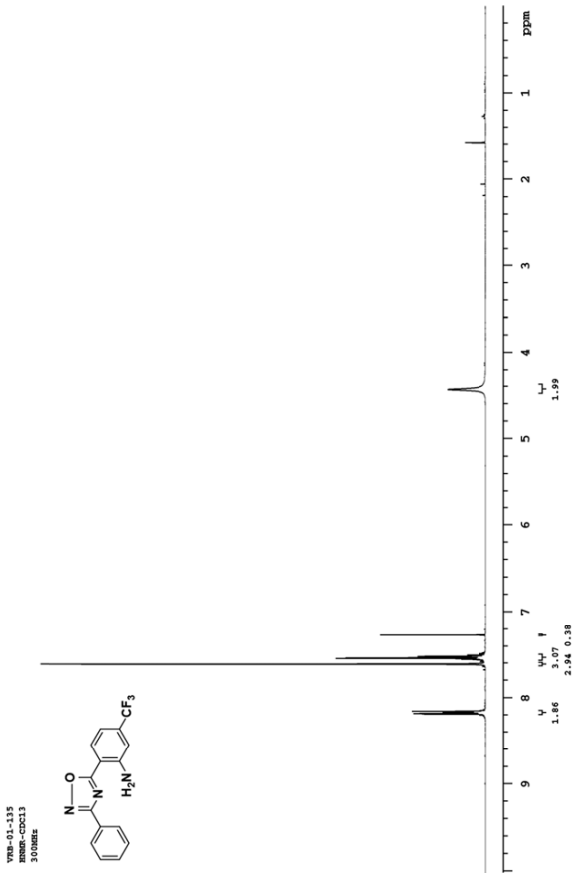
VRB-01-135
mmm-CDCl3
300MHz
CF3
H2N
O
N
N
ppm
1
2
3
4
5
6
7
8
9
1.86
3.07
2.94
0.38
1.99

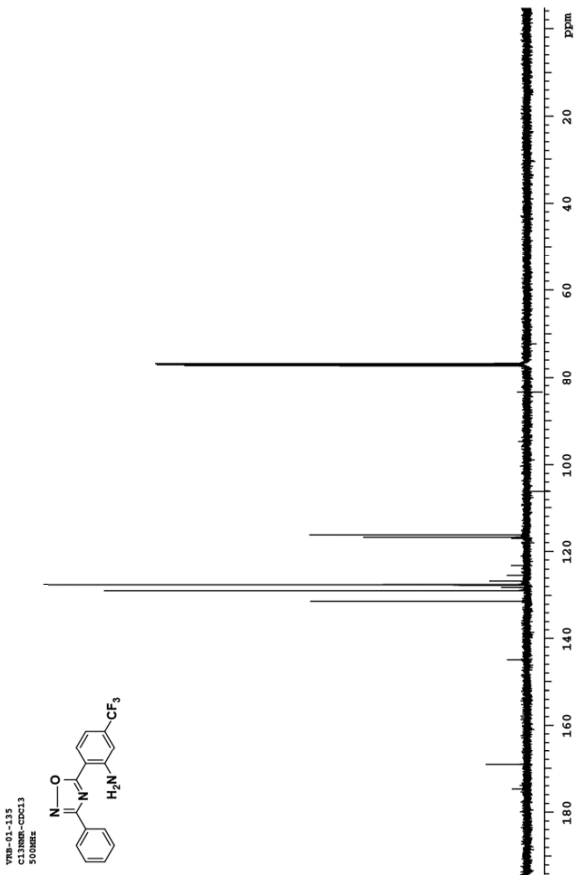
VRB-01-135
C13NMR-CDCl3
500MHz
O
N
N
H_2N
CF_3
ppm
180
160
140
120
100
80
60
40
20

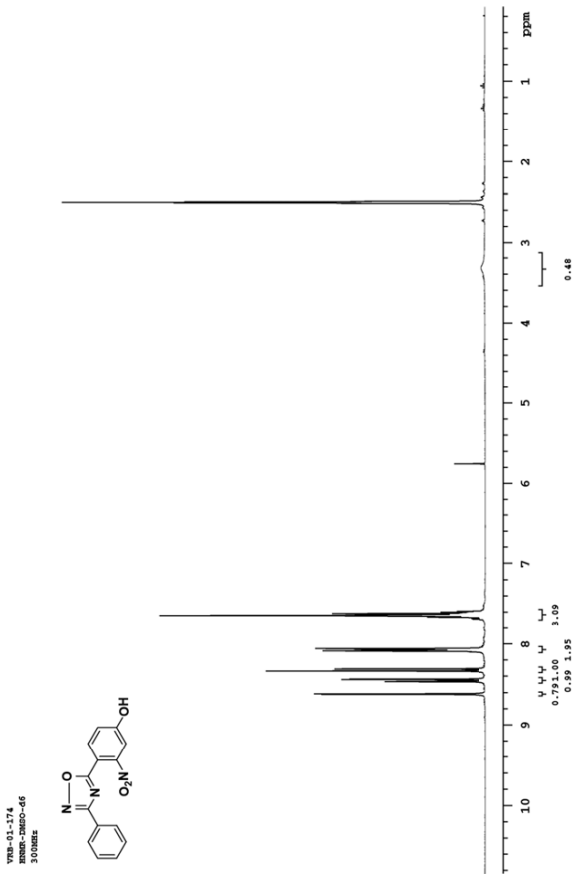
VRB-01-174
HNMR-DMSO-d6
300MHz
OH
O
N
N
O2N
ppm
0.48
0.791.00
0.99 1.95
3.69

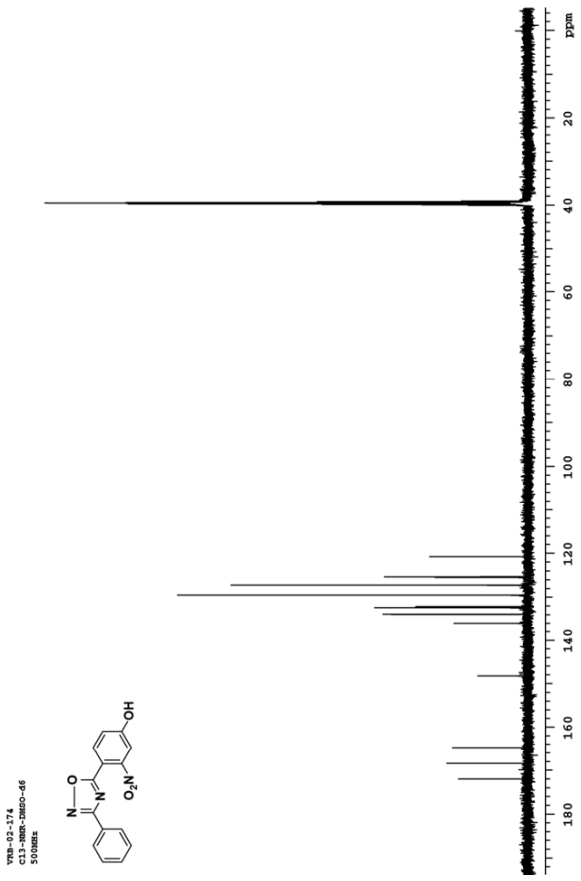
VRB-02-174
C13-NMR-DMSO-d6
500MHz
ppm
20
40
60
80
100
120
140
160
180
OH
O2N
N
O

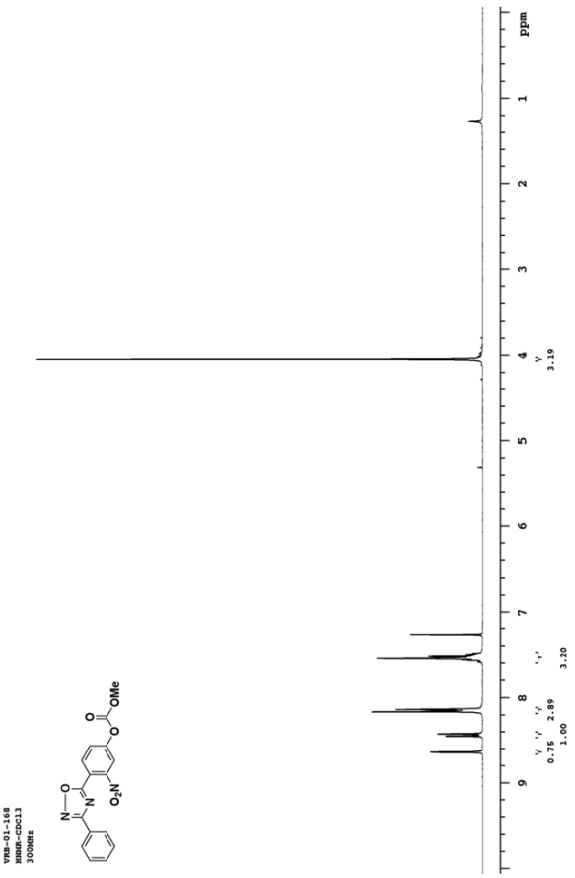
VKB-01-168
HNMR-CDCl3
300MHz
OMe
O_2N
ppm
3.19
3.20
2.89
1.00
0.75

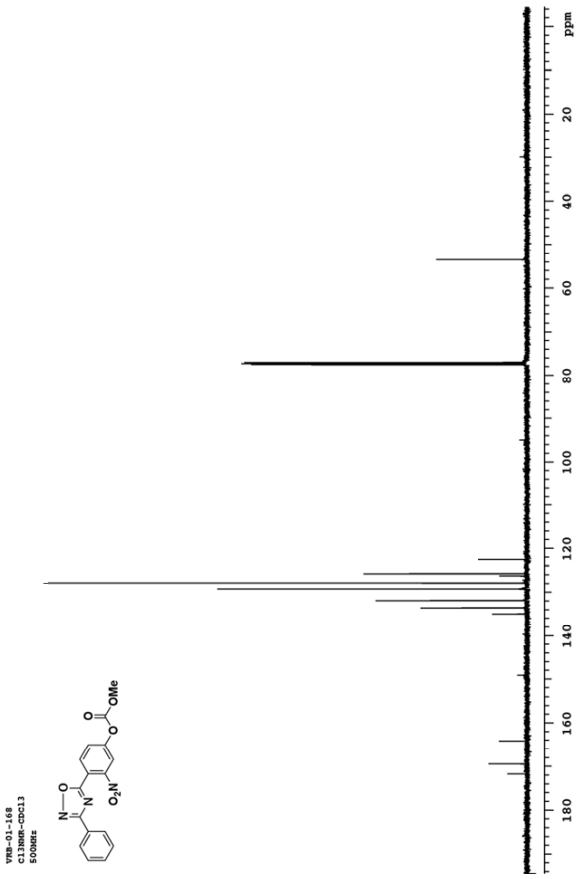
VRS-01-168
C13NMR-CDCl3
500MHz
ppm
20
40
60
80
100
120
140
160
180
OMe
O
O
N
O
N
O2N

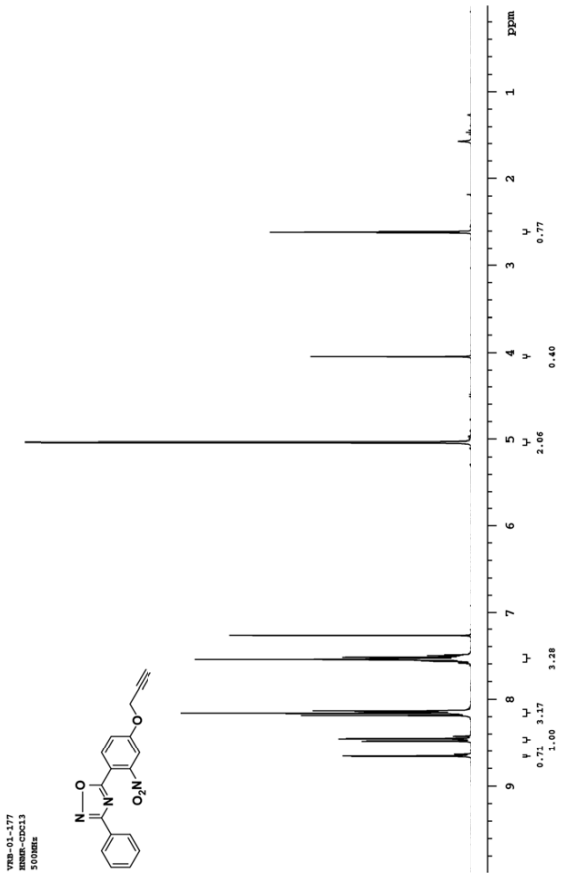
YRB-01-177
NMR-CDCl3
500MHz
ppm
1
2
3
4
5
6
7
8
9
0.77
0.40
2.06
3.28
3.17
1.00
0.71

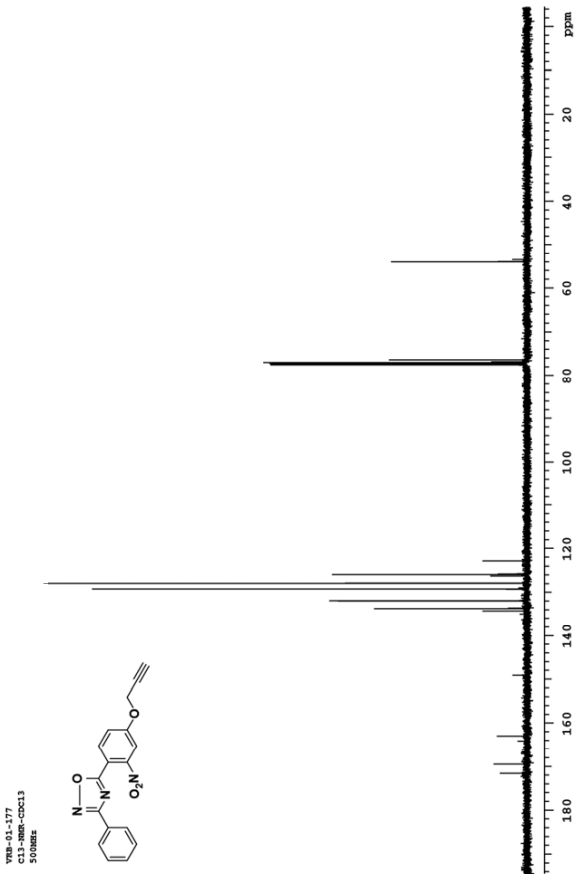
VRS-01-177
C13-NMR-CDCl3
500MHz
ppm
20
40
60
80
100
120
140
160
180

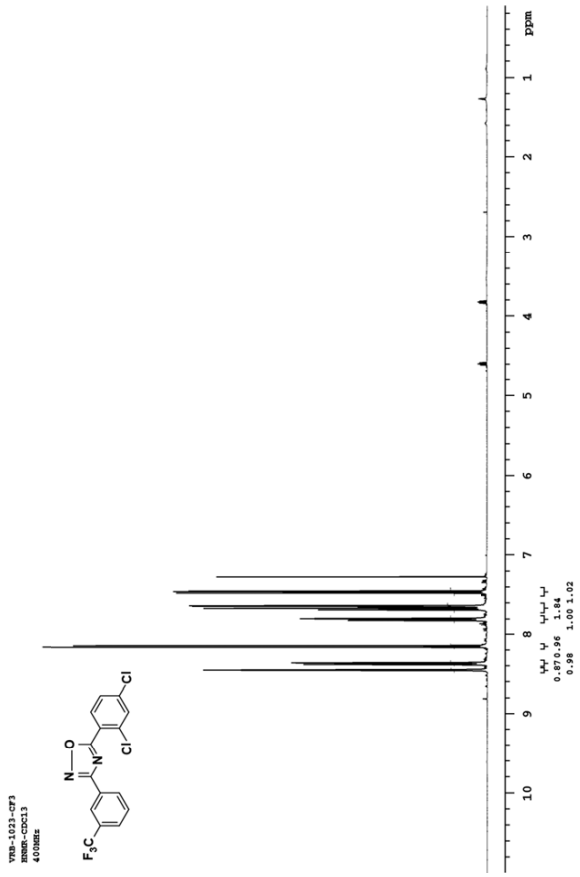
VRB-1023-CF3
HNMR-CDCl3
400MHz
Cl
Cl
F3C
ppm
1
2
3
4
5
6
7
8
9
10
0.87 0.96 1.84
0.98 1.00 1.02

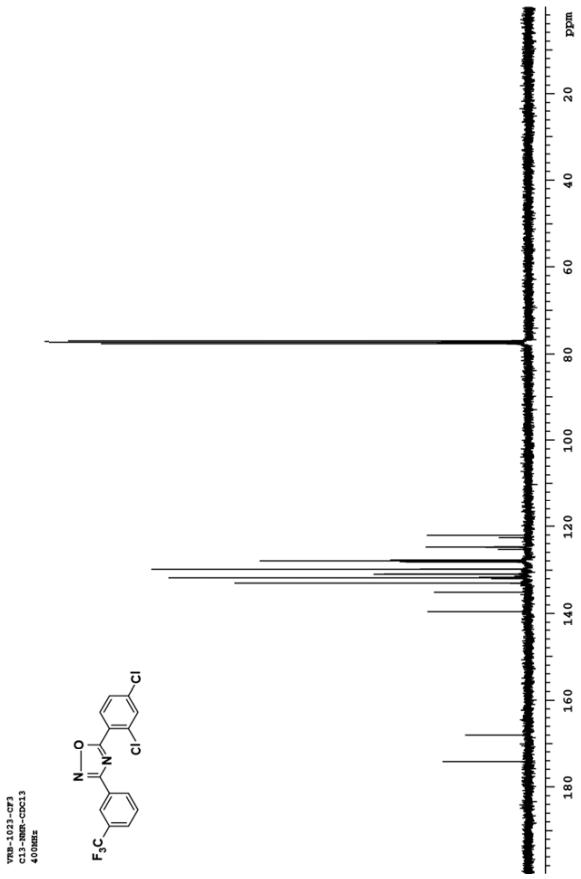
VRS-1023-CF3
C13-NMR-CDCl3
400MHz
Cl
Cl
N
O
N
F3C
ppm
20
40
60
80
100
120
140
160
180

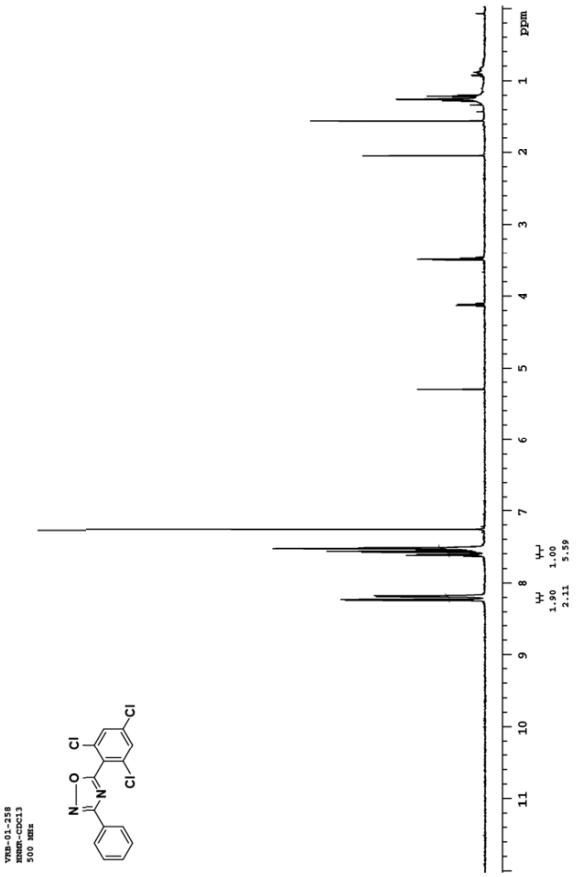
VMA-01-258
PROTON-CDCl3
500 MHz
Cl
Cl
Cl
O
N
N
ppm
1
2
3
4
5
6
7
8
9
10
11
1.90
2.11
1.00
5.59

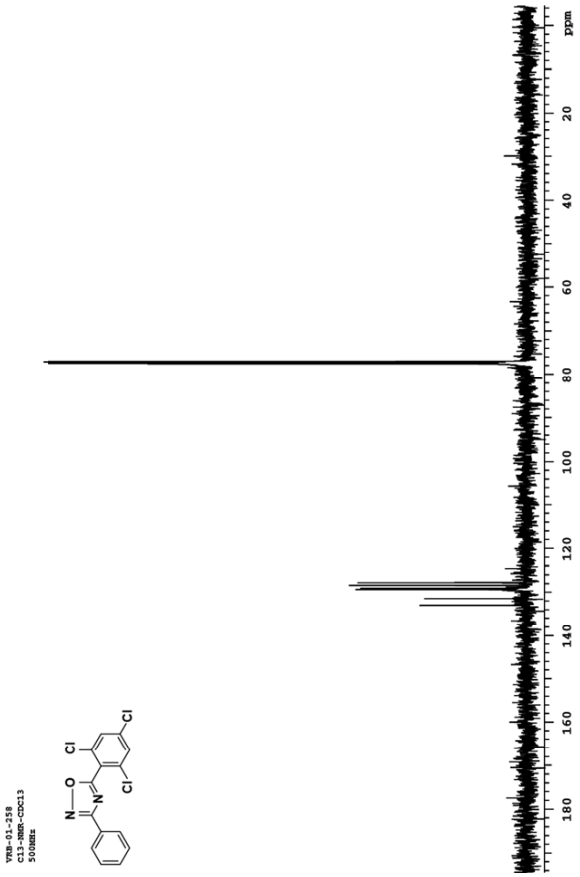
VRB-01-258
C13-NMR-CDCl3
500MHz
Cl
Cl
O
N
N
Cl
ppm
180
160
140
120
100
80
60
40
20

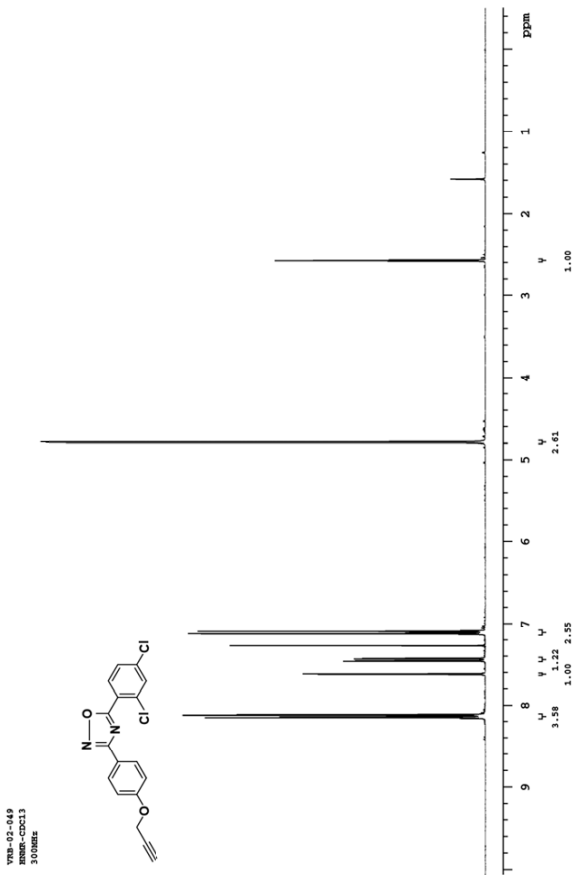
VRB-02-049
HNMR-CDCl3
300MHz
Cl
Cl
O
N
O
N
O
ppm
1
2
3
4
5
6
7
8
9
1.00
2.61
1.22
1.00
2.55
3.58

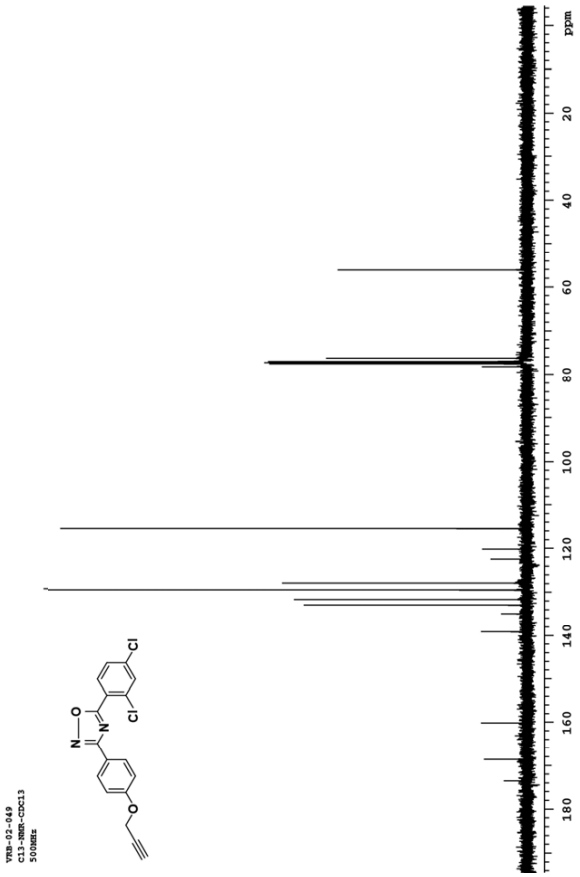
VRB-02-049
C13-NMR-CDCl3
500MHz
ppm
20
40
60
80
100
120
140
160
180
Cl
Cl
N
O
O

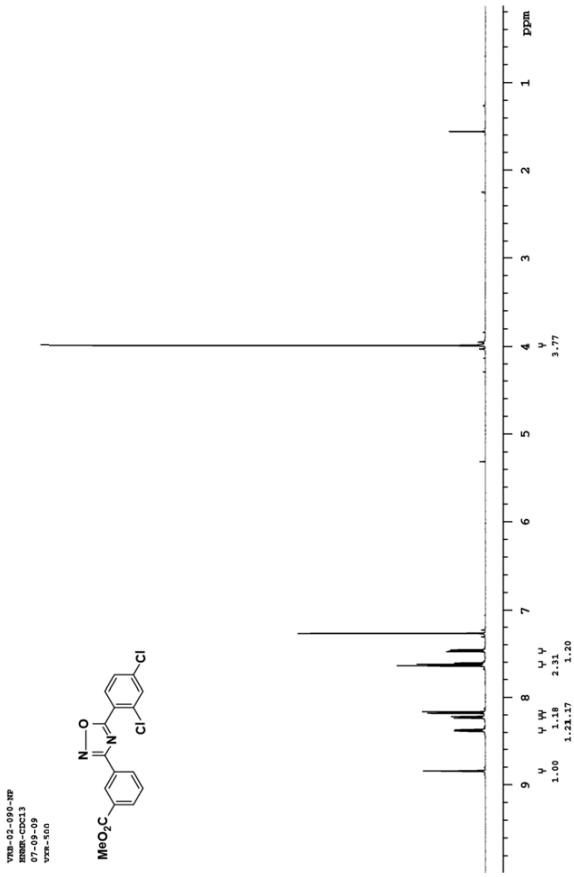
VRB-02-090-MP
RMMR-CDCl3
07-09-09
vrx-400
MeO2C
Cl
Cl
N
O
ppm
1.00
1.18
1.21.17
2.31
1.20
3.77

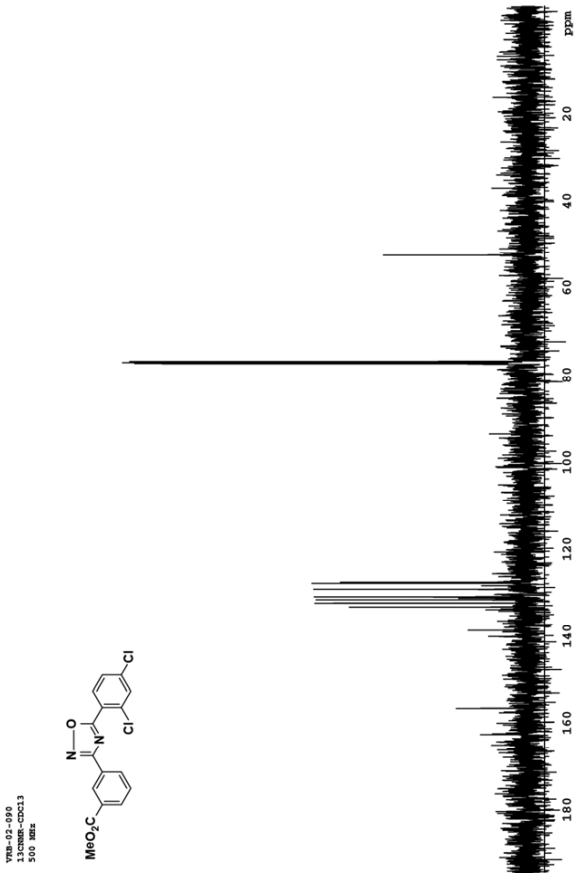
VRB-02-090
13CNMR-CDCl3
500 MHz
MeO2C
Cl
Cl
N
O
N
ppm
20
40
60
80
100
120
140
160
180

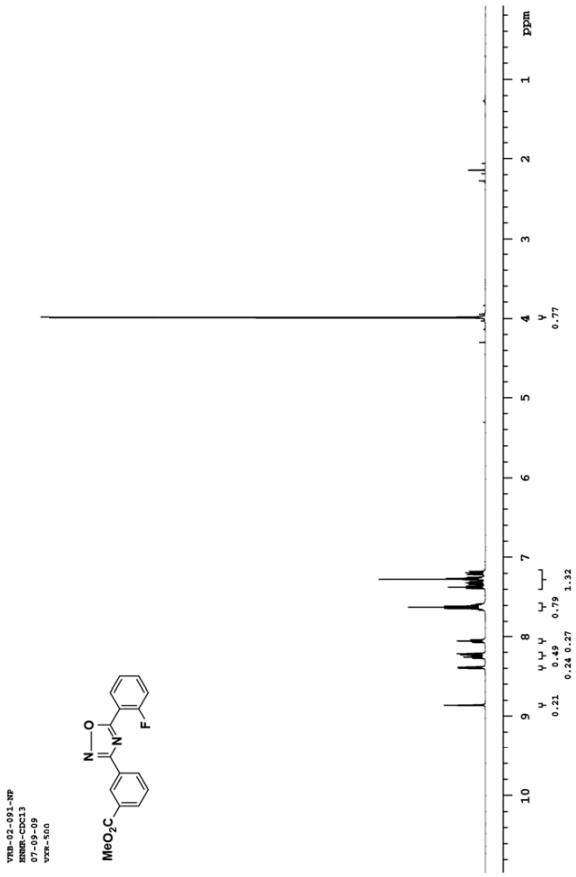
VRB-02-091-HP
RMMR-CDCl3
07-09-09
vrx-400
MeO2C
N
O
F
ppm
1
2
3
4
5
6
7
8
9
10
0.77
1.32
0.79
0.49
0.24
0.27
0.21

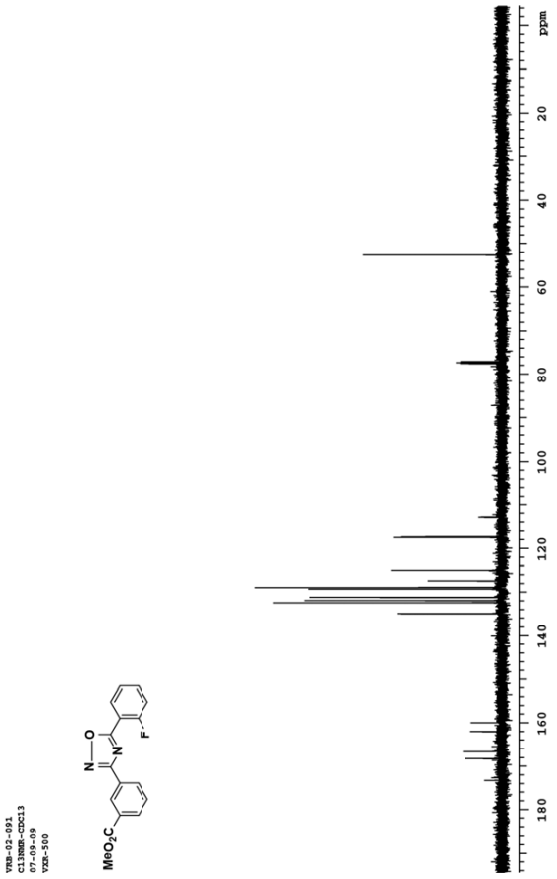
VRS-02-091
C13NMR-CDCl3
07-09-08
YMR-500
MeO2C
N
O
F
ppm
20
40
60
80
100
120
140
160
180

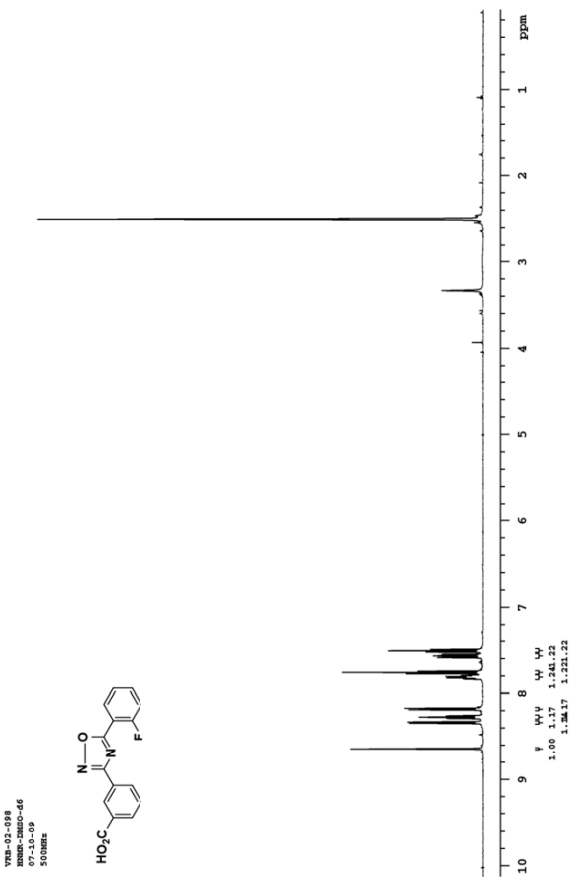
VRB-02-098
HNMR-DMSO-46
07-10-09
500MHz
N
O
N
F
HO2C
ppm
1
2
3
4
5
6
7
8
9
10
1.00
1.17
1.24
1.24
1.22
1.22
1.22

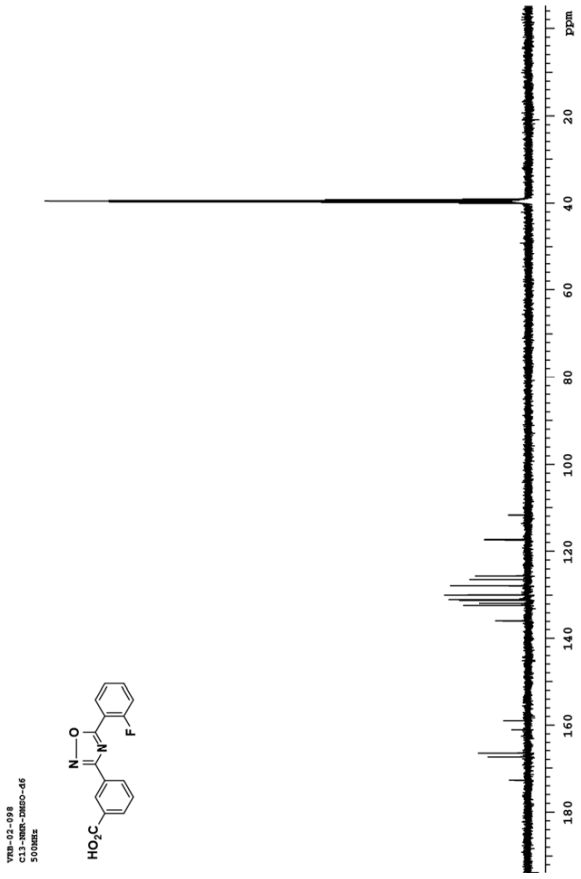
VRB-02-098
C13-NMR-DMSO-d6
500MHz
HO2C
F
ppm
180
160
140
120
100
80
60
40
20

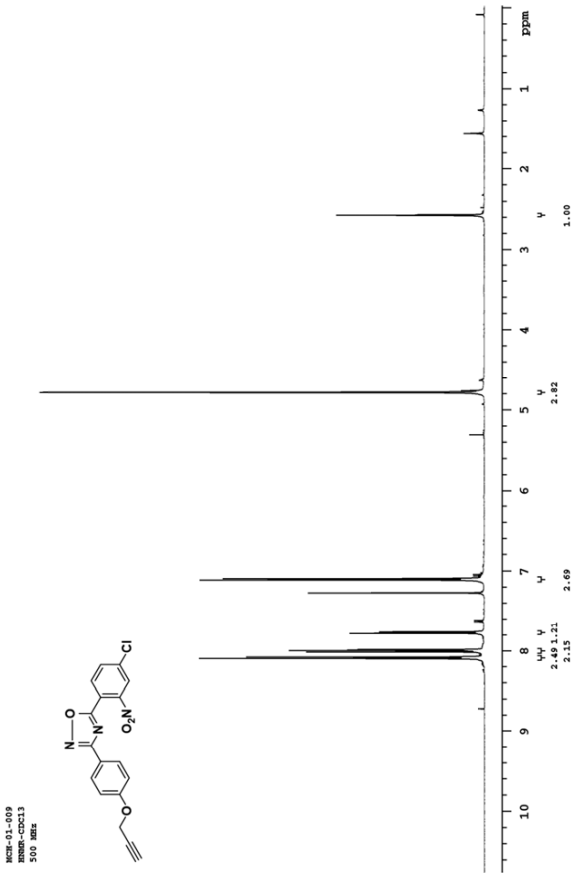
MCM-01-009
HNMR-CDCl3
500 MHz
Cl
O2N
O
N
N
O
ppm
1
2
3
4
5
6
7
8
9
10
1.00
2.82
2.69
2.49 1.21
2.15

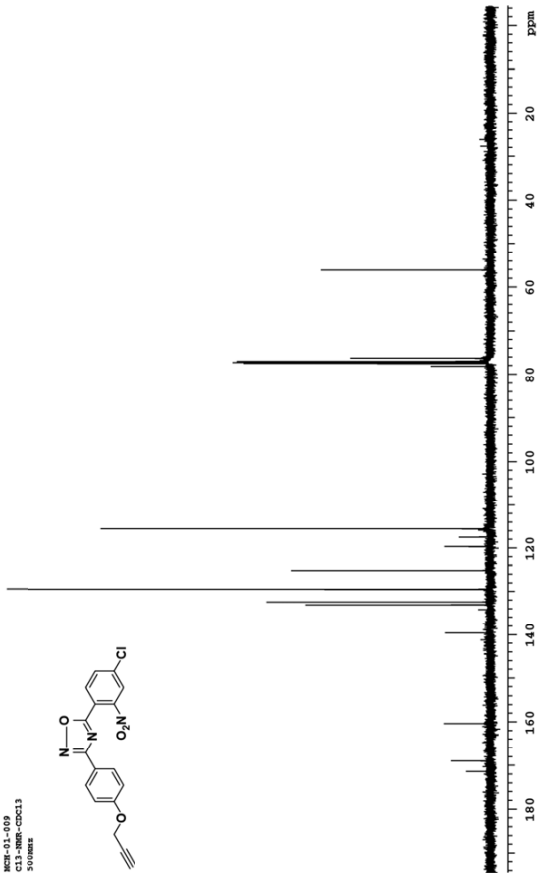
MCM-01-009
C13-NMR-CDCl3
300MHz
ppm
20
40
60
80
100
120
140
160
180
Cl
O
N
N
O2N
O

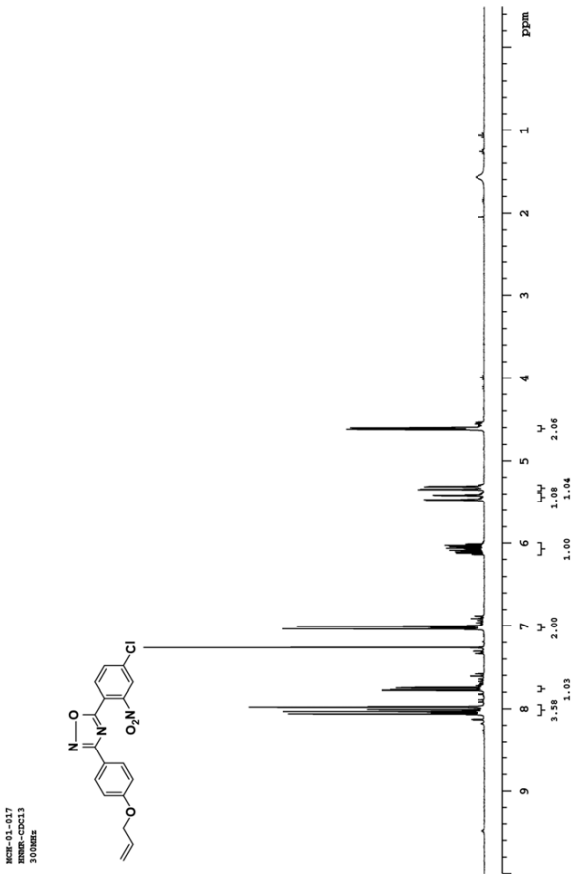
MCM-01-017
HNMR-CDCl3
300MHz
ppm
1
2
3
4
5
6
7
8
9
1.03
3.58
2.00
1.00
1.08
1.04
2.06
Cl
O2N
O
N

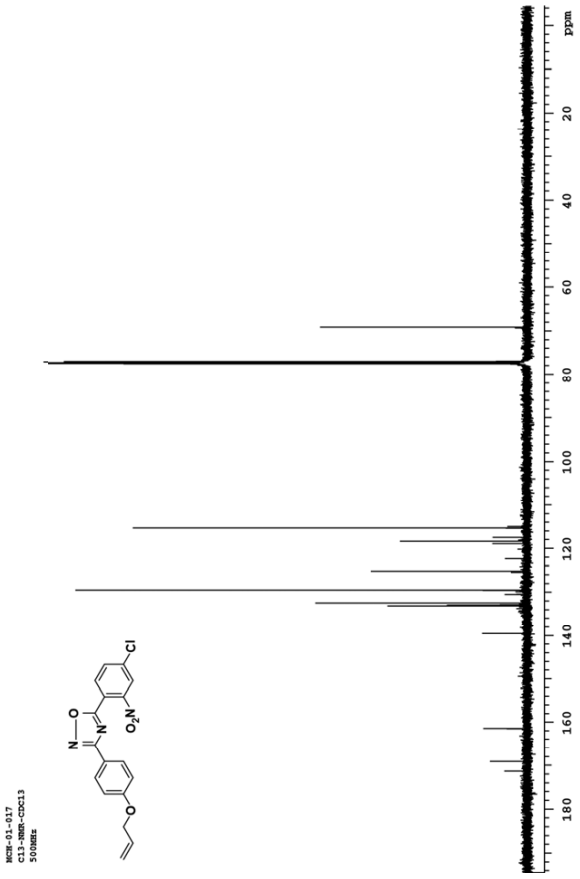
MCM-01-017
C13-NMR-CDCl3
500MHz
ppm
20
40
60
80
100
120
140
160
180
Cl
O2N
O
N
O

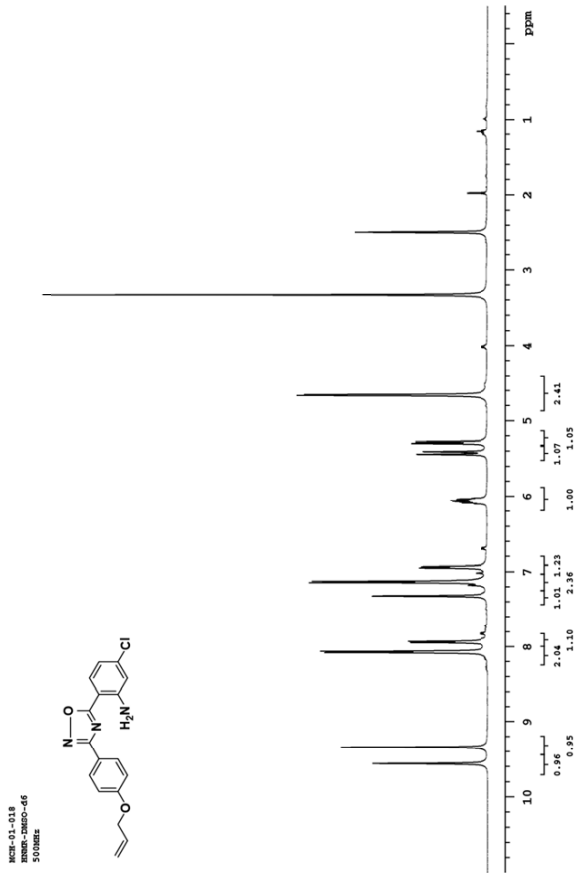
MCM-01-018
NMR-DMSO-46
500MHz
Cl
H_2N
N
O
ppm
10
9
8
7
6
5
4
3
2
1
0.96
0.95
2.04
1.10
1.01
1.23
2.36
1.00
1.07
1.05
2.41

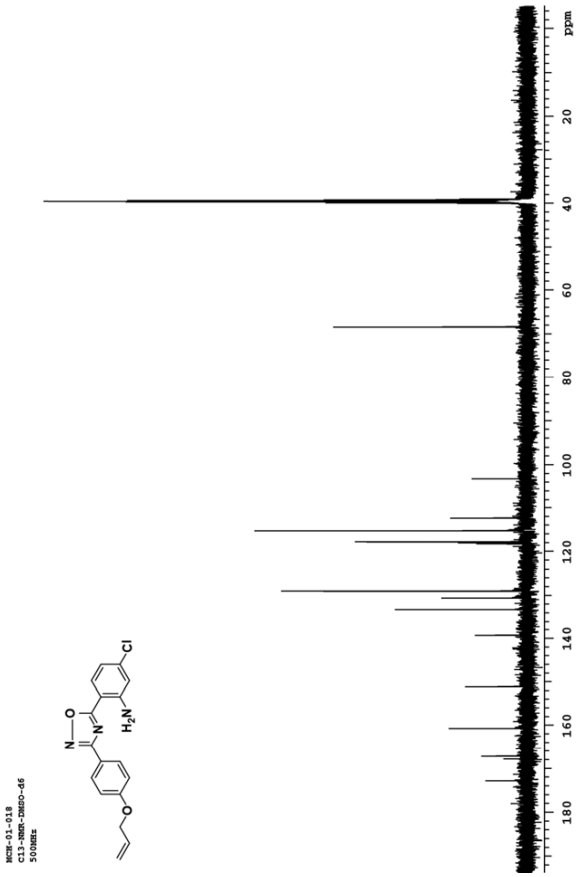
MCM-01-018
C13-NMR-DMSO-d6
500MHz
ppm
20
40
60
80
100
120
140
160
180
Cl
O
N
N
H_2N
O

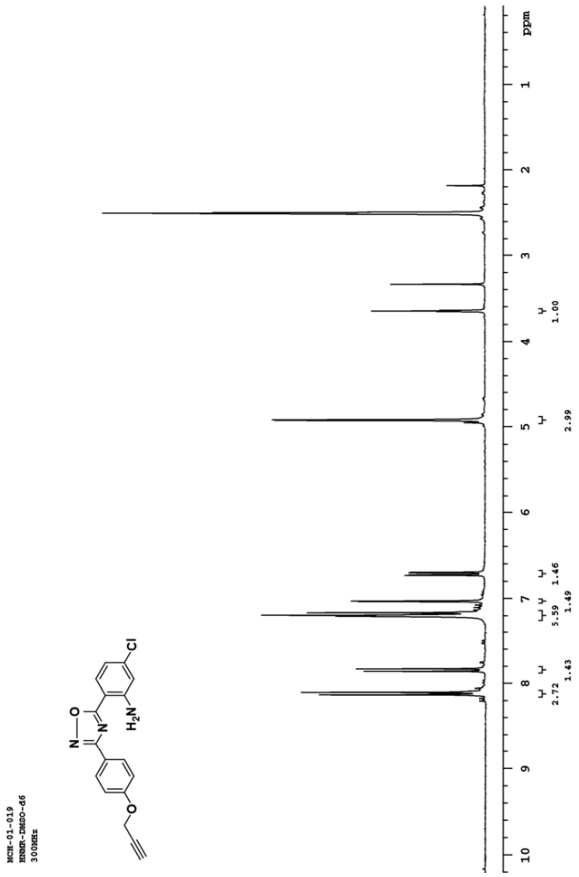
MCM-01-019
HNMR-DMSO-46
300MHz
Cl
H_2N
N
O
O
ppm
1.00
2.99
1.46
1.49
5.59
2.72
1.43

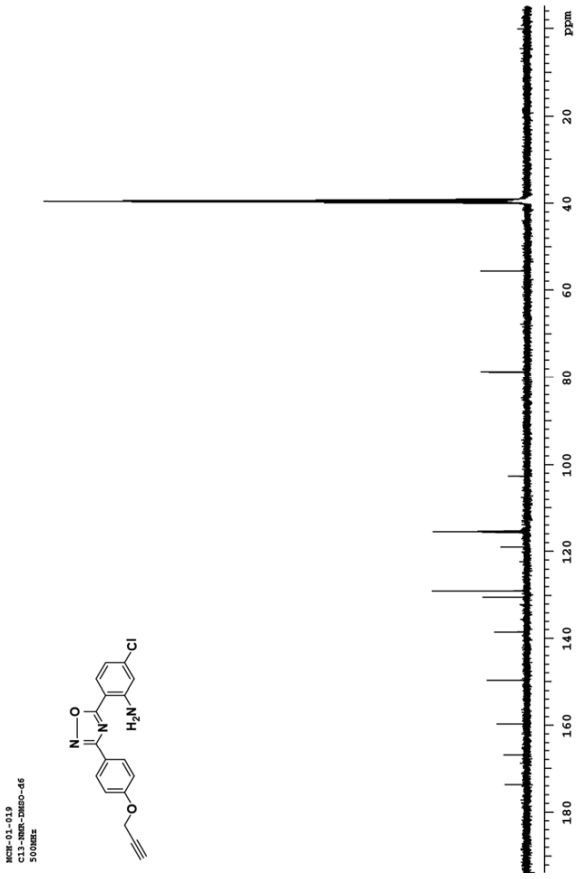
MCM-01-019
C13-NMR-DMSO-d6
500MHz
Cl
H_2N
N
O
O
ppm
180
160
140
120
100
80
60
40
20

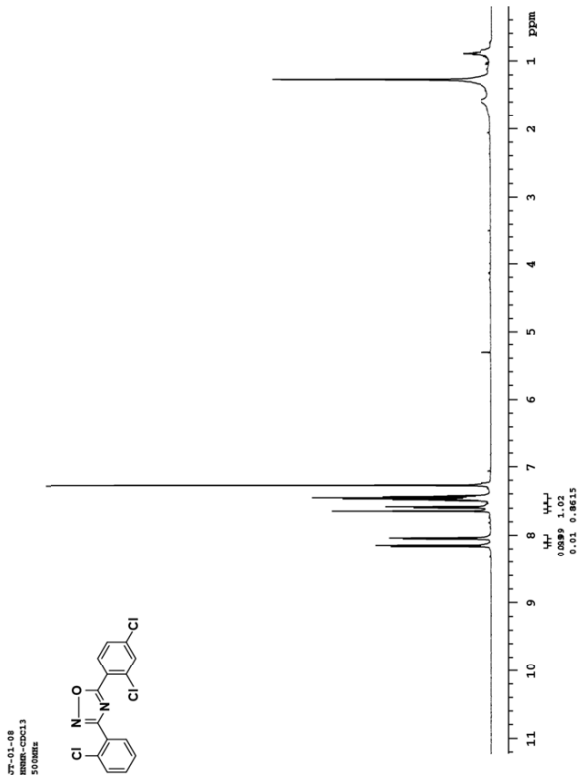
ppm
1
2
3
4
5
6
7
8
9
10
11
Cl
N
O
Cl
Cl

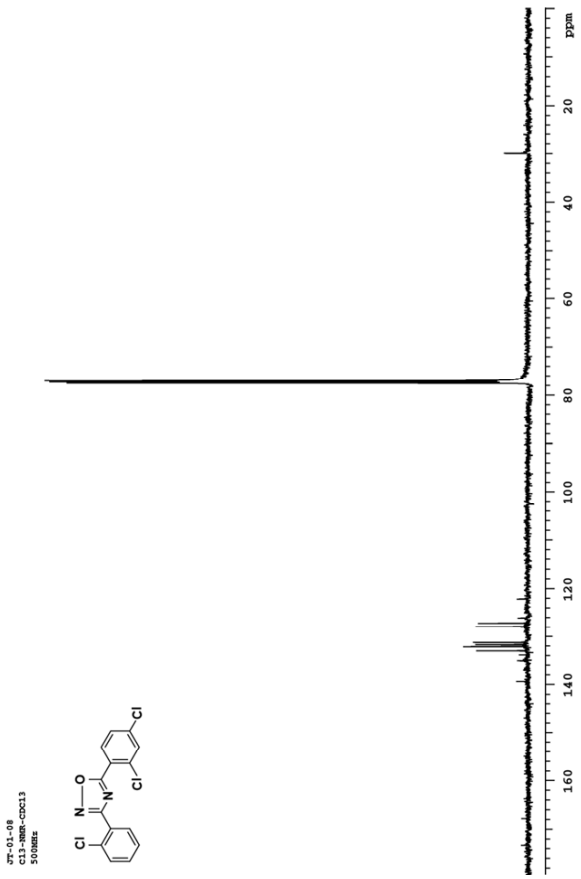
JT-01-08
C13-NMR-CDCl3
500MHz
Cl
N
O
N
Cl
Cl
ppm
160
140
120
100
80
60
40
20

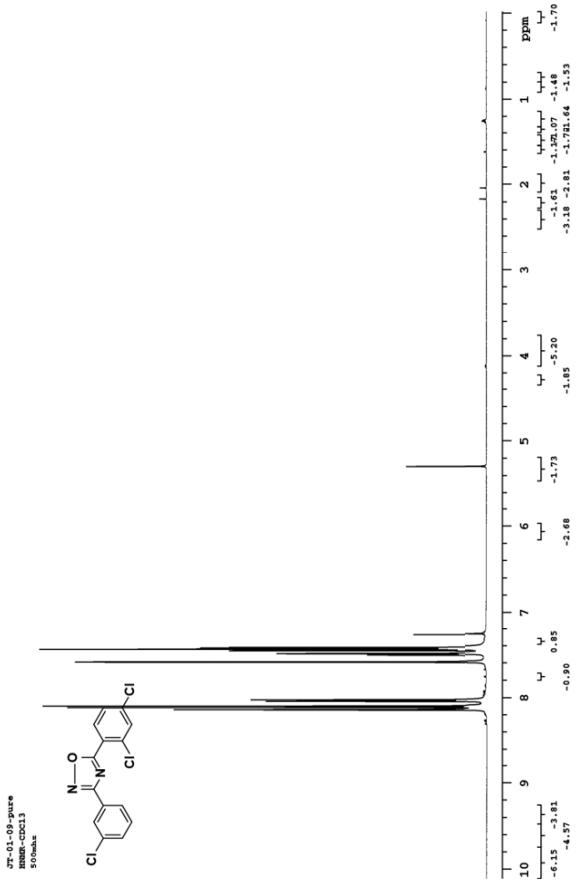
JT-01-09-pure
HNMR-CDCl3
500mhz
Cl
Cl
Cl
O
N
N
ppm

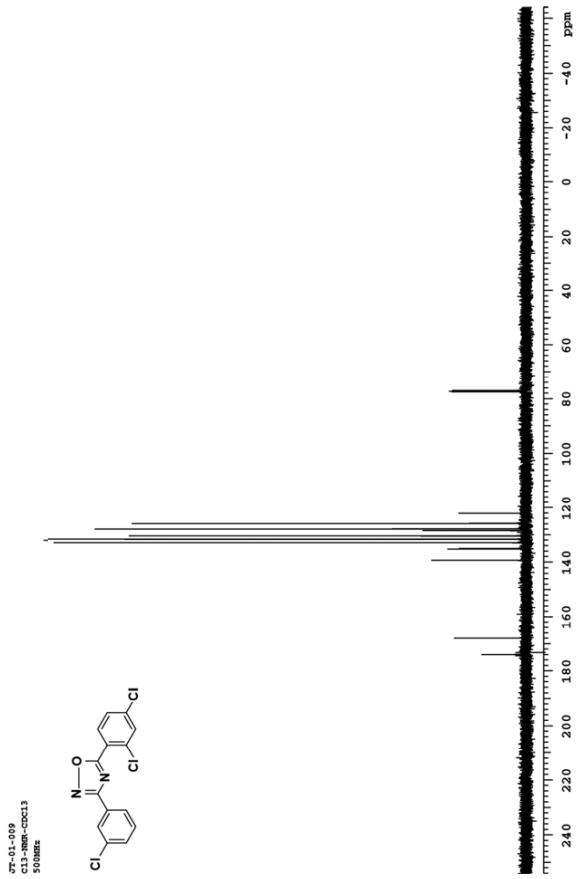
JT-01-069
C13-NMR-CDCl3
500MHz
N
O
N
Cl
Cl
Cl
240
220
200
180
160
140
120
100
80
60
40
20
0
-20
-40
ppm

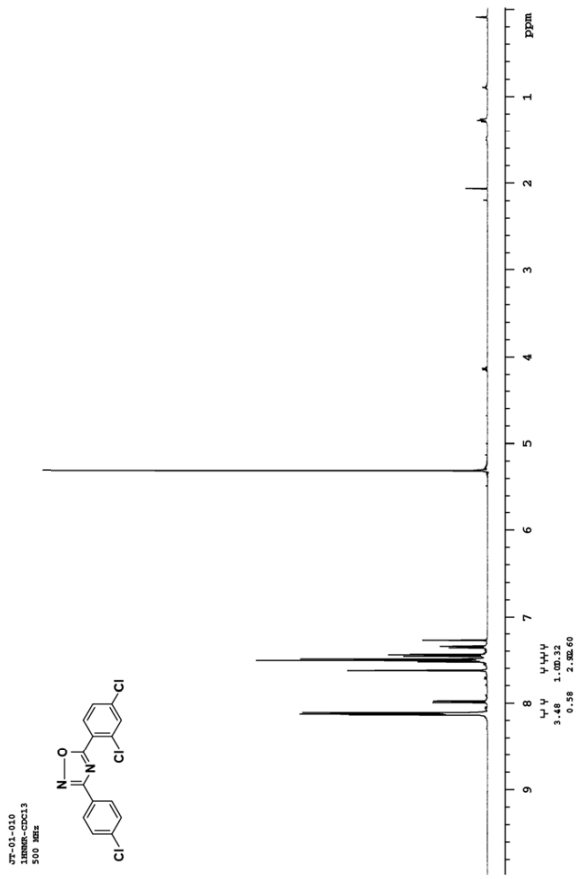
JT-01-010
1HNMR-CDCl3
500 MHz
Cl
Cl
Cl
N
O
N
ppm
1
2
3
4
5
6
7
8
9
3.48
0.58

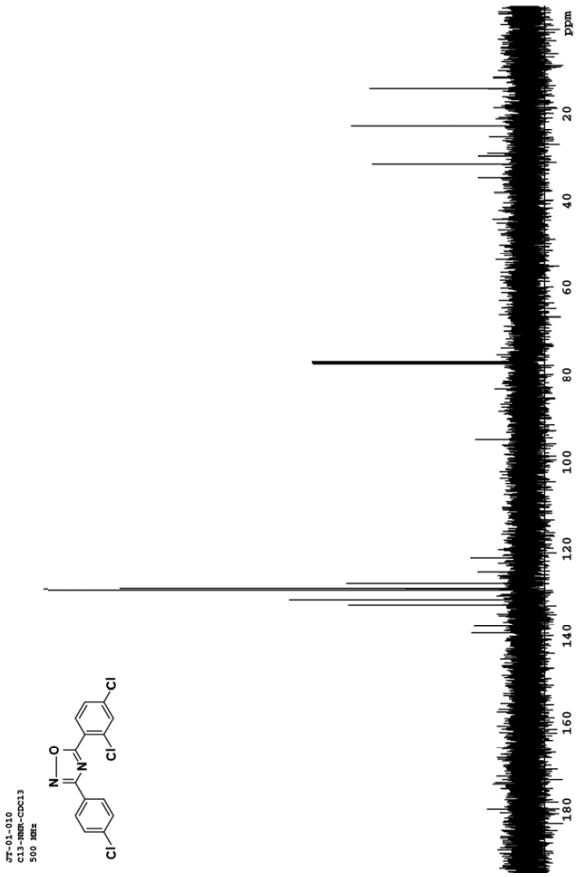
JT-01-010
C13-NMR-CDCl3
500 MHz
O
N
N
Cl
Cl
Cl
ppm
20
40
60
80
100
120
140
160
180

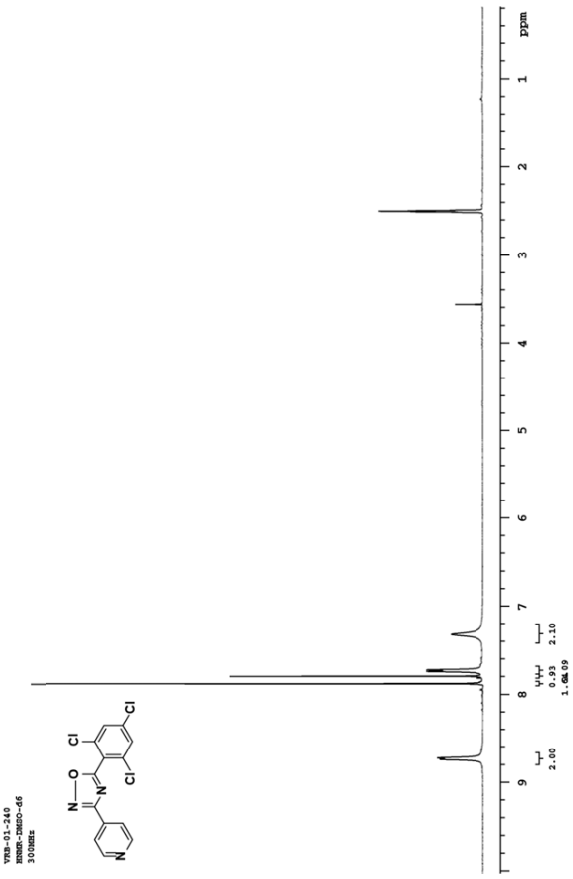
VRB-01-240
NMR-DMSO-d6
300MHz
Cl
Cl
Cl
N
O
N
N
ppm
1
2
3
4
5
6
7
8
9
0.93
1.00
2.10
2.00

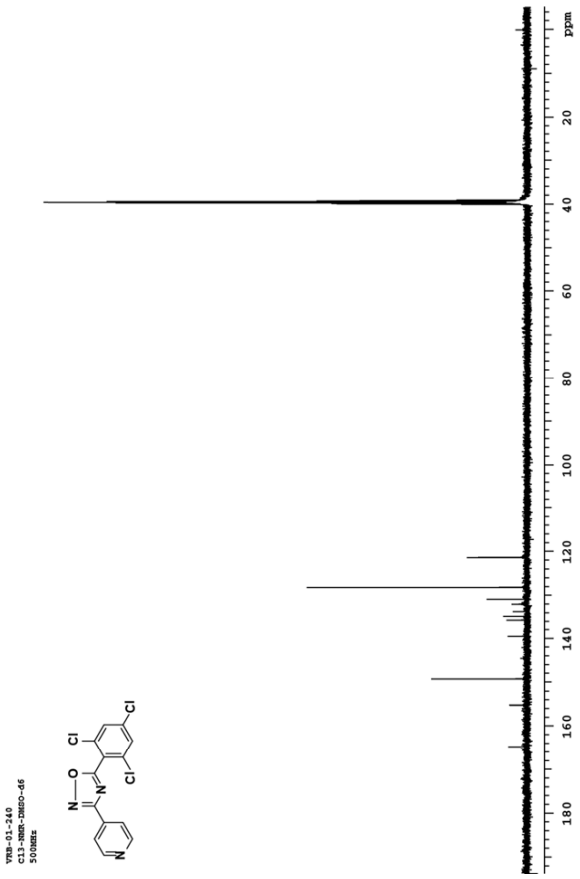
VRB-01-240
C13-NMR-DMSO-d6
500MHz
Cl
Cl
Cl
N
O
N
N
ppm
20
40
60
80
100
120
140
160
180

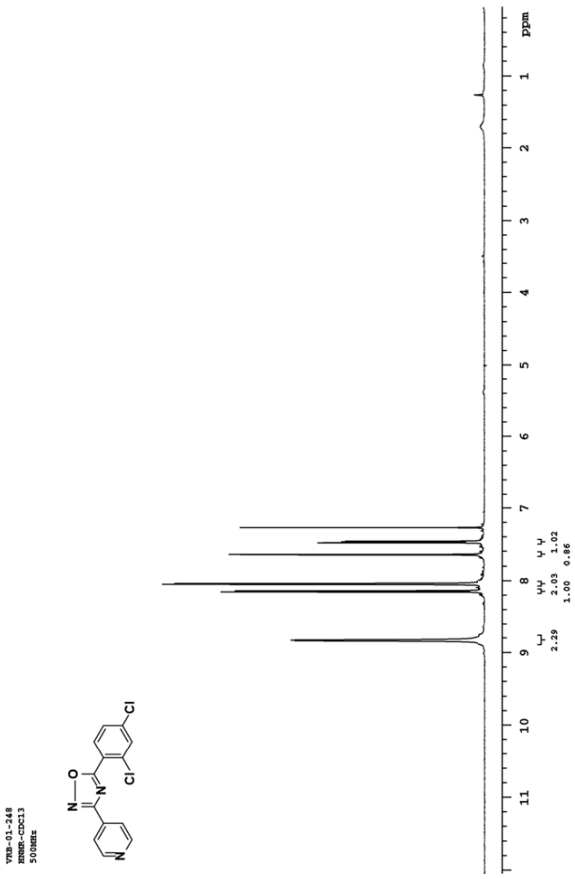
VRB-01-248
NMR-CDCl3
500MHz
Cl
Cl
N
O
N
N
ppm
1
2
3
4
5
6
7
8
9
10
11
2.29
2.03
1.00
1.02
0.86

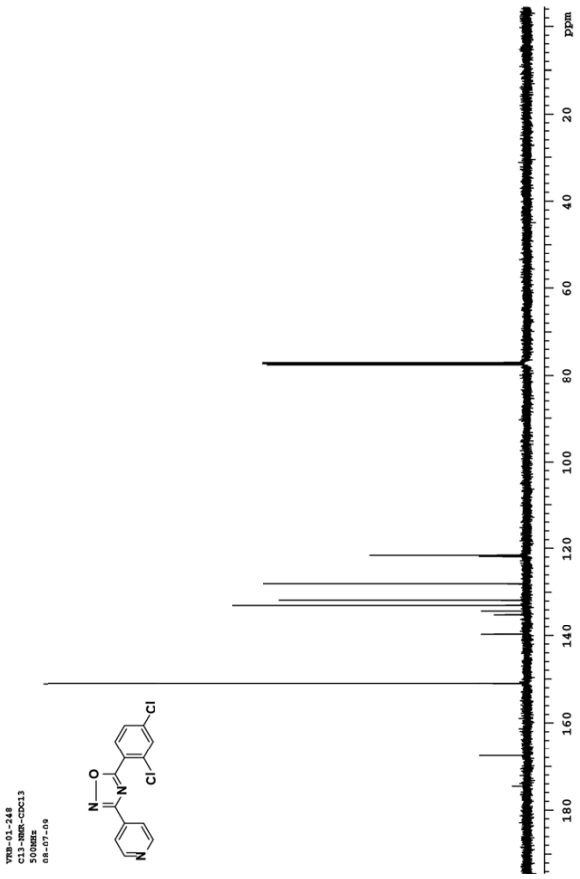
VRB-01-248
C13-NMR-CDCl3
500MHz
08-07-09
Cl
Cl
O
N
N
N
ppm
180
160
140
120
100
80
60
40
20

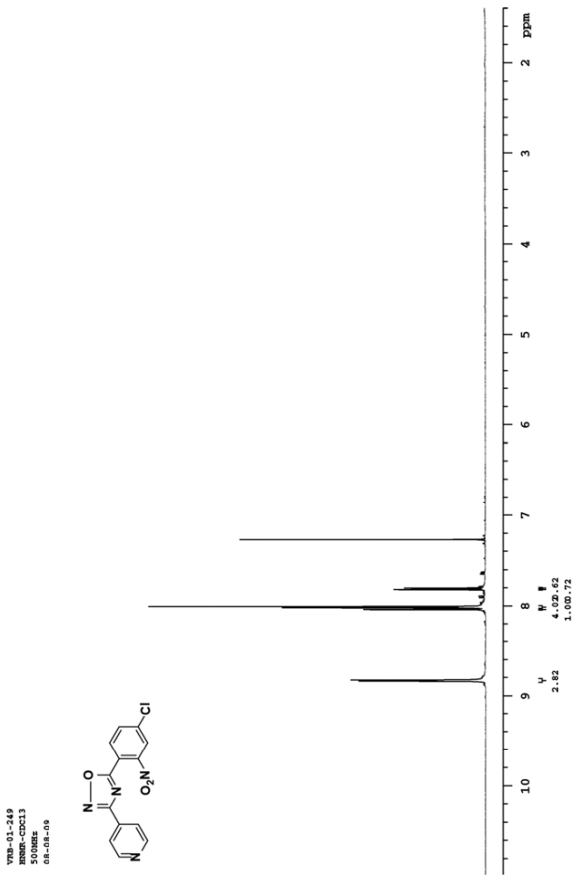
VRB-01-249
HNMR-CDCl3
500MHz
08-08-06
Cl
O2N
N
O
ppm
2
3
4
5
6
7
8
9
10
4.02
2.82
4.02.62
1.00.72

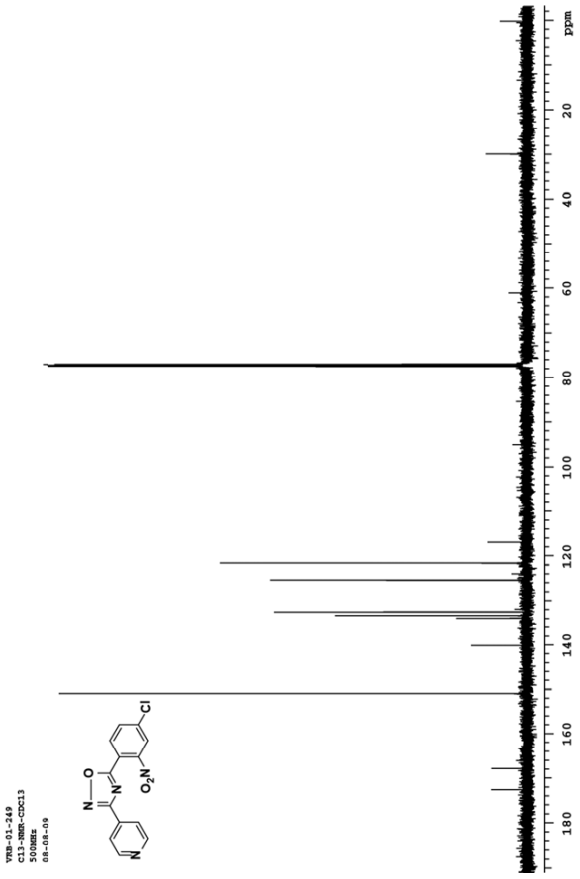
VRB-01-249
C13-NMR-CDCl3
500MHz
08-08-06
Cl
O
N
N
O2N
ppm
20
40
60
80
100
120
140
160
180

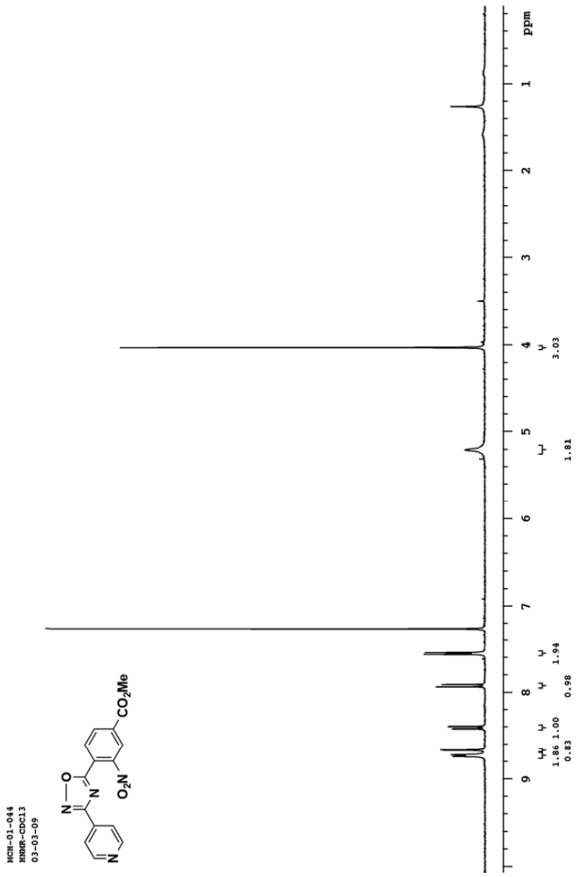
MCM-01-044
HNMR-CDCl3
03-03-09
CO2Me
O2N
ppm
1
2
3
4
5
6
7
8
9
3.03
1.81
1.94
0.98
1.86
1.00
0.83

60

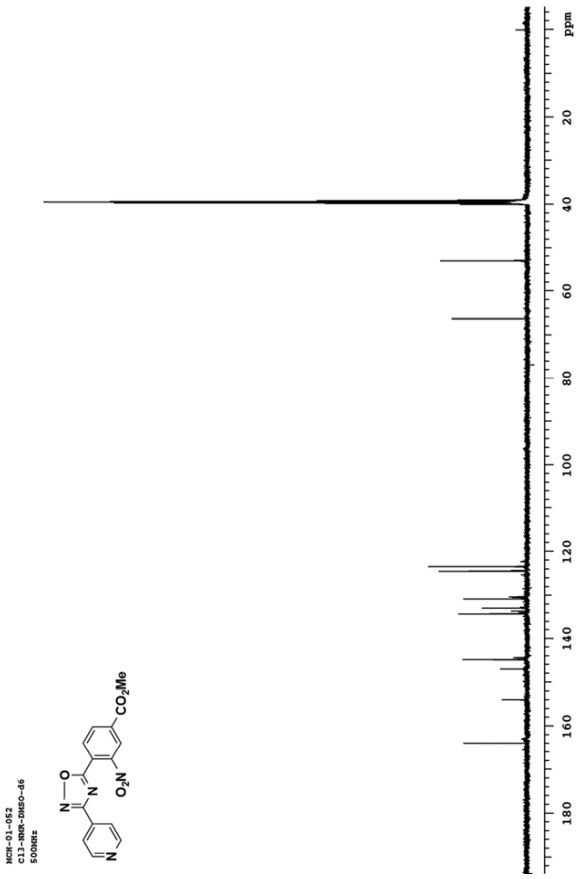
MCH-01-052
C13-NMR-DMSO-d6
500MHz
ppm
20
40
60
80
100
120
140
160
180

2. Biological Experiments:

A. Chemical compounds for screening–TCDD (Cambridge Isotopes Laboratories, Inc., Andover, MA) was obtained as a DMSO stock solution. 1,2,4-*bis*-aryloxadiazole and all associated analogs were synthesized as described above and dissolved in DMSO at a stock concentration of 10 mM.

B. HC11 cell culture–HC11 cells were grown at 37 ºC with 5% CO_2 in RPMI (HyClone) supplemented with 10% FBS (HyClone), 1x ITS-X (Invitrogen), 1X penicillin/streptomycin/glutamine (Invitrogen), and 10 ng/mL murine EGF (BD Biosciences). For all compound treatments, FBS was reduced to 2% 12 hours after seeding cells and cells were treated as indicated.

C. RNA extraction and real-time PCR–HC11 cells were treated for 48 hours with vehicle (0.1% DMSO), TCDD (10 nM), or an analog of 1,2,4-bis-aryloxadiazole (10 μM). RNA isolation and RT-PCR was performed as previously described[1] with the following primer sequences: β-actin forward 5'-GGCTGTGCTGTCCCTGTATG-3', β-actin reverse 5'-CAAGAAGGAAGGCTGGAAAA-3', Cyp1a1 forward 5'-GGTTAACCATGACCGGGAACT-3', Cyp1a1 reverse 5'-TGCCCAAACCAAAGAGAGTGA-3'. Relative gene expression was calculated by direct CT comparison[2] using β-actin as an internal reference gene. Results are shown as mean ± s.e.m.

D. Isolation, aggregation, and culture of primary MECs–Organoids from the fourth inguinal mammary gland were isolated from 8-12 week-old female FVB/n mice[3] (FVB/n mice were maintained following protocols reviewed and approved by the University of Utah Institutional Animal Care and Use Committee). Single cells were aggregated and grown in Matrigel as previously described[1]. Briefly, aggregates were grown in the presence of 2.5 nM FGF2

(Invitrogen) for 144 hours with vehicle (0.1% DMSO) or an analog of 1,2,4-*bis*-aryloxadiazole (10 μM). Results are shown as mean ± s.d.; n = 3.

E. Microscopy–Imaging was performed using an Olympus IX81-ZDC microscope with an ORCAER CCD camera and Slidebook 5.0.0.24 software (Intelligent Imaging Innovations, Inc). DIC images were captured using a 20X long working distance objective lens.

F. Western blot protocol– Cell lysates were harvested and processed as previously described[1]. For each sample, MEC aggregates were grown for 144 hours in Matrigel with 2.5 nM FGF2 and vehicle (0.1% DMSO), TCDD (10 nM) or an analog of 1,2,4-*bis*-aryloxadiazole (10 μM). Three wells of a 24 well plate (1,000 aggregates per well) were combined. Whole cell (10 μg) lysate was separated by 10% SDS-polyacrylamide gel electrophoresis and transferred to PVDF membrane (Millipore) for detection of mouse DSG3 (1:200, MBL #D218-3) and α-tubulin (1:1000, Sigma-Aldrich #T6199). Integrated intensity values were measured on a LI-COR Odyssey Scanner with mean background subtraction. For each sample, DSG3 levels were normalized to α-tubulin levels.

[1]Basham, K. J.; Kieffer, C.; Shelton, D. N.; Leonard, C. J.; Bhonde, V. R.; Vankayalapati, H.; Milash, B.; Bearss, D. J.; Looper, R. E.; Welm, B. E. *J. Biol. Chem.* **2013,** *288*, 2261.
[2]Schefe, J. H.; Lehmann, K. E.; Buschmann, I. R.; Unger, T.; Funke-Kaiser, H. *J Mol Med (Berl)* **2006,** *84*, 901.
[3]Welm, B. E.; Dijkgraaf, G. J.; Bledau, A. S.; Welm, A. L.; Werb, Z. *Cell Stem Cell* **2008,** *2*, 90.

CHAPTER 4

DIOXIN EXPOSURE BLOCKS LACTATION THROUGH A DIRECT EFFECT ON MAMMARY EPITHELIAL CELLS MEDIATED BY THE ARYL HYDROCARBON RECEPTOR REPRESSOR

This research is under review for publication in Toxicological Sciences. Kaitlin J. Basham, Christopher J. Leonard, Collin Kieffer, Dawne N. Shelton, Vasudev R. Bhonde, Ryan E. Looper, and Bryan E. Welm. Dioxin Exposure Blocks Lactation Through a Direct Effect on Mammary Epithelial Cells Mediated by the Aryl Hydrocarbon Receptor Repressor.

Abstract

In mammals, lactation is a rich source of nutrients and antibodies for newborn animals. However, millions of mothers each year experience an inability to breastfeed. Exposure to several environmental toxins, including 2,3,7,8-Tetrachlorodibenzo-*p*-dioxin (TCDD), has been strongly implicated in impaired mammary differentiation and lactation. TCDD and related polyhalogenated aromatic hydrocarbons are widespread industrial pollutants that activate the aryl hydrocarbon receptor (AHR). Despite many epidemiological and animal studies, the molecular mechanism through which AHR signaling blocks lactation remains unclear. We employed *in vitro* models of mammary differentiation to recapitulate lactogenesis in the presence of toxins. We demonstrate AHR agonists directly block milk production in isolated mammary epithelial cells. Moreover, we define a novel role for the aryl hydrocarbon receptor repressor (AHRR) in mediating this response. Our mechanistic studies suggest AHRR is sufficient to block transcription of important milk genes and requires recruitment of a corepressor complex for this function. Since TCDD is a prevalent environmental toxin that affects women worldwide, our results have important public health implications for newborn nutrition.

Introduction

Lactation is a critical biological process in mammals that provides both nutritional and immune support for offspring. However, an estimated 3-6 million human mothers worldwide suffer from impaired lactation each year (1). Several factors contribute to milk production and secretion, but a growing number of studies suggest certain environmental toxins negatively impact the ability of women to initiate and sustain

breastfeeding (2). For example, maternal exposure to pesticides has been associated with shortened duration of lactation in both the United States (3) and Mexico (4).

One specific xenobiotic known to affect lactation is 2,3,7,8-Tetrachlorodibenzo-*p*-dioxin (TCDD). TCDD is a byproduct of natural processes, such as volcanic eruptions and forest fires, and industrial processes, including smelting, waste incineration, pesticide production, and combustion (5). Once produced, TCDD persists in the environment and contaminates air, soil, and food sources (6,7). Although inhalation and skin exposure occur, ingestion of contaminated food sources is the primary route of exposure for humans (8). With an average half-life between 7 and 8 years in humans (9), TCDD is a highly stable chemical that bioaccumulates in fat tissue. Thus, TCDD exposure amasses and persists (10).

Previous studies have demonstrated TCDD exerts its toxicity through activation of the aryl hydrocarbon receptor (AHR) (11). As a ligand activated transcription factor, AHR is restricted to the cytoplasm in its unbound state. Once activated, AHR translocates to the nucleus and forms a transcriptionally active complex with the AHR nuclear translocator (ARNT) to alter expression of specific target genes (12). Although the identity of endogenous AHR activators remains controversial, several exogenous chemicals have been shown to target AHR (13). In particular, we previously identified a 1,2,4-*bis*-aryloxadiazole, referred to as 1023, as a novel AHR agonist (14,15).

An association between AHR activation and changes in milk production has been observed in animal studies. Specifically, pregnant mice exposed to TCDD *in vivo* produced lower levels of the milk proteins β-casein (16) and whey acidic protein (WAP) (17), and were unable to nutritionally support their offspring (17). Moreover, exposure of

pregnant rats to TCDD led to severe defects in mammary gland differentiation and decreased pup size following lactation (18,19), suggesting TCDD exposure impaired functional development of the mammary gland. Together with epidemiological studies in humans, these observations support a strong link between AHR activation and diminished milk production.

Despite these studies, the molecular mechanism through which AHR signaling blocks milk production remains unclear. Moreover, reciprocal transplant studies with AHR null mammary glands implicate both indirect, systemic effects and direct, cellular consequences of AHR signaling on alveolar differentiation (20). Indirectly, TCDD disrupts endocrine function by altering estrogen-mediated signaling (21,22). However, changes in circulating estradiol, progesterone, or prolactin levels were not observed in pregnant mice after *in vivo* TCDD exposure (17), which suggests mammary tissue may respond directly to AHR agonists. Moreover, explant studies, where mammary glands were cultured *ex vivo* under hormonal stimulation with TCDD, showed decreased lobuloalveolar structures (23). Together, these studies suggest AHR signaling contributes to impaired lactogenesis by directly targeting mammary tissue.

We aimed to identify direct epithelial mechanisms through which AHR activation blocks milk production. Using *in vitro* models of mammary morphogenesis and differentiation, we show that both environmental toxins (TCDD) and novel AHR agonists (1023) block lactogenesis directly in mammary epithelial cells. Furthermore, we identify a new role for the aryl hydrocarbon receptor repressor (AHRR) in mediating this response. Our results support a model in which AHRR induction promotes formation of AHRR/ARNT heterodimers, which transcriptionally inhibit milk production.

Results

AHR agonists inhibit milk production in mammary epithelial cells

To study the effect of AHR activation on lactation, we sought to recapitulate this process *in vitro*. Initially, we grew primary mammary epithelial cells (MECs) in the presence of AHR agonists in our three-dimensional branching assay (14) and performed microarray analysis to determine differentially expressed genes. Compared to vehicle treatment (DMSO), cells grown with 10 μM 1023 showed downregulation of several genes important for milk production, including *whey acidic protein* and multiple *casein* genes (Table 4.1). Given the lack of stromal components in this system (14,24), these results suggested AHR activation blocked milk production through a direct mechanism in mammary epithelial cells.

To validate these results, we next utilized the HC11 mammary epithelial cell line. HC11 cells were clonally derived from immortalized COMMA-1D epithelial cells (25), which were isolated from the mammary gland of midpregnant BALB/c mice (26). Importantly, these cells can be induced to differentiate with lactogenic hormones and produce milk proteins in culture (25,27). Using this assay, cells grown in the presence of 10 μM 1023 or 10 nM TCDD failed to produce the milk protein, β-casein, compared to vehicle treated cells (DMSO) (Figure 4.1A). In agreement with our microarray data from primary MECs, a block in *β-casein* production was also observed by RT-PCR (Figure 4.1B), suggesting a transcriptional mechanism of gene regulation.

Previously, we identified and validated AHR as the biological target of 1023 (14). To confirm the observed inhibition of milk protein production was dependent on the AHR pathway, we used lentiviral constructs to generate stable HC11 cell lines expressing

Table 4.1 Genes involved in milk production down regulated in MECs treated for 72 hours with 10 μM 1023

Gene identifier	Gene name	Gene symbol	Ratio*
NM_007784	Casein alpha s1	*Csn1*	+10.97
NM_007786	Casein kappa	*Csn3*	+8.24
NM_011709	Whey acidic protein	*Wap*	+7.88
NM_009972	Casein beta	*Csn2*	+6.84

*Log_2 ratio for 1023-treated *versus* DMSO

either a nonspecific shRNA (Control) or an shRNA against *AHR* (shAHR #1 and shAHR #2). In cells with ~50% *AHR* knockdown (Figure 4.1C), we observed a partial rescue in β-casein expression in the presence of AHR agonists (Figure 4.1D). These results suggested TCDD and 1023 inhibited milk production in mammary epithelial cells through AHR pathway activation.

The aryl hydrocarbon receptor repressor is sufficient to inhibit lactation

Given our data in both primary MECs and mammary HC11 cells, we hypothesized AHR activation blocked milk production through a transcriptional mechanism. Moreover, we became interested in a potential role for AHRR in mediating this process. As a direct target of activated AHR (28), AHRR is highly upregulated in primary MECs treated with 1023 (14) and has a known role as a transcriptional repressor. Specifically, AHRR forms a heterodimer with ARNT and binds to xenobiotic-responsive elements (XREs) in the promoter region of AHR target genes. Subsequent recruitment of a corepressor complex, which includes ANKRA2, HDAC4, and HDAC5, inhibits transcription of AHR target genes (28,29).

Figure 4.1. AHR activation blocks milk production in MECs. Mammary HC11 cells were treated with vehicle control (DMSO), 10 μM 1023, or 10 nM TCDD and induced with lactogenic hormones (LH) to produce milk proteins. A, HC11 cell lysates were probed for β-casein and α-tubulin (control). B, *β-casein* mRNA levels were measured in the same assay by RT-PCR and normalized to *β-actin* expression. Results are shown as normalized mean *β-casein* expression (± SEM). An **** indicates a statistically significant difference compared to vehicle treated cells ($p \leq 0.0001$). C, Lentiviral shRNA constructs (shAHR#1 and shAHR#2) were used to stably knockdown *AHR* expression HC11 cells. *AHR* expression was measured by RT-PCR, normalized to *β-actin* expression, and compared to HC11 cells stably expressing a control shRNA (Control). D, Stable HC11 cell lines were treated, induced, and probed for β-casein and β-actin (control) as described above. Abbreviations: TCDD, 2,3,7,8-Tetrachlorodibenzo-*p*-dioxin; LH, lactogenic hormones; AHR, aryl hydrocarbon receptor.

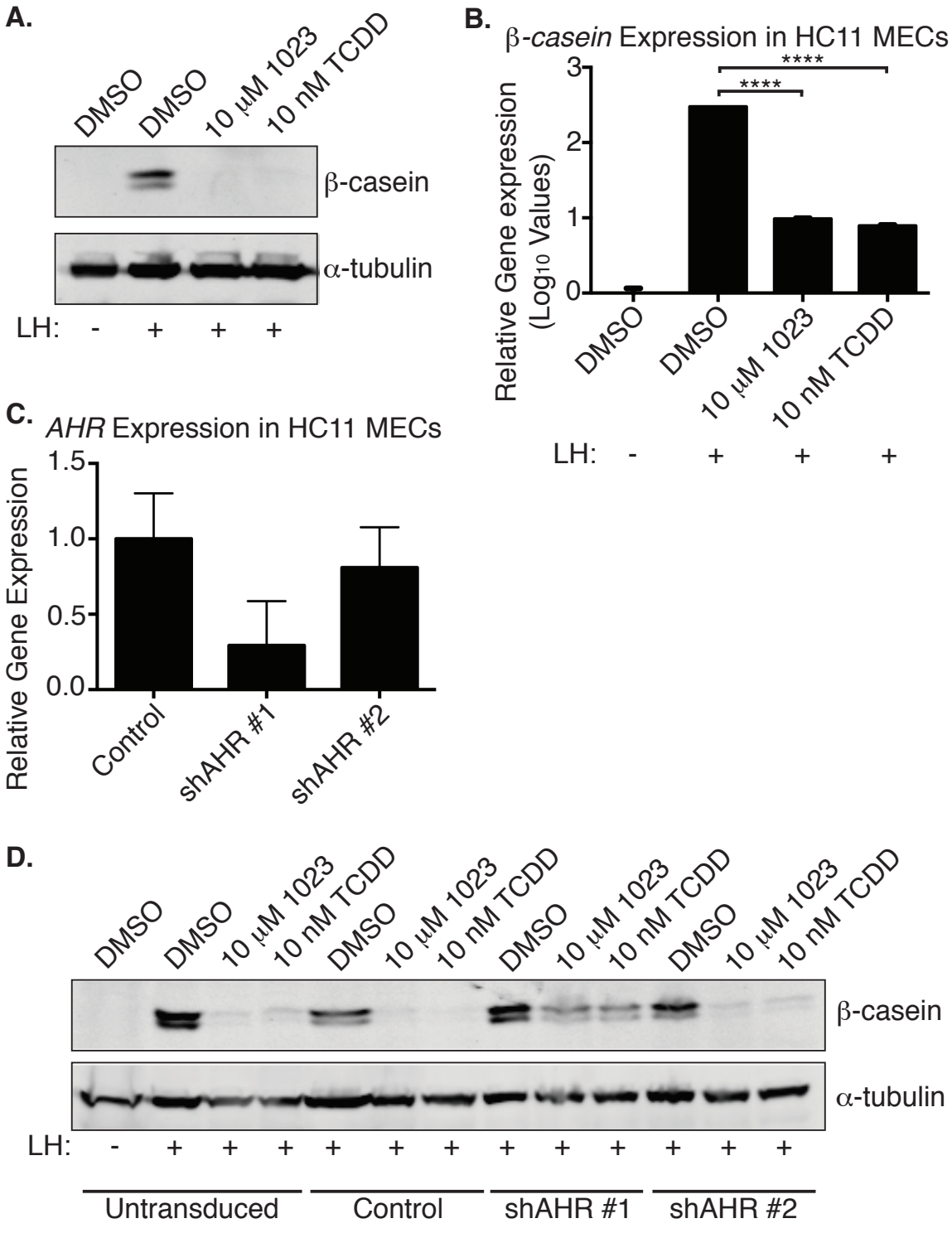
A.
DMSO
DMSO
10 μM 1023
10 nM TCDD
β-casein
α-tubulin
LH: - + + +
B.
β-casein Expression in HC11 MECs
Relative Gene expression (Log10 Values)
****
****
DMSO
DMSO
10 μM 1023
10 nM TCDD
LH: - + + +
C.
AHR Expression in HC11 MECs
Relative Gene Expression
Control
shAHR #1
shAHR #2
D.
DMSO
DMSO
10 μM 1023
10 nM TCDD
β-casein
α-tubulin
LH: - + + + + + + + + + + + +
Untransduced
Control
shAHR #1
shAHR #2

To test the effect of AHRR on milk production, we first stably expressed a lentiviral hemagglutinin (HA)-tagged AHRR construct in HC11 cells. We confirmed overexpression (Figure 4.2A) and validated the construct by measuring a well-characterized AHR response gene, *Cyp1A1*. Compared to control transduced cells, overexpression of AHRR decreased induction of *Cyp1A1* after 48 hours of treatment with 10 μM 1023 (Figure 4.2B). These results verified our tagged AHRR construct interacted with ARNT to functionally repress known target genes.

Next, to examine a potential role for AHRR in repressing milk production, we tested whether AHRR expression was sufficient to block β-casein production in the absence of AHR agonists. In HC11 cells induced with lactogenic hormones, and without exposure to AHR agonists, β-casein production was repressed at both the mRNA (Figure 4.2C) and protein level (Figure 4.2D) in cells expressing HA-AHRR compared to control cells. These results demonstrated the presence of AHRR was sufficient to block lactation.

AHRR contains a transcriptional repression domain within its C-terminal region, which consists of three conserved small ubiquitin-like modifier (SUMO)ylation sites at Lys-542, Lys-583, and Lys-660. Previous studies demonstrated these lysine residues are modified by SUMO-1 to facilitate interaction between AHRR and its corepressor complex (30). To genetically test the requirement of this interaction for AHRR to inhibit milk production, we mutated all three lysine residues to arginine (HA-AHRRmutant). Previously, these mutations in AHRR have been shown to allow interaction between AHRR and ARNT, but prevent interaction between AHRR and its corepressor complex (30). Compared to HC11 cells overexpressing wild-type AHRR, overexpression of the

Figure 4.2. AHRR is sufficient to block milk production in MECs. HC11 cells were transduced with lentivirus to generate cell lines stably expressing hemagglutinin (HA)-tagged AHRR (pEiZ-HA-AHRR) or a control (pEiZ). A, Western blot of lysates from stable cell lines probed for HA and α-tubulin (control). B, Stable HC11 cell lines were treated for 48 hours with vehicle control (DMSO) or 10 μM 1023. *Cyp1A1* mRNA levels were measured by RT-PCR and normalized to *β-actin* expression. Results are shown as normalized mean *Cyp1A1* expression (± SEM). An **** indicates a statistically significant difference compared to control cells ($p \leq 0.0001$). Stable HC11 cell lines were induced with lactogenic hormones (LH) to produce milk proteins. C, *β-casein* mRNA levels were measured by RT-PCR and normalized to *β-actin* expression. Results are shown as normalized mean *β-casein* expression (± SEM). An **** indicates a statistically significant difference compared to control cells ($p \leq 0.0001$). D, Cell lysates were probed for β-casein and α-tubulin (control). E, An HC11 cell line was generated to express AHRR mutated to prevent SUMOylation in the C-terminal region (HA-AHRRmutant). All stable cell lines were induced with LH and probed for β-casein and α-tubulin (control) as before. Abbreviations: HA, hemagglutinin; AHRR, aryl hydrocarbon receptor repressor; MECs, mammary epithelial cells; LH, lactogenic hormones.

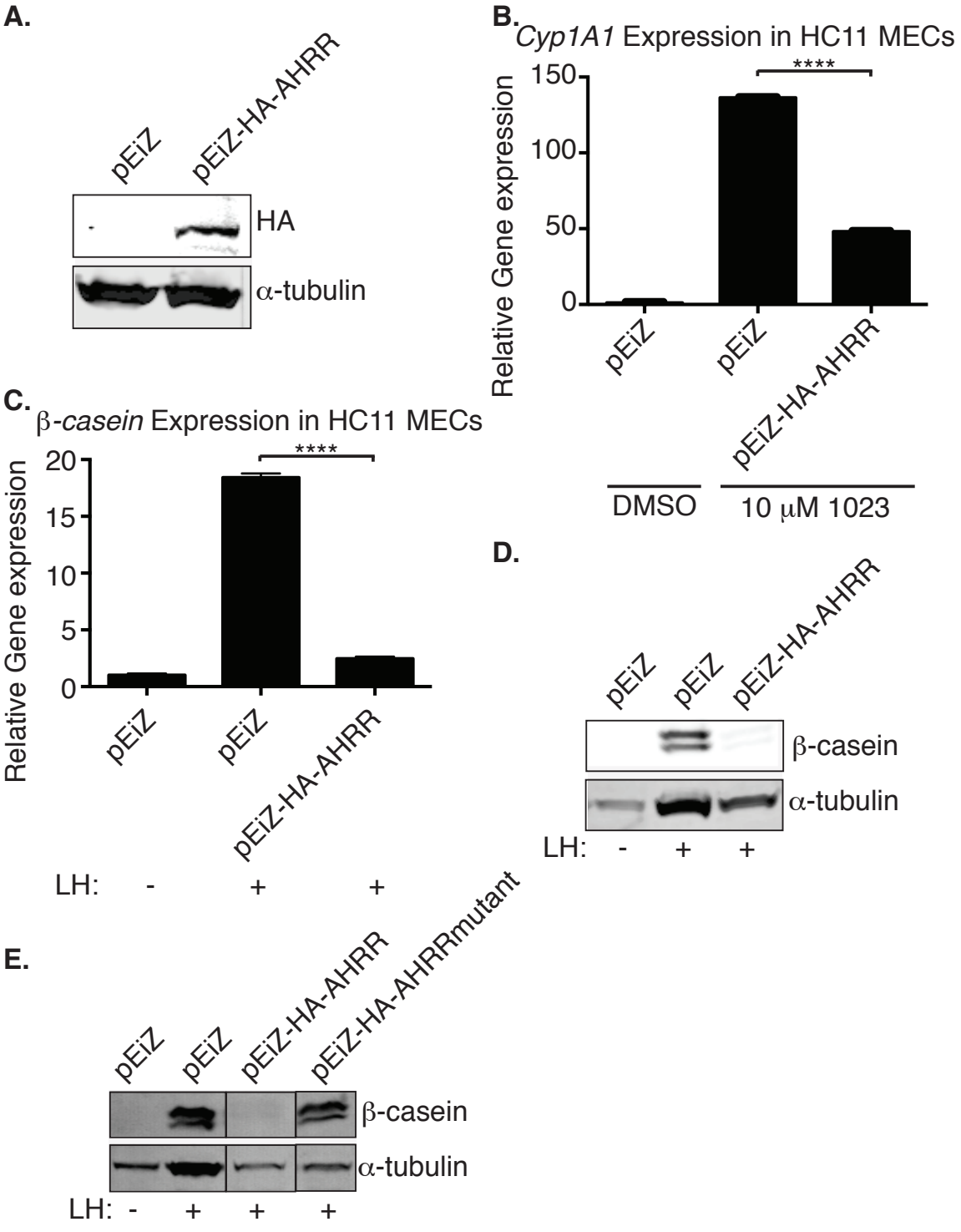
A.
pEiZ
pEiZ-HA-AHRR
HA
α-tubulin
B.
Cyp1A1 Expression in HC11 MECs
****
Relative Gene expression
150
100
50
0
pEiZ
pEiZ
pEiZ-HA-AHRR
DMSO
10 μM 1023
C.
β-casein Expression in HC11 MECs
****
Relative Gene expression
20
15
10
5
0
pEiZ
pEiZ
pEiZ-HA-AHRR
LH: - + +
D.
pEiZ
pEiZ
pEiZ-HA-AHRR
β-casein
α-tubulin
LH: - + +
E.
pEiZ
pEiZ
pEiZ-HA-AHRR
pEiZ-HA-AHRRmutant
β-casein
α-tubulin
LH: - + + +

SUMOylation mutant fully rescued β-casein production (Figure 4.2E), indicating AHRR requires interaction with its corepressor complex to inhibit lactogenesis.

ARNT is required for milk production in mammary epithelial cells

To elucidate the mechanism through which AHRR inhibits milk production, we examined the role of its major binding partner, ARNT, during normal lactation. Stable HC11 cell lines expressing a nonspecific lentiviral shRNA (Control) or a lentiviral shRNA against ARNT (shARNT #1 or shARNT #2) were generated (Figure 4.3A-B). Following induction with lactogenic hormones, knockdown of ARNT inhibited β-casein expression at both the mRNA (Figure 4.3C) and protein level (Figure 4.3D). As loss of AHR had no effect on milk production in HC11 cells (Figure 4.1D), these results implicated an independent role for ARNT during milk production.

Overexpression of ARNT rescues milk production in the presence of AHR agonists

Based on our results, we hypothesized ARNT participated in a transcriptionally active complex to promote expression of milk genes, such as β-casein, during lactogenesis. Furthermore, since ARNT was required for lactogenesis, we speculated AHRR might inhibit milk production through competitive interactions with ARNT. To test this hypothesis, we overexpressed ARNT prior to treatment with AHR agonists and assessed milk production. We reasoned overexpression of ARNT would promote transcriptionally active complexes and restore milk production in the presence of AHR

Figure 4.3. ARNT is required for milk production in MECs. Lentiviral shRNA constructs (shARNT#1 and shARNT#2) were used to stably knockdown *ARNT* expression in HC11 cells. A, *ARNT* expression was measured by RT-PCR, normalized to *β-actin* expression, and compared to HC11 cells stably expressing a control shRNA (Control). Results are shown as normalized mean *ARNT* expression (± SEM). An * indicates a statistically significant difference compared to control cells ($p \leq 0.05$). B, ARNT protein levels were measured in cell lysates from stable lines. Western blot of lysates probed for ARNT and α-tubulin (control). Stable HC11 cell lines were induced with lactogenic hormones (LH) to produce milk proteins. C, *β-casein* mRNA levels were measured by RT-PCR and normalized to *β-actin* expression. Results are shown as normalized mean *β-casein* expression (± SEM). An **** indicates a statistically significant difference compared with control cells ($p \leq 0.0001$). D, Western blot of lysates probed for β-casein and α-tubulin (control). Abbreviations: ARNT, aryl hydrocarbon receptor nuclear translocator; MECs, mammary epithelial cells; LH, lactogenic hormones.

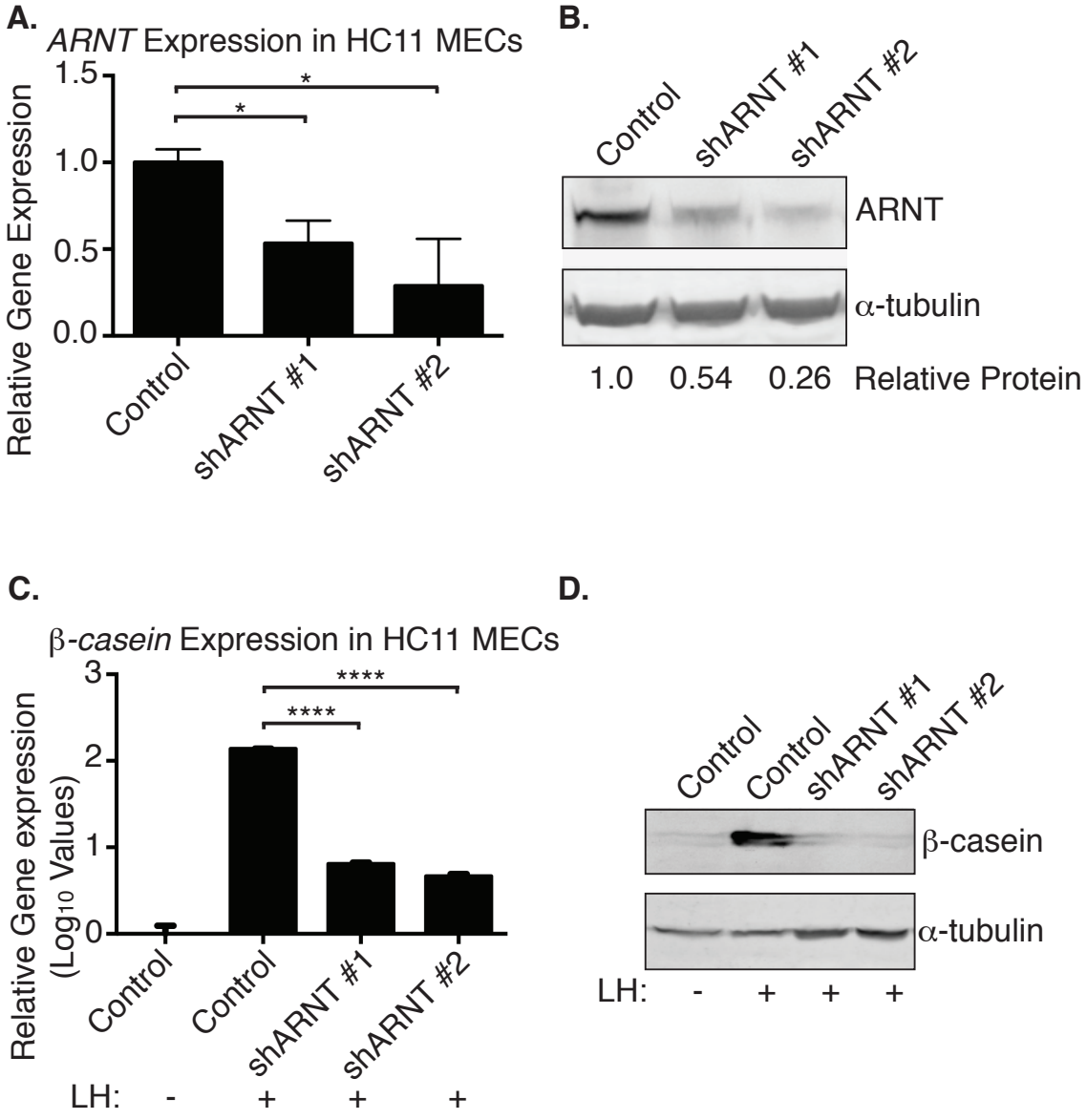
A.
ARNT Expression in HC11 MECs
Relative Gene Expression
1.5
1.0
0.5
0.0
*
*
Control
shARNT #1
shARNT #2
B.
Control
shARNT #1
shARNT #2
ARNT
α-tubulin
1.0 0.54 0.26 Relative Protein
C.
β-casein Expression in HC11 MECs
Relative Gene expression (Log10 Values)
3
2
1
0
****
****
Control
Control
shARNT #1
shARNT #2
LH: - + + +
D.
Control
Control
shARNT #1
shARNT #2
β-casein
α-tubulin
LH: - + + +

agonists. In HC11 cells stably overexpressing a lentiviral HA-ARNT construct (Figure 4.4A), we found milk production partially restored in the presence of both 10 μM 1023 and 10 nM TCDD compared to control cells (Figure 4.4B). These results support a model in which AHRR blocks milk production by acting as a transcriptional repressor to inhibit ARNT signaling.

Discussion

Using an epithelial-based model of mammary lactation, we demonstrate AHR agonists directly block milk production. Specifically, we showed AHRR, a robust downstream target of AHR signaling, was sufficient to inhibit lactogenesis. Although well studied in the context of AHR activation, AHRR is also induced by other toxic insults. In particular, recent studies showed cigarette smoking, including secondhand exposure, caused significant demethylation and increased expression of AHRR (31,32). As women who smoke have consistently been shown to produce significantly less milk volume (33,34) and breastfeed for a shorter duration (33,35-38), our results provide a potential molecular mechanism through which this toxicity occurs.

Following induction, AHRR forms a heterodimer complex with ARNT (39). As loss of ARNT completely blocked milk protein production in mammary epithelial cells, our results implicate an important role for ARNT during lactation. These observations are consistent with the phenotype observed in conditional ARNT knockout mice, where ARNT deletion using the MMTV-Cre transgene resulted in impaired mammary function (40). Specifically, loss of ARNT led to incomplete alveolar development, smaller litter sizes, and 60% of dams that could not support their pups.

Figure 4.4. ARNT overexpression rescues milk production in the presence of AHR agonists. A hemagglutinin (HA) tagged ARNT construct (pEiZ-HA-ARNT) was stably expressed in mammary HC11 cells using lentiviral transduction. An empty expression vector (pEiZ) was used to create a stable control HC11 cell line. A, Western blot of lysates probed for HA and α-tubulin (control). B, Stable HC11 cell lines were treated with vehicle control (DMSO), 10 μM 1023, or 10 nM TCDD and induced with lactogenic hormones (LH) to produce milk proteins. Western blot of lysates probed for β-casein and α-tubulin (control). Abbreviations: HA, hemagglutinin; ARNT, aryl hydrocarbon receptor nuclear translocator; LH, lactogenic hormones; TCDD, 2,3,7,8-tetrachlorodibenzo-*p*-dioxin.

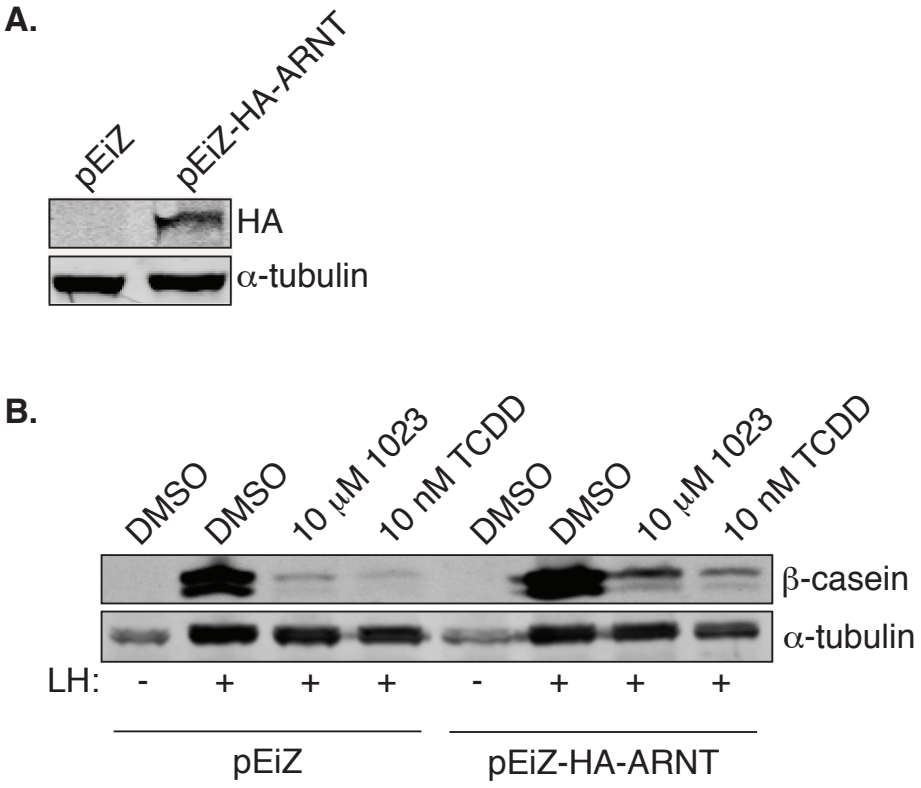
A.
pEiZ
pEiZ-HA-ARNT
HA
α-tubulin
B.
DMSO
DMSO
10 μM 1023
10 nM TCDD
DMSO
DMSO
10 μM 1023
10 nM TCDD
β-casein
α-tubulin
LH: - + + + - + + +
pEiZ
pEiZ-HA-ARNT

However, inactivation of ARNT using WAP-Cre resulted in normal mammary differentiation during pregnancy (40). Furthermore, transplantation of ARNT null mammary epithelium generated using MMTV-Cre into wild type recipients normalized alveolar development (40). Although inconsistent with initial studies and our current findings, these incongruent results may be explained by differences in methodology. Specifically, WAP-Cre reduced ARNT levels in 80% of the mammary epithelium (40,41), resulting in residual ARNT expression that may facilitate normal development. In reciprocal transplant studies, the high selective pressure of transplantation may have induced compensation from other ARNT family members, including ARNT2. Expressed in the mammary gland (42), ARNT2 is known to form functional complexes with AHR (43) and may be capable of contributing to mammary development. Further *in vivo* studies will be required to explain these differences.

Our experiments with AHRR and ARNT suggest a model in which ARNT promotes milk production under lactogenic conditions (Figure 4.5). As a basic helix-loop-helix (bHLH) PER-ARNT-SIM (PAS) family member, ARNT requires dimerization to form a functional transcription complex. Although ARNT is known to interact with multiple proteins, we hypothesize that hypoxia inducible factor-1α (HIF1α) or single-minded 2 (SIM2) interact with ARNT to promote lactation. In previous studies, conditional knockout of ARNT prevented induction of known HIF1α target genes (44), suggesting ARNT is critical for HIF1α signal transduction. Additionally, deletion of HIF1α in the mammary epithelium resulted in severe differentiation defects and failed lactation (45). Previous studies with SIM2 also support its potential role in cooperating with ARNT to regulate lactation. With SIM2 overexpression, precocious production of

Figure 4.5. Working model for the mechanism through which AHR activation blocks milk production in mammary epithelial cells. (Right) In the absence of AHR agonists, we propose ARNT signaling promotes milk production during lactogenic stimulation. (Left) In the presence of AHR agonists, AHR translocates to the nucleus and forms a heterodimer with ARNT. AHR/ARNT heterodimers bind XRE sequences to increase transcription of AHR target genes, including AHRR. Once induced, AHRR competes with AHR for interaction with ARNT and forms a transcriptionally repressive complex, which we propose inhibits expression of milk proteins.

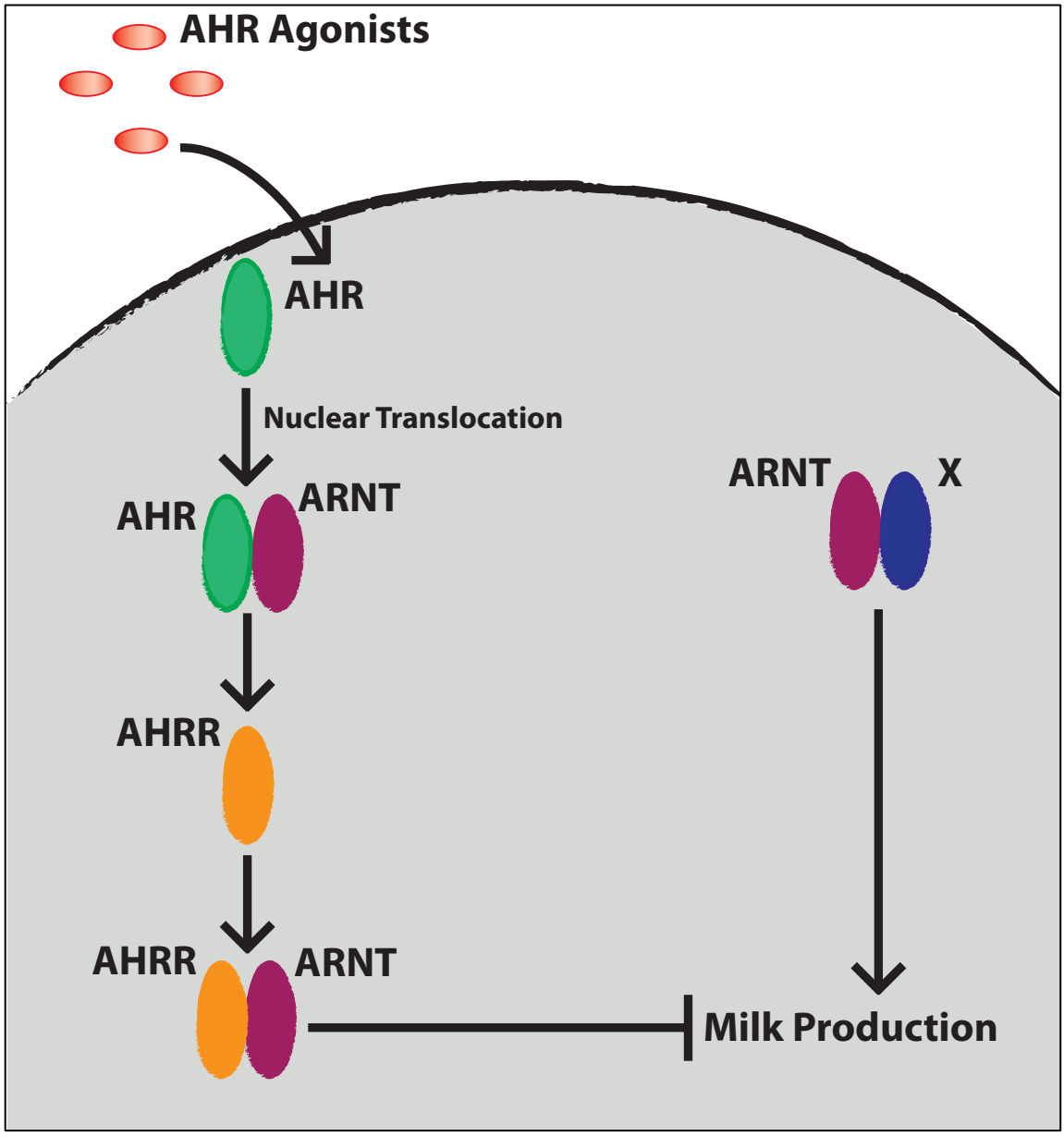
AHR Agonists
AHR
Nuclear Translocation
AHR
ARNT
AHRR
AHRR
ARNT
ARNT
X
Milk Production

β-casein and WAP occurred *in vitro* and *in vivo*, and chromatin immunoprecipitation (ChIP) experiments showed SIM2 associated with the β-casein promoter. Conversely, loss of SIM2 inhibited milk production (46). Taken together, these experiments strongly implicate a role for HIF1α or SIM2 in promoting ARNT-mediated lactogenesis.

In response to toxic stimuli, AHRR/ARNT heterodimers form and are sufficient to block lactation. One potential mechanism of AHRR repression under these conditions is ARNT sequestration. Competition for a limited pool of ARNT has been observed previously, where ARNT availability regulated AHR signaling through HIF1α (47) and SIM1 (48,49). However, our experiments using an AHRR repression mutant that could bind ARNT, but not recruit a corepressor complex, suggested this is not the dominant mechanism. Rather, our results indicate AHRR requires SUMOylation and subsequent recruitment of ANKRA2, HDAC4, and HDCA5 to block milk production. Further experiments will be needed to determine whether activating ARNT complexes and repressive AHRR/ARNT heterodimers bind the same DNA response elements. Additionally, these studies will help determine whether ARNT-mediated complexes bind directly in the promoter region of milk target genes or whether they control activity of an intermediate factor(s).

Our data demonstrate that AHR signaling directly disrupts milk protein production in isolated mammary epithelial cells. Since industrial waste is one of the main sources of TCDD and other related polyhalogenated aromatic hydrocarbons, human exposure to these toxins is highest in industrialized countries (50). However, acute exposure has occurred in several distinct populations worldwide, including exposure to Agent Orange herbicide in Vietnam (51), indigenous Canadian Inuit populations who

consume contaminated marine species (52), and people living in Seveso, Italy during the 1976 industrial explosion (53), among others. Given the prevalence of these environmental toxins and their ability to bioaccumulate over time, our study has substantial implications on public health, particularly with regard to the ability of women to breastfeed. Thus, future efforts to monitor TCDD exposure levels, analyze epidemiological data, and elucidate the molecular mechanism downstream of AHRR are needed to address this problem.

Materials and Methods

Microarray data

Data previously generated (14) were analyzed using GeneSifter software (Geospiza Inc). Microarray data analyzed for this publication can be obtained from the Gene Expression Omnibus database (http://www.ncbi.nlm.nih.gov/geo/) using accession number GSE39249.

Chemical compounds

TCDD (Cambridge Isotopes Laboratories, Inc., Andover, MA) was obtained as a DMSO stock solution. 1023 was synthesized as previously described (14) and dissolved in DMSO at a stock concentration of 10 mM.

HC11 cell culture and induction with lactogenic hormones

HC11 cells were maintained at 37 ^{o}C with 5% CO2 in HC11 culture media (RPMI (HyClone), 10% FBS (HyClone), ITS-X (Invitrogen), 1X

penicillin/streptomycin/glutamine (Invitrogen), and 10 ng/mL murine epidermal growth factor (EGF) (BD Biosciences)). For induction with lactogenic hormones, $1x10^6$ cells per well were seeded in 6-well tissue culture plates. Two-day confluent cultures were washed twice with EGF-free HC11 culture media and grown for 96 additional hours in EGF-free HC11 culture media containing 5 μg/mL ovine prolactin (Sigma) and 1 μM dexamethasone (Sigma). For compound treatments, FBS was reduced to 2% 12 hours after seeding and cells were grown with 0.1% DMSO, 10 μM 1023, or 10 nM TCDD as indicated. Throughout each assay, media were replaced every 48 hours.

Western blot

HC11 cells were washed twice and scraped in 1 mL cold PBS. Cells were pelleted at 1250 x g for 5 minutes, lysed in RIPA buffer (50 mM Tris-HCL pH 8.0, 150 mM NaCL, 0.1% SDS, 0.5% sodium deoxycholate, 1% Triton X-100, 1 mM DTT, 1X protease/phosphatase inhibitor cocktail), and sonicated for 20 seconds. All processing steps occurred at 4^oC or on ice. Whole cell lysate (50 μg) was separated by 10% SDS-polyacrylamide gel electrophoresis and transferred to PVDF membrane (Millipore) for detection of β-casein (1:100, Santa Cruz #sc-17969), α-tubulin (1:1000, Sigma-Aldrich #T6199), HA (1:500, Covance #MMS-101R), or ARNT (1:500, BD Biosciences #611078). Integrated intensity values were measured on a LI-COR Odyssey Scanner with mean background subtraction and normalized to α-tubulin levels.

RNA extraction, cDNA synthesis, and real-time PCR

RNA was isolated, converted to cDNA, and used for real-time PCR as previously described (14). Primer sequences were as follows: *β-actin* forward (5'-GGCTGTGCTGT CCCTGTATG-3'), *β-actin* reverse (5'-CAAGAAGGAAGGCTGGAAAA-3'), *β-casein* forward (5'-CAATCCCGTCCCACAAAA-3'), *β-casein* reverse (5'-TCCAGTTTCAGT CAGTTCAAAAA-3'), *AHR* forward (5'-CTTTGCTGAACTCGGCTTGC-3'), *AHR* reverse (5'-TTGCTGGGGGCACACCATCT-3'), *Cyp1A1* forward (5'-GGTTAACCATG ACCGGGAACT-3'), *Cyp1A1* reverse (5'-TGCCCAAACCAAAGAGAGTGA-3'), *ARNT* forward (5'-CTAAGAGACAGCTTTCAGCAGGT-3'), *ARNT* reverse (5'-AGGGTTTTG GAAGGTAAAGG AG-3').

Plasmids and molecular cloning

Constructs expressing an shRNA against AHR or ARNT were previously generated (14) using the pLentiLox5.0-GFP vector (54) provided by Dr. James Bear (University of North Carolina, Chapel Hill, NC). Lentiviral expression constructs were generated using the pEiZ plasmid (pHIV-Zsgreen, plasmid 18121, Addgene, Cambridge, MA) previously described (24). For generation of pEiZ-HA-AHRR, a mouse AHRR expression plasmid (pcDNA-mAhRR) (55) provided by Dr. Mark Hahn (Woods Hole Oceanographic Institution, Woods Hole, MA) was used to PCR amplify AHRR with addition of an N-terminal HA tag and EcoRI restriction sites. The following primers were used for amplification: forward (5'-CTAGAATTCCCACCATGAGCGTAGTCTG GGACGTCGTATGGGTAATGATGATTCCGTCTGGAGAGTGTACA-3'), reverse (5'-GACGAATTCACTCTAGGGTAGGAAAATTCCATCAGAGCC-3'). The resulting

PCR product was subcloned into the pCR®2.1-TOPO® TA vector to create Topo-HA-AHRR, which was then digested with EcoRI, and ligated into the same site in pEiZ. For generation of pEiZ-HA-AHRRmutant, site-directed mutagenesis was performed using the Strategene QuikChange Site-Directed Mutagenesis Kit (Strategene, La Jolla, CA) and the Topo-HA-AHRR plasmid according to manufactures instructions. Lys-542, Lys-583, and Lys-660 were each mutated to an arginine residue in separate reactions using the following primer sequences: Lys-542-Arg sense (5'-CACTGGATGTGCCAATCAGGATGGAGAATGAATCTGG-3'), Lys-542-Arg antisense (5'-CCAGATTCATTCTCCATCCTGATTGGCACATCCAGTG-3'), Lys-583-Arg sense (5'-CCAGGATGCACCTGAGAACAGAGCCCGACTA-3'), Lys-583-Arg antisense (5'-TAGTCGGGCTCTGTTCTCAGGTGCATCCTGG-3'), Lys-660-Arg sense (5'-ACTGCAGAGCTCCTATTGTTAGGCGTGAGCCTC-3'), Lys-660-Arg antisense (5'-GAGGCTCACGCCTAACAATAGGAGCTCTGCAGT-3'). Following site-directed mutagenesis, Topo-HA-AHRRmutant was digested with EcoRI and the resulting fragment was ligated into pEiZ using the same site. For generation of pEiZ-HA-ARNT, an HA-tagged mouse ARNT expression plasmid (pACTAG-HA-ARNT) (56) provided by Dr. Oliver Hankinson (University of California, Los Angeles, CA) was used to PCR amplify the HA-ARNT fragment with additional EcoRI restriction sites. The resulting PCR product was subcloned into the pCR®2.1-TOPO® TA vector to create Topo-HA-ARNT, which was digested with EcoRI and ligated into the same site in pEiZ. The following plasmids for generating lentivirus have been previously described: pMDLg/pRRE (57), pRSV-Rev (57), and pVSV-G (Clontech). The identity of each plasmid was confirmed by sequencing.

Production and titration of lentivirus

High titer lentivirus was produced, concentrated, and titrated as previously described (14).

Generation of stable HC11 cell lines

For stable HC11 cell lines expressing an shRNA or expression construct, $1.25x10^6$ cells were seeded in a 10-cm dish, cultured for 12 hours, and transduced at an MOI of 20. Transduced cells were sorted 72 hours later based on GFP expression to obtain stable lines.

References

1. Lew, B. J., Collins, L. L., O'Reilly, M. A., and Lawrence, B. P. (2009) Activation of the aryl hydrocarbon receptor during different critical windows in pregnancy alters mammary epithelial cell proliferation and differentiation. *Toxicol. Sci.* **111**, 151-162

2. Neville, M. C., and Walsh, C. T. (1995) Effects of xenobiotics on milk secretion and composition. *Am. J. Clin. Nutr.* **61**, 687S-694S

3. Rogan, W. J., Gladen, B. C., McKinney, J. D., Carreras, N., Hardy, P., Thullen, J., Tingelstad, J., and Tully, M. (1987) Polychlorinated biphenyls (PCBs) and dichlorodiphenyl dichloroethene (DDE) in human milk: Effects on growth, morbidity, and duration of lactation. *Am. J. Public Health* **77**, 1294-1297

4. Gladen, B. C., and Rogan, W. J. (1995) DDE and shortened duration of lactation in a northern Mexican town. *Am. J. Public Health* **85**, 504-508

5. Wong, M. H., Armour, M. A., Naidu, R., and Man, M. (2012) Persistent toxic substances: Sources, fates and effects. *Rev. Environ. Health* **27**, 207-213

6. Travis, C. C., and Hattemer-Frey, H. A. (1991) Human exposure to dioxin. *Sci. Total Environ.* **104**, 97-127

7. Larsen, J. C. (2006) Risk assessments of polychlorinated dibenzo- p-dioxins, polychlorinated dibenzofurans, and dioxin-like polychlorinated biphenyls in food. *Mol. Nutr. Food Res.* **50**, 885-896

8. Carpenter, D. O. (2006) Polychlorinated biphenyls (PCBs): Routes of exposure and effects on human health. *Rev. Environ. Health* **21**, 1-23

9. Geyer, H. J., Schramm, K. W., Feicht, E. A., Behechti, A., Steinberg, C., Bruggemann, R., Poiger, H., Henkelmann, B., and Kettrup, A. (2002) Half-lives of tetra-, penta-, hexa-, hepta-, and octachlorodibenzo-p-dioxin in rats, monkeys, and humans--a critical review. *Chemosphere* **48**, 631-644

10. Consonni, D., Sindaco, R., and Bertazzi, P. A. (2012) Blood levels of dioxins, furans, dioxin-like PCBs, and TEQs in general populations: A review, 1989-2010. *Environ. Int.* **44**, 151-162

11. Fernandez-Salguero, P. M., Hilbert, D. M., Rudikoff, S., Ward, J. M., and Gonzalez, F. J. (1996) Aryl-hydrocarbon receptor-deficient mice are resistant to 2,3,7,8-tetrachlorodibenzo-p-dioxin-induced toxicity. *Toxicol. Appl. Pharmacol.* **140**, 173-179

12. Tijet, N., Boutros, P. C., Moffat, I. D., Okey, A. B., Tuomisto, J., and Pohjanvirta, R. (2006) Aryl hydrocarbon receptor regulates distinct dioxin-dependent and dioxin-independent gene batteries. *Mol. Pharmacol.* **69**, 140-153

13. Denison, M. S., and Nagy, S. R. (2003) Activation of the aryl hydrocarbon receptor by structurally diverse exogenous and endogenous chemicals. *Annu. Rev. Pharmacol. Toxicol.* **43**, 309-334

14. Basham, K. J., Kieffer, C., Shelton, D. N., Leonard, C. J., Bhonde, V. R., Vankayalapati, H., Milash, B., Bearss, D. J., Looper, R. E., and Welm, B. E. (2013) Chemical genetic screen reveals a role for desmosomal adhesion in mammary branching morphogenesis. *J. Biol. Chem.* **288**, 2261-2270

15. Basham, K. J., Bhonde, V. R., Kieffer, C., Mack, J. B., Hess, M., Welm, B. E., and Looper, R. E. (2014) Bis-aryloxadiazoles as effective activators of the aryl hydrocarbon receptor. *Bioorg. Med. Chem. Lett.* **24**, 2473-2476

16. Collins, L. L., Lew, B. J., and Lawrence, B. P. (2009) TCDD exposure disrupts mammary epithelial cell differentiation and function. *Reprod. Toxicol.* **28**, 11-17

17. Vorderstrasse, B. A., Fenton, S. E., Bohn, A. A., Cundiff, J. A., and Lawrence, B. P. (2004) A novel effect of dioxin: Exposure during pregnancy severely impairs mammary gland differentiation. *Toxicol. Sci.* **78**, 248-257

18. Fenton, S. E., Hamm, J. T., Birnbaum, L. S., and Youngblood, G. L. (2002) Persistent abnormalities in the rat mammary gland following gestational and lactational exposure to 2,3,7,8-tetrachlorodibenzo-p-dioxin (TCDD). *Toxicol. Sci.* **67**, 63-74

19. Badesha, J. S., Maliji, G., and Flaks, B. (1995) Immunotoxic effects of exposure of rats to xenobiotics via maternal lactation. Part I 2,3,7,8-tetrachlorodibenzo-p-dioxin. *Int. J. Exp. Pathol.* **76**, 425-439

20. Lew, B. J., Manickam, R., and Lawrence, B. P. (2011) Activation of the aryl hydrocarbon receptor during pregnancy in the mouse alters mammary development through direct effects on stromal and epithelial tissues. *Biol. Reprod.* **84**, 1094-1102

21. Safe, S., Wang, F., Porter, W., Duan, R., and McDougal, A. (1998) Ah receptor agonists as endocrine disruptors: Antiestrogenic activity and mechanisms. *Toxicol. Lett.* **102-103**, 343-347

22. Matthews, J., and Gustafsson, J. A. (2006) Estrogen receptor and aryl hydrocarbon receptor signaling pathways. *Nucl. Recept. Signal.* **4**, e016

23. Hushka, L. J., Williams, J. S., and Greenlee, W. F. (1998) Characterization of 2,3,7,8-tetrachlorodibenzofuran-dependent suppression and AH receptor pathway gene expression in the developing mouse mammary gland. *Toxicol. Appl. Pharmacol.* **152**, 200-210

24. Welm, B. E., Dijkgraaf, G. J., Bledau, A. S., Welm, A. L., and Werb, Z. (2008) Lentiviral transduction of mammary stem cells for analysis of gene function during development and cancer. *Cell Stem Cell* **2**, 90-102

25. Ball, R. K., Friis, R. R., Schoenenberger, C. A., Doppler, W., and Groner, B. (1988) Prolactin regulation of beta-casein gene expression and of a cytosolic 120-kd protein in a cloned mouse mammary epithelial cell line. *EMBO J.* **7**, 2089-2095

26. Danielson, K. G., Oborn, C. J., Durban, E. M., Butel, J. S., and Medina, D. (1984) Epithelial mouse mammary cell line exhibiting normal morphogenesis in vivo and functional differentiation in vitro. *Proc. Natl. Acad. Sci. U. S. A.* **81**, 3756-3760

27. Doppler, W., Hock, W., Hofer, P., Groner, B., and Ball, R. K. (1990) Prolactin and glucocorticoid hormones control transcription of the beta-casein gene by kinetically distinct mechanisms. *Mol. Endocrinol.* **4**, 912-919

28. Mimura, J., Ema, M., Sogawa, K., and Fujii-Kuriyama, Y. (1999) Identification of a novel mechanism of regulation of Ah (dioxin) receptor function. *Genes Dev.* **13**, 20-25

29. Oshima, M., Mimura, J., Yamamoto, M., and Fujii-Kuriyama, Y. (2007) Molecular mechanism of transcriptional repression of AhR repressor involving ANKRA2, HDAC4, and HDAC5. *Biochem. Biophys. Res. Commun.* **364**, 276-282

30. Oshima, M., Mimura, J., Sekine, H., Okawa, H., and Fujii-Kuriyama, Y. (2009) SUMO modification regulates the transcriptional repressor function of aryl hydrocarbon receptor repressor. *J. Biol. Chem.* **284**, 11017-11026

31. Philibert, R. A., Beach, S. R., and Brody, G. H. (2012) Demethylation of the aryl hydrocarbon receptor repressor as a biomarker for nascent smokers. *Epigenetics* **7**, 1331-1338

32. Shenker, N. S., Polidoro, S., van Veldhoven, K., Sacerdote, C., Ricceri, F., Birrell, M. A., Belvisi, M. G., Brown, R., Vineis, P., and Flanagan, J. M. (2013) Epigenome-wide association study in the European Prospective Investigation into Cancer and Nutrition (EPIC-Turin) identifies novel genetic loci associated with smoking. *Hum. Mol. Genet.* **22**, 843-851

33. Vio, F., Salazar, G., and Infante, C. (1991) Smoking during pregnancy and lactation and its effects on breast-milk volume. *Am. J. Clin. Nutr.* **54**, 1011-1016

34. Hopkinson, J. M., Schanler, R. J., Fraley, J. K., and Garza, C. (1992) Milk production by mothers of premature infants: Influence of cigarette smoking. *Pediatrics* **90**, 934-938

35. Andersen, A. N., and Schioler, V. (1982) Influence of breast-feeding pattern on pituitary-ovarian axis of women in an industrialized community. *Am. J. Obstet. Gynecol.* **143**, 673-677

36. Hakansson, A., and Carlsson, B. (1992) Maternal cigarette smoking, breast-feeding, and respiratory tract infections in infancy. A population-based cohort study. *Scand. J. Prim. Health Care* **10**, 60-65

37. Schulte-Hobein, B., Schwartz-Bickenbach, D., Abt, S., Plum, C., and Nau, H. (1992) Cigarette smoke exposure and development of infants throughout the first year of life: Influence of passive smoking and nursing on cotinine levels in breast milk and infant's urine. *Acta. Paediatr.* **81**, 550-557

38. Whichelow, M. J. (1979) Breast feeding in Cambridge, England: Factors affecting the mother's milk supply. *J. Adv. Nurs.* **4**, 253-261

39. Evans, B. R., Karchner, S. I., Allan, L. L., Pollenz, R. S., Tanguay, R. L., Jenny, M. J., Sherr, D. H., and Hahn, M. E. (2008) Repression of aryl hydrocarbon receptor (AHR) signaling by AHR repressor: Role of DNA binding and competition for AHR nuclear translocator. *Mol. Pharmacol.* **73**, 387-398

40. Le Provost, F., Riedlinger, G., Hee Yim, S., Benedict, J., Gonzalez, F. J., Flaws, J., and Hennighausen, L. (2002) The aryl hydrocarbon receptor (AhR) and its nuclear translocator (Arnt) are dispensable for normal mammary gland development but are required for fertility. *Genesis* **32**, 231-239

41. Walton, K. D., Wagner, K. U., Rucker, E. B., 3rd, Shillingford, J. M., Miyoshi, K., and Hennighausen, L. (2001) Conditional deletion of the bcl-x gene from mouse mammary epithelium results in accelerated apoptosis during involution but does not compromise cell function during lactation. *Mech. Dev.* **109**, 281-293

42. Martinez, V., Kennedy, S., Doolan, P., Gammell, P., Joyce, H., Kenny, E., Prakash Mehta, J., Ryan, E., O'Connor, R., Crown, J., Clynes, M., and O'Driscoll, L. (2008) Drug metabolism-related genes as potential biomarkers: Analysis of expression in normal and tumour breast tissue. *Breast Cancer Res. Treat.* **110**, 521-530

43. Hirose, K., Morita, M., Ema, M., Mimura, J., Hamada, H., Fujii, H., Saijo, Y., Gotoh, O., Sogawa, K., and Fujii-Kuriyama, Y. (1996) cDNA cloning and tissue-specific expression of a novel basic helix-loop-helix/PAS factor (Arnt2) with close sequence similarity to the aryl hydrocarbon receptor nuclear translocator (Arnt). *Mol. Cell. Biol.* **16**, 1706-1713

44. Tomita, S., Sinal, C. J., Yim, S. H., and Gonzalez, F. J. (2000) Conditional disruption of the aryl hydrocarbon receptor nuclear translocator (Arnt) gene leads to loss of target gene induction by the aryl hydrocarbon receptor and hypoxia-inducible factor 1alpha. *Mol. Endocrinol.* **14**, 1674-1681

45. Seagroves, T. N., Hadsell, D., McManaman, J., Palmer, C., Liao, D., McNulty, W., Welm, B., Wagner, K. U., Neville, M., and Johnson, R. S. (2003) HIF1alpha is a critical regulator of secretory differentiation and activation, but not vascular expansion, in the mouse mammary gland. *Development* **130**, 1713-1724

46. Wellberg, E., Metz, R. P., Parker, C., and Porter, W. W. (2010) The bHLH/PAS transcription factor singleminded 2s promotes mammary gland lactogenic differentiation. *Development* **137**, 945-952

47. Gradin, K., McGuire, J., Wenger, R. H., Kvietikova, I., fhitelaw, M. L., Toftgard, R., Tora, L., Gassmann, M., and Poellinger, L. (1996) Functional interference between hypoxia and dioxin signal transduction pathways: Competition for recruitment of the Arnt transcription factor. *Mol. Cell. Biol.* **16**, 5221-5231

48. Woods, S. L., and Whitelaw, M. L. (2002) Differential activities of murine single minded 1 (SIM1) and SIM2 on a hypoxic response element. Cross-talk between basic helix-loop-helix/per-Arnt-Sim homology transcription factors. *J. Biol. Chem.* **277**, 10236-10243

49. Probst, M. R., Fan, C. M., Tessier-Lavigne, M., and Hankinson, O. (1997) Two murine homologs of the Drosophila single-minded protein that interact with the mouse aryl hydrocarbon receptor nuclear translocator protein. *J. Biol. Chem.* **272**, 4451-4457

50. Schecter, A., Birnbaum, L., Ryan, J. J., and Constable, J. D. (2006) Dioxins: An overview. *Environ. Res.* **101**, 419-428

51. Schecter, A., Quynh, H. T., Papke, O., Tung, K. C., and Constable, J. D. (2006) Agent Orange, dioxins, and other chemicals of concern in Vietnam: Update 2006. *J. Occup. Environ. Med.* **48**, 408-413

52. Ayotte, P., Carrier, G., and Dewailly, E. (1996) Health risk assessment for inuit newborns exposed to dioxin-like compounds through breast feeding. *Chemosphere* **32**, 531-542

53. Warner, M., Eskenazi, B., Mocarelli, P., Gerthoux, P. M., Samuels, S., Needham, L., Patterson, D., and Brambilla, P. (2002) Serum dioxin concentrations and breast cancer risk in the Seveso Women's Health Study. *Environ. Health Perspect.* **110**, 625-628

54. Cai, L., Marshall, T. W., Uetrecht, A. C., Schafer, D. A., and Bear, J. E. (2007) Coronin 1B coordinates Arp2/3 complex and cofilin activities at the leading edge. *Cell* **128**, 915-929

55. Karchner, S. I., Franks, D. G., Powell, W. H., and Hahn, M. E. (2002) Regulatory interactions among three members of the vertebrate aryl hydrocarbon receptor family: AHR repressor, AHR1, and AHR2. *J. Biol. Chem.* **277**, 6949-6959

56. Moffett, P., Reece, M., and Pelletier, J. (1997) The murine Sim-2 gene product inhibits transcription by active repression and functional interference. *Mol. Cell. Biol.* **17**, 4933-4947

57. Dull, T., Zufferey, R., Kelly, M., Mandel, R. J., Nguyen, M., Trono, D., and Naldini, L. (1998) A third-generation lentivirus vector with a conditional packaging system. *J. Virol.* **72**, 8463-8471

CHAPTER 5

SPATIAL AND TEMOPRAL REGULATION OF MAMMARY DESMOSOMES

Abstract

Desmosomes are specialized adhesion complexes that provide tight contacts between epithelial cells. Previously, we identified a role for desmosomes during mammary morphogenesis. Using a 3D model of *in vitro* mammary branching, we found loss of desmosomes was sufficient to induce branching morphogenesis in primary mammary epithelial cells (MECs). Furthermore, activation of the aryl hydrocarbon receptor (AHR) blocked mammary branching by upregulating desmosomes. In the present study, we investigated desmosome dynamics during *in vivo* mammary branching. In agreement with our previous data, desmosomes were lost in wild type mice during pregnancy. However, we observed differential regulation of desmosomal adhesion during pregnancy, with only myoepithelial specific desmosomes downregulated. These results suggest myoepithelial desmosomes significantly contribute to ductal integrity and regulate initiation of mammary branching morphogenesis. We also investigated desmosomes in the context of AHR activation and found loss of the aryl hydrocarbon receptor repressor (AHRR) increased desmosomes and blocked branching. Since AHRR negatively regulates AHR activity, these results implicate a direct link between activated AHR and desmosomal adhesion.

Introduction

Desmosomes are specialized intercellular junctions expressed in epithelial cells. These highly organized complexes contain proteins from the cadherin, armadillo, and plakin families (1). Cell-cell adhesion is mediated by desmosomal cadherins, which are a family of transmembrane proteins further divided into desmocollin (Dsc1-3) and

desmoglein (Dsg1-4) proteins (2). Armadillo proteins, including plakoglobin and plakophilin, bridge the cytoplasmic domains of the cadherins to desmoplakin (3), which attaches to intermediate filaments (1). By connecting the plasma membrane to the intermediate filament cytoskeleton, desmosomes stabilize tissues during mechanical stress (4). However, desmosomes are dynamic structures that also function in cell and tissue morphogenesis.

Previously, we identified a role for desmosomes during mammary morphogenesis (5). Unlike other organs, the mammary gland undergoes differential development after birth. A rudimentary ductal tree is formed during embryogenesis, but significant mammary growth does not begin until puberty, when hormonal cues stimulate ductal elongation. This process creates an elaborate ductal network that fills the surrounding adipose tissue (6). Mammary ducts maintain a bilayered morphology, with luminal epithelial cells surrounded by myoepithelial cells. During pregnancy, tertiary branching continues to expand the epithelial network and lobuloalveolar development occurs to form alveolar buds. These structures are critical to the function of the mammary gland, as they contain both differentiated luminal cells capable of producing milk proteins and contractile myoepithelial cells that aid milk delivery (7). Ultimately, mammary branching morphogenesis establishes an extensive ductal network capable of producing and delivering milk to newborn animals.

As a highly secretory epithelial tissue, the mammary gland must maintain both barrier integrity and cell permeability. The distinct phases and cyclical nature of mammary gland development requires a highly dynamic relationship between these two functions. Transmission electron microscopy (EM) performed in the 1970s suggests

cellular adhesion helps regulate this balance (8). In the virgin mouse mammary gland, EM analysis shows close interaction between ductal cells. Tight junctions, intermediate junctions, gap junctions, and desmosomes mediate luminal cell interactions. Dispersed desmosomes and gap junctions connect luminal and myoepithelial cells, and hemidesmosomes attach myoepithelial cells to the basal lamina. Alveoli resemble mammary ducts in early pregnancy, but once they gain secretory capacity, desmosomes appear to be lost. As tight and gap junctions remained, these observations suggested loss of desmosomes facilitates mammary morphogenesis and increases cell permeability.

Supporting these early observations, our previous work determined that increased desmosomal adhesion in primary mammary epithelial cells (MECs) blocks mammary branching (5). These results were obtained using an *in vitro* three-dimensional (3D) model of branching morphogenesis in which primary MECs were stimulated with fibroblast growth factor-2 (FGF2). In the first step of this assay, MECs reorganize to form duct-like structures before they initiate branching morphogenesis. Using a forward chemical genetic screen, we found activation of the aryl hydrocarbon receptor (AHR) blocked branching and maintained cells as apparently normal duct-like structures. Functionally, we showed AHR stimulation blocked the transition of MECs from duct-like to branched structures by promoting desmosomal adhesion. Likewise, loss of desmosomes was sufficient to induce mammary branching in MECs grown with epidermal growth factor (EGF), which normally promotes duct-like formation. Together, these results implicated desmosomes as a critical regulator of mammary morphogenesis.

Here, we investigated the temporal and spatial regulation of desmosomes during *in vivo* mammary branching. In support of our previous studies, we observed loss of

desmosomes during pregnancy in wild type mice. However, desmosomal cadherins were differentially regulated, with Dsc3 and Dsg3 exclusively expressed in myoepithelial cells and dramatically downregulated during pregnancy, while Dsc2 and Dsg2 were uniformly expressed and maintained during pregnancy. Our results support loss of myoepithelial specific desmosomes as a driving force during mammary branching. In addition to differences in expression and regulation during pregnancy, desmosomal cadherins also showed differential response to AHR stimulation. To further elucidate the molecular link between AHR activation and desmosomes, we studied primary MECs from aryl hydrocarbon receptor repressor (AHRR) deficient mice. Surprisingly, loss of AHRR alone blocked mammary branching and significantly increased desmosomes. These results strongly implicate a role for activated AHR in directly regulating desmosomal adhesion.

Results

Specific desmosomal cadherins are lost during pregnancy

Based on our previous studies, we hypothesized desmosomes were lost *in vivo* during pregnancy to facilitate branching. To test this, we harvested mammary epithelial tissue from virgin and 15-day pregnant FVB/n female mice (Figure 5.1A) and performed qRT-PCR to measure mRNA levels of desmosomal cadherins. We found d*esmocollin 1* (*Dsc1*), *desmoglein 1* (*Dsg1*), *desmocollin 3* (*Dsc3*), and *desmoglein 3* (*Dsg3*) dramatically downregulated in late pregnancy, compared to the virgin control (Figure 5.1B-E). In contrast, expression of *desmocollin 2* (*Dsc2*) and *desmoglein 2* (*Dsg2*) were

Figure 5.1. Desmosomal cadherins are lost during pregnancy. (A.) Representative whole mount analysis of mammary glands from (left) virgin and (right) 15 day pregnant FVB/n female mice. Glands were collected and stained with carmine alum. Scale bar, 250 μm. (B-E.) *Desmocollin 1* (*Dsc1*), *desmoglein 1* (*Dsg1*), *desmocollin 3* (*Dsc3*), and *desmoglein 3* (*Dsg3*) mRNAs were significantly down regulated at 15 days pregnancy compared to the virgin control. *Dsc1*, *Dsg1*, *Dsc3*, and *Dsg3* gene expression was measured in primary mammary epithelial cells (MECs) by qRT-PCR and normalized to *β-actin* expression. Results are shown as mean ± S.E. (error bars); **, $p < 0.01$; ***, $p < 0.001$.

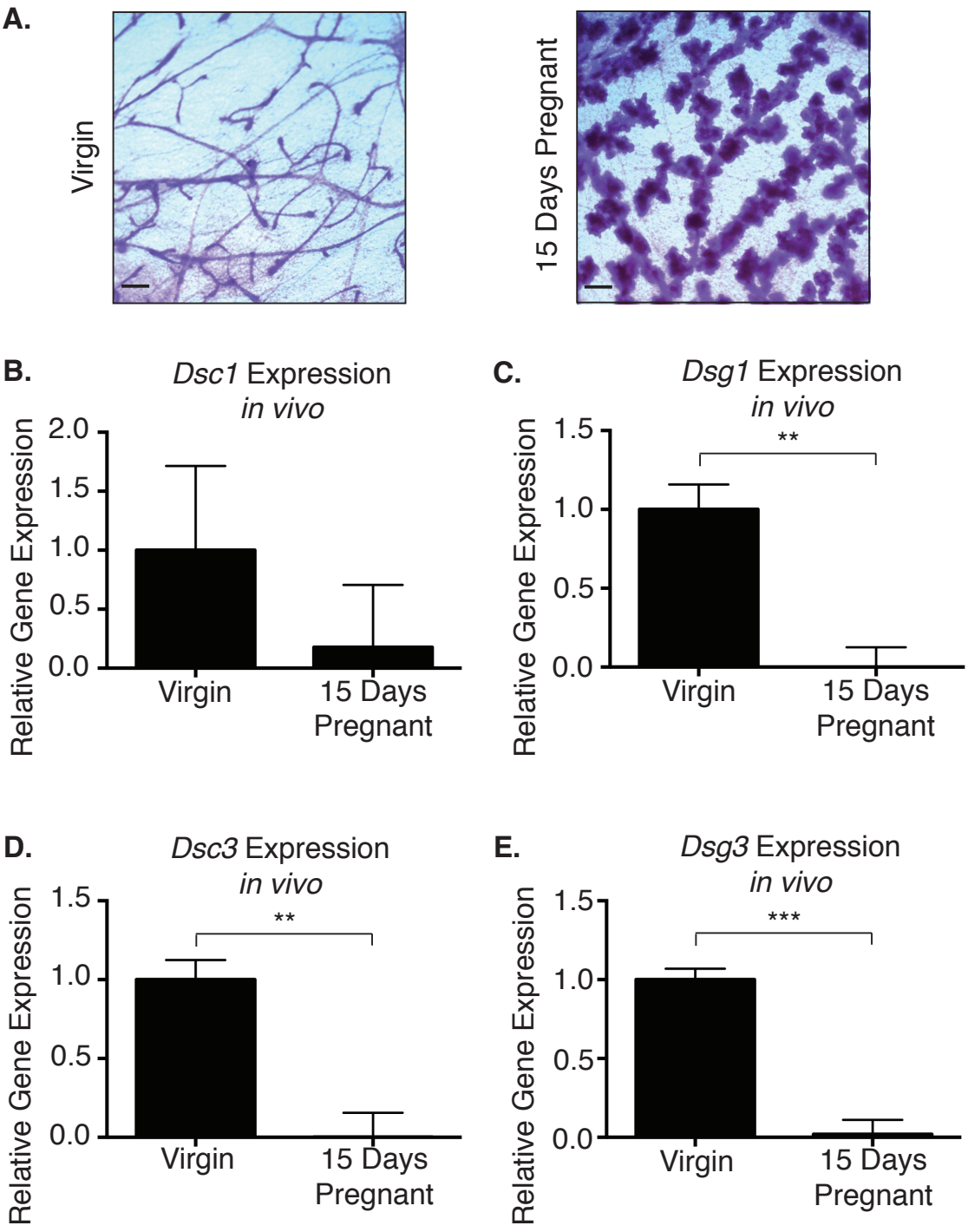
A.
Virgin
15 Days Pregnant
B.
Dsc1 Expression
in vivo
Relative Gene Expression
2.0
1.5
1.0
0.5
0.0
Virgin
15 Days Pregnant
C.
Dsg1 Expression
in vivo
**
Relative Gene Expression
1.5
1.0
0.5
0.0
Virgin
15 Days Pregnant
D.
Dsc3 Expression
in vivo
**
Relative Gene Expression
1.5
1.0
0.5
0.0
Virgin
15 Days Pregnant
E.
Dsg3 Expression
in vivo
***
Relative Gene Expression
1.5
1.0
0.5
0.0
Virgin
15 Days Pregnant

maintained during pregnancy (Figure 5.2A-B). Unlike the other desmosomal cadherins, *Dsc2* and *Dsg2* were not upregulated by AHR activation in our 3D culture system (Figure 5.2C-D). Only cadherin isoforms regulated by AHR signaling were altered *in vivo* during branching morphogenesis. These results demonstrate the differential *in vivo* regulation of desmosome components during pregnancy.

Desmosomal cadherins have distinct expression patterns
in the mammary gland

To better characterize these complexes, we next determined the expression pattern of desmosomal cadherins in the normal mammary gland. With a bilayered morphology, the mammary gland consists of cytokeratin-8 (K8) positive luminal epithelial cells surrounded by cytokeratin-14 (K14) positive myoepithelial cells (Figure 5.3A). Since Dsc1 and Dsg1 are not expressed in the human mammary gland (9), we focused our studies on Dsc2, Dsg2, Dsc3, and Dsg3. Primary MECs from virgin FVB/n female mice were FACS sorted using CD49f expression to enrich for mammary stem and myoepithelial cells (10). Using gene expression analysis, we found *Dsc3* and *Dsg3* were exclusively expressed in *K14*-positive, CD49f-high MECs, and *Dsc2* and *Dsg2* were expressed in both CD49f-low and CD49f-high populations (Figure 5.3B). These results were consistent with previous studies analyzing human (9) and bovine (11) mammary epithelial cells and suggested *Dsc3* and *Dsg3* were restricted to the myoepithelial cell population.

Figure 5.2. Dsc2 and Dsg2 are maintained during pregnancy. (A-B.) Expression of *desmocollin 2* (*Dsc2*) and *desmoglein 2* (*Dsg2*) mRNAs were not significantly changed between the virgin and pregnant state. Gene expression was measured in primary mammary epithelial cells (MECs) from FVB/n female mice. (C-D.) Similarly, epidermal growth factor (EGF) or aryl hydrocarbon receptor (AHR) agonists did not induce expression of *Dsc2* or *Dsg2* mRNA. Gene expression was measured in aggregated primary MECs grown in Matrigel for 96 hours with 2.5 nM EGF or 2.5 nM fibroblast growth factor-2 (FGF2) and 0.1% DMSO or 10 nM TCDD or 10 μM 1023. Gene expression was measured by qRT-PCR and normalized to *β-actin* expression. Results are shown as mean ± S.E. (error bars).

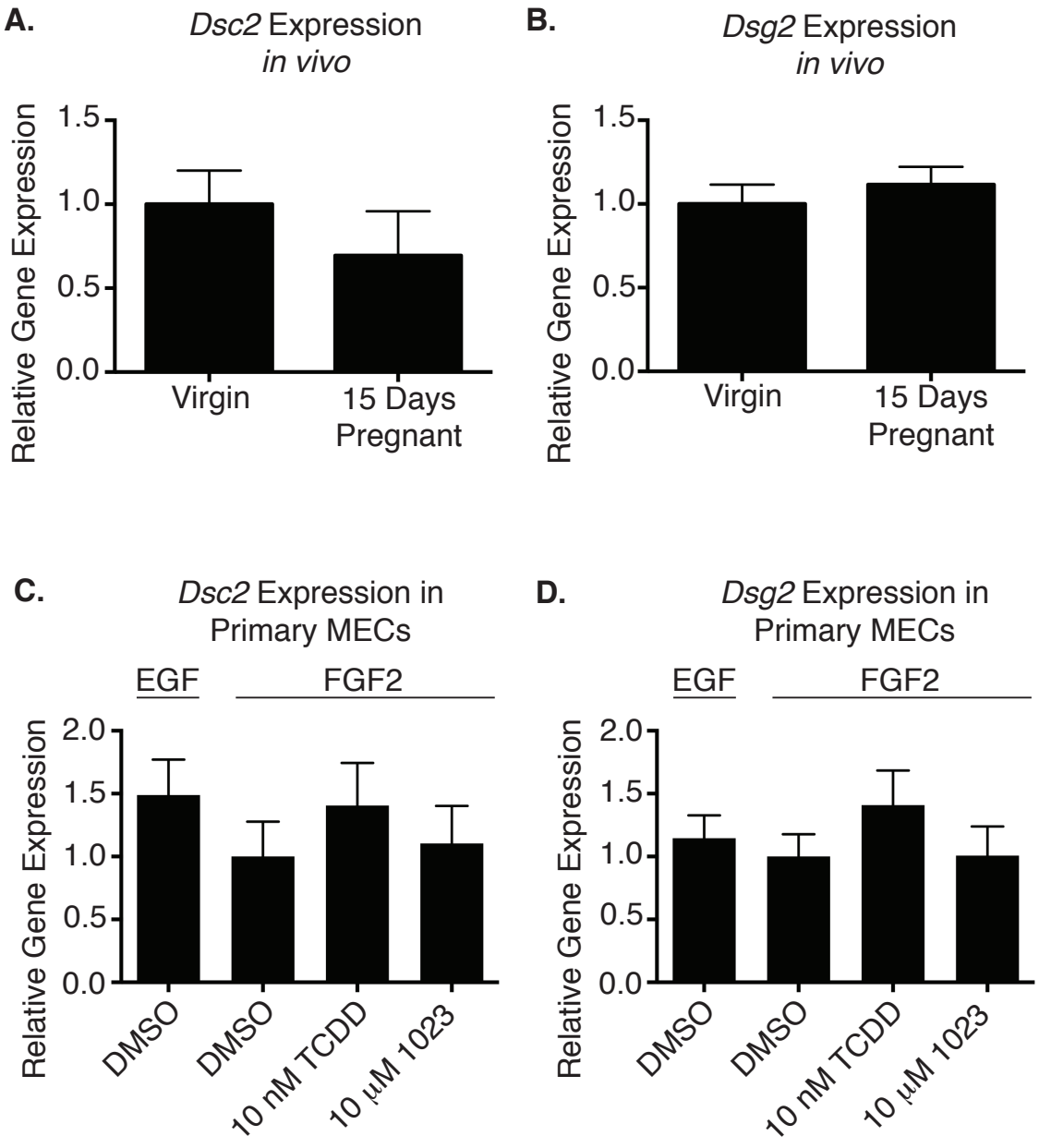
A.
Dsc2 Expression
in vivo
Relative Gene Expression
1.5
1.0
0.5
0.0
Virgin
15 Days
Pregnant
B.
Dsg2 Expression
in vivo
Relative Gene Expression
1.5
1.0
0.5
0.0
Virgin
15 Days
Pregnant
C.
Dsc2 Expression in
Primary MECs
EGF
FGF2
Relative Gene Expression
2.0
1.5
1.0
0.5
0.0
DMSO
DMSO
10 nM TCDD
10 μM 1023
D.
Dsg2 Expression in
Primary MECs
EGF
FGF2
Relative Gene Expression
2.0
1.5
1.0
0.5
0.0
DMSO
DMSO
10 nM TCDD
10 μM 1023

Figure 5.3. Desmosomes are differentially expressed in mammary epithelial cells (MECs). (A.) (Left) The virgin mammary gland contains a lymph node (LN) and large surrounding ductal network. Whole mount analysis from a virgin FVB/n female mouse is shown. Scale bar, 250 μm. (Right) Mammary ducts are composed of an epithelial bilayer, with cytokeratin-14 (K14, red) positive myoepithelial cells surrounding cytokeratin-8 (K8, green) positive luminal epithelial cells. Immunofluorescence was performed on a cross section of a duct from a virgin FVB/n female mouse and nuclei were stained with DAPI (blue). Scale bar, 40 μm. (B.) *Desmocollin 3* (*Dsc3*) and *desmoglein 3* (*Dsg3*) mRNA expression were highly enriched in myoepithelial cells, which also express high levels of *K14*. In contrast, *desmocollin 2* (*Dsc2*) and *desmoglein 2* (*Dsg2*) mRNA expression was similar in both myoepithelial cells and luminal epithelial cells. Luminal epithelial cells were enriched for *milk fat globule-EGF factor 8* (*Mfge8*) and *lactotransferrin* (*Ltf*), as expected. Gene expression was measured by qRT-PCR in CD49f sorted primary MECs isolated from virgin FVB/n female mice. Gene expression was normalized to *β-actin* expression.

A.

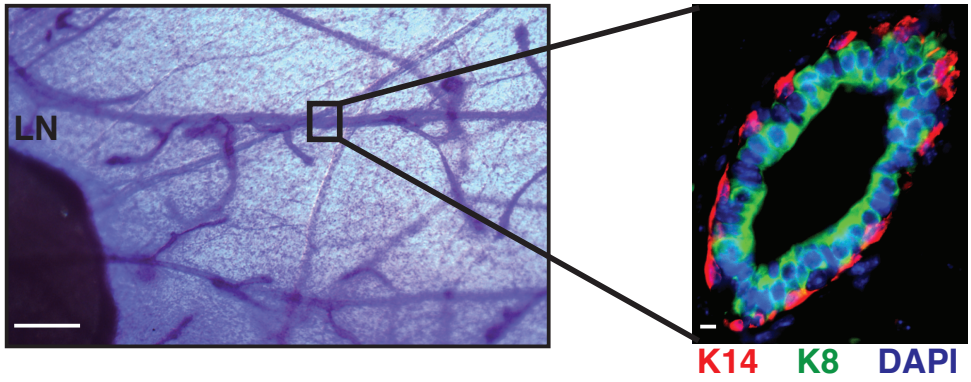
LN
K14
K8
DAPI

B.

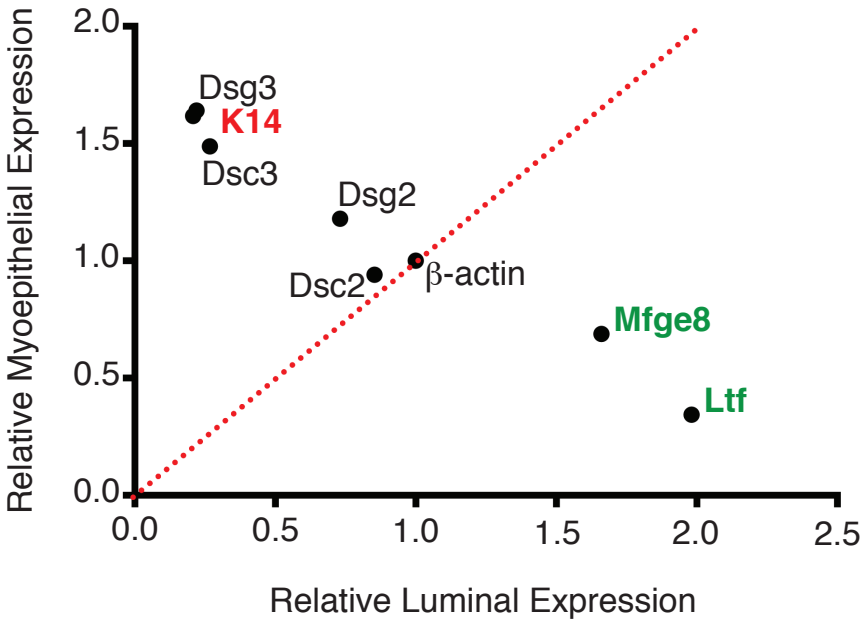
Relative Myoepithelial Expression
Relative Luminal Expression
2.0
1.5
1.0
0.5
0.0
0.0
0.5
1.0
1.5
2.0
2.5
Dsg3
K14
Dsc3
Dsg2
Dsc2
β-actin
Mfge8
Ltf

Expression of EMT factors correlates with desmosome dynamics

Next, we sought to determine how desmosomes were differentially regulated in the mammary gland. Although desmosome turnover can be controlled by endocytosis (12,13), our data implicated a transcriptional mechanism. As a result, we focused our studies on Snai1 and Snai2, which are two critical epithelial-to-mesenchymal transition (EMT) factors that act as transcriptional repressors. Snai1 and Snai2 are necessary and sufficient for branching morphogenesis in organotypic culture of MECs (14). Furthermore, Snai1 was shown to induce cell scattering in MDCK cells by disrupting cellular adhesion (15) and Snai2 dissociated desmosomes in NBT-II cells (16), a rat bladder carcinoma cell line. Based on these studies, we hypothesized Snai1 or Snai2 differentially regulated desmosomal cadherins in the mammary gland to induce branching morphogenesis.

To begin assessing these EMT factors as potential negative regulators of desmosomes, we first looked at their expression in response to AHR stimulation. We hypothesized *Snai1* or *Snai2* would be downregulated in TCDD-treated primary MECs, thus allowing for upregulation of desmosomes. Based on time-lapse imaging, 48 hours in culture represented a critical decision point in primary MEC cultures between cyst formation and branching morphogenesis (Figure 5.4A), and was also when robust upregulation of desmosomal cadherins began (Figure 5.4B-C). We observed ~50% reduction in *Snai1* expression (Figure 5.4D) and no significant change in *Snai2* expression (Figure 5.4E) after 48 hours of TCDD treatment. These results implicated a more likely role for *Snai1* than *Snai2* in regulating mammary desmosomes.

Figure 5.4. AHR activation downregulates *Snai1* expression. (A.) Time-course imaging of primary MECs grown in Matrigel with 2.5 nM fibroblast growth factor-2 (FGF2). Early initiation of branching is observed between 48 and 72 hours in culture. (B.) Primary MECs treated for 48 hours with 10 nM TCDD showed upregulation of *desmocollin 3* (*Dsc3*) and (C.) *desmoglein 3* (*Dsg3*) mRNAs. At this same time point, (D.) S*nai1* mRNA expression was reduced, but (E.) *Snai2* showed no change. Gene expression was measured by qRT-PCR and normalized to *β-actin* expression. Results are shown as mean ± S.E. (error bars); *, $p < 0.05$; ****, $p < 0.0001$.

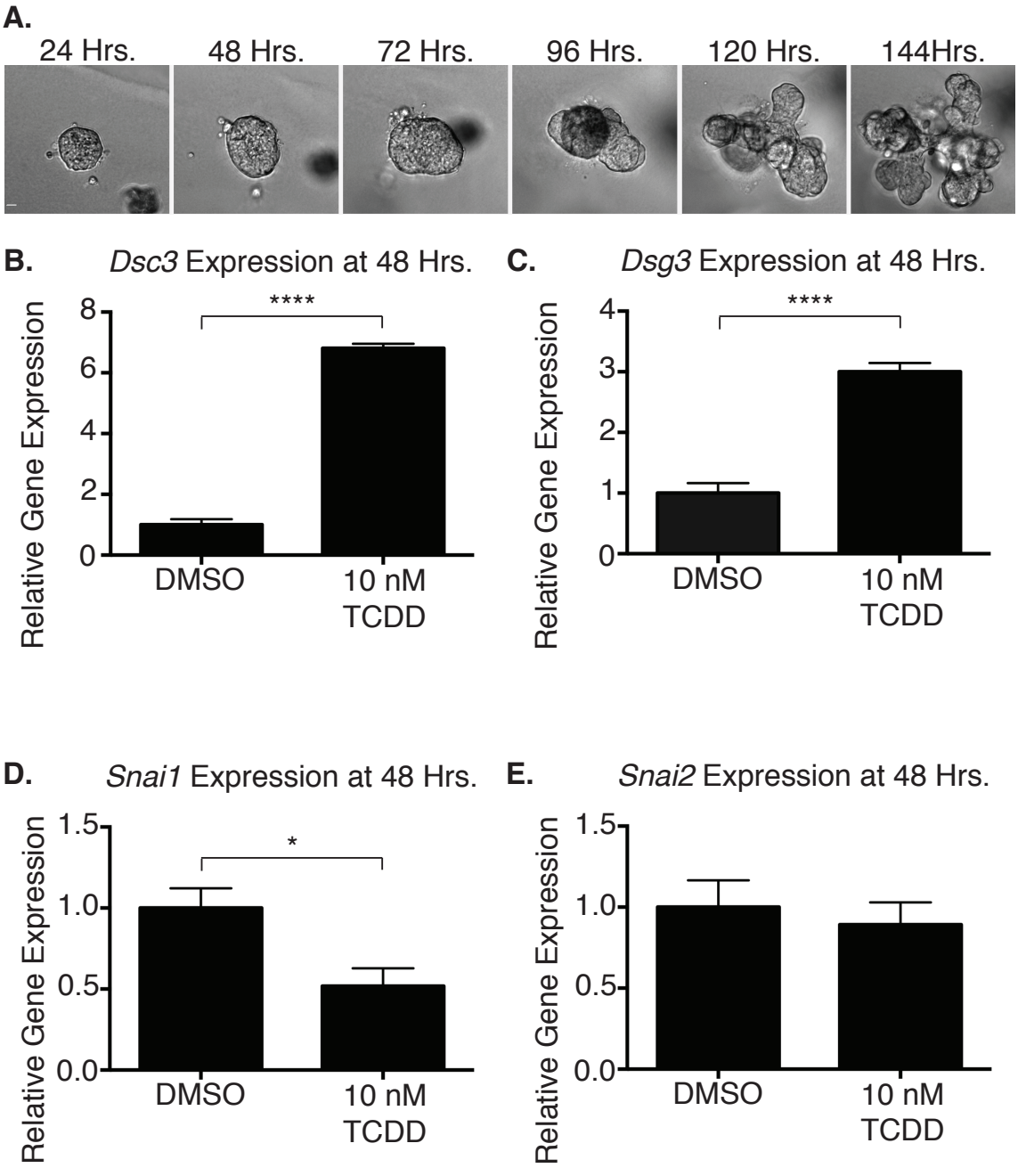
A.
24 Hrs.
48 Hrs.
72 Hrs.
96 Hrs.
120 Hrs.
144Hrs.
B.
Dsc3 Expression at 48 Hrs.
Relative Gene Expression
8
6
4
2
0
****
DMSO
10 nM TCDD
C.
Dsg3 Expression at 48 Hrs.
Relative Gene Expression
4
3
2
1
0
****
DMSO
10 nM TCDD
D.
Snai1 Expression at 48 Hrs.
Relative Gene Expression
1.5
1.0
0.5
0.0
*
DMSO
10 nM TCDD
E.
Snai2 Expression at 48 Hrs.
Relative Gene Expression
1.5
1.0
0.5
0.0
DMSO
10 nM TCDD

After identifying *Snai1* as a strong candidate, we next measured its expression in the virgin gland. We isolated primary MECs from virgin FVB/n female mice and FACS sorted based on CD49f expression. Since we previously observed high expression of *Dsc3* and *Dsg3* in virgin myoepithelial cells, we hypothesized that *Snai1* expression would be relatively low in this cellular compartment. Consistent with our previous observations, *Snai1* displayed higher expression in luminal epithelial cells from virgin MECs compared to myoepithelial cells (Figure 5.5A).

Next, we assessed *Snai1* expression during pregnancy. Our data demonstrated myoepithelial desmosomes were dramatically downregulated at day 15 of pregnancy. As a result, we hypothesized *Snai1* expression would be increased in pregnant primary MECs. In agreement with this prediction, *Snai1* expression was induced in primary MECs from 15-day pregnant FVB/n mice compared to the virgin control (Figure 5.5B). Taken together, these results show an inverse relationship in the mammary gland between *Snai1* and myoepithelial desmosomes.

Loss of the aryl hydrocarbon receptor repressor blocks
mammary branching morphogenesis

Our next goal was to determine the intersection of normal FGF2-mediated branching and AHR signaling. Once activated, AHR translocates to the nucleus and forms a dimer with the AHR nuclear translocator (ARNT). As a heterodimer, AHR/ARNT binds xenobiotic-responsive elements (XREs) in the promoter region of AHR target genes, including the aryl hydrocarbon receptor repressor (AHRR) (17). We became interested in a potential role for AHRR in regulating *Snai1*. Previously, AHRR

Figure 5.5. *Snai1* expression increases during pregnancy. (A.) In mammary epithelial cells (MECs) isolated from virgin FVB/n female mice, *Snai1* mRNA expression was enriched in the luminal cell population. Luminal and myoepithelial cell populations were isolated based on CD49f expression. (B.) Compared to MECs isolated from virgin mice, MECs from 15-day pregnant FVB/n female mice showed higher levels of *Snai1* mRNA expression. Gene expression was measured by qRT-PCR and normalized to *cytokeratin-14* expression. Results are shown as mean ± S.E. (error bars); *, $p < 0.05$; **, $p < 0.01$.

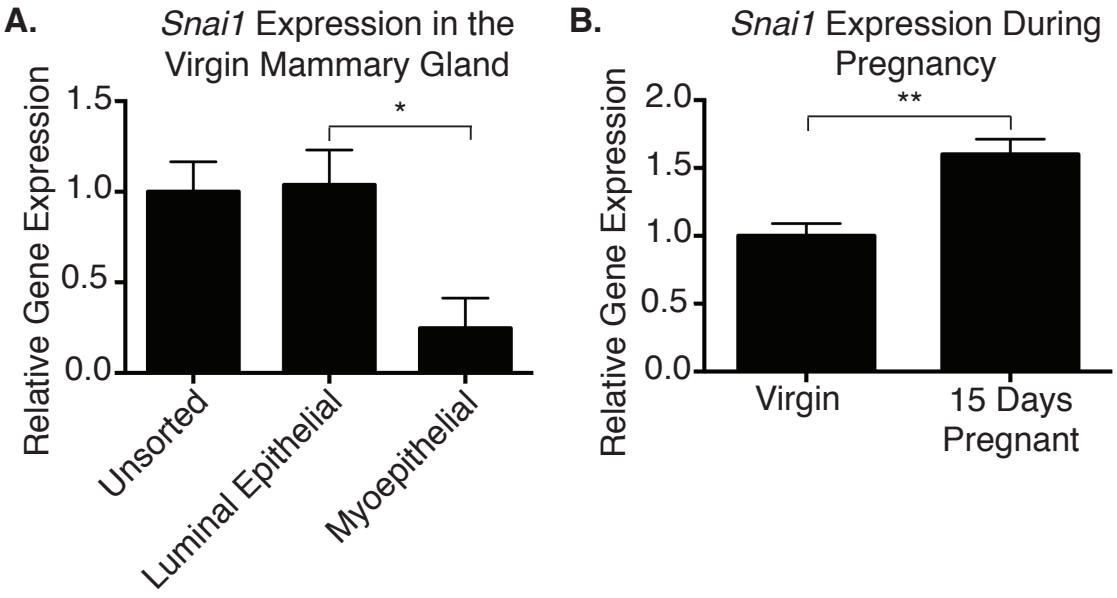
A.
Snai1 Expression in the Virgin Mammary Gland
Relative Gene Expression
1.5
1.0
0.5
0.0
*
Unsorted
Luminal Epithelial
Myoepithelial
B.
Snai1 Expression During Pregnancy
Relative Gene Expression
2.0
1.5
1.0
0.5
0.0
**
Virgin
15 Days Pregnant

was shown to regulate *Snai1* through *CK2α* (18,19), a serine/threonine kinase that contains multiple XREs in its promoter region (20). Based on these observations, we hypothesized that AHRR was a critical downstream mediator of AHR signaling required for activation of desmosomes and blocked branching morphogenesis. To test our hypothesis, we generated an AHRR knockout (KO) mouse using targeted sperm obtained from the Knockout Mouse Project (KOMP) Repository.

First, we isolated primary MECs from wild type (WT) and AHRR KO mice and treated them with 10 nM TCDD. Since AHRR drives a repressive feedback loop that inhibits AHR activity (21), we expected AHRR KO cells to display heightened AHR activation. In our assay, AHRR KO MECs showed significantly higher induction of the AHR readout gene, *Cyp1A1*, than WT MECs (Figure 5.6A). These results confirmed AHRR was properly targeted.

Next, we isolated primary MECs from WT and KO female mice and performed an *in vitro* 3D branching assay. We reasoned if AHRR was critical for activation of desmosomal cadherins, loss of AHRR would rescue branching in the presence of TCDD. Unexpectedly, primary MECs from AHRR KO mice failed to undergo FGF2-induced branching morphogenesis, even in the absence of AHR ligands. Rather, we observed large, fluid-filled cysts in KO MECs grown with 2.5 nM FGF2. In the presence of 10 nM TCDD, we observed cyst arrest with both WT and KO MECs (Figure 5.6B).

Loss of AHRR highly upregulates desmosomes

We previously demonstrated AHR activation blocked branching morphogenesis by upregulating desmosomes (5). Based on these observations, we hypothesized AHRR

Figure 5.6. Loss of AHRR blocks mammary branching. (A.) Primary mammary epithelial cells (MECs) isolated from aryl hydrocarbon receptor repressor (AHRR) knockout (KO) mice showed increased *Cyp1A1* mRNA induction in the absence of AHR agonists. AHRR KO cells treated with 10 nM TCDD also showed elevated *Cyp1A1* induction compared to primary MECs isolated from wild type (WT) mice. Gene expression was measured by qRT-PCR and normalized to *β-actin* expression. Results are shown as mean ± S.E. (error bars); ****, $p < 0.0001$. (B.) Primary MECs isolated from AHRR KO mice failed to branch in 3D. Aggregated MECs were grown in Matrigel for 144 hours with 2.5 nM fibroblast growth factor-2 (FGF2) and 0.1% DMSO or 10 nM TCDD. Results are shown as mean ± S.D. (error bars); **, $p < 0.01$; ***, $p < 0.001$.

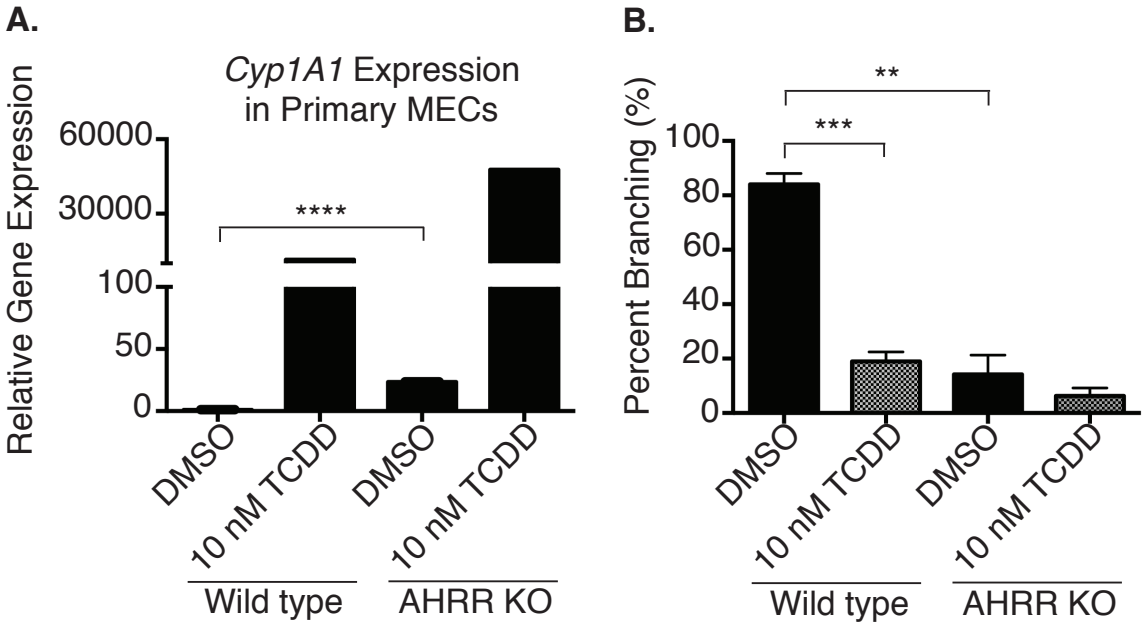
A.
Cyp1A1 Expression
in Primary MECs
Relative Gene Expression
60000
30000
100
50
0
****
DMSO
10 nM TCDD
DMSO
10 nM TCDD
Wild type
AHRR KO
B.
Percent Branching (%)
100
80
60
40
20
0
**
***
DMSO
10 nM TCDD
DMSO
10 nM TCDD
Wild type
AHRR KO

KO MECs failed to branch due to increased desmosomal adhesion. To test this, we measured expression of the desmosome cadherins previously induced by AHR signaling (5) in WT and AHRR KO MECs. Compared to WT MECs grown with 10 nM TCDD, AHRR KO MECs grown in the absence of TCDD showed higher levels of D*sc1* and *Dsg1* and comparable levels of *Dsg3*. In the presence of 10 nM TCDD, AHRR KO MECs showed exceptionally high levels of these isoforms (Figure 5.7). Contrary to our original hypothesis, these results demonstrated AHRR was not required for AHR agonists to activate desmosomes. Rather, loss of AHRR alone was sufficient to induce levels of desmosomal adhesion capable of functionally blocking mammary branching.

Discussion

Using a 3D model of mammary morphogenesis, we previously demonstrated loss of desmosomal adhesion is sufficient to induce mammary branching (5). In the present study, we further investigated the dynamic regulation of desmosomes in the mammary gland. In the virgin gland, we observed differential expression of desmosomal cadherins. Specifically, we found Dsc2 and Dsg2 expressed in both luminal and myoepithelial cells, while Dsc3 and Dsg3 were restricted to the myoepithelial cell population.

The differential expression pattern we observed in the mammary gland parallels the tissue- and cell-type specific expression of desmosomes. In particular, Dsc2 and Dsg2 are uniformly expressed in all tissues that form desmosomes while Dsc1, Dsg1, Dsc3 and Dsg3 are restricted to stratified epithelia (22,23). Additionally, expression of desmosomal cadherins shows cell-type specificity. In the epidermis for example, Dsg1 and Dsc1 are dominant in the differentiated upper skin layer where the strongest barrier

Figure 5.7. Loss of AHRR activates desmosomal adhesion. (A.) Primary mammary epithelial cells (MECs) isolated from aryl hydrocarbon receptor repressor (AHRR) knockout (KO) mice showed increased *desmocollin 1* (*Dsc1*), (B.) *desmoglein 1* (*Dsg1*), and (D.) *desmoglein 3* (*Dsg3*) mRNA induction in the absence of aryl hydrocarbon receptor (AHR) stimulation. These levels were comparable or higher than wild type (WT) MECs grown with 10 nM TCDD. (C.) Increased *desmocollin 3* (*Dsc3*) mRNA expression was not observed in AHRR KO MECs. Aggregated MECs were grown in Matrigel for 144 hours with 2.5 nM fibroblast growth factor-2 (FGF2) and 0.1% DMSO or 10 nM TCDD. Gene expression was measured by qRT-PCR and normalized to *β-actin* expression. Results are shown as mean ± S.E. (error bars); **, $p < 0.01$; ****, $p < 0.0001$.

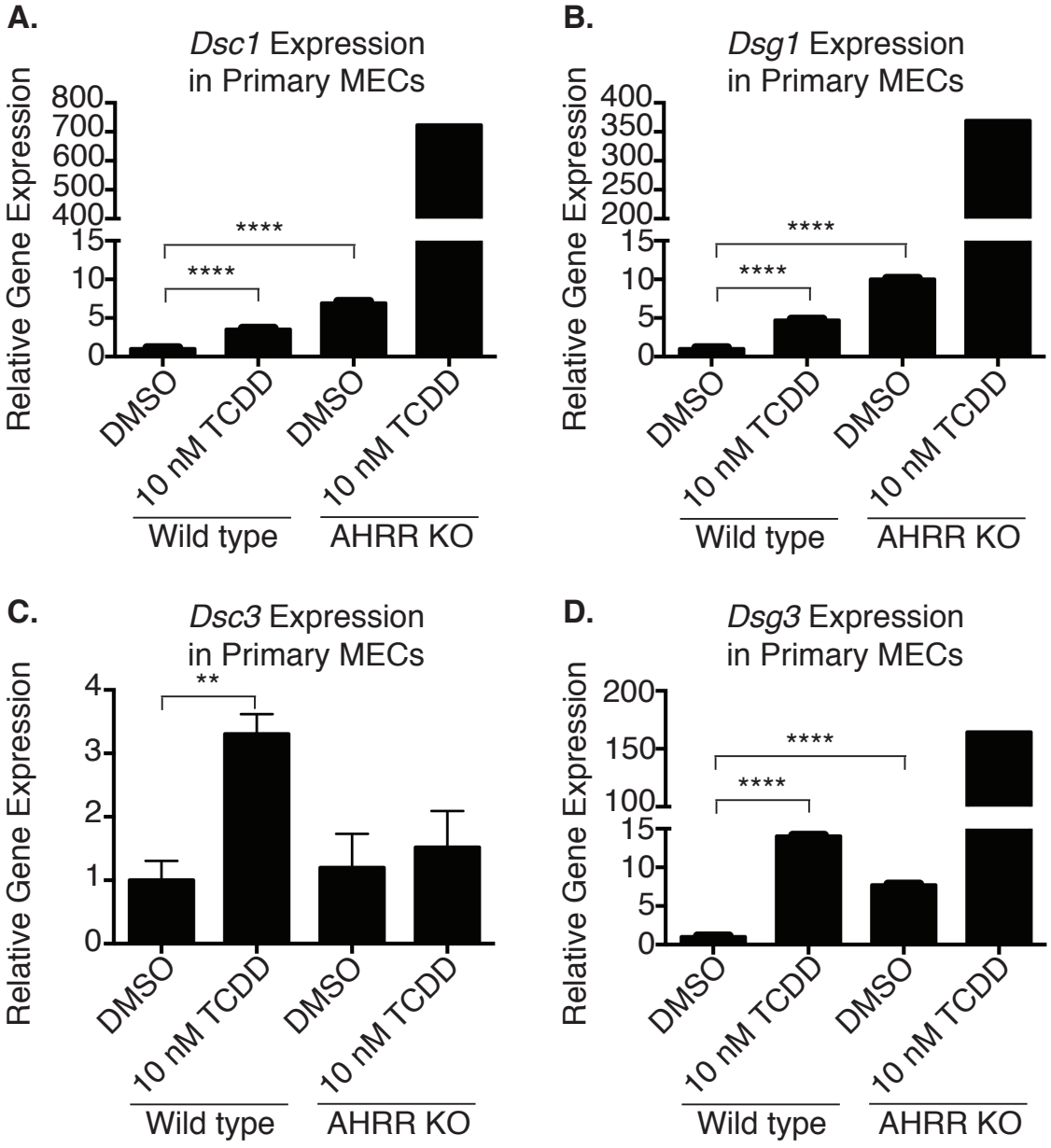
A.
Dsc1 Expression in Primary MECs
Relative Gene Expression
800
700
600
500
400
15
10
5
0
****
****
DMSO
10 nM TCDD
DMSO
10 nM TCDD
Wild type
AHRR KO
B.
Dsg1 Expression in Primary MECs
Relative Gene Expression
400
350
300
250
200
15
10
5
0
****
****
DMSO
10 nM TCDD
DMSO
10 nM TCDD
Wild type
AHRR KO
C.
Dsc3 Expression in Primary MECs
Relative Gene Expression
4
3
2
1
0
**
DMSO
10 nM TCDD
DMSO
10 nM TCDD
Wild type
AHRR KO
D.
Dsg3 Expression in Primary MECs
Relative Gene Expression
200
150
100
15
10
5
0
****
****
DMSO
10 nM TCDD
DMSO
10 nM TCDD
Wild type
AHRR KO

function is observed. Dsc3 and Dsg3 are concentrated in the spinosum layer, and Dsc2 and Dsg2 are dominant in the basal layer, where proliferation is highest (24). These observations suggest desmosomes have differentiation-dependent expression patterns in epidermal tissue.

In addition to the expression pattern, we also observed differences in the temporal regulation of mammary desmosomes. Dsc2 and Dsg2 were unaffected by AHR stimulation and were maintained during pregnancy. Conversely, Dsc1, Dsg1, Dsc3, and Dsg3 were induced during AHR-mediated cyst formation in 3D culture and lost during pregnancy. Given our data, we hypothesize myoepithelial specific desmosomal cadherins are preferentially lost during both *in vitro* and *in vivo* branching (Figure 5.8). The restricted loss of Dsc3 and Dsg3 would facilitate breaks in myoepithelial cell coverage, where luminal branch points have been previously shown to arise in organotypic mammary cultures (25). Additionally, maintenance of Dsc2 and Dsg2 during branching would support collective migration of luminal epithelial cells, where desmosomes are thought to be maintained (26).

To fully test this model, selective inhibition of desmosomal cadherins is required. We predict loss of Dsc3 and Dsg3 in the virgin gland, but not Dsc2 or Dsg2, will induce precocious branching. Previously, distinct desmosomes have been indirectly targeted in the mammary gland. In particular, Perp (p53 apoptosis effector related to PMP-22) deficiency led to loss of Dsg1/2 and Dsc2 in the mammary epithelium. Although Perp null mammary glands had increased immune infiltration, normal ductal development was observed (27). In addition to Perp, conditional deletion of the tumor suppressor gene liver kinase B1 (Lkb1) caused loss of mammary desmosomes. Interestingly, Lkb1

Figure 5.8. Working cellular model for how desmosomes regulate mammary branching morphogenesis *in vitro* and *in vivo*. (Left) In the virgin mammary gland or during AHR activation, desmosomal adhesion is induced in all cell types, allowing ductal architecture to be maintained. (Middle) As branching morphogenesis initiates, we propose myoepithelial specific desmosomes are downregulated, which allows branch points to form. (Right) Luminal epithelial cells maintain desmosomes and migrate collectively during mammary branching morphogenesis.

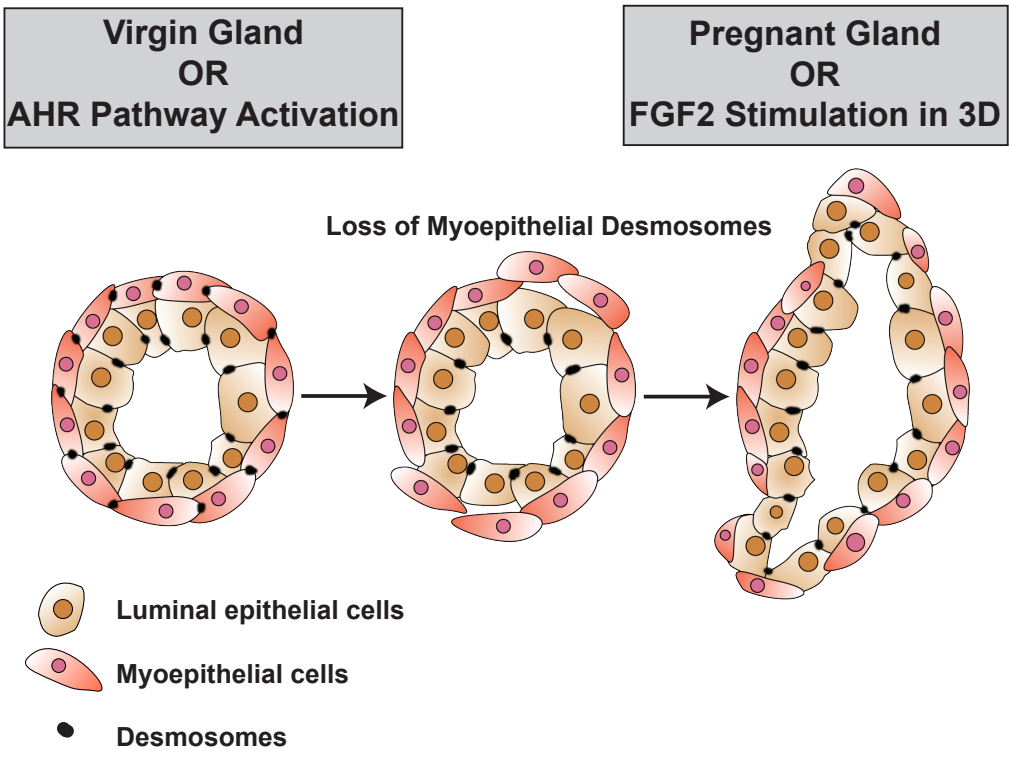
Virgin Gland
OR
AHR Pathway Activation
Pregnant Gland
OR
FGF2 Stimulation in 3D
Loss of Myoepithelial Desmosomes
Luminal epithelial cells
Myoepithelial cells
Desmosomes

deletion induced *in vitro* and *in vivo* hyperbranching (28). Since desmosome defects were visualized by transmission electron microscopy, it is unclear which cadherin isoforms were inhibited by Lkb1. Direct *in vivo* targeting of individual desmosomal cadherins will be needed to fully understand how desmosomes regulate the dynamics of mammary branching morphogenesis.

Our studies of desmosomes and mammary morphogenesis have focused on postnatal stages of development, namely puberty and pregnancy. However, remodeling of cellular adhesion is also thought to drive early mammary morphogenesis. At E15, desmosomes are absent in the mammary bud. However, desmosomes are restored at E17 as the mammary bud elongates and begins cavity formation. Importantly, desmosomes remain absent in the distal region of the elongating bud, where branches create the mammary sprout (29). Similar to our current observations, these studies of embryonic mammary gland development suggest increases in desmosomes are linked to lumen formation while decreases in desmosomes coincide with branch point formation.

Supporting our model in the mammary gland, differential desmosomal adhesion is thought to drive morphogenesis of other ectoderm-derived tissues. In early hair follicle morphogenesis, placode formation is accompanied by downregulation of desmosomes. As cell masses form in epithelial buds, desmosomes are almost completely lost and do not reform again until hair follicle elongation begins (30). Similar to the high expression of mammary desmosomes during ductal morphogenesis, re-expression of desmosomes in the elongating hair follicle coincides with cavity formation. In addition to the hair follicle, remodeling of cellular adhesion is also associated with tissue morphogenesis in the submandibular gland. Desmosomes are absent in the early cell mass, but

strengthened during lumen formation. Interestingly, desmosomes are strongest in cells near the lumen and weaker in the terminal lobules (31), thus paralleling the distribution of desmosomes during mammary morphogenesis. Taken together, these studies strongly implicate desmosomes as a critical force driving tissue morphogenesis.

Aside from normal mammary development, we previously demonstrated AHR agonists upregulated desmosomes to functionally block mammary branching. Here, we hypothesized AHRR was a key downstream mediator of AHR activation required for desmosome regulation. Surprisingly, loss of AHRR alone upregulated desmosomes and inhibited mammary branching. These results were inconsistent with a role for AHRR promoting desmosomes downstream of AHR activation. Rather, our results implicated a more direct role for activated AHR in regulating desmosomes.

Loss of AHRR results in hyperactivation of AHR/ARNT heterodimers (17). Since desmosomes were upregulated under these conditions, our data suggest AHR/ARNT complexes regulate desmosomes. Directly, AHR/ARNT may bind the promoter region of desmosomal cadherins, which are organized in a tandem array on chromosome 18 (32). Alternatively, AHR/ARNT may indirectly regulate desmosomal cadherins through other transcription factor(s), such as *Snai1*. ChIP-sequencing experiments will be required to parse out direct and indirect effects of AHR/ARNT on desmosomal cadherins.

Overall, our data demonstrate desmosomal adhesion helps regulate invasion and migration of normal primary MECs. Desmosomes promote ductal integrity in the virgin gland and undergo dynamic remodeling to drive mammary morphogenesis during pregnancy. In the context of tumorigenesis, these results predict deterioration of

desmosomal adhesion would enhance cellular motility and facilitate a more aggressive tumor phenotype. Interestingly, estrogens are known to increase desmosome formation in normal and malignant breast cells (33), which may contribute to the less invasive phenotype observed in estrogen receptor-positive tumors (34). Additionally, desmosomes are disrupted in several types of breast cancer cells. Shedding of Dsg2 was observed in A431 cells due to stabilization of ADAM17 through EGF signaling (35). Furthermore, Dsc3 expression was downregulated in breast cancer cell lines and primary breast tumors (36,37) primarily due to methylation-mediated epigenetic silencing (37). Thus, understanding the molecular mechanisms that regulate mammary desmosomes will help identify new strategies to inhibit tumor growth and invasion.

Materials and Methods

Mice

Mice were maintained following protocols reviewed and approved by the University of Utah Institutional Animal Care and Use Committee.

Whole mount analysis

Mammary glands were prepared for whole mount analysis as previously described (38). Briefly, the fourth inguinal mammary gland was removed, spread on a slide, and fixed in Carnoy's fixative (60% ethanol, 30% chloroform, 10% glacial acetic acid) for 2 hours at room temperature. Fixed mammary glands were rehydrated, stained in carmine alum overnight, dehydrated, and cleared in xylene overnight. Stained glands were imaged between two slides and mounted with permount for long-term storage.

Isolation of primary MECs

Organoids from the fourth inguinal mammary gland were isolated from virgin (8-12-week-old) and 15-day pregnant female mice and processed to single epithelial cells as previously described (5).

RNA isolation and real-time PCR

RNA was isolated from primary MECs, converted to cDNA, and used for real-time PCR as previously described (5). Primer sequences are shown in Table 5.1.

Chemical compounds

TCDD (Cambridge Isotopes Laboratories, Inc., Andover, MA) was obtained as a DMSO stock solution. 1023 was synthesized as previously described (5) and dissolved in

Table 5.1 Primer sequences used for RT-PCR

Target	Forward (5'->3')	Reverse (5'->3')
β-actin	GGCTGTGCTGTCCCTGTATG	CAAGAAGGAAGGCTGGAAA
Dsc1	CAGTAGTGGCGACAGATACA	CCTTCTCCTGCTGACAAATG
Dsg1	GGGATAACCACCATCTGTGT	CCTCCCAGATCTTGCATTTC
Dsc3	TAAAGATGTTGCAAACCG	GCACTCCTTGATCTGAGC
Dsg3	AGGTTCTGGCCATAGACGAA	TCACTGAGAGGGTCACAGAA
Dsc2	CATTTTGAAGGGCAATG	ATGATTCCCAGAGTTCC
Dsg2	GAGGAATCTGATCGTCCCAA	CCATCCCCCAATAATCACAG
Snai1	CTTGTGTCTGCACGACCTGT	AGTGGGAGCAGGAGAATGG
Snai2	GGCTGCTTCAAGGACACATT	GATGTGCCCTCAGGTTTGAT
Cyp1A1	GGTTAACCATGACCGGGAACT	TGCCCAAACCAAAGAGAGTG

DMSO at a stock concentration of 10 mM.

Aggregation and culture of primary MECs in 3D

Primary MECs were aggregated overnight, embedded, and grown in Matrigel as previously described (5). For branching studies and imaging, 250 aggregates per well were plated in 48-well tissue culture plates. To calculate percent branching, samples were fixed in 4% paraformaldehyde and quantified using bright field microscopy at low magnification. Branching was defined as three ducts or more, as previously established (39). Three independent samples were averaged for each experiment. For RNA extraction, 1,000 aggregates per well were plated in 24-well tissue culture plates and three wells were combined for each sample.

Immunofluorescence

Staining for cytokeratin-8 (Developmental Studies Hybridoma Bank, Troma-I, 1:100) and cytokeratin-14 (Covance, PRB-155P-100, 1:400) was performed on sections of mammary gland from virgin FVB/n mice as previously described (5).

Microscopy

Mammary whole mounts were imaged using an Olympus MVX10 dissecting microscope with a SPOT Insight FireWire 4 CCD camera and Spot Alias 4.6.1.38 software (Diagnostic Instruments, Inc). Immunofluorescence and DIC imaging were performed using an Olympus IX81-ZDC microscope with an ORCAER CCD camera and Slidebook 5.0.0.24 software (Intelligent Imaging Innovations, Inc.).

Immunofluorescence imaging was performed using a 40X U-Plan objective lens and DIC images were captured using a 20X long working distance objective lens. For immunofluorescence imaging, deconvolution was performed using Slidebook software and the nearest neighbor method.

FACS sorting

Primary MECs were aggregated overnight as described. After 16 hours, aggregates were collected into a 15 mL conical tube (450 x g for 2 minutes) and washed twice with 10 mL DMEM/F-12 base media (HyClone). Pelleted aggregates were trypsinized (0.05% trypsin/EDTA, Gibco) for 10 minutes at 37 ^{o}C with gentle pipetting every 5 minutes. Single cells were washed with Hanks' balanced salt solution (HBSS) (Gibco) containing 2% fetal bovine serum (FBS) (Gibco) to inactivate trypsin. Pelleted cells were resuspended in HBSS/2% FBS at a concentration of 5 x 10^6 cells per mL. The following aliquoted samples were kept on ice and in the dark: 1) 200 μL unstained control, 2) 200 μL 7AAD control, 3) 200 μL CD49f-FITC control, 4) experimental sample. Cells were incubated with primary antibody (1:100, BD Pharmingen) for 15 minutes, washed (1 mL HBSS/2% FBS, 1000 x g for 2 minutes), and resuspended in 400 μL HBSS/2%FBS. 7AAD (10 μL per 1 x 10^6 cells) was added as indicated and cells were filtered through a 40 μm sterile filter (BD Biosciences). Samples were sorted directly into RLT buffer (Qiagen) for subsequent RNA extraction.

AHRR knockout mice

Targeted sperm used to rederive Ahrr$^{tm1a(KOMP)Wtsi}$ mice was generated by the trans-NIH Knock-Out Mouse Project (KOMP) and obtained from the KOMP Repository (www.komp.org). NIH grants to Velocigene at Regeneron Inc (U01HG004085) and the CSD Consortium (U01HG004080) funded the generation of gene-targeted ES cells for 8500 genes in the KOMP Program and archived and distributed by the KOMP Repository at UC David and CHORI (U42RR024244). Oocytes from C57Bl6/CBA F1 female mice were used for in vitro fertilization (IVF). After heterozygous Ahrr$^{tm1a(KOMP)Wtsi}$ mice were backcrossed to FVB/n mice for 9 generations, heterozygous matings were used to generate WT and AHRR KO mice for experiments as indicated.

References

1. Garrod, D., and Chidgey, M. (2008) Desmosome structure, composition and function. *Biochim. Biophys. Acta.* **1778**, 572-587

2. Garrod, D. R., Merritt, A. J., and Nie, Z. (2002) Desmosomal cadherins. *Curr. Opin. Cell Biol.* **14**, 537-545

3. Hatzfeld, M. (1999) The armadillo family of structural proteins. *Int. Rev. Cytol.* **186**, 179-224

4. Getsios, S., Huen, A. C., and Green, K. J. (2004) Working out the strength and flexibility of desmosomes. *Nat. Rev. Mol. Cell Biol.* **5**, 271-281

5. Basham, K. J., Kieffer, C., Shelton, D. N., Leonard, C. J., Bhonde, V. R., Vankayalapati, H., Milash, B., Bearss, D. J., Looper, R. E., and Welm, B. E. (2013) Chemical genetic screen reveals a role for desmosomal adhesion in mammary branching morphogenesis. *J. Biol. Chem.* **288**, 2261-2270

6. Sternlicht, M. D. (2006) Key stages in mammary gland development: The cues that regulate ductal branching morphogenesis. *Breast Cancer Res.* **8**, 201

7. Sternlicht, M. D., Kouros-Mehr, H., Lu, P., and Werb, Z. (2006) Hormonal and local control of mammary branching morphogenesis. *Differentiation* **74**, 365-381

8. Pitelka, D. R., Hamamoto, S. T., Duafala, J. G., and Nemanic, M. K. (1973) Cell contacts in the mouse mammary gland. I. Normal gland in postnatal development and the secretory cycle. *J. Cell Biol.* **56**, 797-818

9. Runswick, S. K., O'Hare, M. J., Jones, L., Streuli, C. H., and Garrod, D. R. (2001) Desmosomal adhesion regulates epithelial morphogenesis and cell positioning. *Nat. Cell Biol.* **3**, 823-830

10. Stingl, J., Eirew, P., Ricketson, I., Shackleton, M., Vaillant, F., Choi, D., Li, H. I., and Eaves, C. J. (2006) Purification and unique properties of mammary epithelial stem cells. *Nature* **439**, 993-997

11. Runswick, S. K., Garrod, D. R., and Streuli, C. H. (1996) The differential expression of desmocollin isoforms in mammary epithelia. *Biochem. Soc. Trans.* **24**, 346S

12. Calkins, C. C., Setzer, S. V., Jennings, J. M., Summers, S., Tsunoda, K., Amagai, M., and Kowalczyk, A. P. (2006) Desmoglein endocytosis and desmosome disassembly are coordinated responses to pemphigus autoantibodies. *J. Biol. Chem.* **281**, 7623-7634

13. Delva, E., Jennings, J. M., Calkins, C. C., Kottke, M. D., Faundez, V., and Kowalczyk, A. P. (2008) Pemphigus vulgaris IgG-induced desmoglein-3 endocytosis and desmosomal disassembly are mediated by a clathrin- and dynamin-independent mechanism. *J. Biol. Chem.* **283**, 18303-18313

14. Lee, K., Gjorevski, N., Boghaert, E., Radisky, D. C., and Nelson, C. M. (2011) Snail1, Snail2, and E47 promote mammary epithelial branching morphogenesis. *EMBO J.* **30**, 2662-2674

15. Ohkubo, T., and Ozawa, M. (2004) The transcription factor Snail downregulates the tight junction components independently of E-cadherin downregulation. *J. Cell Sci.* **117**, 1675-1685

16. Savagner, P., Yamada, K. M., and Thiery, J. P. (1997) The zinc-finger protein slug causes desmosome dissociation, an initial and necessary step for growth factor-induced epithelial-mesenchymal transition. *J. Cell Biol.* **137**, 1403-1419

17. Mimura, J., Ema, M., Sogawa, K., and Fujii-Kuriyama, Y. (1999) Identification of a novel mechanism of regulation of Ah (dioxin) receptor function. *Genes Dev.* **13**, 20-25

18. Zudaire, E., Cuesta, N., Murty, V., Woodson, K., Adams, L., Gonzalez, N., Martinez, A., Narayan, G., Kirsch, I., Franklin, W., Hirsch, F., Birrer, M., and Cuttitta, F. (2008) The aryl hydrocarbon receptor repressor is a putative tumor suppressor gene in multiple human cancers. *J. Clin. Invest.* **118**, 640-650

19. Kanno, Y., Takane, Y., Izawa, T., Nakahama, T., and Inouye, Y. (2006) The inhibitory effect of aryl hydrocarbon receptor repressor (AhRR) on the growth of human breast cancer MCF-7 cells. *Biol. Pharm. Bull.* **29**, 1254-1257

20. Hahn, M. E., Allan, L. L., and Sherr, D. H. (2009) Regulation of constitutive and inducible AHR signaling: Complex interactions involving the AHR repressor. *Biochem. Pharmacol.* **77**, 485-497

21. Evans, B. R., Karchner, S. I., Allan, L. L., Pollenz, R. S., Tanguay, R. L., Jenny, M. J., Sherr, D. H., and Hahn, M. E. (2008) Repression of aryl hydrocarbon receptor (AHR) signaling by AHR repressor: Role of DNA binding and competition for AHR nuclear translocator. *Mol. Pharmacol.* **73**, 387-398

22. Nuber, U. A., Schafer, S., Schmidt, A., Koch, P. J., and Franke, W. W. (1995) The widespread human desmocollin Dsc2 and tissue-specific patterns of synthesis of various desmocollin subtypes. *Eur. J. Cell Biol.* **66**, 69-74

23. King, I. A., Sullivan, K. H., Bennett, R., Jr., and Buxton, R. S. (1995) The desmocollins of human foreskin epidermis: Identification and chromosomal assignment of a third gene and expression patterns of the three isoforms. *J. Invest. Dermatol.* **105**, 314-321

24. Yin, T., and Green, K. J. (2004) Regulation of desmosome assembly and adhesion. *Semin. Cell Dev. Biol.* **15**, 665-677

25. Ewald, A. J., Brenot, A., Duong, M., Chan, B. S., and Werb, Z. (2008) Collective epithelial migration and cell rearrangements drive mammary branching morphogenesis. *Dev. Cell* **14**, 570-581

26. Ewald, A. J., Huebner, R. J., Palsdottir, H., Lee, J. K., Perez, M. J., Jorgens, D. M., Tauscher, A. N., Cheung, K. J., Werb, Z., and Auer, M. (2012) Mammary collective cell migration involves transient loss of epithelial features and individual cell migration within the epithelium. *J. Cell Sci.*

27. Dusek, R. L., Bascom, J. L., Vogel, H., Baron, S., Borowsky, A. D., Bissell, M. J., and Attardi, L. D. (2012) Deficiency of the p53/p63 target Perp alters mammary gland homeostasis and promotes cancer. *Breast Cancer Res.* **14**, R65

28. Partanen, J. I., Tervonen, T. A., Myllynen, M., Lind, E., Imai, M., Katajisto, P., Dijkgraaf, G. J., Kovanen, P. E., Makela, T. P., Werb, Z., and Klefstrom, J. (2012) Tumor suppressor function of Liver kinase B1 (Lkb1) is linked to regulation of epithelial integrity. *Proc. Natl. Acad. Sci. U. S. A.* **109**, E388-397

29. Nanba, D., Nakanishi, Y., and Hieda, Y. (2001) Changes in adhesive properties of epithelial cells during early morphogenesis of the mammary gland. *Dev. Growth Differ.* **43**, 535-544

30. Nanba, D., Hieda, Y., and Nakanishi, Y. (2000) Remodeling of desmosomal and hemidesmosomal adhesion systems during early morphogenesis of mouse pelage hair follicles. *J. Invest. Dermatol.* **114**, 171-177

31. Hieda, Y., Iwai, K., Morita, T., and Nakanishi, Y. (1996) Mouse embryonic submandibular gland epithelium loses its tissue integrity during early branching morphogenesis. *Dev. Dyn.* **207**, 395-403

32. Hunt, D. M., Sahota, V. K., Taylor, K., Simrak, D., Hornigold, N., Arnemann, J., Wolfe, J., and Buxton, R. S. (1999) Clustered cadherin genes: A sequence-ready contig for the desmosomal cadherin locus on human chromosome 18. *Genomics* **62**, 445-455

33. Maynadier, M., Chambon, M., Basile, I., Gleizes, M., Nirde, P., Gary-Bobo, M., and Garcia, M. (2012) Estrogens promote cell-cell adhesion of normal and malignant mammary cells through increased desmosome formation. *Mol. Cell. Endocrinol.* **364**, 126-133

34. Osborne, C. K. (1998) Steroid hormone receptors in breast cancer management. *Breast Cancer Res. Treat.* **51**, 227-238

35. Santiago-Josefat, B., Esselens, C., Bech-Serra, J. J., and Arribas, J. (2007) Post-transcriptional up-regulation of ADAM17 upon epidermal growth factor receptor activation and in breast tumors. *J. Biol. Chem.* **282**, 8325-8331

36. Klus, G. T., Rokaeus, N., Bittner, M. L., Chen, Y., Korz, D. M., Sukumar, S., Schick, A., and Szallasi, Z. (2001) Down-regulation of the desmosomal cadherin desmocollin 3 in human breast cancer. *Int. J. Oncol.* **19**, 169-174

37. Oshiro, M. M., Kim, C. J., Wozniak, R. J., Junk, D. J., Munoz-Rodriguez, J. L., Burr, J. A., Fitzgerald, M., Pawar, S. C., Cress, A. E., Domann, F. E., and Futscher, B. W. (2005) Epigenetic silencing of DSC3 is a common event in human breast cancer. *Breast Cancer Res.* **7**, R669-680

38. Kordon, E. C., McKnight, R. A., Jhappan, C., Hennighausen, L., Merlino, G., and Smith, G. H. (1995) Ectopic TGF beta 1 expression in the secretory mammary epithelium induces early senescence of the epithelial stem cell population. *Dev. Biol.* **168**, 47-61

39. Fata, J. E., Mori, H., Ewald, A. J., Zhang, H., Yao, E., Werb, Z., and Bissell, M. J. (2007) The MAPK(ERK-1,2) pathway integrates distinct and antagonistic signals from TGFalpha and FGF7 in morphogenesis of mouse mammary epithelium. *Dev. Biol.* **306**, 193-207

CHAPTER 6

CONCLUSIONS AND FUTURE DIRECTIONS

Mammary Branching Morphogenesis

Mammary gland development is a highly coordinated process that ultimately establishes an elaborate network of epithelial ducts poised for differentiation and milk production (1). Over the course of several distinct stages, the gland undergoes robust proliferation and branching. Many hormonal and local signals have long been recognized as important factors regulating this process (2). These include estrogen and progesterone, as well as epidermal growth factor (EGF) and fibroblast growth factor (FGF). Despite identification of these major factors, the downstream mediators of these pathways that more directly drive morphogenesis have remained unclear.

We established an *in vitro*, three-dimensional (3D) model of mammary development using primary mammary epithelial cells (MECs) stimulated with fibroblast growth factor-2 (FGF2) (3). Using this system, primary MECs underwent considerable reorganization and established proper cellular polarity, thus recapitulating key aspects of *in vivo* development. We then coupled this assay with a library of small molecules to identify compounds that block FGF2-mediated mammary branching. Follow-up studies with our lead compound elucidated a new role for desmosomal adhesion during mammary branching morphogenesis. Specifically, our results suggested loss of desmosomes facilitated mammary branching.

To fully understand the implications of this work, we next need to determine which type(s) of mammary branching desmosomes participate in. Bifurcation of terminal end buds (TEBs), side branching, and lobuloalveolar formation are distinct branching processes that all occur during mammary development. TEBs are club shaped structures that form at the tips of elongating ducts during puberty (4). Composed of a multilayered

inner core of body cells and an outer layer of cap cells, TEBs bifurcate to create new primary ducts (4). In contrast, side branching occurs to create new secondary and tertiary branches during puberty and early pregnancy (5). These branch points form in the main portion of ducts, which contain an inner layer of luminal epithelial cells surrounded by an outer layer of myoepithelial cells. As a result, new branch points must invade through both the myoepithelial layer and the basement membrane. Finally, lobuloalveolar development occurs during pregnancy. This process is characterized by formation of sphere-shaped alveolar structures (6), which each contain a single layer of milk-producing luminal epithelial cells surrounded by a discontinuous myoepithelial layer. This cellular arrangement promotes contact between luminal epithelial cells and the basement membrane, which is required for full differentiation (7,8).

Based on cellular composition and architecture, our 3D branching model appears to most closely resemble side branching. Primary MECs in our assay consist of luminal epithelial cells and myoepithelial cells, which reorganize to form bilayered cysts prior to branching (3). Moreover, the specific growth signals present in our system are more consistent with TEBs or side branching than lobuloalveolar development. Rather than progesterone and prolactin, which are required for alveolar formation, our system includes insulin and FGF2. These signals are known to be important *in vivo* during puberty (2,5,9) and bypass the need for upstream factors like estrogen and EGF. Together, the cellular composition, branching mode, and regulatory growth signals present in our assay implicate side branching as the primary branching mode.

These observations suggest loss of desmosomes specifically facilitates side branching. One way to test this hypothesis is to extend our original findings to an *in vivo*

system. We anticipate that loss of desmosomes *in vivo* would induce precocious side branching. However, desmosomes may also play a role in other branching mechanisms, which could result in increased TEBs and/or alveoli formation.

In addition to these studies, investigating the role of desmosomes during breast cancer progression is an important next phase of the project. Our data suggest desmosomes limit FGF2-induced cellular invasion. Although desmosomes are not as well studied as related adhesion complexes, they are beginning to be appreciated as important players in breast cancer. Mechanisms that destabilize and downregulate desmosomal cadherins, including Dsg2 and Dsc3, have been observed in breast cancer cell lines and primary breast tumors (10-12). Conversely, signals that increase desmosome formation in breast cells, such as estrogen (13), are associated with less invasive tumor phenotypes (14). Together, these studies support our findings in primary MECs and underlie the importance of further characterizing desmosomes in the context of malignant breast growth.

In studying the relationship between desmosomes and breast cancer, it will be important to look specifically at myoepithelial cells. Our work demonstrates that desmosomes expressed exclusively in myoepithelial cells have the most significant impact on mammary branching (3). As a result, we hypothesize desmosomal adhesion creates a myoepithelial barrier to prevent invasion. These observations are consistent with the known capacity of myoepithelial cells to function as tumor suppressors in the context of breast cancer (15,16). Although rarely transformed (16,17), myoepithelial cells are significantly lost during cancer progression (18). These cells preferentially contain many tumor suppressor proteins (19) and have a higher capacity for DNA repair

than neighboring luminal epithelial cells (20). Additionally, our work suggests that myoepithelial cells restrain tumor growth through expression of specific desmosome complexes that are able to robustly block cellular invasion. By inhibiting myoepithelial desmosomes *in vivo* and assessing the invasive and metastatic behavior of transformed primary MECs, we can functionally validate this idea.

AHR Signaling and Mammary Differentiation

The lead compound from our chemical screen was a *bis*-aryloxadiazole, referred to as 1023, which increased desmosomes by activating the aryl hydrocarbon receptor (AHR) (3). Discovered nearly 40 years ago, AHR is a ligand-activated transcription factor and important mediator of vertebrate toxicity (21). Specifically, a wide range of synthetic and naturally occurring compounds activates AHR and subsequently induces expression of metabolic enzymes to help eliminate these harmful substances (22).

Consistent with its role remediating toxins, AHR is thought to significantly affect normal physiological processes, including mammary gland development and function. Epidemiological studies in humans suggest exposure to the environmental toxin and AHR agonist, 2,3,7,8-Tetrachlorodibenzo-*p*-dioxin (TCDD), impairs mammary development and negatively impacts the ability of women to breastfeed (23-25). Studies in rodents support these observations and demonstrate TCDD severely blocks mammary branching and milk production (26-31). Despite these findings, the molecular mechanism through which AHR signaling alters mammary function has remained unclear.

In terms of mammary development, our work identified desmosomes as a novel downstream target critical for AHR-mediated inhibition of mammary branching (3). We observed a strong correlation between AHR activation, desmosome levels, and a block in mammary branching morphogenesis (32), suggesting desmosomes are a robust indicator of AHR activity in the mammary gland. Beyond branching, we also assessed the effect of AHR stimulation on lactogenesis. Using an *in vitro* model of mammary differentiation, we found AHR activation inhibited milk production through a direct effect on MECs. Moreover, we defined downstream targets of activated AHR that block transcription of critical milk genes (Figure 6.1).

Interestingly, different cellular compartments appear to mediate the different effects of AHR activation on the mammary gland. The desmosomal cadherin isoforms upregulated by the AHR pathway, which functionally block branching, are exclusively expressed in myoepithelial cells. Conversely, milk production occurs in luminal epithelial cells, which are negatively impacted by AHR signaling during lactation. We would like to more elegantly demonstrate this differential effect of AHR activation by reconstituting the mammary gland *in vivo* with MECs from wild type and AHR knockout mice. Following treatment with TCDD, glands containing wild type luminal epithelial cells and knockout myoepithleial cells should display normal mammary branching, but impaired milk production.

To further elucidate the mechanism through which AHR signaling blocks mammary development and differentiation, we have focused on the aryl hydrocarbon receptor repressor (AHRR). AHRR is a key component of the AHR pathway and normally drives a negative feedback loop to dampen AHR signaling (33). We found loss

Figure 6.1. Working molecular model for how AHR activation disrupts mammary function. Stimulation of the aryl hydrocarbon receptor (AHR) by both novel small molecules (1023) and environmental pollutants (TCDD) blocks mammary branching and lactation. (Left) Activated AHR upregulates desmosomal adhesion to functionally block branching. This phenotype appears to be mediated by myoepithelial cells, as the desmosomal cadherin isoforms targeted by AHR are exclusively expressed in this compartment. Overall, these results suggest loss of desmosomes facilitates mammary branching morphogenesis. (Right) The aryl hydrocarbon receptor repressor (AHRR), which is upregulated by the AHR pathway, is sufficient to block milk production. Since milk production occurs in luminal epithelial cells, the luminal epithelial cell compartment mediates this phenotype.

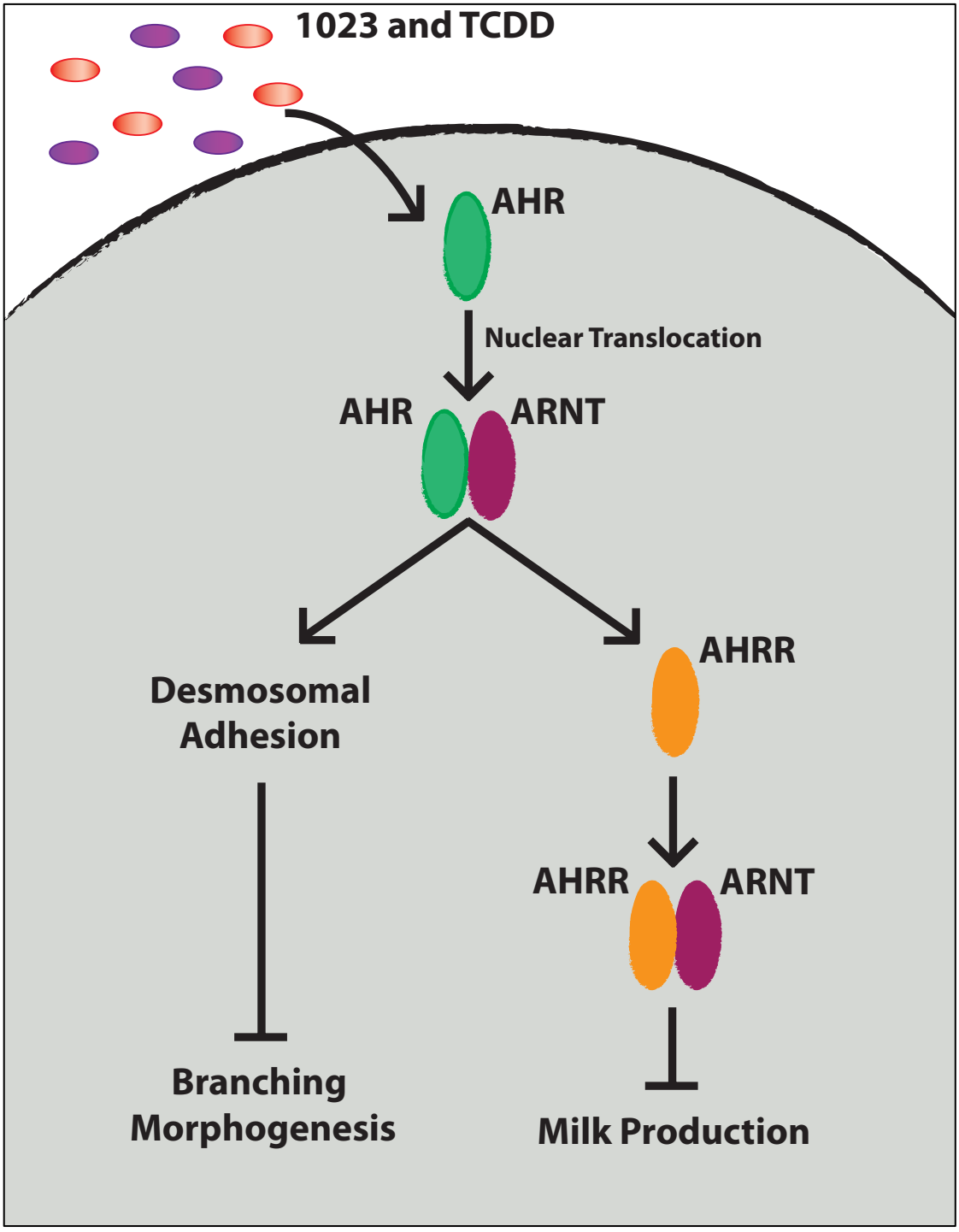
1023 and TCDD
AHR
Nuclear Translocation
AHR
ARNT
Desmosomal
Adhesion
AHRR
AHRR
ARNT
Branching
Morphogenesis
Milk Production

of AHRR alone upregulated desmosomes and inhibited mammary branching in our 3D assay. Since AHR signaling is promoted under these conditions, these results suggest AHR and its binding partner, ARNT, regulate desmosomes. Additionally, overexpression of AHRR was sufficient to block milk production, implicating AHRR as a critical factor inhibiting lactogenesis.

In the broader context, our results suggest the AHR pathway may be active and dynamically regulated during normal mammary gland development. If AHR signaling were completely inactive during mammary development, loss of AHRR would have little impact. Thus, the block in mammary branching observed in AHRR deficient MECs suggests the AHR pathway may have a basal level of activity. This is consistent with expression studies in developing mice, where indicators of AHR activity, including both nuclear AHR and Cyp1A1 expression, were observed in a portion of mammary epithelial cells (34).

However, given the robust ability of the AHR pathway to inhibit mammary branching and lactation, any basal activity is likely restricted to earlier stages of development. This is supported by the dynamic expression of AHR (34) and ARNT (35) in the mammary gland, which is very high during puberty. AHR activity during ductal elongation would support epithelial integrity and prevent hyperbranching. Moreover, the induction of AHRR would inhibit premature mammary differentiation and milk production. With the onset of pregnancy, we expect the AHR pathway to be dramatically downregulated. However, we anticipate ARNT remains active throughout this period since our mechanistic studies with AHRR show this protein likely blocks milk production by disrupting a normal function of ARNT. Supporting this idea, AHR expression

declines rapidly in pregnancy (34) while ARNT does not decrease significantly until involution (35). The sustained expression of ARNT during lactation is consistent with a critical role for ARNT during normal milk production.

Overall, our study of the AHR pathway in the mammary gland has revealed new aspects of both mammary gland biology and AHR signaling. In particular, we have discovered a novel role for AHRR in regulating mammary branching and differentiation. Through the characterization of AHRR knockout mice, we hope further define the complexities of this pathway.

References

1. Macias, H., and Hinck, L. (2012) Mammary gland development. *Wiley Interdiscip. Rev. Dev. Biol.* **1**, 533-557

2. Sternlicht, M. D., Kouros-Mehr, H., Lu, P., and Werb, Z. (2006) Hormonal and local control of mammary branching morphogenesis. *Differentiation* **74**, 365-381

3. Basham, K. J., Kieffer, C., Shelton, D. N., Leonard, C. J., Bhonde, V. R., Vankayalapati, H., Milash, B., Bearss, D. J., Looper, R. E., and Welm, B. E. (2013) Chemical genetic screen reveals a role for desmosomal adhesion in mammary branching morphogenesis. *J. Biol. Chem.* **288**, 2261-2270

4. Hinck, L., and Silberstein, G. B. (2005) Key stages in mammary gland development: The mammary end bud as a motile organ. *Breast Cancer Res.* **7**, 245-251

5. Sternlicht, M. D. (2006) Key stages in mammary gland development: The cues that regulate ductal branching morphogenesis. *Breast Cancer Res.* **8**, 201

6. Oakes, S. R., Hilton, H. N., and Ormandy, C. J. (2006) The alveolar switch: Coordinating the proliferative cues and cell fate decisions that drive the formation of lobuloalveoli from ductal epithelium. *Breast Cancer Res.* **8**, 207

7. Streuli, C. H., Edwards, G. M., Delcommenne, M., Whitelaw, C. B., Burdon, T. G., Schindler, C., and Watson, C. J. (1995) Stat5 as a target for regulation by extracellular matrix. *J. Biol. Chem.* **270**, 21639-21644

8. Fata, J. E., Werb, Z., and Bissell, M. J. (2004) Regulation of mammary gland branching morphogenesis by the extracellular matrix and its remodeling enzymes. *Breast Cancer Res.* **6**, 1-11

9. Lu, P., Ewald, A. J., Martin, G. R., and Werb, Z. (2008) Genetic mosaic analysis reveals FGF receptor 2 function in terminal end buds during mammary gland branching morphogenesis. *Dev. Biol.* **321**, 77-87

10. Santiago-Josefat, B., Esselens, C., Bech-Serra, J. J., and Arribas, J. (2007) Post-transcriptional up-regulation of ADAM17 upon epidermal growth factor receptor activation and in breast tumors. *J. Biol. Chem.* **282**, 8325-8331

11. Klus, G. T., Rokaeus, N., Bittner, M. L., Chen, Y., Korz, D. M., Sukumar, S., Schick, A., and Szallasi, Z. (2001) Down-regulation of the desmosomal cadherin desmocollin 3 in human breast cancer. *Int. J. Oncol.* **19**, 169-174

12. Oshiro, M. M., Kim, C. J., Wozniak, R. J., Junk, D. J., Munoz-Rodriguez, J. L., Burr, J. A., Fitzgerald, M., Pawar, S. C., Cress, A. E., Domann, F. E., and Futscher, B. W. (2005) Epigenetic silencing of DSC3 is a common event in human breast cancer. *Breast Cancer Res.* **7**, R669-680

13. Maynadier, M., Chambon, M., Basile, I., Gleizes, M., Nirde, P., Gary-Bobo, M., and Garcia, M. (2012) Estrogens promote cell-cell adhesion of normal and malignant mammary cells through increased desmosome formation. *Mol. Cell. Endocrinol.* **364**, 126-133

14. Osborne, C. K. (1998) Steroid hormone receptors in breast cancer management. *Breast Cancer Res. Treat.* **51**, 227-238

15. Sternlicht, M. D., and Barsky, S. H. (1997) The myoepithelial defense: A host defense against cancer. *Med. Hypotheses* **48**, 37-46

16. Sternlicht, M. D., Kedeshian, P., Shao, Z. M., Safarians, S., and Barsky, S. H. (1997) The human myoepithelial cell is a natural tumor suppressor. *Clin. Cancer Res.* **3**, 1949-1958

17. Lakhani, S. R., and O'Hare, M. J. (2001) The mammary myoepithelial cell--Cinderella or ugly sister? *Breast Cancer Res.* **3**, 1-4

18. Ronnov-Jessen, L., Petersen, O. W., and Bissell, M. J. (1996) Cellular changes involved in conversion of normal to malignant breast: Importance of the stromal reaction. *Physiol. Rev.* **76**, 69-125

19. Barsky, S. H. (2003) Myoepithelial mRNA expression profiling reveals a common tumor-suppressor phenotype. *Exp. Mol. Pathol.* **74**, 113-122

20. Angele, S., Jones, C., Reis Filho, J. S., Fulford, L. G., Treilleux, I., Lakhani, S. R., and Hall, J. (2004) Expression of ATM, p53, and the MRE11-Rad50-NBS1 complex in myoepithelial cells from benign and malignant proliferations of the breast. *J. Clin. Pathol.* **57**, 1179-1184

21. Poland, A., Glover, E., and Kende, A. S. (1976) Stereospecific, high affinity binding of 2,3,7,8-tetrachlorodibenzo-p-dioxin by hepatic cytosol. Evidence that the binding species is receptor for induction of aryl hydrocarbon hydroxylase. *J. Biol. Chem.* **251**, 4936-4946

22. Denison, M. S., and Nagy, S. R. (2003) Activation of the aryl hydrocarbon receptor by structurally diverse exogenous and endogenous chemicals. *Annu. Rev. Pharmacol. Toxicol.* **43**, 309-334

23. Rogan, W. J., Gladen, B. C., McKinney, J. D., Carreras, N., Hardy, P., Thullen, J., Tingelstad, J., and Tully, M. (1987) Polychlorinated biphenyls (PCBs) and dichlorodiphenyl dichloroethene (DDE) in human milk: Effects on growth, morbidity, and duration of lactation. *Am. J. Public Health* **77**, 1294-1297

24. Gladen, B. C., and Rogan, W. J. (1995) DDE and shortened duration of lactation in a northern Mexican town. *Am. J. Public Health* **85**, 504-508

25. Neville, M. C., and Walsh, C. T. (1995) Effects of xenobiotics on milk secretion and composition. *Am. J. Clin. Nutr.* **61**, 687S-694S

26. Vorderstrasse, B. A., Fenton, S. E., Bohn, A. A., Cundiff, J. A., and Lawrence, B. P. (2004) A novel effect of dioxin: Exposure during pregnancy severely impairs mammary gland differentiation. *Toxicol. Sci.* **78**, 248-257

27. Fenton, S. E., Hamm, J. T., Birnbaum, L. S., and Youngblood, G. L. (2002) Persistent abnormalities in the rat mammary gland following gestational and lactational exposure to 2,3,7,8-tetrachlorodibenzo-p-dioxin (TCDD). *Toxicol. Sci.* **67**, 63-74

28. Lewis, B. C., Hudgins, S., Lewis, A., Schorr, K., Sommer, R., Peterson, R. E., Flaws, J. A., and Furth, P. A. (2001) In utero and lactational treatment with 2,3,7,8-tetrachlorodibenzo-p-dioxin impairs mammary gland differentiation but does not block the response to exogenous estrogen in the postpubertal female rat. *Toxicol. Sci.* **62**, 46-53

29. Lew, B. J., Manickam, R., and Lawrence, B. P. (2011) Activation of the aryl hydrocarbon receptor during pregnancy in the mouse alters mammary development through direct effects on stromal and epithelial tissues. *Biol. Reprod.* **84**, 1094-1102

30. Lew, B. J., Collins, L. L., O'Reilly, M. A., and Lawrence, B. P. (2009) Activation of the aryl hydrocarbon receptor during different critical windows in pregnancy alters mammary epithelial cell proliferation and differentiation. *Toxicol. Sci.* **111**, 151-162

31. Collins, L. L., Lew, B. J., and Lawrence, B. P. (2009) TCDD exposure disrupts mammary epithelial cell differentiation and function. *Reprod. Toxicol.* **28**, 11-17

32. Basham, K. J., Bhonde, V. R., Kieffer, C., Mack, J. B., Hess, M., Welm, B. E., and Looper, R. E. (2014) Bis-aryloxadiazoles as effective activators of the aryl hydrocarbon receptor. *Bioorg. Med. Chem. Lett.* **24**, 2473-2476

33. Mimura, J., Ema, M., Sogawa, K., and Fujii-Kuriyama, Y. (1999) Identification of a novel mechanism of regulation of Ah (dioxin) receptor function. *Genes Dev.* **13**, 20-25

34. Hushka, L. J., Williams, J. S., and Greenlee, W. F. (1998) Characterization of 2,3,7,8-tetrachlorodibenzofuran-dependent suppression and AH receptor pathway gene expression in the developing mouse mammary gland. *Toxicol. Appl. Pharmacol.* **152**, 200-210

35. Le Provost, F., Riedlinger, G., Hee Yim, S., Benedict, J., Gonzalez, F. J., Flaws, J., and Hennighausen, L. (2002) The aryl hydrocarbon receptor (AhR) and its nuclear translocator (Arnt) are dispensable for normal mammary gland development but are required for fertility. *Genesis* **32**, 231-239